Title
Seismic and Acoustic Investigations of Rock Fall Initiation, Processes, and Mechanics

Author
Zimmer, Valerie Louise

Publication Date
2011

Peer reviewed|Thesis/dissertation

Seismic and Acoustic Investigations of Rock Fall Initiation, Processes, and Mechanics

by

Valerie Louise Zimmer

A dissertation submitted in partial satisfaction of the

requirements for the degree of

Doctor of Philosophy

in

Engineering – Civil and Environmental Engineering

in the

Graduate Division

of the

University of California, Berkeley

Committee in charge:

Professor Nicholas Sitar, Chair
Professor James Rector
Professor Douglas Dreger

Fall 2011

Abstract

Seismic and Acoustic Investigations of Rock Fall Initiation, Processes, and Mechanics

by

Valerie Louise Zimmer

Doctor of Philosophy in Engineering – Civil and Environmental Engineering

University of California, Berkeley

Professor Nicholas Sitar, Chair

Rock falls were monitored in Yosemite Valley using seismic and infrasound sensors in order to gain insights into the feasibility of rock fall detection and rock fall processes. The research objectives were to characterize the rock fall seismic signal and use that data to study the initiation, triggering, and dynamics of rock falls, correlate the data with physical and environmental conditions, and to search for potential rock fall precursors. Yosemite Valley has approximately one rock fall per week in an area that measures 15 km^2, making it an ideal laboratory for monitoring rock falls. Data were collected continuously at 500-1000 sps using a network of one to four stations during two winter seasons. Three stations were located within a 600 m long footprint on the cliff or at the base of the historically active Middle Brother formation and one station was located 2 km to the east. There were three widely reported rock falls that were also easily identifiable in the seismic data: these three events were critical in the development of a triggering algorithm and criteria for distinguishing rock falls from the thousands of triggers. In addition to rock falls, snow avalanches, construction activity, rain, wind, pressure waves generated from Yosemite Falls, thermally-driven long period seismic anomalies, and earthquakes triggered or were identified in the seismic and acoustic data. A total of twelve to seventeen rock falls were recorded, out of which only eight were reported by eyewitnesses. All but one rock fall event came from within one kilometer of the seismic network and originated at four distinct source areas. The spectral similarities between some events allowed them to be placed with high certainty as coming from a particular talus slope even when there were too few stations in operation to precisely locate the source. Detachment and impact signals were recorded for multiple rock fall events, and timing delay between detachment and impact correlated well with physical parameters such as falling and impact distances. The Ahwiyah Point rock fall on 28 March 2009 was a large enough event to have been widely captured on regional seismic networks and is the only rock fall recorded at a distance greater than 1 km. The Ahwiyah Point rock fall was uniquely well-documented with pre and post rock fall high resolution photography and LiDAR to supplement the seismic and acoustic data. The rock fall dynamics were

resolved by integrating these different data to show that a large block detached, slid off of a steeply dipping ledge, launched into a ballistic trajectory, impacted the cliff with enough force to detach another large volume of rock, continued down the cliff face to the talus, and produced an airblast upon impact. P and Rayleigh wave phases were recorded for multiple rock falls, although S-waves were generally not detected. P-waves were calculated to have arrived via granitic cliff faces rather than directly through unconsolidated valley sediments via single station polarities and multiple station timing delays. Rayleigh waves generated by rock falls on the same cliff as the seismic sensor travel along and are oriented to the cliff face (e.g. tilted from normal). However Rayleigh waves do appear to travel through the valley when arriving from other cliffs and can be difficult to identify due to boundary interactions at the base of the cliff. Distances were calculated using the phase arrival differences of P and Rayleigh waves and the arrival time differences of P and infrasound acoustic waves. Thus, rock falls were successfully detected, located, and their dynamics reconstructed with the seismic and acoustic data.

Table of Contents

Acknowledgements

I wish to thank my advisor, Professor Nicholas Sitar, for being supportive and encouraging of my research pursuits. Professor Sitar introduced me to rock fall research and cutting edge sensor technology and shared his creative insights with me in many interesting discussions. I wish to thank the members of my research committee, Douglas Dreger and James Rector, for their advice and support on dissertation research and other projects over the years. I also wish to thank Greg Stock and Bob Sas for facilitating field research in Yosemite National Park, for providing critical information for data analysis, and for engaging in fruitful technical discussions. I thank Brian Collins at the US Geological Survey for his support in collecting, processing, and interpreting LiDAR data that was used to correlate seismic signatures with physical parameters. I thank Bob Reinke and Al Leverette of the Defense Threat Reduction Agency for lending me an instrumentation system and providing training for it at a critical moment at the beginning of my research. I thank Ernie Majer, Ramsey Haught, and Kenzi Karasaki for support, lending me instruments and allowing me to tinker up at Lawrence Berkeley National Laboratory. I wish thank the Berkeley Seismological Laboratory for allowing me to use their tools and supporting me when requested. Thanks also go out to the helpful and supportive folks at PASSCAL, who loaned me instruments during the second winter. I also wish to thank the volunteers who came to Yosemite National Park and helped to carry and install instrumentation, by name: Shee Zhiqiang, Hunter Philson, Kent Richards, Phil Boudreau, Bill Chen, Greg Valiant, Sara Weinstein, Seth Green, Anand Varma, Kelsey Richardson, Evan Battaglia, Bryce Nesbitt, Chrissy Bloomer, Ingrid Gennity, Martha Quenon, Meg Schwarzman, James Boudreau, Ed Hartouni, Kurt Amundson, Yngve Antonsen, Jonas Thelemann, Max Schubert, Aaron Dresden, Dave Wang, Sonya King, Nick Holt, Hillary Raya, and James Sonu.

I wish to thank those entities who offered instrumentation, data management, and funding support, and am extremely grateful to them to have had the opportunity to conduct this research. Thanks for funding support go to Hitachi, Ltd. and the National Science Foundation (NSF) SGER Grant # 0840580 to Nicholas Sitar. Airborne LiDAR data collected in 2010 was provided through a National Center for Airborne Laser Mapping (NCALM) graduate student Seed project grant. Seismic instruments were provided by the Defense Threat Reduction Agency and by the PASSCAL Instrument Center at New Mexico Tech, of the Incorporated Research Institutions for Seismology (IRIS). Data collected during this experiment will be available through the IRIS Data Management Center. The facilities of the IRIS Consortium are supported by the National Science Foundation under Cooperative Agreement EAR-0552316 and by the Department of Energy National Nuclear Security Administration. Acoustic microphones were kindly loaned by the InfraVolc Research Group at New Mexico Tech. Thanks also go to the National Park Service for providing high-resolution photography and field observations and for allowing research to be conducted inside the park.

I wish to thank my close friends and family for their constant love and support during this process, and for providing much needed laughter, soul-cleansing adventures, and introspective discussions on life. To my sister Erica and brother Kurt, to my extended family and my new family, especially James Boudreau for being so easy and accepting, to my lifelong friends from Vermont, to my roommates at 56th Street, to the CHAOS tribe, and to many others who don't fit neatly in those categories, I am grateful and blessed for your presence in my life. I especially would like to thank my parents, Fred and Terry Zimmer, for their unconditional love, for always encouraging and believing in my potential, and for letting me be myself while growing up. And finally, I wish to thank Phil Boudreau, whose love and understanding never wavered and who has been my rock these past few years.

1 Introduction

This thesis presents a multi-year project in which geophysical instruments were selected and installed in Yosemite Valley for the purpose of rock fall monitoring and the results, analysis of data, and ideas that emerged from the study. Geophysical monitoring can identify and locate rock falls and associated phenomena as well as possibly identify the conditions required for rock fall triggering and the dynamics of a rock fall in progress. Rock falls pose a hazard in steep, mountainous terrain and a risk to roads, villages, and people living nearby. The risk can be managed only with a good understanding of the hazard. Previous rock fall studies address the location, frequency, geologic structure, rock type, environmental conditions, and geomorphological processes. There are only a handful of cases where geophysical instruments were employed and those that successfully recorded rock falls were either short-term, or targeted small cliffs at close range. In contrast, this dissertation targeted a large, historically active cliff in Yosemite Valley and monitored it continuously for several months with a network of sensors.

Yosemite Valley has approximately one rock fall per week in an area that measures 15 km^2, making it an ideal laboratory for monitoring rock falls. Large rock falls have damaged facilities and killed and injured people, which is not surprising considering that nearly four million people visit the Yosemite Valley each year. Monitoring protocols and rock fall specific zoning are actively being developed in response to an evolving need for rock fall risk management. Rock falls in Yosemite Valley are, thus far, only documented when people happen to witness and report them. Therefore, not only are there presumably rock falls that go unreported, there is also a location distribution bias toward areas with higher populations. In some cases, large rock falls were preceded by cracking noises and small rock falls. In retrospect, these were precursory events, but witnesses usually do not think to report them until after a catastrophic rock fall. Thus, there is a lack of data on the frequency of these phenomena without subsequent rock falls as well as a lack of data on the propensity of precursors occurring before a rock fall. Rock fall monitoring in Yosemite Valley can help in understanding rock fall frequency and associated phenomena, which can be used to assess the hazard.

1.1 Scientific Objectives

The objectives of this study were to characterize seismic phenomena, analyze the rock fall signal, and correlate the data with physical parameters and environmental conditions. The first objective was to simply observe signals related to rock falls and document them without relying on human reporting. Thus far, the seismic characteristics of Yosemite rock fall are unknown, and finding rock fall events in the seismic record requires identifying those characteristics and differentiating them from other signals related to other seismic events and noise. The next objective was to examine the geophysical records in detail to ascertain if there is information about environmental conditions at the site or nearby common noise that may or may not be related to rock falls. Once rock falls have been identified, they can be studied in detail to identify physical processes such as the mechanics of block detachment and the dynamics of the rock fall in progress. Physical parameters such as rock fall volume, energy, fall height, and runout may be identifiable with a large enough dataset. Questions about the triggering of rock falls persist, and an objective is to correlate the data with potential triggers and assess whether or not some rock falls are progressive events. Finally, documentation of the frequency of phenomena such as cracking noises and small rock falls preceded larger rock falls was another important objective of the project.

1.2 Definition of a Rock Fall

Rock falls specific events that involve individual blocks of rock failing suddenly and falling in a primarily vertical trajectory. In contrast, a rockslide is an episodic event that involves rock blocks moving downslope en-mass. A rock fall can initiate in a stress-induced burst, by sliding off of a dipping ledge, or by toppling over. The initial failure of the cliff, the breakup and ricocheting of falling rock while bouncing down the cliff face, the mid-cliff dislodging of additional material, multiple large ground impacts, airblasts strong enough to topple trees, and deceleration of the rocks as they come to a stop are all part of a rock fall event.

1.3 Experiment Design

The first step was to determine whether or not geophysical rock fall monitoring in Yosemite Valley was feasible. In order to accomplish this, several monitoring studies at mines, volcanoes, and landslides were reviewed in order to determine the type instrumentation needed to monitor small seismic events several hundred meters away in granitic rock. Then, a single station feasibility study with a geophone and accelerometer was conducted during the winter of 2007-08. The station was placed high on a cliff near the historically active Middle Brother formation, in an attempt to get as close as possible to a rock fall initiation zone. This initial feasibility study was a success, recording several rock falls at a cliff location 600 meters from a rock fall source area.

The success of the feasibility study prompted the second phase of the project: the installation of a network of sensors. The sensor locations were constrained by the number of instruments available, access to cliff locations, power, and wilderness restrictions in a National Park. The small network was optimized for the target location, Middle Brother, by getting as close as possible to the rock fall source areas, spacing instruments at two ledge locations and one talus site. One additional instrument was installed in Yosemite Village, two kilometers away, as part of a second feasibility study at a new site. In addition, infrasound acoustic microphones were tested, thereby increasing the scope of the project to search for precursory cracking, rumbling, and airblasts that sometimes accompany rock falls.

During the second phase, a large rock fall occurred that spurred interest beyond the scope of the original project. Other researchers conducted geomorphological studies using lidar and high-resolution photography. With support from these collaborators, an airborne lidar data grant was awarded to this project to provide post rock fall lidar data that could be compared to the pre rock fall data that had been collected several years prior. These different sets of geophysical, lidar, and photography data were combined into an analysis that is being published in a collaborative scientific paper (Zimmer et al., 2012 in prep).

1.4 Data Processing

A major part of the project effort was searching for rock falls in the seismic record. Continuous recording at several stations for several months generates a dataset that is too large to be searched manually. Thus, designing a rock fall search algorithm is an important part of the project. Characterizing the known rock falls and noise allows the data to be filtered in order to enhance rock falls while eliminating as much noise as possible. Next, a processing method and algorithm were designed, tested, and applied to the entire dataset to look for additional rock falls; events that met the criteria of the algorithm are called triggers. The full waveforms of triggered events were reviewed systematically in order to determine whether or not they were indeed rock falls. Finally, seismic triggering and rock fall event trends were reviewed and correlated with weather events and human activity. The data processing methods developed for this project have potential to be applied to additional data sets in near real time and require less time for processing in the future.

2 Background

This dissertation builds upon a previous body of research in rock fall and rockslide in Yosemite National Park as well as locations worldwide, and applies monitoring and analysis methods developed in mining and seismology. Rock falls and rockslides are landslide events that occur in primarily rocky terrain. A rock fall chiefly involves individual blocks of rock failing suddenly and falling in a primarily vertical trajectory, which is distinguished from a rockslide, which are rock blocks that move downslope en-mass in episodes at regular intervals. The initiation of a rock fall can occur in several ways; the rock can fail in a stress-induced burst, it can slide off a ledge from which it has been meta-stable for years, and it can topple over. In many cases, there is no known trigger associated with the rock fall, and the mechanics by which the rock fall was initiated was unknown.

Scientific studies specific to rock falls are limited. However, in the mining industry, rock mass failures have been a subject of intense research. Most mining studies focused on rockbursts, which are sudden, catastrophic, stress-induced failures in deep, underground mines. There are some studies on roof-falls and bench collapse, both of which occur under lower stress conditions and are often progressive in nature. Of particular interest to this dissertation are mining studies that use microseismic and acoustic emission sensors in attempts to predict impeding failure and pinpoint the triggering conditions. Thus, it is relevant to this research to review the mining failure monitoring efforts in addition to research specific to rock falls.

2.1 Geologic Setting: Yosemite Valley, California, USA

The Yosemite Valley is a glacial valley carved into an intact granitic batholith in the Sierra Nevada, California, USA (Figure 1). Several episodes of glaciation left a classic U-shaped valley with steep granitic walls that are nearly as tall as the valley is wide (approximately 1000 meters). The Yosemite Valley is the main attraction in the Yosemite National Park, registering nearly 3.9 million visitors in 2009 (NPS Statistics, 2011). The steep rock walls present a significant rock fall hazard and a corresponding risk to visitors, the majority of whom are located in the narrow valley.

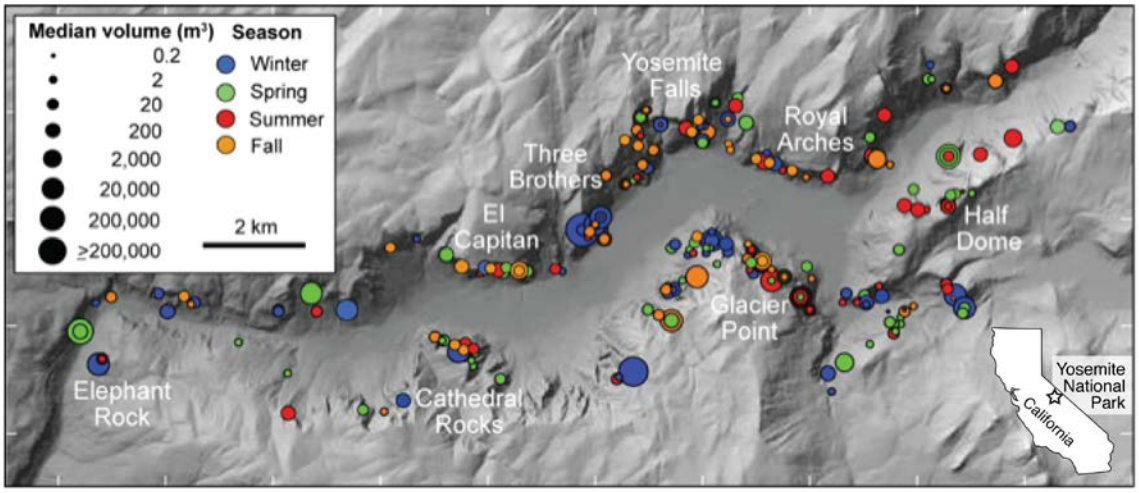

Figure 1. Historic rock falls in Yosemite Valley. Figure courtesy Greg Stock, NPS.

Rock fall activity has been recorded since 1857, although certainly it has been occurring for far longer, as evidenced by the large amount of talus that has accumulated since the last ice age approximately 10,000 years ago. In one famous account, the naturalist John Muir, living in the valley, was "awakened by a tremendous earthquake", and, taking meager cover, reported that a formation known as Eagle Rock "gave way and I saw it falling in thousands of … great boulders." Muir goes on to report that rock falls continued to shake the valley daily for over two months (Muir, 1912).

The history of rock falls and assessment of rock-fall hazards in Yosemite has been extensively studied through a cooperative program between the U.S. Geological Survey, National Park Service, and outside researchers (Wieczorek et al., 1995, 1999, 2000, 2002, 2008; Wieczorek and Jäger, 1996; Wieczorek and Synder, 1999; Guzzetti et al., 2003; Stock and Uhrhammer, 2010; Stock et al., 2011a, b; Zimmer et al., 2012 in prep.). Because Yosemite Valley experiences a high frequency of rock falls contained in a very small geographic area, it has been an ideal laboratory for closely monitoring rock fall activity. More than 800 rock falls and other landslide events have been documented during the period 1857 to 2010 (Figure 1), with the majority of events occurring as rock falls in Yosemite Valley. Rock falls have caused fifteen fatalities, numerous injuries, and many incidents where buildings, roads, and trails were damaged (Stock et al., 2011b).

Several high profile rock fall events have occurred in the past 15 years, bringing new attention to the hazard. The Glacier Point rock face (Figure 2) has been the source of most of the damaging rock fall events, due to the proximity of the Curry Village and Happy Isles facilities and the extremely popular John Muir and Mist Trails, which lead to premier Yosemite attractions at Nevada Falls and Half Dome. Thousands of visitors occupy Curry Village and thousands more tread the nearby trails on a busy summer day. At 6:52 pm on July 10, 1996, 60,000 m^3 of rock detached above Happy Isles, slid off a inclined rock face, fell on a vertical trajectory, and created an airblast that knocked over 1000 trees, crushed a snack bar, destroyed a bridge, and killed a hiker (Wieczorek et al., 2000). On June 13, 1999, at 7:35 pm, roughly 200 m^3 of rock detached above the Glacier point Apron, killing a young rock climber and struck a Curry Village Terrace tent (Wieczorek and Snyder, 1999). In December 2003 and June 2007, rock falls from Staircase Falls damaged occupied visitor cabins (Wieczorek et al., 2007; Wieczorek et al., 2008). And finally, on October 7-8, 2008, 6000 m^3 of rock detached above Curry Village and completely destroyed 7 cabins, some of which had been occupied moments before the rock fall (Figure 3). It is notable to consider that rock falls occurred during a variety of weather and hydrological conditions on the cliff face, thus, there is no single cause or trigger to which they can be attributed.

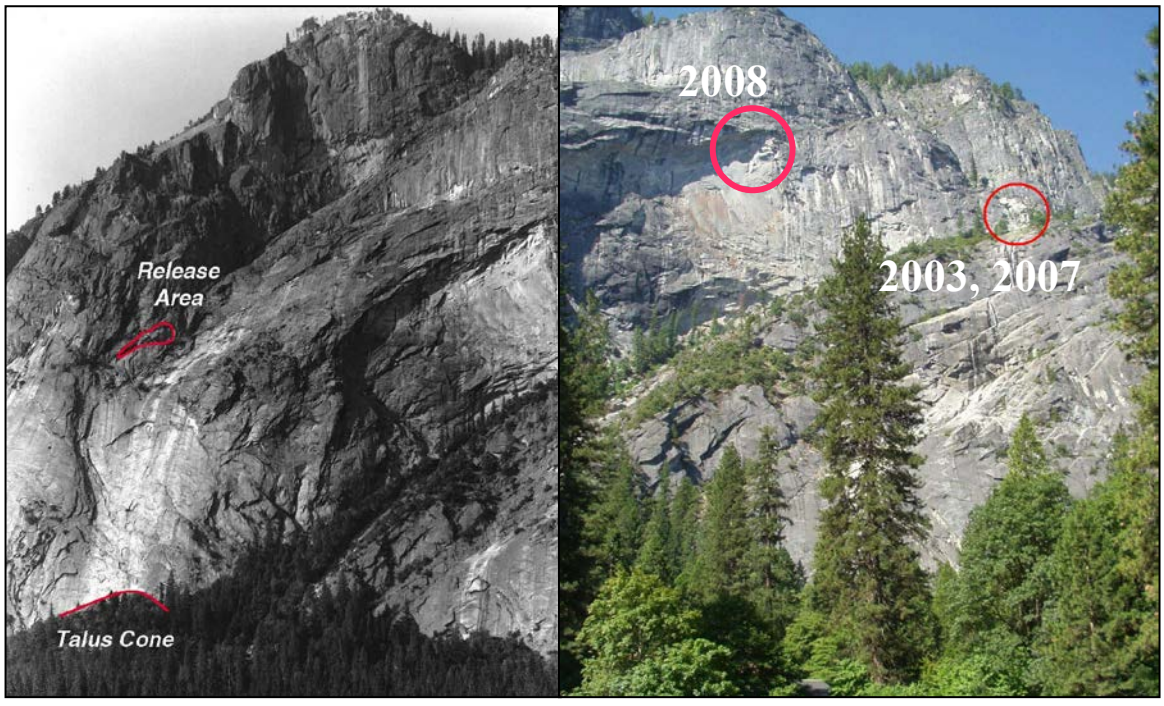

Figure 2. Glacier Point rock face, showing release point in 1999 (left), and 2003, 2007, and 2008 (right). The 1996 Happy Isle release zone is around the corner to the right of this face, and is not shown.

Figure 3. Curry Village visitor cabins crushed by October 8, 2008 rock fall (Greg Stock/NPS photo).

The trigger that causes a metastable block of rock to fall at a particular time is difficult to determine. Ultimately, rock falls are a part of an erosional process of weathering and fracturing of the rock mass. Rock fall triggering has been a subject of considerable research in Yosemite (Wieczorek and Jäger, 1996; Stock et al., 2011b). Research has shown that approximately half of all documented failures in Yosemite are correlated with commonly recognized triggering mechanisms such as earthquakes, intense rainfall, snowmelt, or freeze-thaw cycles (Stock et al., 2011b). Still, approximately half of all documented rock falls in Yosemite have no recognized trigger. Furthermore, most rock fall events are not part of a clear pattern of continuing events from a particular source area over a long period of time. Historically, rock falls have been distributed throughout the Yosemite Valley, and most above average rock fall frequency (in a particular area) can be attributed to a reporting bias (e.g. more visitors in that area to witness the rock falls) (Stock, personal communication, 2011). Thus, it is currently impossible to predict whether or not a particular rock mass is unstable enough to precipitate a failure in the near future, even when known triggering events (such as rain and snow) are occurring.

Traditional geological engineering hazard modeling techniques, developed for mining and highway cuts, evaluate the regional and site-specific settings to obtain a probabilistic assessment of overall risk, often with a high degree of success (Vandewater et al., 2005). When such a technique is applied to Yosemite Valley, most of the area near the cliff faces and corresponding talus slopes are identified as being high hazard, a result that is not practical for rock fall prediction (Guzzetti et al., 2003). Current planning efforts in Yosemite National Park are focused on avoiding these areas by moving structures down and away from the cliff faces, rather than trying to determine which cliffs and rock masses are stable. For example, 233 cabins were closed following the 2008 Curry Village rock fall, nearly 1/3 of all available cabins. New recommendations for Yosemite Valley development and relocation will include a policy of rock fall avoidance for facilities, thus acting in a proactive manner (rather than reactive) with regards to rock fall risk management (Stock, personal communication, 2011). Such planning is challenging due to the Merced River floodplain, which encompasses much zone deemed safe from rock fall. Damages from the January 1997 Yosemite Valley flood totaled $178 million, closed the Valley for 2.5 months, and permanently forced the closing of several campgrounds. In 2005, the Yosemite Valley flooded again, although the closure and damage were less severe. Furthermore, this level of planning does not extend to most trails, with a few notable exceptions, such as those closed due to very recent rock fall (e.g. the Southern Mirror Lake trail below Ahwiyah Point), and those deemed to have an exceptionally high hazard (e.g. the former Ledge Trail at Glacier Point).

Despite new efforts by NPS to avoid rock falls by moving infrastructure away from the most hazardous areas, most trails and by extension, many visitors are still subject to the rock fall hazard in Yosemite Valley when participating in recreational activities. Managing the risk in high hazard areas, such as trails, is usually done only after a failure has occurred, by visually inspecting the source area for potential additional loose material, monitoring the area for continuing rock falls, and relying on prior experience to decide when to reopen that area (Snyder, Stock, NPS, personal communication, 2004-2011). Occasionally, precursors, e.g. loud cracking noises, a showering of small showering of small pebbles and rocks, or small rock falls from the same source area, have been reported following a large rock fall. The 2008 Curry Village rock falls that crushed several visitor cabins occurred less than a day after of cracking noises (that were reported later by eyewitnesses) and a smaller rock fall event (Stock, personal communication, 2008).

While post-event reporting of apparent precursors does not help in risk management, it does suggest that instrumented cliff monitoring may be able to identify precursors in order to raise an increased hazard alarm. In 1987, small rock falls and cracking noises at Middle Brother started occurring with enough frequency over a two-day period that the National Park Service closed Northside Drive, the Yosemite Park exit road (Wieczorek and Snyder, 2004; Wieczorek, 2002; Wieczorek et al., 1995; Wieczorek et al, 1992; Yosemite Association, 1987). This closure was followed two hours later by the largest rock fall in recording history on March 10, 1987 at 2:47pm, when 600,000 m^3 of rock detached and buried Northside Drive to a depth of four meters. In this particular case, the fact that precursors were noted did in fact lead to a successful prediction and management of the risk.

There was one attempt to monitor rock falls with seismic instruments following the 1996 and 1999 Glacier Point rock falls. The results were inconclusive, as there were no notable rock falls during the time period, and at a distance of 650 meters from the rock fall release zone, there were no other signals that could be definitely related to rock falls (Myers et al., 2000).

2.2 Rockslide and Rock Fall Monitoring by Non-Seismic Techniques

The current state of the practice in geological engineering is to target known unstable rock slopes and cliffs for monitoring using many of the same methods used for landslides. Many rockslides are progressive and known to be failing, although rock falls are generally catastrophic, and thus harder to target. Monitoring can be done through the use of photography, damage mapping, hydrological surveys, extensometers, real-time GPS stations, and InSAR. Techniques of specific interest to this dissertation are acoustic emission/microseismic (AE/MS), seismic, and scanning laser systems (LiDAR). Ground and airborne-based LiDAR surveys can be used to document earth movements over time (Collins and Sitar, 2005), as well as pinpoint the exact location of rock detachment and impact, and changes to the talus slope (Zimmer et al., 2012 in prep). LiDAR data has been used to study rock fall in other studies, although the majority of such research consisted only of post-rock fall data, or were part of larger slope failures that are better characterized as rockslides or landslides. For example, Rosser et al. (2007) used LiDAR to identify small rock fall, which occurred prior to larger slope failure in sedimentary rocks.

In Yosemite National Park, airborne LiDAR data from the National Center for Airborne Laser Mapping (NCALM) have been collected twice: a general survey in 2006 and a second dataset in 2010 under a graduate student Seed grant for this awarded to support this research. Terrestrial LiDAR data have been collected at several locations in Yosemite National Park between 2007 to the present, including Glacier Point, Middle Brother, and following the 2009 Ahwiyah Point failure. LiDAR results from the Ahwiyah Point rock fall are presented in later chapters in this dissertation, and much of the remaining LiDAR data is being used in current research efforts or as baseline data in preparation for future rock falls at these locations (Stock and Collins, personal communication).

While LiDAR is a valuable tool for monitoring progressive failures such as rockslides, and for developing a better understanding of the rock fall process by precisely mapping the fracture systems and rock fall source and impact areas, it is currently impractical to use it to identify impeding rock fall failures or the temporal pattern of rock fall, unless LiDAR surveys are conducted on a very regular and frequent basis (an expensive proposition). More importantly, the typical LIDAR resolution (2.5 cm at 200 m) can only detect movement once the failure has initiated and cannot be used to detect precursors to failure. Given the brittle nature of most crystalline rocks, e.g. granite, movement of sufficient magnitude to be detected optically means that failure is already in process. Thus, the search for previously unreported rock falls and precursors requires constant monitoring, which is more suitable for seismic and acoustic monitoring techniques.

2.3 Seismic Studies of Rock Falls and Rockslides

Seismic studies of rock falls and rockslides have been conducted on a wide range of scales, in different rock types, and with different scientific objectives. Seismic signatures can help distinguish the type (rock fall vs. rockslide vs. degassing event at a volcano), size, location, progression, and triggering mechanism of failure. Precursory activity to rock falls and rockslides has been observed in the form of smaller rock falls or cracking noises in the days or hours leading up to a large failure, most often noted after the fact. In Yosemite National Park, loud popping noises have been reported before occurrence of rock falls in 1987 ((Wieczorek and Snyder, 2004; Wieczorek, 2002; Wieczorek et al., 1995; Wieczorek et al, 1992; Yosemite Association, 1987) and have been heard preceding small rock falls by park geologist Greg Stock (Stock, personal communication, 2010), and by the author of this thesis on one occasion. This indicates that the movement or fracture propagation prior to failure produces rock noise with sufficient energy to be audible and possibly seismically detectable.

The seismic signatures associated with rock falls have been noted by seismologists since, at least, the early 1970s. The early researchers were primarily interested in earthquakes or volcanic activity and noted the rockslide or rock fall activity only to distinguish it from events of more immediate interest. Tilling et al. (1975) took interest rock fall seismicity in an attempt to correlate seismic duration with rock fall volume at Makaopuhi Crater in Hawaii, finding poor correlation. In the Cascades, Norris (1994) analyzed seismic records of 14 large ($> 10^4$ m^3) rock falls and avalanches between 1963 and 1992, and noted that the events with significantly different volumes (orders of magnitude) were distinguishable in the seismic record, but events closer in size were not. He also found good correlation between seismic amplitude and slide volume of successive rock falls from the same sources areas and runout, a result confirmed by other (Dammeier, 2010; Dammeier et al., 2011) on rockslides in the central Alps.

Rock falls occurring at volcanoes have been frequently noted due to the existence of dense seismic networks and to the dynamic nature of volcanoes that triggers rock falls through surface topography changes, tremors, and degassing (Luckett et al., 2002). An event at Mt. St. Helens was confirmed as an usually large rock fall that registered as a M3.1 earthquake and produced a significant air blast recorded on infrasound microphones. The seismic signature of such an event appears similar to a volcanic explosion, but visual reconnaissance confirmed it as a rock fall with no explosive (ballistic) component (Moran et al., 2008).

Rock falls and rockslides have been detected in several cases by strong motion seismic networks designed for earthquakes. In the French Alps, Deparis et al. (2008) studied 10 rock fall events that had been seismically detected by at least three stations in an attempt to evaluate the magnitude, identify seismic phases, and correlate with physical parameters. In the central Alps, a similar study was conducted on 20 rockslide events using different methods of analysis (Dammeier, 2010; Dammeier et al., 2011). McSaveney and Downes (2002) reviewed large rockslides in the New Zealand Alps and suggested that tsunami-causing landslides might be detected with existing seismic networks. The July 10, 1996 Happy Isles rock fall in Yosemite National Park was recorded by seismic stations as far as 200 km away and was, at the time, the largest vertical rock free-fall ever recorded. This rock fall occurred in two main impacts 13.6 seconds apart, registering as 2 earthquakes of magnitudes 1.5 and 2.1, respectively, and produced an airblast that knocked over 1000 trees (Wieczorek et al., 1999; Uhrhammer, 1996).

Special monitoring networks used to predict catastrophic failure of a specific rockslide have been installed at several sites, including the Åknes rockslide in Norway (Roth and Blikra, 2009), the Randa rockslide in Switzerland (Spillman et al., 2007), the Séchilienne rockslide in the French Alps (Helmstetter and Garambois, 2010; Lacroix and Helmstetter, 2011), and a limestone cliff in southeast France (Got et al., 2010). These research efforts monitor the background seismicity rate, assess the relationship of the seismic activity with rock falls and rockslide acceleration, and correlate with rainfall and other potential triggering phenomena. Localization is of special interest to researchers trying to define the active parts of rockslides and identify triggering mechanisms (LaCroix and Helmstetter, 2011). Rock falls, for example, are often used as a metric for forecasting when and where a much larger progressive rockslide is becoming active. Furthermore, the seismic signature from rock falls is characterized by multiple bursts (or sources), while a rockslide or talus slide has an emergent and constant energy release (Moore et al., 2007; Vilajosana et al., 2008; Helmstetter and Garambois, 2010).

The mechanics of triggering and failure of a rock fall can be different than a rockslide, and in some cases, rock falls are the primary hazard. Moore et al. (2007) monitored an alpine cirque with both seismic instruments and a human observer, finding good correlation between the seismic records and the observed rock falls. In Spain, researchers took advantage of an artificially triggered rock fall and instrumented the slope, finding that individual impacts were easily distinguished in the record and used polarization analysis to locate each impact (Vilajosana et al., 2008). Following the 1996 Happy Isles and the 1999 Glacier Point rock falls, there was an attempt to monitor rock fall in Yosemite Valley with seismic instruments. The results were inconclusive: there were no notable rock falls during that time period and no other signals that could be definitively related to rock falls, although the instruments were placed at the base of the cliff 650 meters below the rock fall release zone (Myers et al. 2000).

The detection of precursors for rock fall events requires recording of seismic events that are not caused by failures themselves. In order to study these phenomena, researchers in Normandy, France installed instruments on a chalk cliff within several meters of known source areas and observed precursory seismic activity up to 2 hours before cliff failure (Amitrano et al., 2005). Their instruments consisted of a geophone with range of 40 Hz to 1.5 kHz and an accelerometer in the 2 Hz to 10 kHz range, spaced 50 meters apart, although the detected failure was quite close (within 5m) of a sensor. They also developed a working hypothesis of the failure mechanism processes via decreasing spectral frequency patterns associated with seismic events progressing toward a rock fall (Senfaute et al., 2009). Researchers in Italy attempting to develop rock fall forecasting methods using AE/MS monitoring techniques used hydraulic jacks and hammers to induce fractures and seismic waves; thus far they have mixed results (Arosio et al., 2009).

2.3.1 Comparisons of seismic and physical parameters

Links between the seismic and physical parameters of a rockslide or rock fall are being made in order to study the mechanism of failure, in-progress falling dynamic, and to identify previously unknown events. For example, the different seismic phases (e.g. compressional (P) and shear (S) wave arrivals) can help to locate and determine the type of failure. Other parameters, such as peak ground acceleration and seismic moment are compared with physical parameters such as potential energy and runout.

Many researchers have difficulty in picking P and S first breaks associated with rock falls or rockslides due to heterogeneity of the talus and rockslide material, reporting emergent P-wave onsets and unreliable S-wave picks (Lacroix and Helmstetter, 2011; Spillman et al., 2007). Only Dammeier (2010, 2011) was able to reliably identify S-waves at most rockslides using polarization analysis. The difficulties with determining P-wave first breaks and lack of discernable S-waves in rockslides were the motivation behind developing alternative source localization methods (Lacroix and Helmstetter, 2011).

Significant Rayleigh and Love wave excitation has been reported in several studies, including the 1996 Happy Isles Rock fall (Uhrhammer, 1996; Wieczorek et al., 1999) and the 2006 Mt St. Helens rockslide (Moran et al., 2008), and several rockslides in the French Alps (Deparis, 2008); in contrast, Dammeier (2010, 2011) did not find strong Rayleigh wave excitation in rockslides in the central Alps.

Both studies in the European Alps linked seismic signal characteristics such as magnitude, significant duration, rise time, envelope area, and peak ground motion with known physical parameters such as potential energy, fall height, rock volume, and runout. In the French Alps, Deparis et al. (2008) found a rough correlation with seismic duration and rock fall runout, but reported poor correlations with other parameters. Dammeier (2010, 2011) found loglog attenuation behavior between many of the seismic characteristics and distance and correlations between seismic velocity envelope area and event volume and between seismic duration and potential energy.

Comparisons between rock fall potential energy and seismic energy were reported in three different studies using widely different methodologies. Deparis et al. (2008) took a two-step approach: first, they developed their own magnitude scale (M_{rf}) using multiple stations to define the decay in seismic amplitudes at distance for each of 10 rock falls in the central Alps; then they used Kanamori's (1977) equation relating radiated seismic energy and surface wave magnitude, and found that the radiated seismic energy was 10^{-3} to 10^{-6} less than the ratio in a typical earthquake. Dammeier (2010, 2011) did not attempt to relate absolute energy values or ratios, instead using peak ground velocity from a seismic velocity envelope (ePGV) at each distance to correlate with potential energy. Vilajosana et al. (2008) also used a seismic velocity envelope and corrected for distance using assumptions about ground density, an attenuation factor, and phase velocity picks, finding that potential energy was four times that of seismic energy.

2.4 Seismic Monitoring in Mining

Hard rock mining often occurs in environments with inherently unstable rock masses, thus, there are far more monitoring studies in mining than on rock falls or rockslides. Furthermore, many of the techniques for studying rock falls are rockslides were developed, in part, from mining engineering and thus, it is useful to review the state-of-the-art in mine monitoring.

The removal of the rock in a mine changes the *in-situ* stress conditions, leaving the mine prone to catastrophic failures. There are three main types of failures: rockbursts (called bumps in coal mines), i.e. sudden violent tension failures, roof falls, i.e. gradual failures of poorly-supported blocks of rock in low stress (shallow) mines, and slope failures in open-pit mines. Rockbursts, due to their sudden and violent nature, are the focus of most of the mine monitoring efforts. Mine monitoring takes many different forms; most frequently, displacement devices are placed in areas of low stability, and the level of standard practice reinforcements is meant to prevent all failures.

Acoustic emission/microseismic (AE/MS) techniques for monitoring the stability of rock masses were first developed in the 1930s (Obert and Duvall, 1942; Obert, 1977). The U.S. Bureau of mines took serious interest in these techniques in the late 1960s and 1970s and laid the groundwork for later studies (Blake & Leighton, 1970; Blake et al., 1974; Blake, 1978; Leighton, 1982). The early rock engineering research efforts in AE/MS application were aimed at monitoring and preventing (or predicting) catastrophic failures in underground mines. The critical question under study was whether such failures are precipitated by unusual behavior and whether such anomalies could be accurately located. Unusual behavior was generally defined as either an increase in the sheer number of events (Brady & Leighton, 1977), or an increase in the accumulated energy of all events (Blake, 1978), in the weeks, days, or hours before a hazardous failure.

A review of the state of the art by Blake (1984) identified only 10 rock bursts worldwide that had been successfully predicted (in time) despite automatic monitoring in mines since the 1970s. Furthermore, Blake concluded that readily distinguishable precursor phenomena were identified only 30% of the time prior to a rock burst, and 60% of diagnostic precursor patterns were not followed by a rockburst. Therefore, although historically microseismic monitoring appears to be often successful, it also seems to be unreliable (Langstaff, 1978; Gibbons, 1978).

Rockburst research studies have since become more specialized and utilize advanced sensor networks in order to map natural rock structures (such as fractures or joints), determine the in-situ state of stress before, during, and after mining operations, analyze sequences of activity before and after main shocks or failures, determine source mechanisms, and more accurately locate events (Archibald et al., 1990; Boler & Swanson, 1992; Calder et al.; 1990; Chavan et al., 1993; Ellenberger et al., 2001; Gale et al. 2001; Gibowicz, 1990; Hardy & Ersavci, 1990; Iannacchione et al., 2005 (a, b, c); Iannacchione et al., 2004; Li, 1989; Marcak, 1998; Neumann & Makauch, 1989; Rudajev, 1990; Swanson & Sines, 1991; Wong, 1992). Most modern mine monitoring systems are capable of recording and evaluating individual events for their time, location, and energy level (with limitations on accuracy and energy due to equipment sensitivity and/or background noise).

Roof falls are different from rockbursts because they occur under low stress conditions, are largely gravity driven, tend to be progressive (as opposed to catastrophic) in nature, and often fail on existing fracture planes (Iannacchione et al., 2005 a, b). Although the research on roof falls is more limited than rockbursts, it may be more applicable to rock falls than rockburst research since both rock falls and roof falls occur in low stress (surface or shallow mine) environments.

The state-of-the-art in roof fall monitoring does not employ acoustic emission monitoring in the vast majority of mines: instead, these techniques rely on convergence monitoring and observations. NIOSH has begun studying the applicability of AE to this problem and has determined that microseismic activity and convergence trend well with a failing roof. Mines are instrumented with both acoustic emission sensors and roof-to-fall convergence monitors. In one short-term time scale study, analysis of microseismic patterns were used for forecasting of imminent roof-falls and the results are promising: roof-falls were successfully predicted 73% of the time, 90% of the roof-falls had a warning time of > 1 minute, and 50% of warnings resulted in no (immediate) roof-fall (which might be due, in part, to the fact that mining operations were stopped which may have halted the failure) (Iannacchione et al., 2005 a). Furthermore, longer-term studies found that unstable areas were preceded by a buildup of microseismic activity that preceded any noticeable convergence for 1-3 days (although the actual failure occurred days, or even weeks later) (Iannacchione, 2004 a).

Direct rock slope monitoring methods are commonplace in mining where high rock walls in open pit mines often present significant challenges. Given the financial risk that a major failure entails, not even considering the potential for injury, the mining industry has been a leader in adopting new technologies. Research specific to rock slopes is far more limited than that of underground mine monitoring, but the mining research has set the framework for this type of application. AE/MS studies have been conducted in some open pit mines with success, but these may only have limited application to natural rock slopes (Hardy & Kimble, 1991; Shiotani, 1998).

Unfortunately, most data and analyses from mine monitoring remains undocumented in scientific literature because the mining industry is less concerned with actual predictions, and more concerned with identifying areas in need of reinforcement. A typical response to an increase in noise in a mine is to reinforce that area until noise levels drop, a tactic effective for improving safety and production in a working environment. The following sections contain a review of mine monitoring research efforts documented in scientific literature as pertaining to general underground mining, specifically roof falls, and also rock slopes in open pit mines.

2.5 Infrasound Monitoring of Natural Phenomena

Infrasound microphones are being used to monitor volcanic vents and eruptions in addition to more traditional seismic networks. Infrasound spectral energy appears to exceed the audible acoustic energy by several magnitudes, and the near infrasound band (1-20 Hz) appears to be the primary energy band for vent degassing (Johnson et al., 2004). These volcanic networks have also identified other infrasound sources in the form of nearby large waterfalls, which are continuous radiators, and thunder, which has a very broadband but short duration signal (Johnson et al., 2006).

Rock falls associated with volcanic activity have been observed to produce infrasound signals in both the higher frequency bands, which correspond to distinct impacts, as well as very low frequencies (~0.02 Hz), associated with the initial collapse and mass air movement (Moran et al., 2008). The signature, or coda, associated with a rock fall differs from that associated with eruptions, which allows rock falls to be identified even at noisy volcanoes (Johnson et al., 2011).

2.6 Seismology

The techniques of seismic monitoring and post-processing were developed on a large body of seismology research that began nearly a hundred years ago. Charles Richter's earthquake magnitude scale was a breakthrough that condensed the information contained in seismograms recorded by a Wood-Anderson seismometer (Anderson and Wood, 1925) into a coherent earthquake energy measurement (Richter, 1935). The extraction of information from the seismograms recorded while monitoring for rock fall is the main objective of this thesis, and thus, a brief introduction to the main concepts used for this research is included in the background.

The differentiation of an earthquake or other seismic event of interest such as a rock fall from the continuously recorded seismic record is a problem that exists for all networks worldwide. Most use a algorithm that measures a ratio of the short term average over the long term average of the time series or some function based on it (Ambuter and Solomon, 1974; Stevenson, 1976; Allen, 1978). The frequency range of interest of the rock fall should be understood in order to differentiate from other seismic sources. Filtering techniques and spectral analysis, using techniques such the Fourier or Hilbert transform can be used for this task (Bracewell, 1999; Morrison et al., 2004; Huang et al., 1999).

Seismic waves are an elastic strain response of the earth's crust to a physical stress such as an earthquake or a rock fall impact. Three main wave types that might expected for a rock fall are compressional (P), shear (S), and surface (Rayleigh) waves (Lay and Wallace, 1995; Aki and Richards, 2002). The P-wave particle motion is radial to the direction the wave is traveling; the S-wave particle motion is transverse; the Rayleigh wave has a retrograde looping particle motion traveling at the surface. The differences in particle motion, frequency, and velocity are used to identify the different phases. The distance to a seismic event is calculated primarily by taking advantage of the velocity difference between P and S waves, which results in increased wave separation with increasing distance. A network of stations can then triangulate the location of the seismic event, but even with just a single station, the P-wave polarities indicate the azimuth of the incoming wavefront. Automatic processing uses these basic concepts to locate earthquakes today using many different methods (for example Geiger, 1912; Lee and Lahr, 1972; Uhrhammer et al, 2001).

One of the main objectives in modern seismology is to identify the source mechanics. Many linear inversion methods have been developed to calculate the source parameters based on wave amplitudes and good earth models (for example, Stump and Johnson, 1977; Dziewonski et al., 1981; Jost and Hermann, 1989; Dreger and Helmberger, 1993; Dreger, 2003; Minson and Dreger, 2008). These methods can be difficult to apply without good geological models and are, in general, tuned for seismic events occurring at depth and traveling through many kilometers of crust before reaching seismic stations on the surface. The complex topography of Yosemite Valley, where the closest stations are located, and the fact that most rock falls are not detectable at distances greater than a few kilometers make it difficult to apply these methods. Alternate methods of have been developed based on the amplitudes of radiated seismic waves (Ebel and Bonjer, 1990; Nakamura et al., 1999; Pearce and Rogers, 1989; Pearce 1977) but structural heterogeneity can distort the amplitudes, and some of these methods are designed for teleseismic distances, which are too far for rock fall detection. Polarity of seismic phases can also resolve the source mechanism, although this method works best for double couple mechanisms (Reasenberg and Oppenheimer, 1985; Hardebeck and Shearer, 2002), which may not be the correct solution for a rock fall. Amplitude ratio comparisons may work for rock falls since they may remain less distorted by heterogeneity and do not always require double couple solutions (Julian & Foulger, 1996; Nakamura et al., 1999; Hardebeck and Shearer, 2003). Comparisons between the amplitude ratios of P, SH, and SV waves can be used to rule out double-couple (typical earthquake) solutions in geothermal areas (Julian & Foulger, 1996).

The are several different magnitude scales to assign the energy release of an earthquake based on the amplitude of a particular wavefront, but whenever possible, seismologists use the moment magnitude scale to relate the seismic moment, which is a function of fault area, rigidity, and displacement, to the radiated seismic energy (Hanks and Kanamori, 1979). The seismic moment is calculated using low frequency information but is difficult to assess accurately for smaller events, such as rock falls. The seismic coda provides another method of assessing energy in scattered waveforms (Baltay et al., 2010). Rock fall potential energy can be assessed if the fall height and mass of the rock, but it is unknown how much of that energy is radiated seismically. The ratio of radiated seismic energy to earthquake energy is small, on the order of 10^{-5} (Kanamori and Anderson, 1975; Kanamori, 1977; Vassilou and Kanamori, 1982). The complex envelope of a seismic signal may be a better representation of radiated seismic energy for a rock fall than a calculation of magnitude (Farnbach, 1975).

2.7 Summary

The research presented in this thesis would not be possible without an enormous body of knowledge that came before. The preceding paragraphs touch upon some basic concepts used widely as well as research efforts that are closely related to this dissertation. As seismic monitoring efforts increase and ideas in rock fall analysis progress, additional bodies of research will become relevant.

3 Data Collection Methods

The objective of the project was to test the feasibility of seismic monitoring for the purpose of rock fall detection (Phase 1), and if successful, then install a network of sensors intended to monitor rock falls (Phase 2). The project was permitted (by the National Park Service) to run during the winter months at limited sites on cliffs in the wilderness, defined as any site located > 200 feet above the Yosemite Valley floor, when visitor impact and interference was minimal.

3.1 Site Selection

The ideal site for this project is one that is potentially active during winter, has accessibility to source areas without requiring climbing equipment, and can be approached during the winter months with minimal exposure to avalanches, icefall, and rock fall. The original intent was to place instruments as close as possible to a rock fall source area in the hope of capturing acoustic emissions associated with rock fracture and using high frequency (> 1 kHz) instrumentation. However, most source areas are several hundred meters high on rock faces and require roped climbing to access. Furthermore, many source areas are hundreds of meters across, meaning that even if an instrument is installed, it may still be hundreds of meters away from any rocks that happen to fracture or fall, if any at all. Most of the south side (north-facing) cliffs in Yosemite Valley are completely inaccessible during the winter months due snow and ice avalanches that roar down on a daily basis, ruling out locations such as Glacier Point, which has been the location of many notable rock falls and an area with a high risk due to park infrastructure, including overnight facilities for tourists and housing for employees. Cliffs on the north side (south-facing) may be inaccessible for over two weeks in winter for the same reason, but are far safer in winter due to rapid melting of snow and ice, preventing accumulation. Finally, any instrument installed in an area with difficult access should not need regular maintenance: it needs to have ample backup power and send data wirelessly to a base station on a regular basis. Installing large solar panels, battery banks, and antennas on the side of a sheer cliff is not only difficult, it is not permitted in a National Park for aesthetic reasons.

The Middle Brother rock formation (Figure 4) was selected for monitoring in large part to accommodate the attempt to place instruments as close as possible to a rock fall source area. There are three major rock fall source areas: "A", the westernmost and largest with a rough diameter of 300m, "B", and "C", of a diameter of 100 m, all of which happened to be active while instruments were in place. Middle Brother has a prominent ledge system (Michael's Ledge), which passes just below source area "A" and just above "B" and "C", theoretically allowing access to all three areas. However, in practicality, the part of the ledge that passes below source area "A" requires several hundred meters of roped traversing, and is exposed to very small rock fall on a (probably) daily basis. Therefore, the risk of traversing that part of the ledge every two weeks during winter was not worth the small benefit of installing an instrument nearer to a source area that may or may not be active, and may still be more than hundred meters away even if it is active. The rest of the ledge, however, can be safely accessed without ropes which still allows instruments to be placed high on a cliff.

Figure 4. Middle Brother, showing locations of significant rock falls and seismic stations (red triangles).

The Middle Brother formation also has a very-active freeze-thaw cycle, which is a strong potential rock fall trigger. A significant amount of ice and snow builds up during a storm cycle and melts out rapidly (within one week following a storm) under a warm sun on the exposed southeast-facing ledges. The warming of the cliff also means that this site is a reasonably safe place to work during winter, as it is not exposed to avalanches and icefall after drying. Historically, Middle Brother has been active in winter, including a series of rock falls in March 1987 that cumulated in the largest recorded rock fall in historic times in Yosemite Valley. Middle Brother is located on the north side of Yosemite Valley (Figure 5).

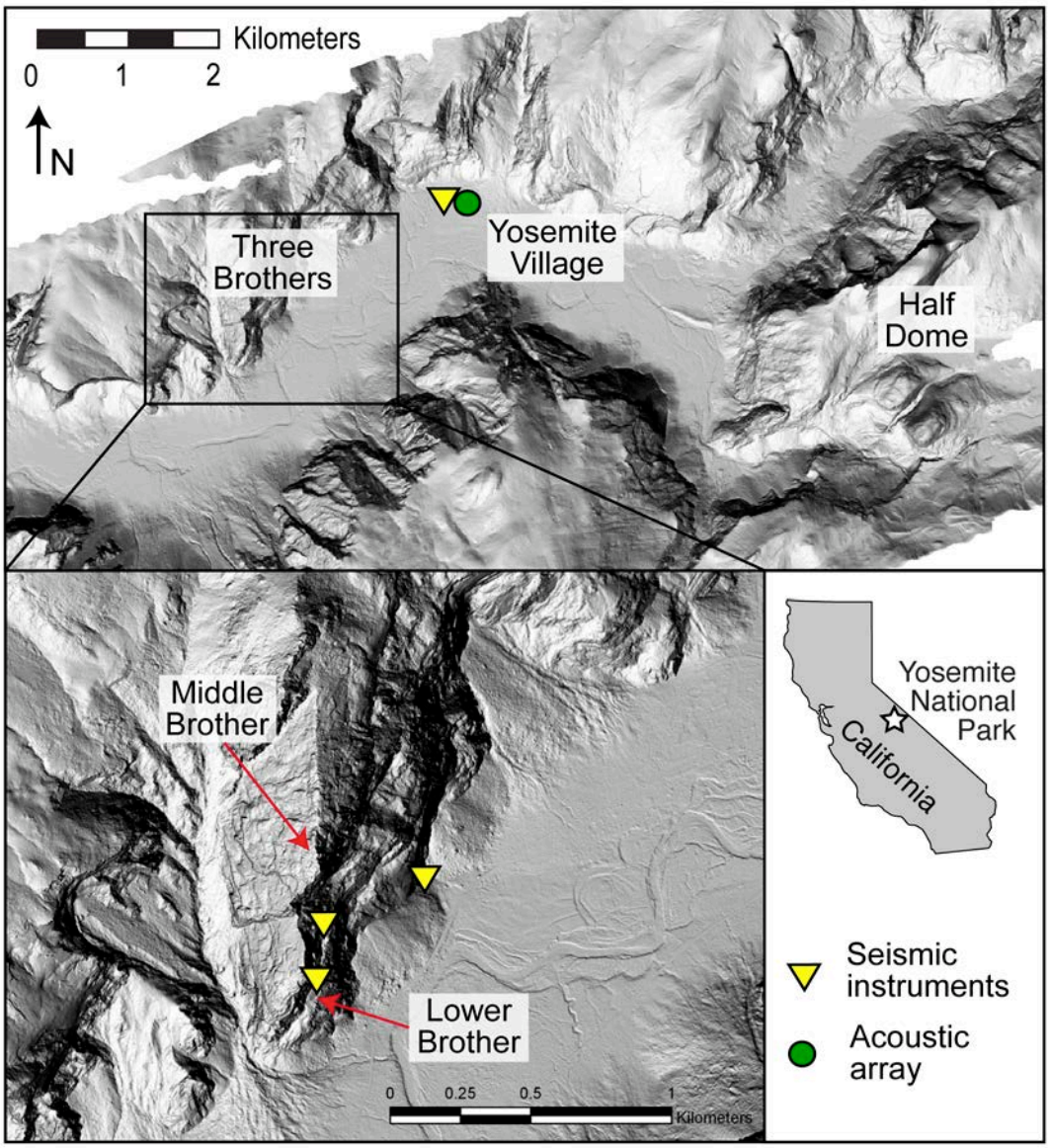

Figure 5. Location of Middle Brother and instruments.

3.2 Instrumentation

The selection of instruments for this project was a process that balanced ideal instrumentation configurations with practical options. The first step in designing an instrumentation scheme is to focus on the sensors required for capturing the signal of interest, in this case, anything related to rock falls. Rock fall signals are thought to come from two main sources: fracturing (e.g. initiation), and impacts. Large impacts have been picked up by strong motion seismic stations in Yosemite National Park and worldwide (Uhrhammer, 1996; Wieczorek et al., 1999; Deparis et al., 2008; Dammeier, 2010), thus, should be recordable by standard strong motion seismic equipment.

The fracturing signal of the rock prior to a rock fall is of great interest to this research, should it exist. Rock fracturing has been recorded by microseismic sensors in the laboratory, in underground mining, and at a chalk cliff in France (Amitrano et al., 2005), and is frequently referred to as microseismic or acoustic emission (AE/MS). The frequency sensitivity range is variable for AE/MS studies, but ranges from tens of Hz to MHz, at a range of 250 m to just a few centimeters (respectively). The frequency of any given seismic signal is a function of the source function and the attenuation characteristics due to distance and rock type. Thus, picking up any microseismic signal requires proximity to the source, even in granitic rock with good seismic transmission characteristics.

The source areas in Yosemite National Park are not only numerous, but they can be many hundreds of meters wide on cliffs that tower over 1000 m tall. Even targeting specific source areas can result in sensor placement well over 100 m from the source in a rugged terrain. Thus, it is unlikely that high frequency microseismic signals would propagate far enough to be picked up by any sensors that could be practically installed on Yosemite's cliff faces.

The use of wireless motes was considered as a platform for sensor placement. Wireless sensor networks offer a number of advantages; they are small, discreet, power-efficient, and communicate remotely, and thus could be placed in many difficult to reach places for long periods of time. However, continuous seismic recording, even at relatively low sampling rates for microseismic (e.g. 100 Hz) requires very high amounts of onboard data storage capacity, high amounts of power and, most important, bandwidth that would exceed the capacity of any modern network. It might be possible to collect only triggered data, which would solve the data storage and bandwidth problems, but the system still requires extra power (at rugged, near-vertical cliffs where solar panels would be difficult to install, possibly in shade, or not allowed for aesthetic reasons) and a prior knowledge of the seismic characteristics pertaining to events of interest. Future projects may take advantage of the results of this study to design such a triggering algorithm for rock fall monitoring, but at the time of this project, there were no appropriate wireless sensor network seismic monitoring prototypes.

Thus, the best choice, given the practical limitations and scientific objectives, was to use field-tested standard seismic equipment at as high a sampling rate as possible and place it as close to rock fall source areas as possible while still being accessible for the duration of the field installation.

3.2.1 Dataloggers (and GPS)

Reftek RT130 dataloggers (Figure 6) were used at all stations for the duration of the project. The RT130 is a 3 or 6-channel 24-bit analog to digital convertor (ADC) capable of recording data up to 1000 samples-per-second (sps). Data storage is through two compact flash (CF) cards; the manufacturer sells and recommends 2 or 4 GB cards, but 8 GB generic CF cards also worked. The RT130 consumes little power (1-2 watts), and is enclosed in a ruggedized plastic case that is nearly waterproof. Serial and ethernet ports are available for data communications, but were not used except for monitoring the state of health of the unit and when downloading data manually. A Global Positioning System (GPS) attached externally to the unit updated the internal clock regularly.

Figure 6. Reftek RT130 datalogger with instruments attached.

3.2.2 Seismic Sensors

Both accelerometers and geophones were tested and installed as part of this project. Two accelerometers, a Reftek RT131A 02/03 and a Terratech SSA-320, were available, compatible with the datalogger, and enclosed in ruggedized, weather-resistant cases. The Reftek RT131A 02/03 is a MEMS force-balance accelerometer with DC - 500 Hz frequency response. This instrument was used during Phase 1 at Michael's Ledge and moved to station GH08 in Yosemite Valley during Phase 2. The Terratech SSA-320 accelerometer has a frequency response of DC - 50Hz with a 120 dB of dynamic range. This instrument was affixed vertically to the cliff during Phase 2. The geophones used were one triaxial SM-6 8 Hz geophone in Phase 1 and five triaxial L-28 4.5 Hz geophones during Phase 2 (Figure 7). The instruments were installed with minimal protection from the elements during Phase 1, and under sandbags during Phase 2, except for the geophone at LB05, which was placed in the same position and under the same minimal protection as the Phase 1 geophone, for consistency.

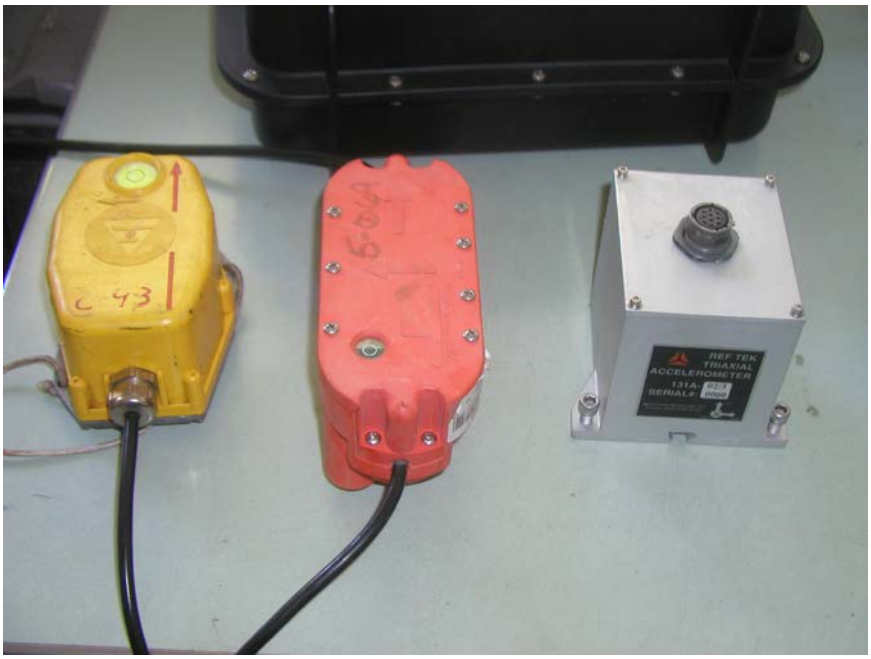

Figure 7. Triaxial geophones (yellow 8 Hz SM-6 and orange 4.5 Hz L-28) and RT131A-02/03 accelerometer.

3.2.3 Barometric Microphones

Three barometric microphones packaged by the Volcano Infrasound Group at New Mexico Tech were borrowed for feasibility testing during Phase 2. These microphones have been used successfully in conjunction with seismic sensors at several volcanoes. The microphones sensor is a differential pressure transducer that has a response from 0.02 Hz to frequencies > 20 Hz (unspecified). There is an optional 22.9 Hz low pass filter built-in, which may have been used with some of the microphones for part of the project. These microphones are enclosed in a weatherproof box and are designed to work with an RT130 datalogger.

3.2.4 Power

The power system requirements for the installation were one to two weeks of backup power and an appropriately sized solar panel to recharge the batteries during sunny periods. The system was also designed to be as small and light as possible such that it would be possible to carry equipment up the cliffs and also to be discreet, in accordance with National Park Service aesthetics. Thus, the selection of battery and solar panel size was conducted with these conditions in mind.

The power requirement of the RT130 datalogger was assumed to be 3 watts using a 12-volt supply, which translates into a consumption of 6 amp-hours per day (Ah/day). True deep cycle batteries are typically discharged to about 80% over time without damage, although the hybrid dual-cycle (marine) batteries used for this project typically perform less well ((http://www.windsun.com/Batteries/Battery_FAQ.htm 07/20/2011 15:48). Thus, a 75 Ah battery (the heaviest battery that can be carried up the ledge weighing ~ 55 lbs.) can be expected to last about ten days with no recharge.

The size of the solar panel selected must account for the typical insolation of a Yosemite winter while providing at least 6 Ah-day of recharge power to the battery. Winter insolation in Yosemite National Park is approximately 4 hours per day (http://rredc.nrel.gov/solar/old_data/nsrdb/redbook/atlas/ 07/20/2011 15:50), which means that 1 m^2 of ground receives 4 kW of sunlight per day, on average. Assuming typical values for efficiency (10%), losses (20%) and peak power point (17 V) results in a minimum requirement of a 30-watt solar panel. Thus, all stations were equipped with at least 75 Ah of battery power and one 30-watt solar panel except in Yosemite Valley, where line power was available. The power system worked as expected, only failing after storm cycles lasting more than one week when stations were inaccessible and covered with snow for an extended period of time (Figure 8). Solar panels and stations were dug out after storm cycles on more than one occasion (Figure 9).

Figure 8. Solar panel exposure on cliff ledge at station LB01.

Figure 9. Digging out the station after a snowstorm.

3.2.5 Communications

Data was collected manually rather than wirelessly for the duration of the project despite the RT130's onboard ethernet capability, due to technical reasons. First, the amount of data collected in a continuous 500-1000 sps mode is large enough to overwhelm most modern cellular phone and wireless mote networks. Second, while cellular phone service is available at most of the remote field sites, there was no cellular data service in Yosemite Valley. Internet WIFI routers, which require extra power, a larger antenna, and a base station in the valley, were also considered. However, there are no facilities within sight of most of the stations, and antennas were not allowed for aesthetic reasons within the national park, so this plan was abandoned.

Although remote data downloading capability was not installed, an ARGOS satellite was linked to some of the stations during the second phase and allowed remote monitoring of the health of the stations via webpage (http://www.passcal.nmt.edu/~argos2/), thus reducing the number of site visits.

3.3 Field Data Collection: Phase 1

The first phase occurred from December 11, 2007 to April 24, 2008 and was designed to test the feasibility of installing a seismic network for the purpose of rock fall monitoring on the side of a cliff in Yosemite Valley. A single station (LB01) consisting of an SM-6 triaxial geophone and an RT131A-2/3 triaxial accelerometer attached to a 6-channel RT130 datalogger was installed on Michael's Ledge at a location shown in Figure 4 and Figure 10. This location (Table 1) is at an elevation of 1480 m and approximately 270 m above the floor of Yosemite Valley, with east/southeast exposure. The geophone is located a few meters east of the datalogger on a small ledge (Figure 11) and the accelerometer a few meters west, also on a small ledge (Figure 12). Although the instruments were located in two different locations approximately 10 meters apart, they are still very close to one another and the characteristics of the two locations are similar in that they are sitting on the same major ledge and exposed to the same environmental conditions. Remarkably, this station was in operation for all but two days and a few hours in January, during a storm cycle, and a five-day period in May when the solar power system charge controller malfunctioned.

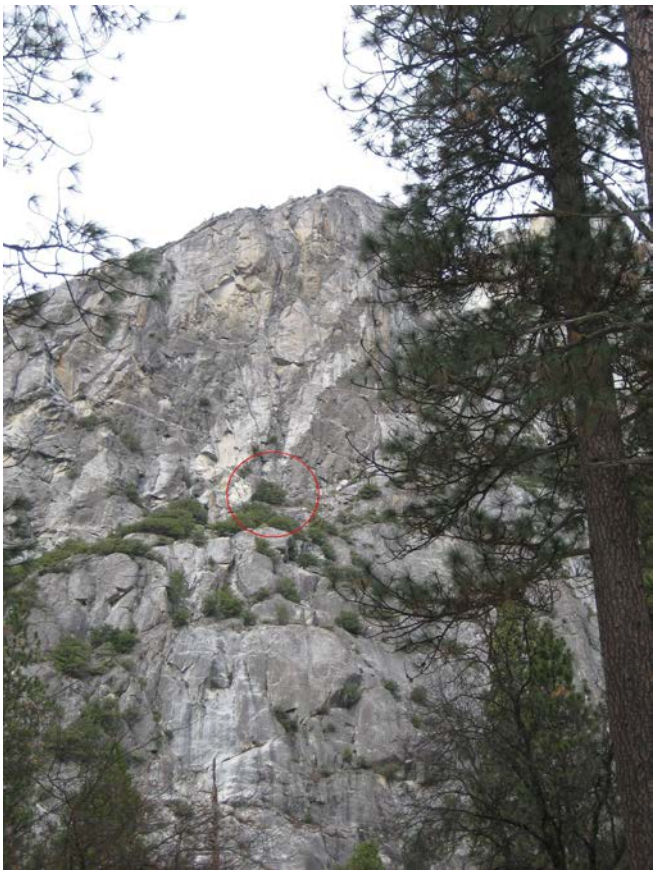

Figure 10. Michael's Ledge area and the location of LB01, LB03, and LB05 circled in red, at an elevation of ~270 m above the valley floor.

Table 1. Station coordinates.

	UTM coordinates			Error in Coordinates		
STATIONS	**Northing (m)**	**Easting (m)**	**Elev (m)**	**N**	**E**	**Z**
LB01, LB03, LB05	4179587	269645	1484	4	6	6.5
MB04, MB06	4179828	269715	1626	7	2	4
MB02, MB07	4180032	270062	1250	15	15	21
GH08	4181115	271728	1215	15	15	15

Figure 11. LB01 (Phase 1) SM-6 geophone on a small ledge 270 m above the valley floor later covered in a pile of rocks. The L-28 geophone at station LB05 was installed during Phase 2 at this same location and under the same conditions.

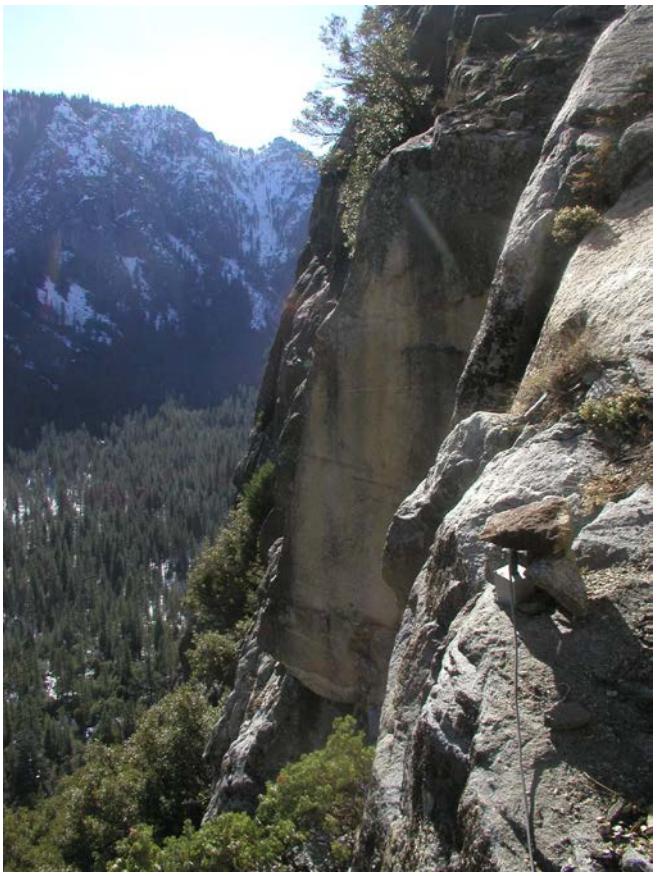

Figure 12. LB01 (Phase 1) RT131A/B accelerometer on a small ledge 270 m above the valley floor.

3.4 Field Data Collection: Phase 2

The success of the first phase led to the installation of a network of sensors from October 24, 2008 to June 18, 2009. Two geophones (stations LB03 and LB05) were installed at the same location as the Phase 1 station LB01 (Figure 4 and Figure 10) at an elevation of 1484 m (270 m above the valley floor). An L-28 geophone (station MB06) and a Terratech SSA-30 (station MB04) accelerometer, mounted to the cliff wall vertically under an overhang, were installed 250 m farther east and 140 m higher (410 m above the valley floor) on Michael's Ledge (Figure 4 and Figure 13). Two L-28 geophones were installed at the base of Middle Brother (stations MB02 and MB07) to the 400 m and 610 m east of the MB04/6 and LB03/5 stations, respectively (Figure 4 and Figure 14) at an elevation of 1250 m between two prominent talus piles. Infrasound microphones were installed for a short period of time on exposed ledges below the large Middle Brother rock fall source area, but were removed due to harsh conditions. The three infrasound microphones were relocated to a site in Yosemite Village 2.5 km to the east (GH08) and installed along with an RT131A-02/03 accelerometer, which was later replaced with an L-28 geophone. All station locations can be found in Table 1, and the relative infrasound microphone locations are in Table 2. Not all stations were in operation at all times; the installation and removal occurred in stages and there were station and power outages during periods of extended storms and snowfall. There were also a few instrument malfunctions and periods of poor quality data that was not used for analysis. A full time accounting can be found in the Appendix A station operation log.

Figure 13. Stations MB04 and MB06 were placed as high on Michael's Ledge as possible with using climbing ropes, 410 m above the valley floor and at an elevation of 1626 m.

Figure 14. Stations MB02 and MB07 were placed to the right (east) of the prominent talus pile below Middle Brother, behind these trees against the rock wall.

Table 2. Infrasound microphone relative locations at GH08.

Mic - Mic	Distance (m)	Azimuth
1-2	24.7	275
2-3	13.4	146
1-3	15.4	230

3.5 Data Archiving

The data were collected from the field, converted into miniSEED format, and archived with the IRIS Data Management Center under the network code "X7" from 2007-2009. Data can be accessed and download online at http://www.iris.edu/dms/dmc/. MiniSEED is a data-only version of SEED (Standard for the Exchange of Earthquake Data); the metadata is stored in an Antelope database and associated with the appropriate miniSEED files.

3.6 Lessons Learned and Problems Solved from Field Work

The field installation provided an excellent test for the design and installation of future networks with the goal of studying rock fall. In this case, at Yosemite National Park, technical issues limited wireless communication since there was no cellular phone data coverage, and large amounts of data were generated during continuous recording at 500 or 1000 sps). Aesthetics limited electrical power generation since, in a National Park, large mounted solar arrays and antennas are considered to be an eyesore and were not permitted. Nevertheless, a large amount of data was collected during harsh weather conditions with few serious problems, although frequent site visits were required to check on the instruments, download data, shovel snow, and perform maintenance.

The Reftek RT-130 dataloggers proved to be remarkably robust under harsh conditions such as cold and snowy storms, melting snow, heavy rain, and hot sun. The dataloggers were placed in water-resistant but not waterproof boxes and river drybags (Figure 15 and Figure 16), and experienced little to no problems due to environmental conditions, even when water was found inside the box or bag with the datalogger. The RT130 dataloggers are designed to operate in continuous mode from 1 to 1000 samples per second sampling rate. Our experience with the RT130 dataloggers suggests that the maximum data throughput of the instrument is very near the 1000 sps rate when run in the 3 and 6-channel modes, and that lower sampling rates resulted in a significant reduction in data gaps and glitches. There were a few minor glitches with the RT-130: one PASSCAL datalogger stopped working for unknown reasons and was replaced, and there were a few timing errors when GPS units malfunctioned, but overall the dataloggers performed well.

Figure 15. River drybag used to protect RT130 datalogger.

Figure 16. Box used to contain most of the instrumentation at stations in the valley.

The geophones performed significantly better than the accelerometers, and would be preferred in the future, with corner frequencies of 4.5 Hz or lower. The 1000 samples per second recording rate is higher than necessary for recording rock fall events; 100 sps is the highest frequency necessary to detect all rock falls, and has the added benefit of increasing the length of time the instrument can record data without running out of storage space. Reftek RT130 dataloggers proved to be robust and reliable in the field, but recording at sampling rates higher than 500 sps pushes the capacity of the datalogger, is likely to result in data errors, and is not recommended. The infrasound microphones performed well, and are useful in detecting mass air movements (airblasts) not seen on seismic records.

The solar and battery configuration had a minimally acceptable capacity and robustness for a remote winter installation, although they were more than adequate for spring conditions. It is recommended that additional batteries be installed when feasible and that solar panels be mounted off the ground to prevent snow from building up on top, if allowed.

4 Data Processing: Searching for Events with Triggering Algorithm

In order to identify rock fall seismic records, the collected data must be sifted through. The sheer volume of data precludes careful, manual review. Thus the data is sifted automatically using processing techniques and algorithms designed to select events with certain characteristics for further review. A triggering algorithm is the search engine that helps to identify these events. A simple example of a triggering algorithm is one that selects any datum above a certain threshold as a trigger and stores the timing of that datum so that it may be reviewed later. The implementation of an effective triggering algorithm requires knowing the characteristics of typical noise, characteristics of events of interest, and the instrument response to these phenomena. Before triggers can be selected, the data should be filtered and normalized in order to consistently find events of interest while avoiding false triggers. Thus, the process of running a triggering algorithm usually involves filtering of the data in the band of interest, removing static offsets, and normalizing the data so that the sensitivity of the algorithm is consistent.

4.1 STA/LTA triggering algorithm and data preparation

The triggering algorithm chosen for this project is a Short-Term Average over Long-Term Average (STA/LTA) ratio trigger. The use of such ratio eliminates the need for absolute data values and thus, in theory, can be used for a variety of sensors, noise levels, and scientific units. In strong motion seismic applications an STA/LTA algorithm is used primarily to determine accurate start times of seismic signals in order to determine event location. For this project, the STA/LTA algorithm was used to filter out non-rock fall seismic events (such as wind and rain noise) and the triggers were then carefully reviewed to identify those that were potentially related to rock falls. Therefore, parameters different than those in strong motion seismic applications were used, such as longer windows in order to eliminate additional transient signals and speed up processing times.

Before a triggering algorithm can be run, the data should first be filtered to enhance signals of interest and eliminate noise, and then normalized to get consistent STA/LTA ratios. Rock falls usually respond strongly in frequencies ranging from a few Hz (and limited by the geophone corner frequency) to about 15-20 Hz, as determined by reviewing known rock fall signals. Low pass filtering can eliminate most noise from rain (>100 Hz) and wind (several resonant bands, most >20 Hz). High pass filtering is important to remove long period (daily) instrument drift (Figure 17), which poses problems since it shifts both short term and long term averages, thereby changing the ratio. Any ratio shift causes the algorithm to record either fewer triggers (insensitive) or an overabundance of false triggers (oversensitive). Therefore, bandpass filtering the data between 1 and 20 Hz helps to eliminate both long period drift and weather-related noise, while still retaining the frequency band in which most rock falls are strongly recorded. The data were also re-sampled to 25 samples-per-second (sps) to reduce the file size and speed up processing time.

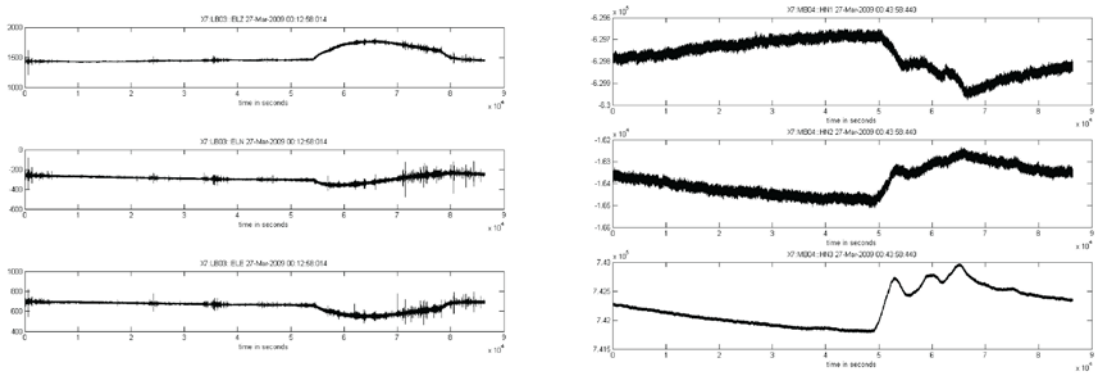

Figure 17. Geophone long period drift at LB03 on March 27, 2009 (left), accelerometer long period drift at MB04 on March 27, 2009 (right).

After filtering, the data were normalized to ensure that the sensitivity of the algorithm at different stations is as consistent as possible. Without normalization, the STA/LTA ratio is highly sensitive to the mean value of the data. Mean removal renders the LTA to near zero and makes the algorithm oversensitive, but simply adding a static offset instead can result in highly variable sensitivities depending on the units and starting mean value. Traditional normalization divides the data by a maximum value, but this can cause sensitivity problems if there are transient spikes. Thus, the objective is to apply a data processing technique that works similarly on all data, regardless of initial mean value, scientific units, type of sensor, or presence of transient spikes in order to produce a relatively consistent sensitivity to unusual events.

The technique devised to normalize all of the data in this study consisted of the following steps. First, the mean was removed. Next, each datum of the mean-removed data was replaced by its absolute value so that all points were between zero and the maximum absolute value. The LTA of this new data was equal to the new mean (approximately 0.7 standard deviations of the original data) with event signals located primarily above the mean, and therefore the LTA. Finally, the act of dividing the STA by the LTA effectively normalized the data and rendered it unitless. An STA/LTA ratio of less than one represents signals that are less energetic than 0.7 standard deviations of the original signal, while a ratio of two represents signals that are 1.4 standard deviations above the original signal.

4.1.1 STA/LTA Triggering Parameters

The time length of the short term (STA) and long term (LTA) averaging windows, the designated triggering ratio, and the window overlap are all parameters that must be chosen for the triggering algorithm. The values of these parameters are determined by the noise and target event characteristics such as duration, dominant spectral frequency, and waveform character.

The LTA window needs to be long enough to represent an average background noise level and be relatively uninfluenced by the onset of a event signal, but not so long as to slow down processing time or be influenced by longer-term noise level drift. The length of the STA window must at minimum capture a few periods of the target signal of interest and be shorter than the duration of the shortest target events so that these events are not lost in the averaging. When possible, the STA window should be longer than short duration noise events (e.g. rain) so that averaging obscures these events. The triggering ratio controls the sensitivity of the algorithm: too low and there will be an overabundance of noise triggers and too high it may not capture events of interest. Window overlap helps to find smaller events that may be obscured by averaging if split into two adjacent windows.

Typically, the duration of a rock fall ranges from a few seconds to over a minute, with the highest spectral energy happening in short bursts. The rock fall response can be very broadband in energetic bursts at close range. At a distance of a few kilometers, most of the energy centers around 8 Hz (0.125 seconds), in our experience. In contrast, the duration of a raindrop is less than 0.1 second. Thus, an STA window of one second will capture eight cycles of a rock fall signal and be too long to trigger on most raindrops. The LTA window was set to 100 seconds, which is longer than a typical rock fall to ensure that the onset of a rock fall signal does not overly influence the value of the LTA. Two windows were selected to overlap each data point, so that short, weaker events are more likely to be captured while only slowing down the processing by a factor of two. After some trial and error, it was determined that a triggering ratio of three, or approximately 2 standard deviation above normal noise levels, was adequate to detect rock falls while remaining relatively insensitive to normal levels of noise.

The filtering and normalization techniques and triggering algorithm parameters were tested on a small data set to confirm that they were successfully picking out earthquakes and known rock fall events at different stations. Stations that did not trigger on known events were reviewed manually, and it was confirmed that there was no distinct seismic signals associated with that event. Figure 18 shows filtered signal (top) and the calculated STA/LTA ratio after normalization (bottom) and triggers (red stars) for an entire day.

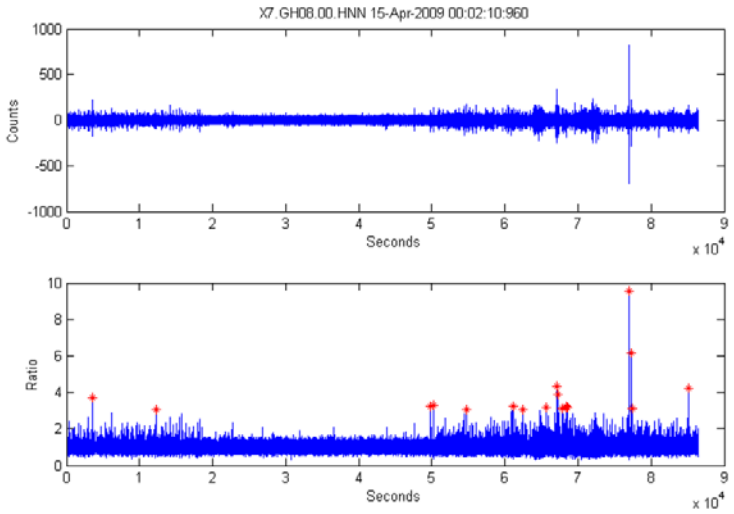

Figure 18. One day of filtered 1-20 Hz accelerometer data (top) and calculated STA/LTA ratio after normalization (bottom) and triggers (red stars).

4.1.2 Special Case: Deliberately Aliased Data

There was one confirmed case of a small local rock fall and an accelerometer located at a distance of 600 meters where the accelerometer failed to trigger. However, it should be noted, the geophone triggered normally. The spectral record clearly shows a record of the rock fall in from 20 to 150 Hz, with the highest spectral energy at ~70 Hz. Filtering from 1-20 Hz removes the rock falls signal, but filtering in a higher band means that the data cannot be re-sampled at 25 sps before running the algorithm. Thus, while the higher frequency filtering and analysis works, it takes four to eight times as long, which is a significant amount of time when reviewing months of continuous data. Instead, an alternate technique was devised and tested which consisted of filtering the data in the band of interest (e.g. 20-150 Hz) and then deliberately aliasing it by under-sampling at 50 sps, thus reducing the file size by a factor of 20. This technique successfully triggers on the confirmed rock fall event at stations that previously did not record a trigger using a shorter STA window (0.5 seconds) and a lower triggering ratio (2). However, after testing this technique and these parameter settings on a sample dataset during periods of wind and rain, it was found to be overly sensitive to environmental noise, triggering ten times as often. This method was abandoned due to the high number of false triggers and the fact that the geophones triggered using the original filtering, normalization, and triggering algorithm parameters, thus detecting this event.

4.2 Identifying Potential Rock Falls from Recorded Triggers

The data processing techniques and triggering algorithm were applied to the entire dataset encompassing nearly a year's worth of data at up to six stations each with three components. Overall, a total of ~500,000 triggers were recorded, far more than could be reviewed individually. Thus, the first step in reviewing the triggers is to eliminate as many as possible from consideration and identify triggers with high probability of being associated with a real event. Trigger elimination and identification occurred in four major steps: 1 – removal of triggers due to transient spike instrumentation noise, 2 – identification of triggers occurring on all three (N, E, Z) components, at multiple stations, and/or multiple wide-network locations as having a high probability of being real, 3 – removal of remaining triggers associated with known regional earthquakes, and 4 – ignoring triggers recorded by a low number and/or low percentage of operating stations. These steps are described in detail in the following sections.

The terminology used for describing the triggers is as follows: a station trigger is a triggered event detected by all three of the station's components, unless otherwise noted. A network trigger is a trigger detected at two or more stations. A wide-network trigger is a trigger detected at two or more locations. Some stations were co-located and thus, a trigger detected only at two co-located stations is not a wide-network trigger.

4.2.1 Transient Spike Instrument Noise Removal

The removal of triggers due to instrument noise (e.g. transient spikes) is a logical first step since they can be identified by direct inspection of the timing of the triggers on a single channel. Instrument noise primarily occurs during starting and stopping of the datalogger (e.g. when experiencing power problems during a storm period) and when the on-board memory cache is overwhelmed at high sampling rates (e.g. 500 or 1000 sps).

Transient spike triggers due to power problems are primarily diagnosed by noting the timing of a particular trigger: if it occurs at the beginning of a new data file and the timing of the data files is irregular, the instrument has most likely been restarted due to power issues and thus, that trigger can be ignored. Since triggers of this type occur only at a single datalogger, they are already screened out if only network triggers are being considered for further review, which is the case for all Phase 2 data. However, during Phase 1, both of the instruments are attached to a single datalogger and considered to be a pseudo two-station network. Thus, these transient spikes appear on the data records for both and populate the list of network triggers. During Phase 1, 121 network triggers were recorded, and 91 of them have been attributed to power problem instrument noise (Table 3).

Table 3. Total numbers of triggers during Phase 1; 121

Station	LB01	LB01	LB01	Triggers
Sensor	Accelerometer	Geophone	Both	121
Z / 1	838	1856	Transient Spike Noise	91
N / 2	344	1887	Earthquakes	1
E / 3	340	1504	MB RF	3
All 3	178	713		

Memory cache problems manifest as regularly spaced transient noise spikes, repeating approximately every 200 seconds (Figure 19 to Figure 21). Repeating triggers with spacing greater than 180 seconds are identified and eliminated using a filtering algorithm. The filter was imperfect, leaving some false triggers in the record, but reasonably effective at removing transient spike triggers. Examples of the eliminated triggers (red stars) and the kept triggers (green stars) are shown in Figure 19 to Figure 21. Stations MB07, LB03, and GH08 experienced severe levels of repeating transient spike noise which caused thousands of false triggers, as shown by comparing total numbers of triggers before and after removing instrument noise (Table 4). Transient spikes account for (at least) 13%, 20%, 64%, and 46% of the original station triggers at stations LB03, MB02, MB07, and GH08 (accelerometer), respectively. The total number of network triggers before filtering for transient spikes is 5788, and after filtering it is reduced by 7% to 5382.

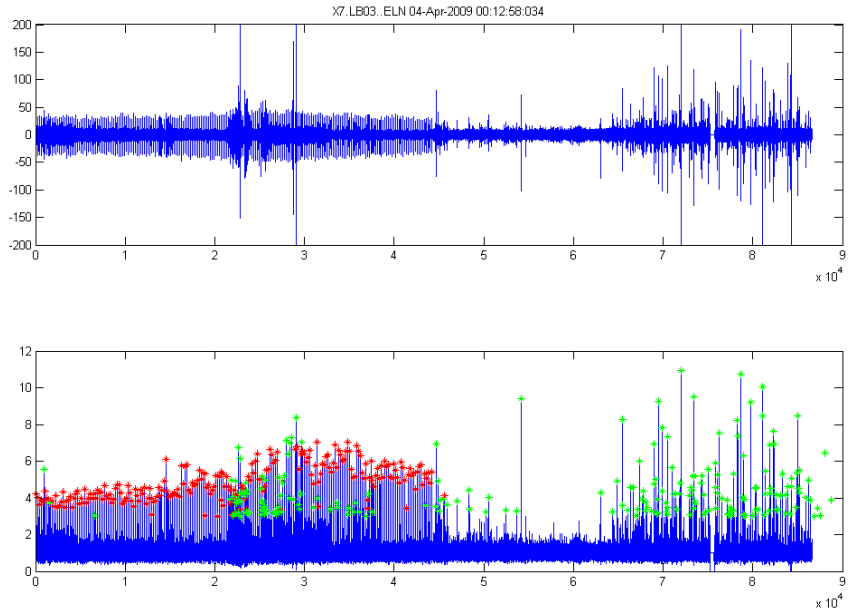

Figure 19. LB03 ELN showing transient spike noise for a one-day period. Filtered record between 1 and 20 Hz (top); the STA/LTA ratio (bottom) and triggers (stars). An algorithm was run to eliminate triggers related to instrumentation noise: eliminated triggers are shown as red stars, and kept triggers shown as green stars.

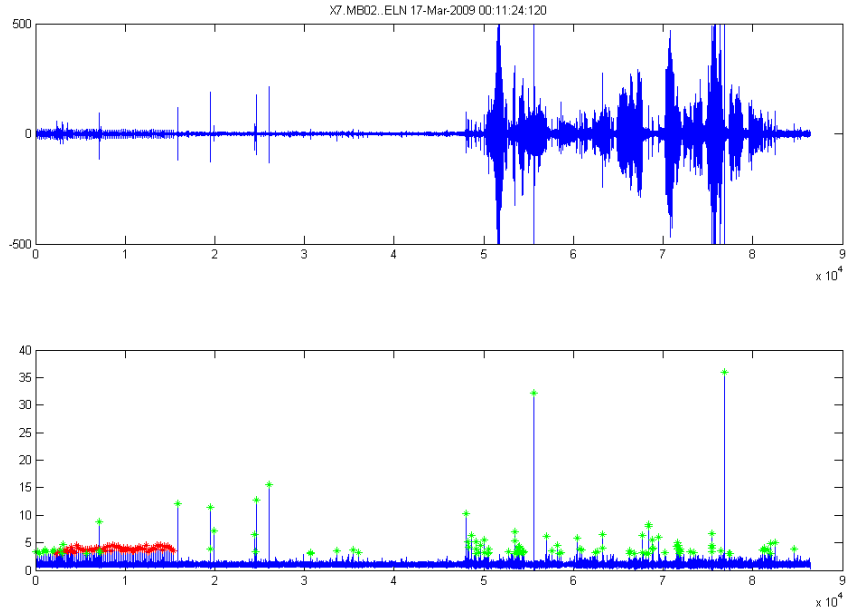

Figure 20. MB02 ELN showing transient spike noise for a one-day period. Filtered record between 1 and 20 Hz (top); the STA/LTA ratio (bottom) and triggers (stars). An algorithm was run to eliminate triggers related to instrumentation noise: eliminated triggers are shown as red stars, and kept triggers shown as green stars.

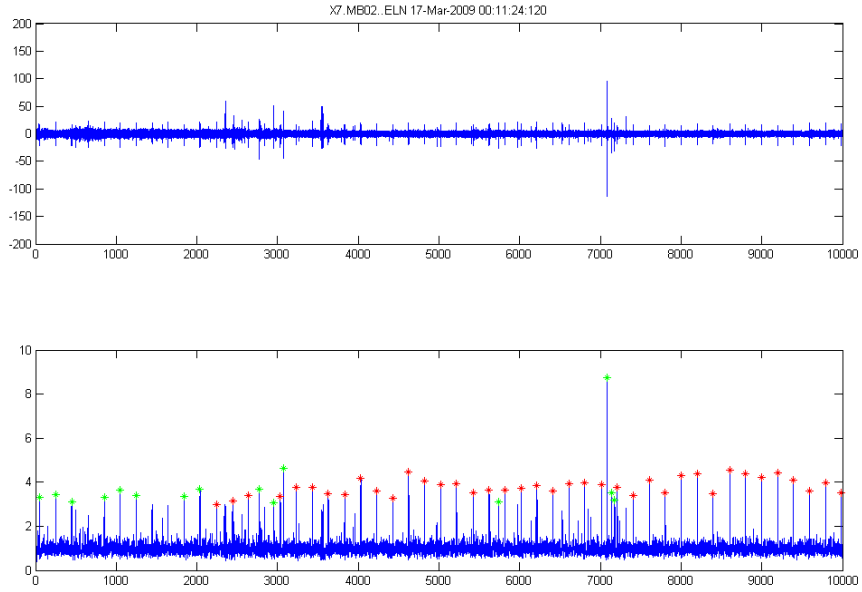

Figure 21. MB02 ELN close-up of the first 10000 seconds from Figure 20. Automatically filtering for transient spikes does not successfully remove all of the bad triggers (the first 8 green stars) because there are not enough successive triggers and they are not consistent enough in timing.

Table 4. Triggers recorded at each station filtered and unfiltered for repetitive instrument noise.

Station	LB03	LB05	MB02	MB07	MB06	GH08	GH08	MB04	MB06	GH08
Sensor	Geo	Geo	Geo	Geo	Geo	Geo	Accel	Accel	HDF	HDF
Hours run	4142	3224	4753	2757	1703	729	1366	3464	--	1104
Unfiltered									*	*
Z / 1	48118	31513	17207	14472	6226	956	19945	77	11490	13425
N / 2	60322	33919	25814	13414	8149	1236	1460	101	3573	12302
E / 3	57357	36848	20732	19208	5517	1910	1858	3825	--	8577
All 3	30952	18734	8990	3074	2583	190	264	24	--	702
trigs/hr	7.47	5.81	1.89	1.11	1.52	0.26	0.19	0.01	--	0.64
Filtered										
Z / 1	43153	31513	13557	10670	6226	956	1256	77	11490	13424
N / 2	52773	33919	22758	4071	8149	1236	1460	101	3573	12298
E / 3	52835	36848	18784	13662	5517	1910	1761	152		8577
All 3	26861	18734	7195	1108	2583	190	142	22	--	702
trigs/hr	6.49	5.81	1.51	0.40	1.52	0.26	0.10	0.01	--	0.64
% cut	13%	0%	20%	64%	0%	0%	46%	8%		0%
* all sensors not running during all hours										

4.2.2 Station Triggers, Network Triggers, and Wide-Network Triggers

Rock fall events that are scientifically interesting should be large enough to trigger at multiple stations on all three components at each of those stations. Triggers that are detected on all three of the instrument's components are considered to be station triggers. In some cases, there are two or more sensors attached to a particular station (e.g. LB01 or GH08), in which case each instrument is considered as a single station for trigger processing. Thus, the single station with two instruments is, for all practical purposes, identical in configuration to two co-located stations (e.g. LB03/LB05, MB02/MB07, and MB04/MB06). Only station triggers (all three components triggering) were considered in determining network triggers (two or more stations triggering) and wide-network triggers (triggers occurring at two or more independent locations). Out of the 5382 network triggers during Phase 2, only 1362 (25%) were wide-network. There were no wide-network triggers for Phase 1 as there was only a single location.

4.2.3 Elimination of known seismic events

Earthquakes are recorded by the regional strong motion seismic network and are most likely also picked up by the rock fall monitoring network. Earthquake event times were downloaded for local, regional, and worldwide distances, depending on the size of the earthquake (Table 5), resulting in a database of >12000 earthquakes spanning both phases of the project. Earthquakes at teleseismic distances were not expected to cause a trigger since the spectral frequency of such earthquakes is highly dampened above 1 Hz, and the geophone corner frequencies are 4.5 Hz and 8 Hz.

Table 5. Criteria for downloading earthquake to compare to wide-network triggers.

EQ Mw	Distance
M -1 to 2	< 300km
M 2 - 3	< 600 km
M 3+	< 2000 km

Next, the earthquakes were compared to the wide-network triggers in the following manner: for each trigger, the algorithm compared local, then regional, and then worldwide earthquakes and back-calculated the seismic velocity to determine if the timing matched. In this manner, 373 earthquakes ranging from moment magnitude 0 to 5.9, at distances of 14.6 to 1468 kilometers were matched to Phase 2 triggers. Only one of the 30 remaining Phase 1 network triggers was attributed to an earthquake, however 53 of the 592 remaining geophone-only triggers were attributed to earthquakes. Figure 22 shows earthquakes matched to Phase 2 triggers by magnitude and by distance. No earthquakes at distances greater than 2000 km were matched with triggers.

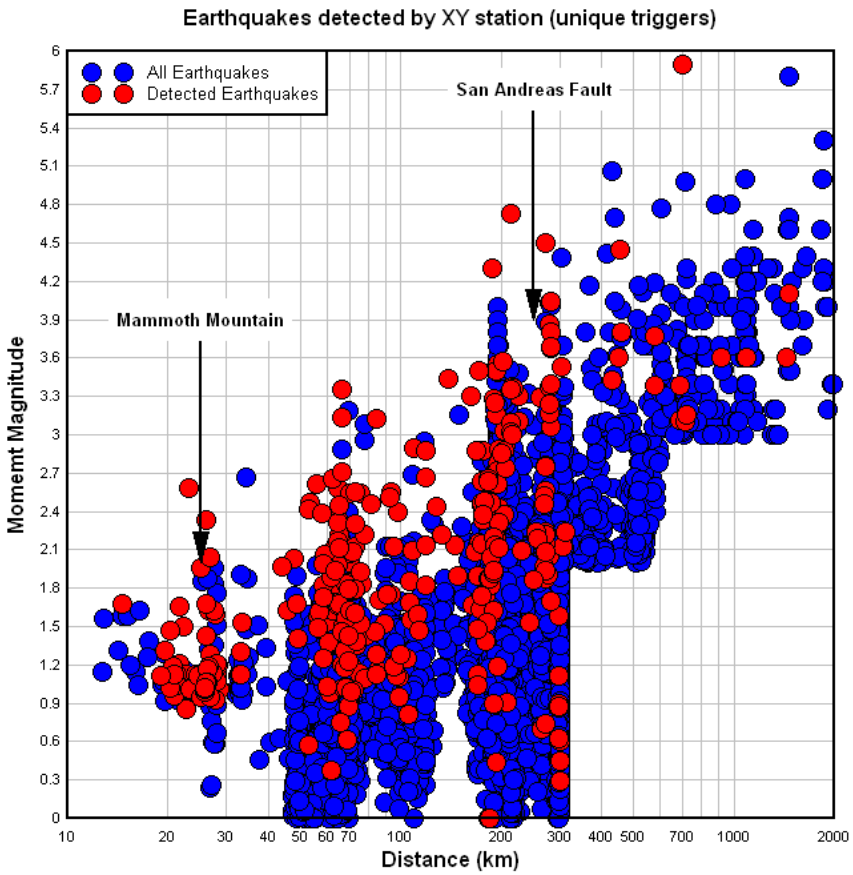

Figure 22. Detection limits of earthquakes compared to rock falls.

The matching of an earthquake with a trigger does not guarantee that the trigger is actually due to an earthquake as it may be a coincidence or a false positive. It is also possible that small earthquakes have been omitted by the database but cause a trigger on the network. The false positive earthquake scenario is only a concern if a potential rock fall event happens around the same time as the earthquake, but a failure to eliminate an earthquake simply results in an extra trigger to be reviewed.

False positive triggers are most likely to be associated with earthquakes of some combination of very small magnitude or very large distance. The probability of each earthquake matching one of the triggers is a function of the time window length for the events to match and the total length of time that the stations were in operation. The time window length is itself a function of distance; more distant events have longer time windows due to the range of allowed seismic velocities, and thus, are more likely to trigger falsely. The probability of false positives can be estimated with the known number of triggers and earthquakes and assumptions about median time windows, window overlap, and number of days when high quality stations were operating.

For the Phase 2 dataset of 1362 triggers and 8930 earthquakes, the probability of matching any given trigger is 1-5%, which in theory results in 14 to 60 false positive triggers. Initial reviews of a random sample of 26 triggers all were confirmed to be earthquakes (true). When triggers correlated with distant, low magnitude earthquakes were reviewed, many did indeed turn out to be false positives. Most of the earthquake-correlated triggers fall within the same earthquake size and distance boundaries, and thus, the overwhelming majority are most likely earthquakes.

4.3 Summary

The technique of data processing by bandpass filtering, normalization, and STA/LTA triggering algorithm followed by elimination of "bad" triggers and identification of potentially interesting triggers leaves a short list of times at which rock falls may have occurred and produced seismic waves. There are a total of 30 remaining network triggers from Phase 1 to review, although the fact that 53 earthquakes were detected by the geophone but not the accelerometer suggests that some of the 539 remaining geophone-only triggers should be reviewed. Since rain and wind are known to produce false positive triggers, geophone-only triggers that occur during periods of stable weather are both uncommon and good candidates for review. During Phase 2, wide-network triggers are the most likely to be rock falls events, although there are still 989 wide-network triggers remaining. Thus, the triggers that are the best candidates from this list to be scientifically interesting are those that occur at a high number and/or high percentage of stations in operation, as well as those that occur during known periods of calm weather. Details pertaining to specific triggers that were selected for review and the results of that review are presented in the next chapter.

5 Instrument Response to Daily and Monthly Changes

There were two observed temporal patterns in the seismic data that appear to be related to the temperature, time of day, or relative aspect of the sun. The first was a noticeable daily periodic fluctuation in the mean of the data, e.g. a daily instrument drift. The second pattern is an apparent fluctuation in the number of triggers. Possible physical explanations are instrumentation response to thermal fluxes, anthropogenic noise, rock deformation due to thermal fluxes, or weather phenomena.

The first two possibilities, instrumentation response and anthropogenic noise are only interesting insomuch as they help in understanding and processing the data. The third explanation, however, could provide insight into one of the possible mechanisms for rock fall triggering. If the rock is deforming in response to temperature fluctuations and exposure to the sun, then it might provide an explanation for summer and evening rock falls that have occurred in the past. In Yosemite National Park, a detached rock flake on a sun-exposed cliff was instrumented with a crackmeter, thermometer, and solar radiation instruments (Collins and Stock 2010). While the final results have not yet been published, preliminary analysis indicates that the rock is in fact deforming on both daily and annual cycles, with a 10 cm crack opening as much as 1 to 1.5 cm on a daily or weekly basis. Thus, the idea that some of the temporal fluctuations in the data baseline and number of triggers might be due to rock deformation is supported by other research. To assess that idea, the following questions were posed:

1. Is the effect seen at each general location?
2. Does the orientation of the sensor matter?
3. How does the effect differ for geophones and accelerometers?
4. Does the effect correlate with temperature, temperature change, or something else?

5.1 Daily Instrument Drift (Tilt)

The daily instrument drift is likely caused by direct instrument response to heating, rock response to heating, or some combination of both. It is possible that the daily drift is relating to the rock expanding and thus, tilting slightly in the vicinity of the instrument. This question would be best answered using instruments in a variety of physical locations at the cliffs and far from the cliffs, including control instruments both exposed to the sun and in the shade at each location, and comparing those results with known temperature and sun exposures. However, this experiment was not designed for the purpose of measuring thermal fluxes. Nevertheless, overall site distribution is good, with instruments on the cliffs, at the base, and in the valley.

The instruments were placed in four locations; on Michael's Ledge at the Lower and Middle Brother rock formations, the talus slope just below the Brothers, and in Yosemite Valley, well away from cliff faces. Michael's Ledge faces east / southeast and thus, is exposed to direct sunlight in the morning and warms up early. In contrast, the warmest ambient temperature is typically in the early afternoon. During mid-winter, Michael's Ledge may become covered in snow during storms, but is still exposed to the sun, sits above a cold air pool created by a temperature inversion, and thus, can be warmer than the Yosemite Valley.

The nature and placement of the instruments is important in interpreting the data (Table 6). The geophones at the Lower Brother location are more exposed to direct sunlight than the geophone at Middle Brother, which has more trees and shrubbery nearby. One geophone at Lower Brother is placed in sand, while the other is sitting on rock on a small ledge. The geophone at Middle Brother is placed in sand. Sandbags protect all three geophones on Michael's Ledge. The accelerometer at Middle Brother was fixed directly on the cliff face and underneath an overhang, thus, in the shade most or all of the time. On the talus slope, two geophones were placed near the wall, buried under a sandbag, and surrounded by trees in a mostly shady location. The one station in Yosemite Village is located several hundred meters from the nearest cliff and sitting on hundreds of meters of sediment. For most of the project duration, it was equipped with an accelerometer and several barometric microphones. For the last month, a geophone replaced the accelerometer. Thus, this station serves as a control point away from the rock faces, but is located nearer to sources of anthropogenic noise.

Table 6. Exposure of instrumentation at different sites.

Station	Instrument	Location	Placement	Sun Exposure
LB03	L-28 geophone	Michael's Ledge*, Lower Brother	In sand under sandbag	Very exposed
LB05	L-28 geophone	Michael's Ledge*, Lower Brother	On small ledge under sandbag (not level)	Very exposed
MB04	Terratech SSA-320 accelerometer	Michael's Ledge*, Middle Brother	Affixed to cliff wall vertically	Shade under overhang
MB06	L-28 geophone	Michael's Ledge*, Middle Brother	In sand under sandbag	Some exposure, nearby trees
MB02	L-28 geophone	Talus slope under Middle Brother	In sand under sandbag	Some exposure, nearby trees
MB07	L-28 geophone	Talus slope under Middle Brother	In sand under sandbag	Some exposure, nearby trees
GH08	RT-131A/B accelerometer	Yosemite Village (no cliffs)	Placed on ground, snow	Some exposure, nearby trees
GH08	L-28 geophone (short time)	Yosemite Village (no cliffs)	Placed on ground	Some exposure, nearby trees
* Michael's Ledge has East / Southeast exposure				

Each instrument is attached to a datalogger recording internal temperature, which is used as a proxy for ambient temperature plus direct sun heating of the black plastic datalogger. In some cases, the temperature that is estimated for a particular instrument is recorded at a datalogger in a different location that is believed to have a similar exposure to the sun as the instrument. In addition, there is a weather station in Yosemite Valley recording temperature and precipitation events. While these are not ideal temperature or solar radiation measurements, they do help to assess the on-site conditions.

A ten-day representative set of data was chosen in early May to check whether the effect is seen at all locations. The temperature during that time period fluctuates between 38 and 80 °F, according to the official record, but higher temperatures are recorded on the ledge in places exposed to a great deal of sun (Figure 23). Daily instrument drift for the ten-day period is examined in detail for all locations.

Next, the drift effect was compared to local, sun-exposed ambient temperature and Yosemite Valley ambient temperature in both winter and summer. This can both show the difference between sun and shade temperature, but also highlight the temperature inversion that develops in winter when cold air pools at the valley floor. This address whether or not the drift is correlated with ambient air temperature of the instrument or rock temperature due to solar radiation.

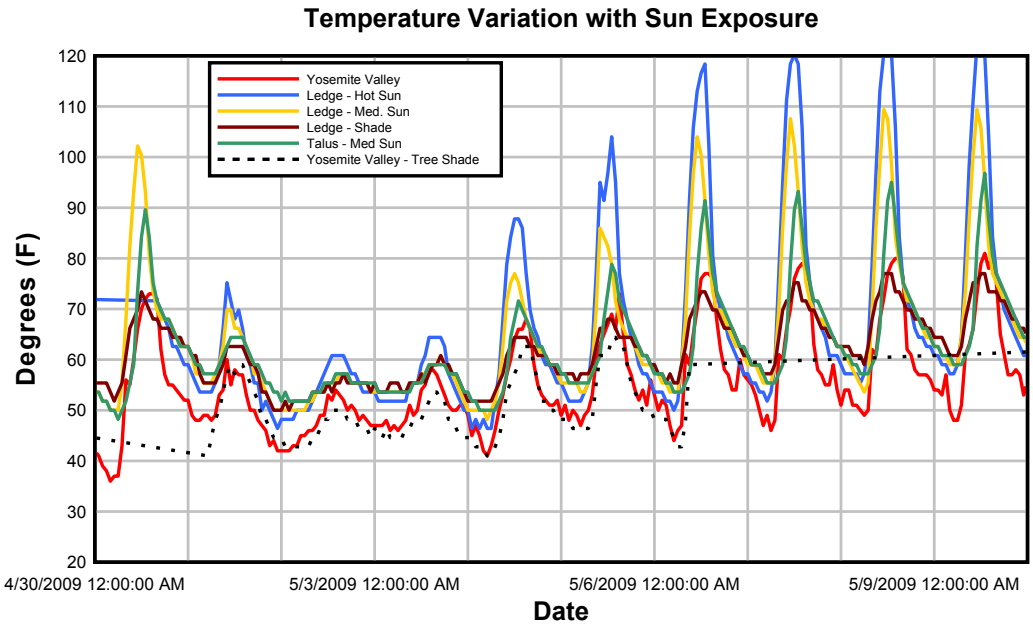

Figure 23. Temperature range from 04/30/2009 to 05/09/2009 in Yosemite Valley.

5.1.1 Michael's Ledge, Exposed to Hot Sun

The warmest location is on Michael's Ledge on Lower Brother. Station LB03 is exposed to the morning sun, which makes this location several degrees warmer than the ambient temperature. Looking at the ten-day period in May, it is clear that this station is experiencing a daily change (Figure 24) and the maximum value happens between 9am and noon, consistent with the east-facing exposure. Furthermore, it is noted that the Z component, roughly parallel to the wall, shows the greatest amount of movement each day, followed by the E-W component, roughly perpendicular to the wall. Lower Brother faces roughly east/southeast with a roughly 70 degree angle.

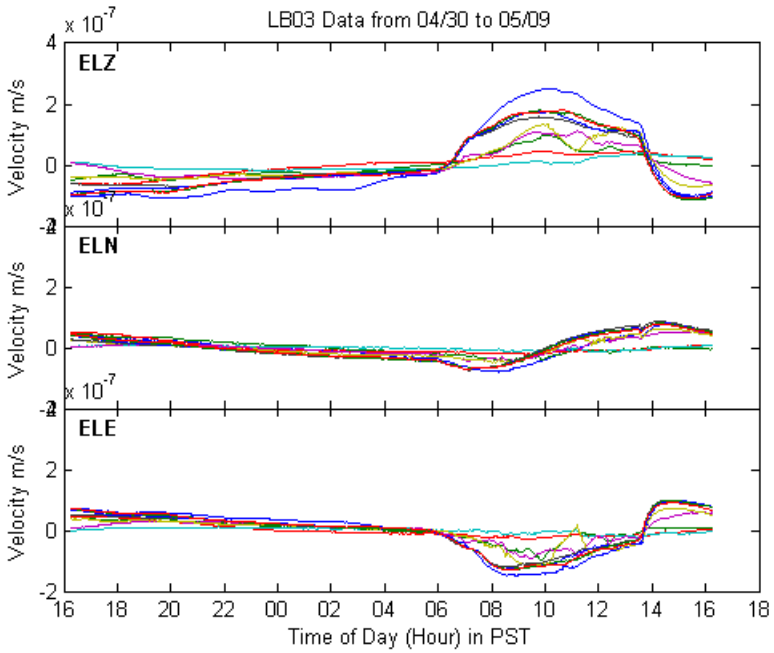

Figure 24. Michael's Ledge (sunny) geophone showing long period drift during a 10-day period.

Comparing the seismic response to temperature during the summer reveals that the maximum drift occurs on the warmest day (June 4th). However, the seismic response peaks at 8am, but the ledge ambient temperature peaks at 2pm after the whole morning of hot sun and the Yosemite Valley (YYV) temperature peak at 1pm (Figure 25). In January, the response peak is still earlier (~9am) than the peak temperature peak on the ledge (~noon) and at YYV (1:30pm) (Figure 26). Table 7 compares in detail the maximum seismic response and temperature during those two periods. When all of the data for the entire installation are compiled and plotted to show maximum seismic activity vs. maximum temperature (Figure 27) it is clear that the median time of maximum seismic response is occurring four hours earlier than the median time of maximum temperature at the hot ledge and two hours earlier than Yosemite Valley when there is no precipitation. Thus the drift is correlated to the onset of intense solar radiation, and thus, rapid warming at this hot, sunny location.

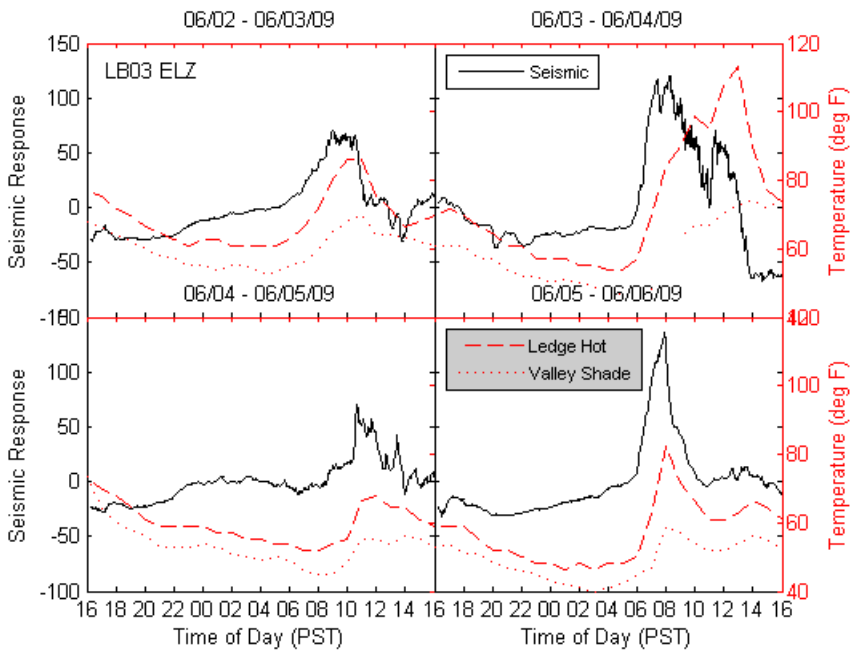

Figure 25. Seismic signal (black) compared with hot sun temperature (red dash) and YYV temperature (red dotted) for LB03 ELZ in June 2009.

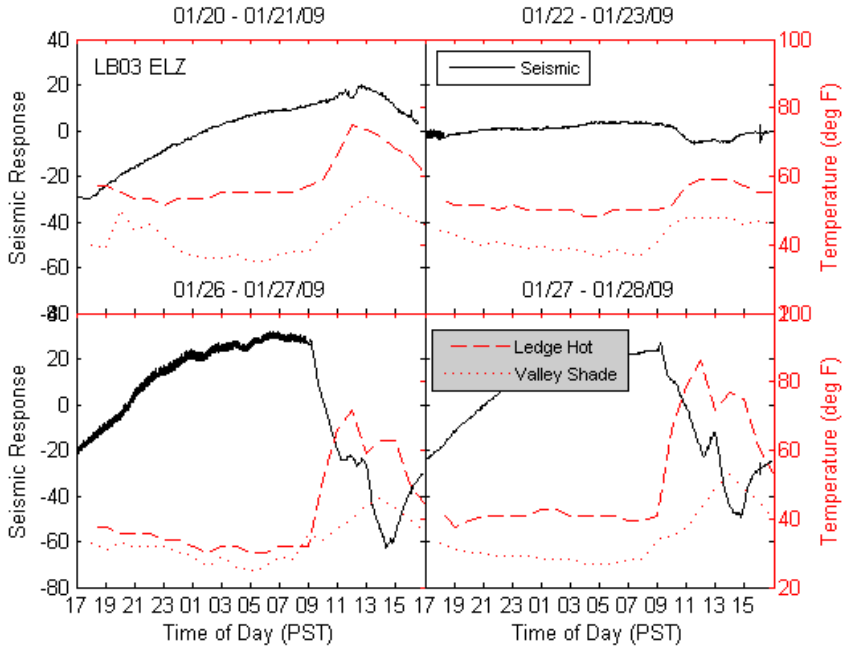

Figure 26. Seismic signal (black) compared with hot sun temperature (red dash) and YYV temperature (red dotted) for LB03 ELZ in January 2009.

Table 7. Time of maximum seismic response and temperature for LB03 ELZ in June and January.

May-June	Time of Maximum			January	Time of Maximum		
Date	Seismic (PST)	Hot Sun	YYV	Date	Seismic (PST)	Hot Sun	YYV
6/1/2009	10	15	10	1/14/2009	11	14	12
6/2/2009	8	13	10	1/15/2009	10	13	12
6/3/2009	9	11	10	1/16/2009	11	14	12
6/4/2009	8	14	13	1/18/2009	11	14	12
6/5/2009	11	14	12	1/19/2009	11	14	12
6/6/2009	8	8	8	1/20/2009	11	14	12
6/7/2009	9	15	13	1/21/2009	13	13	12
6/8/2009	9	11	12	1/23/2009	7	11	12
6/9/2009	7	12	12	1/24/2009	5	14	15
6/10/2009	12	12	12	1/26/2009	10	15	12
6/11/2009	8	11	11	1/27/2009	7	14	12
6/12/2009	9	13	10	1/28/2009	9	14	12
6/13/2009	9	10	9	1/29/2009	9	14	12
6/14/2009	8	11	12	1/31/2009	9	13	12
Blue = Precipitation							

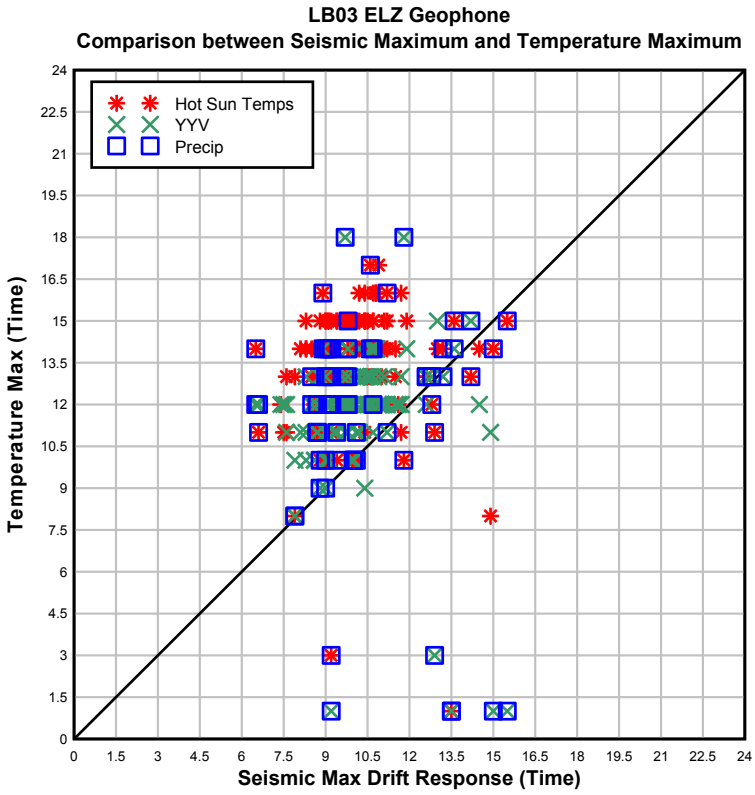

Figure 27. Maximum seismic drift response vs. temperature for sunny LB03.

5.1.2 Michael's Ledge, Shaded

Michael's Ledge continues northeast and higher, crossing from Lower to Middle Brother. Located at the highest point reachable without ropes are two stations shaded by trees and overhanging rock: a geophone (MB06) and an accelerometer affixed vertically to the cliff wall underneath an overhang (MB04). The maximum change at the geophone (Figure 28) and the accelerometer (Figure 29) is recorded by the Z component, roughly parallel to the wall, although the effect is earlier and more pronounced for the accelerometer.

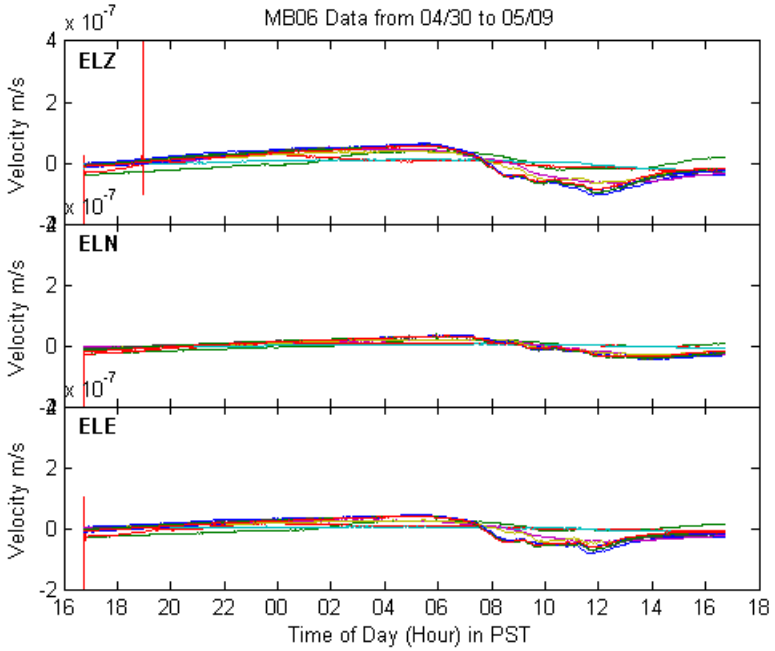

Figure 28. Michael's Ledge (shady) geophone showing long period drift during a 10-day period.

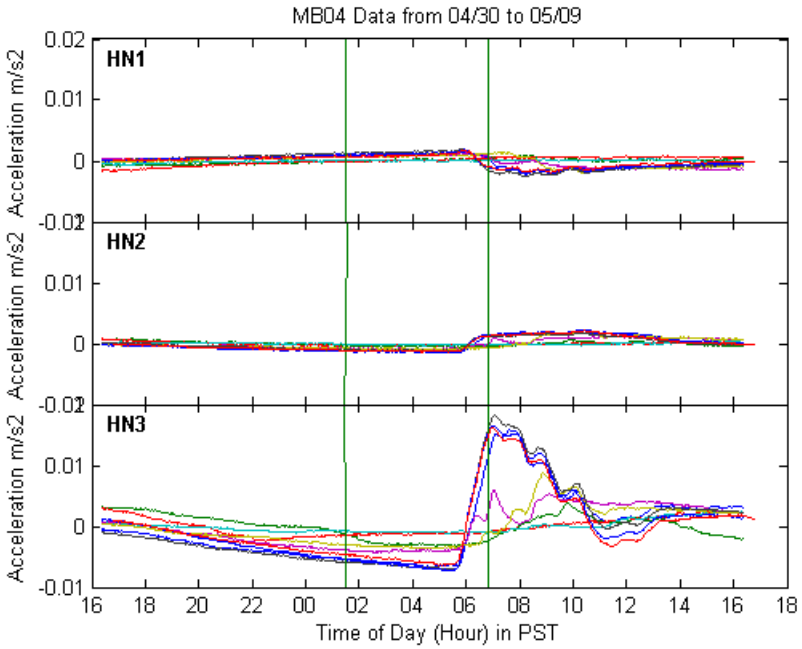

Figure 29. Michael's Ledge (shady) accelerometer showing long period drift during a 10-day period.

Comparison of seismic response and temperature during warm temperatures (and a few rainy days) for the geophone, sitting in sand, is shown in Figure 30, and winter records are shown in Figure 31. The seismic response closely tracks the moderately shaded ledge temperature in this case, peaking at around noon while the ledge temperature peaks within the same hour. When all of the data for the entire installation are compiled and plotted to show maximum seismic activity vs. maximum temperature (Figure 32) it is clear that the median time of maximum seismic response is occurring at roughly the same time as the local ledge temperature.

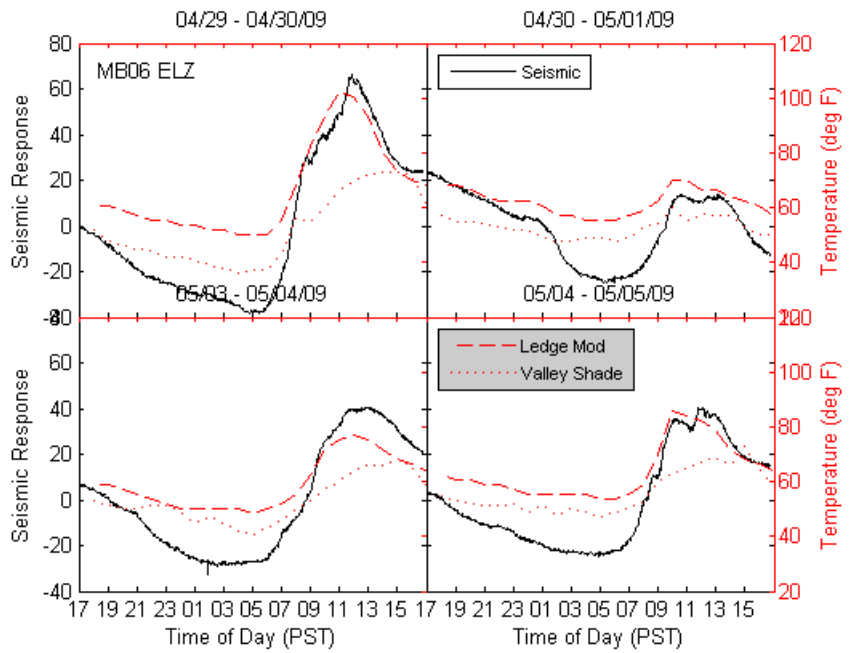

Figure 30. Seismic signal (black) compared with hot sun temperature (red dash) and YYV temperature (red dotted) for MB06 ELZ in May 2009.

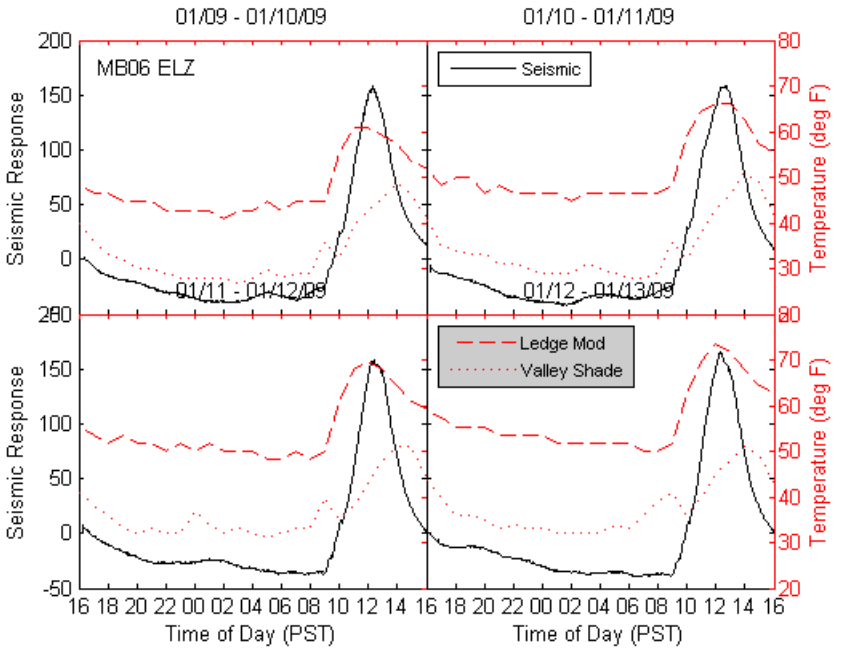

Figure 31. Seismic signal (black) compared with hot sun temperature (red dash) and YYV temperature (red dotted) for MB06 ELZ in January 2009.

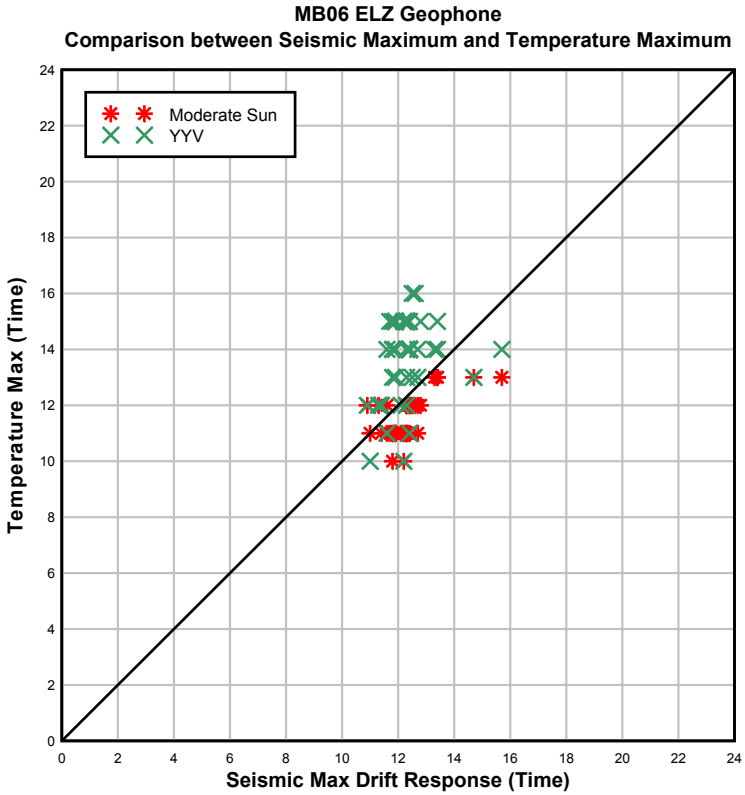

Figure 32. Maximum seismic drift response vs. temperature for partially shaded MB06.

The seismic drift of the even shadier accelerometer is also compared to warm (Figure 33) and colder (Figure 34) temperatures. The seismic response maximizes early in the day (~7am) on warm sunny days, but more closely tracks shade temperature curve on cloudy days. This implies that the accelerometer, which is always shaded and attached directly to the rock, responded to the temperature of the surrounding rock, some of which is exposed to the sun, rather than an internal temperature of the instrument. When all of the data for the entire installation are compiled and plotted to show maximum seismic activity vs. maximum temperature (Figure 35) it is clear that the median time of maximum seismic response is two to three hours earlier than the time of maximum temperature. This indicates that this shaded instrument is correlated more with solar radiation on the rock than with ambient temperature.

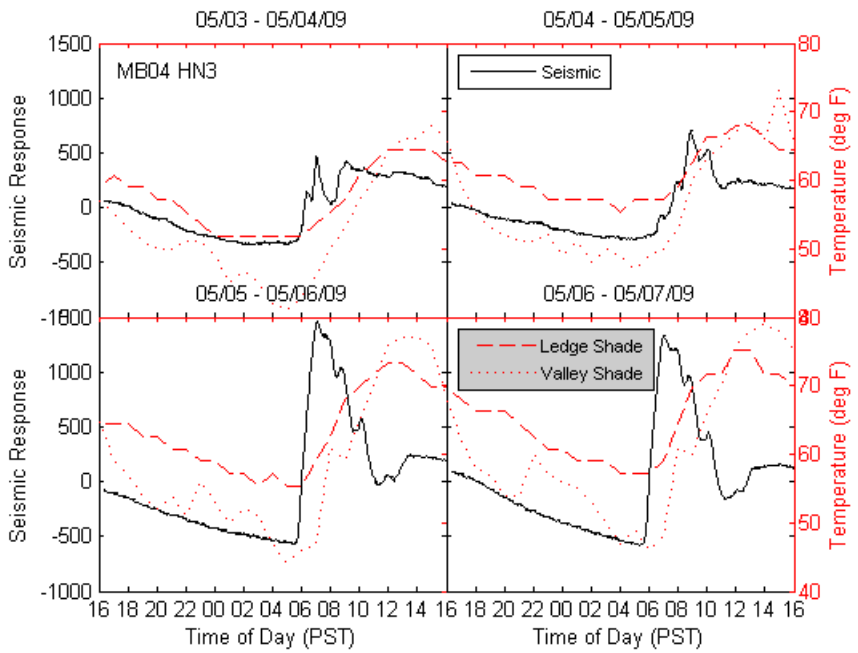

Figure 33. Seismic signal (black) compared with hot sun temperature (red dash) and YYV temperature (red dotted) for MB04 HN3 in May 2009.

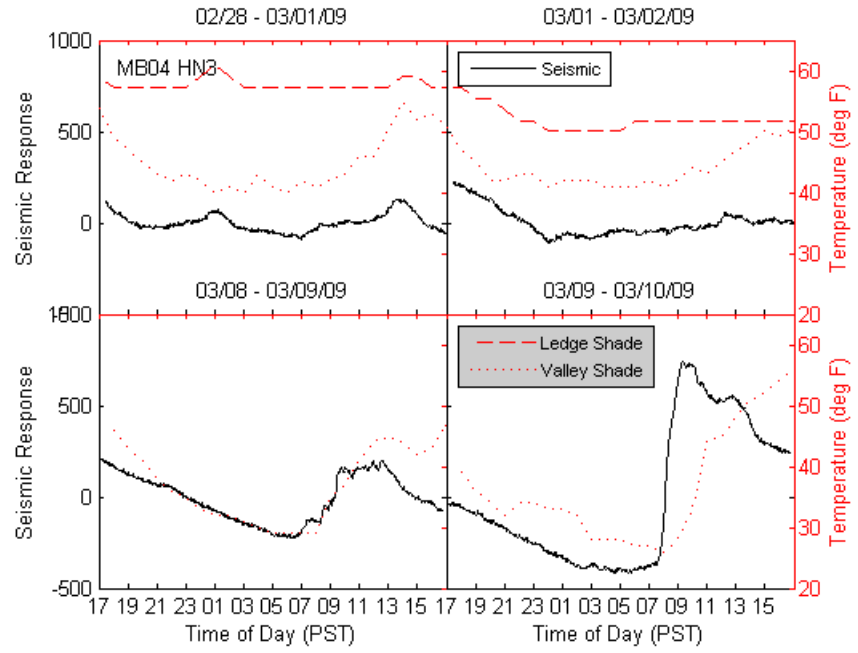

Figure 34. Seismic signal (black) compared with hot sun temperature (red dash) and YYV temperature (red dotted) for MB04 HN3 in March 2009.

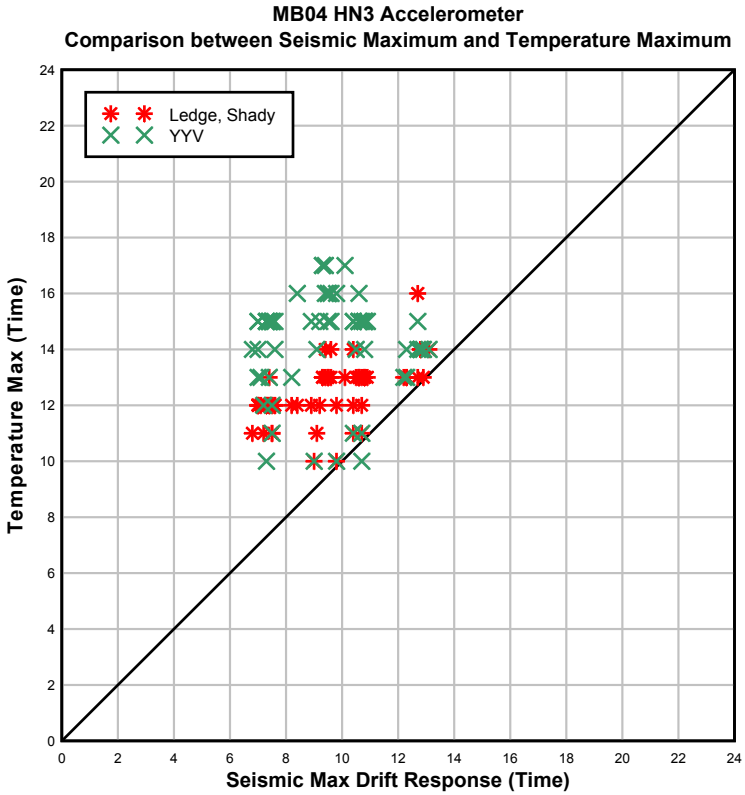

Figure 35. Maximum seismic drift response vs. temperature for shady MB04.

5.1.3 Talus near Rock Wall, Partially Shaded

Below Middle Brother at the low point between two talus slopes, one foot from the rock wall, is a partially shaded geophone (MB02). There is a daily drift signal here, but it occurs at noon or shortly thereafter instead of the morning, like the other shady geophone. Again, the maximum change is seen on the Z component followed the E-W component, which is nearly perpendicular to the wall.

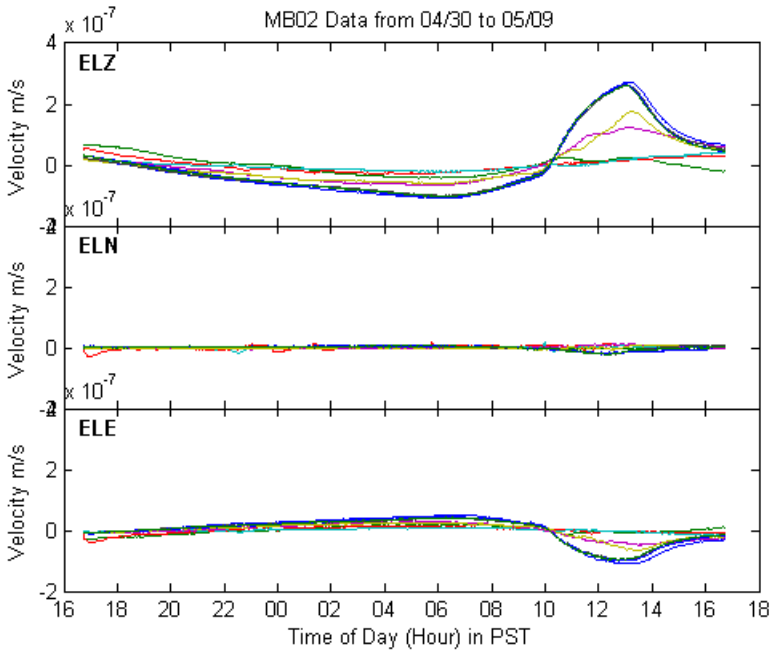

Figure 36. Talus slope (some trees) geophone showing long period drift during a 10-day period.

Comparison of seismic drift in summer (Figure 37) and winter (Figure 38) shows that the seismic response closely tracks the forested talus temperature, peaking at around 1pm while the talus temperature peaks within the same hour. When all of the data for the entire installation are compiled and plotted to show maximum seismic activity vs. maximum temperature (Figure 39) it is clear that the median time of maximum seismic response is occurring at roughly the same time as the local talus temperature, which is a similar result to the shaded geophone up on Michael's Ledge.

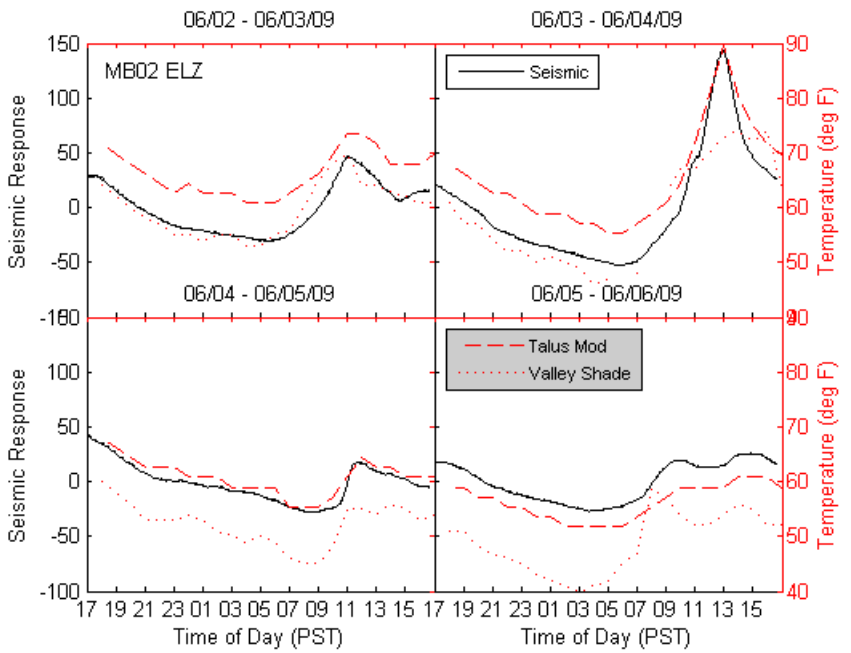

Figure 37. Seismic signal (black) compared with hot sun temperature (red dash) and YYV temperature (red dotted) for MB02 ELZ in June 2009.

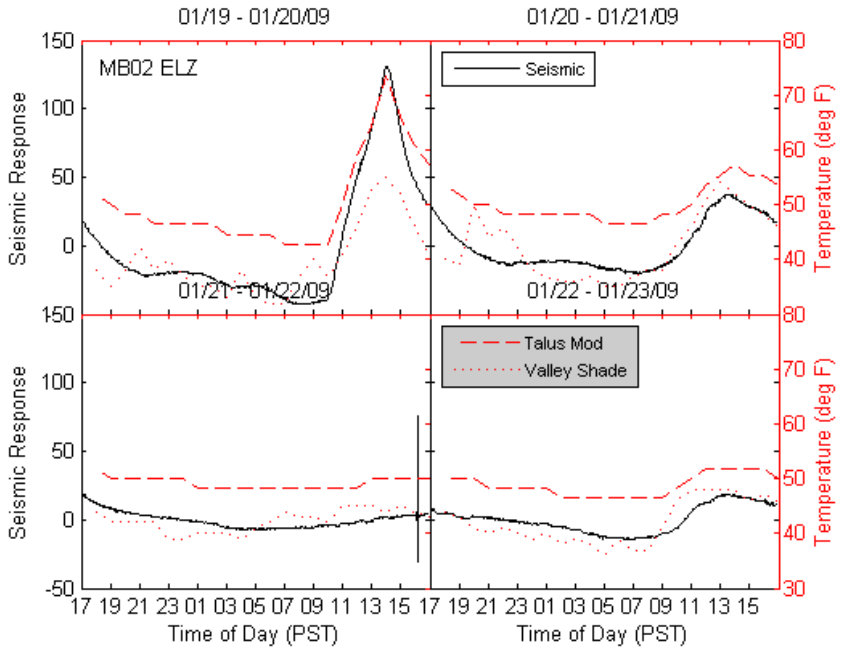

Figure 38. Seismic signal (black) compared with hot sun temperature (red dash) and YYV temperature (red dotted) for MB02 ELZ in January 2009.

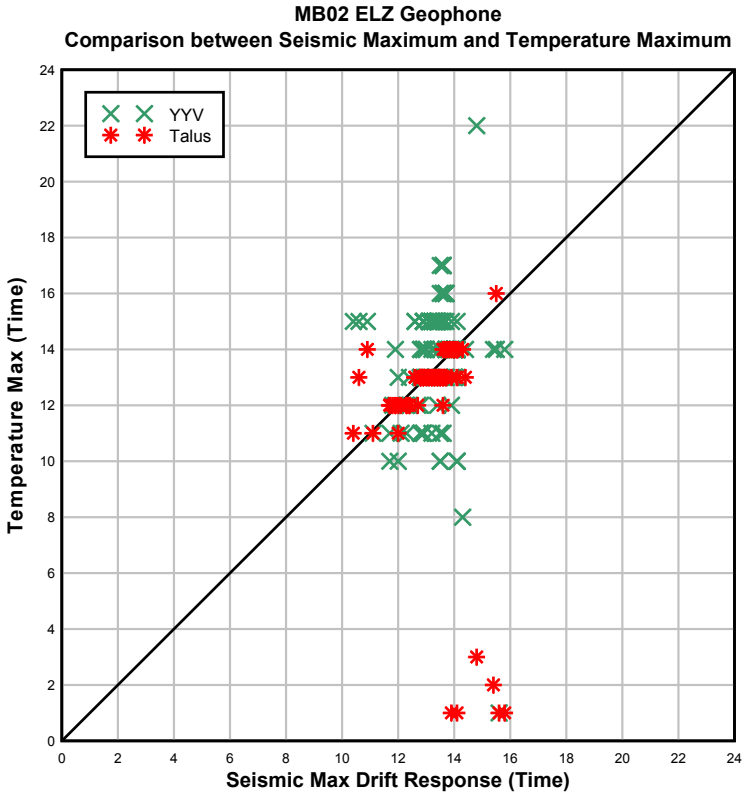

Figure 39. Maximum seismic drift response vs. temperature for partially shaded talus, MB02.

5.1.4 Yosemite Valley Away From Cliff, Partially Shaded

Finally there was an accelerometer (GH08) located in Yosemite Valley under tree canopy several hundred meters from the cliff face. This station featured an accelerometer from January to May, and a geophone from May to June. The accelerometer appears to experience daily fluctuations, but the effect is markedly less pronounced (Figure 40). It should be noted that the accelerometer was removed in early May and was not running during the hottest days. For comparison, some accelerometer data from warm days in April is also shown (Figure 41). The Z component shows the strongest response, consistent with results at other stations. Geophone data is shown to make a comparison with the accelerometer (Figure 42). It too appears to show a daily fluctuation, although unusually, this effect is seen primarily on the N-S component instead of the Z component.

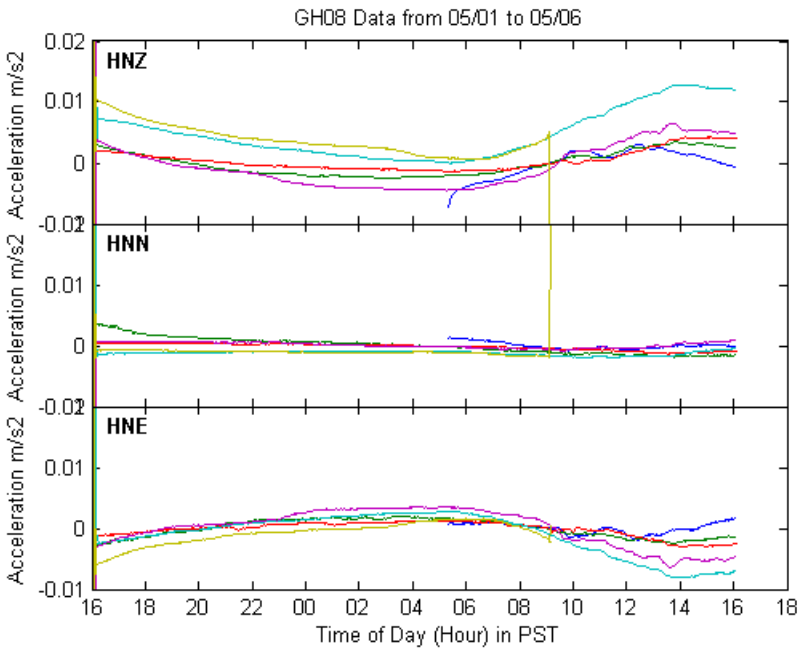

Figure 40. Yosemite Valley (moderately shady) accelerometer showing long period drift during a 6-day period.

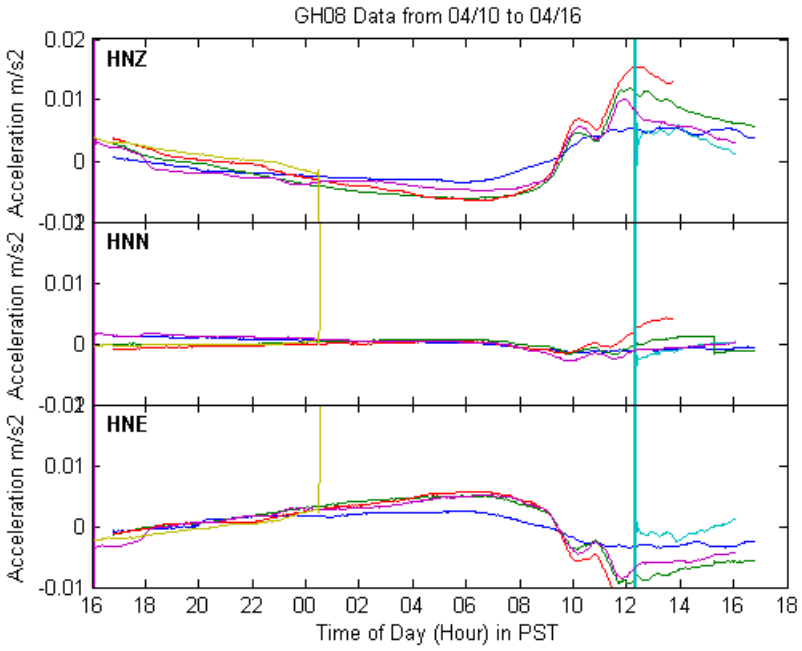

Figure 41. Yosemite Valley (moderately shady) accelerometer showing long period drift during a 7-day period.

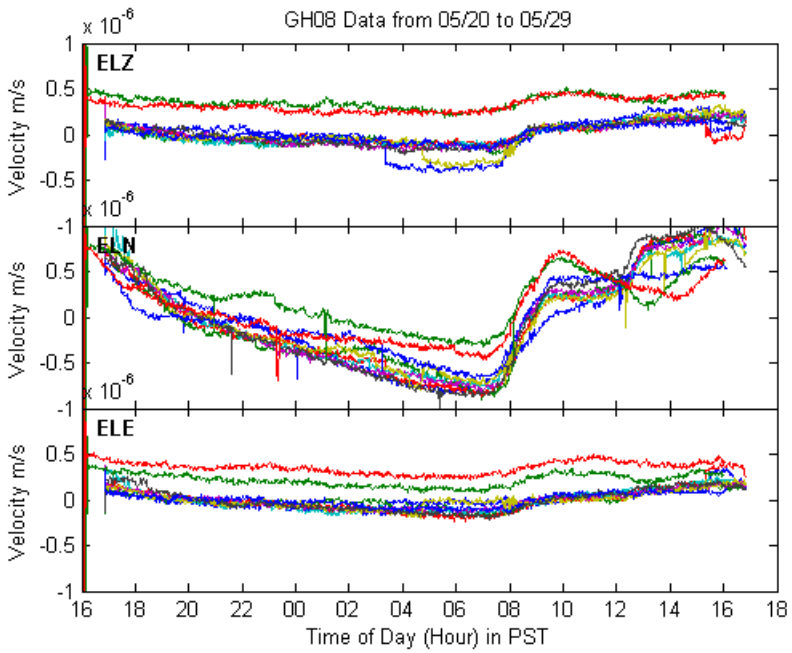

Figure 42. Yosemite Valley (moderately shady) geophone showing long period drift during a 10-day period.

Comparisons of seismic drift to temperature for the accelerometer on warm days and cold days are shown in Figure 43 and Figure 44, respectively. Warm day geophone response is compared to temperature in Figure 45. The seismic response closely tracks the valley temperature for all three cases, peaking at 1-2pm. When all of the data for the entire installation is compiled and plotted (Figure 46) it is clear that the correlation with valley temperature holds.

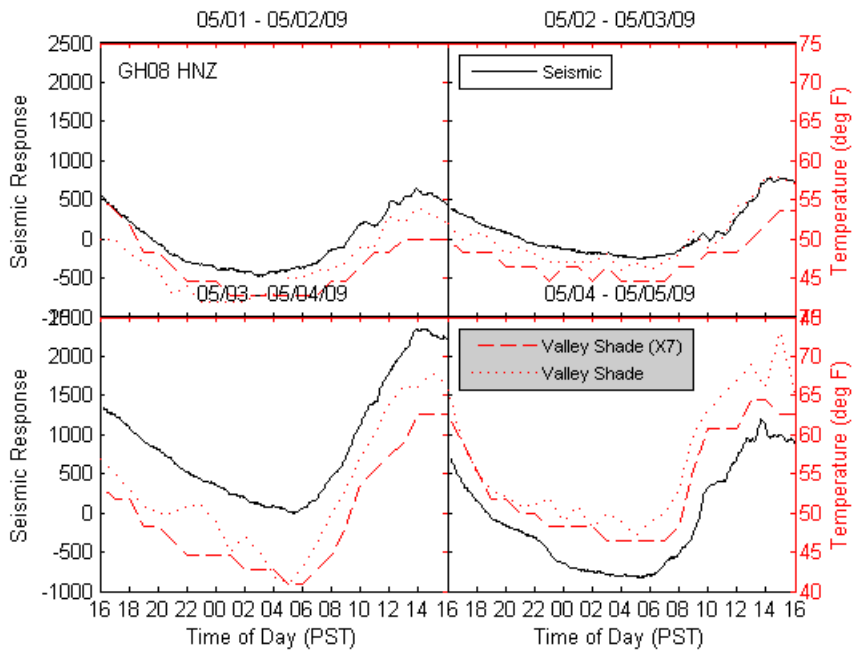

Figure 43. Seismic signal (black) compared with hot sun temperature (red dash) and YYV temperature (red dotted) for GH08 HNZ in May 2009.

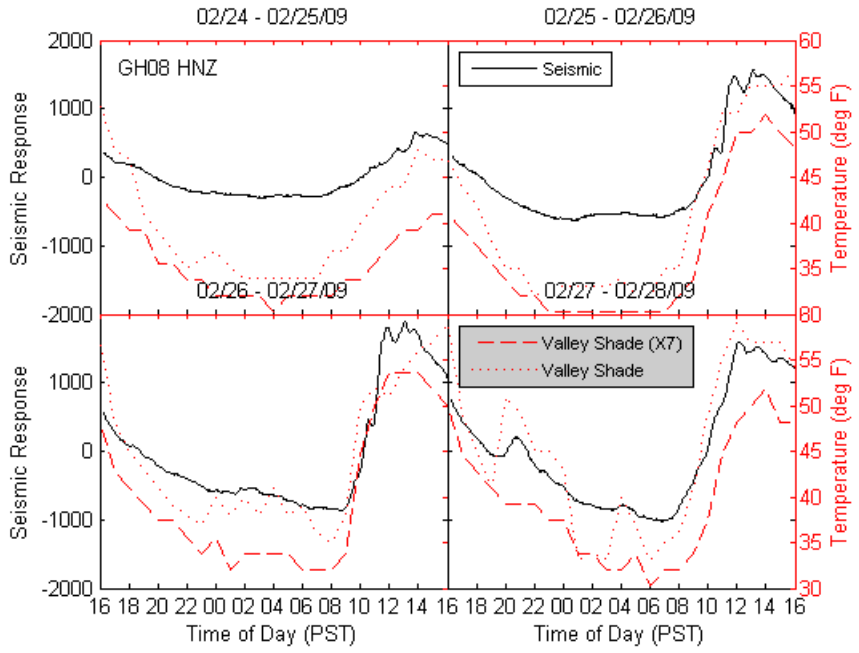

Figure 44. Seismic signal (black) compared with hot sun temperature (red dash) and YYV temperature (red dotted) for GH08 HNZ in February 2009.

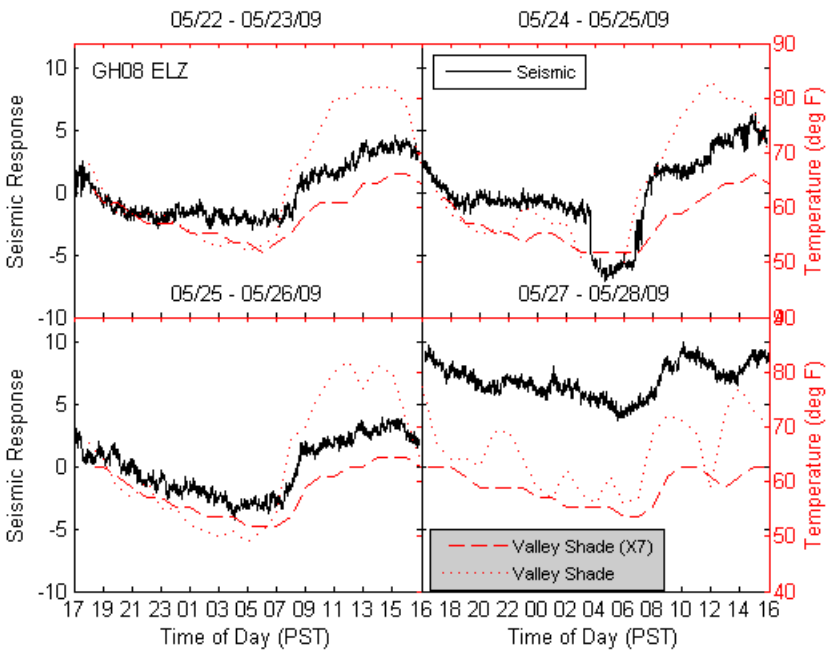

Figure 45. Seismic signal (black) compared with hot sun temperature (red dash) and YYV temperature (red dotted) for GH08 ELZ in May 2009.

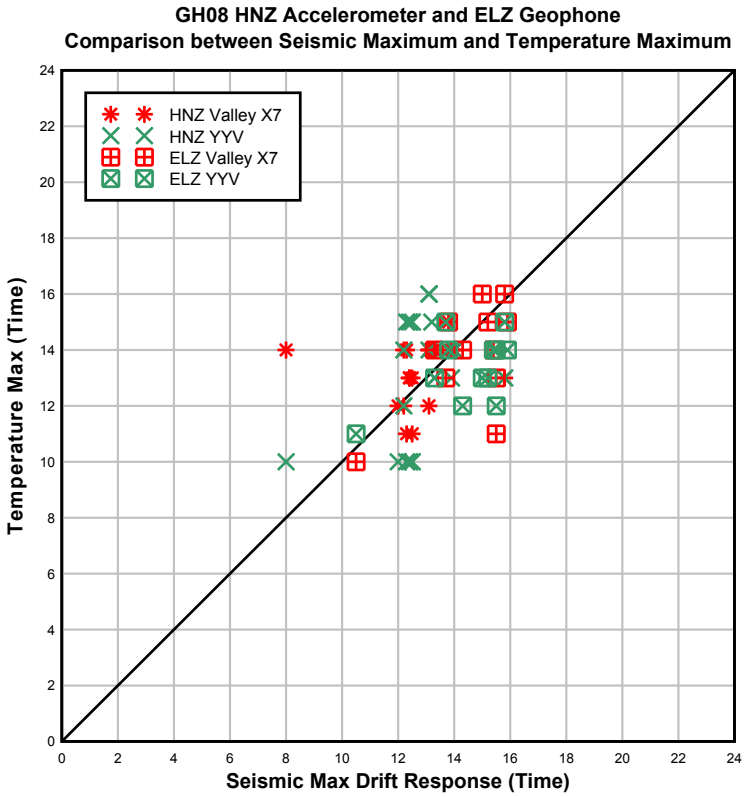

Figure 46. Maximum seismic drift response vs. temperature for partially shaded valley, GH08.

5.1.5 Summary

The daily instrument drift has been shown to occur at all stations regardless of location or instrument type, but the magnitude and timing of the drift is highly variable. In all cases, the maximum drift is correlated with either ambient temperature or with solar radiation, which helps to rule out an anthropogenic source, especially when it peaks early in the morning, is not correlated with peak human activity, and does not last all day long. The Z component is the most sensitive to these thermal effects, followed by the E-W component, which is roughly perpendicular to the cliff orientation.

Although the seismic drift signal is correlated with thermal fluxes, the evidence does not eliminate the possibility that instrumentation components are internally responding to thermal fluxes and causing the signal. Some stations are inconsistent in their readings and track the local ambient temperature, recorded at a similarly sun-exposed datalogger, very well. There are two situations where the seismic drift peaks around 7am on sunny days while the ambient temperature peaks much later. Neither case shows this early anomaly on cloudy days, suggesting that rapid warming is a stronger driver of the drift signal than ambient temperature. One of these cases is the sun-exposed geophone at warmest location, which does not rule out an internal instrument response. The other case is the accelerometer at MB04, which is located in an extremely shady spot under an overhang, behind some trees and attached directly to the rock wall. This case presents the strongest case that the early morning signal is due to expansion and tilting of the nearby sun-exposed rock since the instrument is always in the shade. However, there are also shady geophones near sun-exposed rock, and they do not show an early morning peak on sunny days. It is likely that either the instrument type, an accelerometer instead of a geophone, or the placement, attached directly to the rock instead of placed on a sandy ledge, is responsible for this difference. Thus, at this time, it is difficult to state with certainty whether the signal is originating from the rock or the instrumentation, although there is some evidence that suggests that at least part of the recorded signal is due to rock deformation. A complete record of the instrument drift for the duration of the project is presented in Appendix B.

5.2 Trigger Fluctuation

The dataset was processed to find times of anomalous seismic activity, called triggers. In total, nearly 500,000 triggers were recorded, but only triggers that occurred on all three components for any instrument (station triggers) and those that were recorded at more than one station (network triggers) were kept for rock fall review. Triggers have resulted from wind, rain, rock falls, earthquakes, instrumentation noise, human activity, snow avalanches, and some unexplained phenomena. Triggers do not occur evenly distributed throughout the day and thus, the question is raised whether rock deformation due to thermal changes might be responsible for some seismic anomalies that cause triggers to be recorded. We might not expect that a particular thermal trigger would be recorded at more than one location, and indeed, network triggers are weakly anti-correlated with warming trends, even after removing rainy or windy days from the dataset (Figure 47).

The distribution of triggers is uneven, with geophones accounting for the vast majority (98%) of station triggers, but only 74% of all network hours. Even more interesting is that the two co-located geophones, LB03 and LB05, which happen to be at the warmest spot, accounted for 79% of all station triggers, but only 32% of all network hours. Thus, these two stations are skewing the data, but it might be significant.

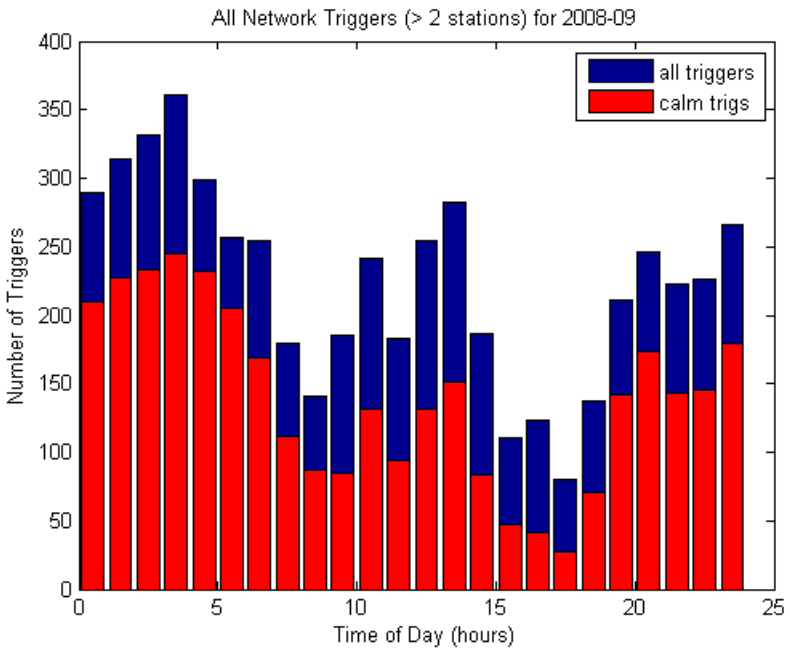

Figure 47. Network triggers sorted by time of day.

If only network triggers recorded at more than one location are considered, any trigger recorded only at LB03 and LB05 is removed. In that case, the results now show an increase in the number of triggers started around 8am and rising until the early afternoon before quickly dropping off again at around 3pm, when the sun has moving behind the east-facing cliff (Figure 49). However, the only possible explanation for thermally driven wide-network triggers is that two stations at two different locations happen to record a thermal trigger at the same time. Thus, neither pattern is likely to be due to thermal fluxes in rock, although they may be related to other weather phenomena, like wind, which may have a thermal driver. Therefore, the effect at each station is examined in the following sections.

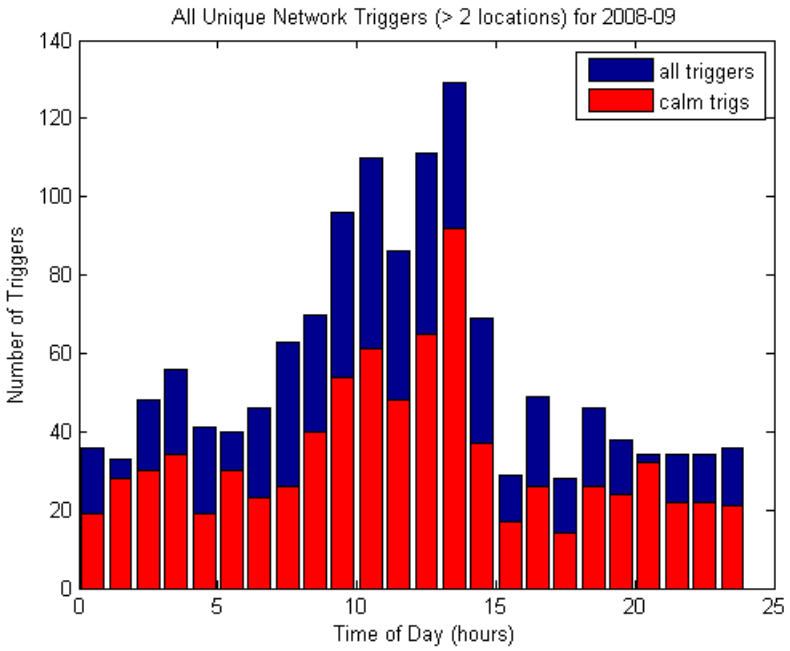

Figure 48. Wide-network triggers sorted by time of day.

5.2.1 Michael's Ledge, Exposed to Hot Sun

Two geophone stations, LB03 and LB05, were located on Michael's Ledge in an area where the entire ledge was highly exposed to solar radiation, especially in the morning. These two stations recorded the highest average triggering rate of the entire network, at 6.5 and 5.8 triggers per hour, respectively. LB03 experienced high levels of instrumentation noise while LB05 did not, which may explain some of the difference between the two. When the triggers were plotted by time of day, it is found that the triggering rate drops off during warm daytime hours. The similarity in the daily temporal triggering pattern between the two stations suggests an association with a natural phenomenon at that location.

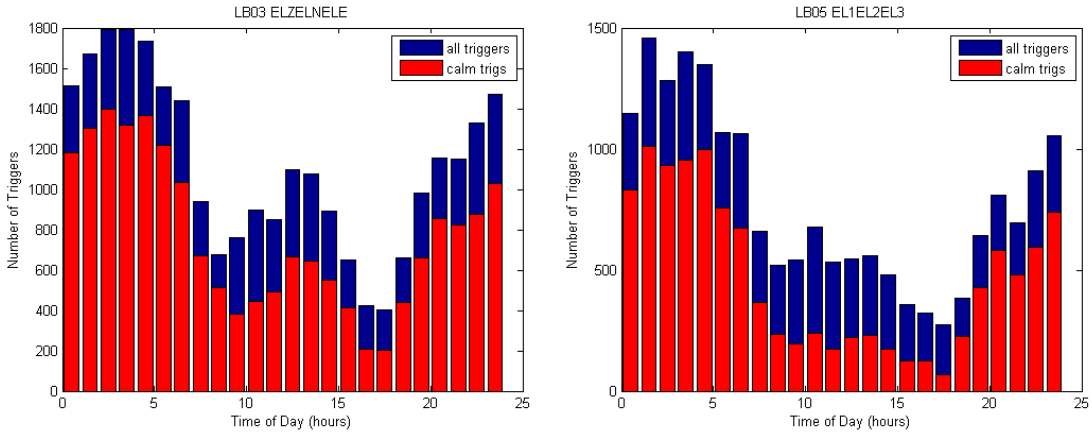

Figure 49. Station triggers at LB03 (left) and LB05 (right), which are located near each other on Michael's Ledge.

Both stations were active throughout the winter and examination of the trigger pattern over the winter and spring months (Figure 50 and Figure 51) shows that most of the triggers occurred after large winter storms. This association suggests that the triggers are related to warming following a large snow and ice storms, or, a freeze-thaw mechanism. There are two possible explanations for triggers: small avalanches caused by melting, or refreezing and expansion of snow and rock cracks. Since the majority of triggers are happening at night and this is the warmest location on sunny days, refreezing is the likely cause of most of the triggers.

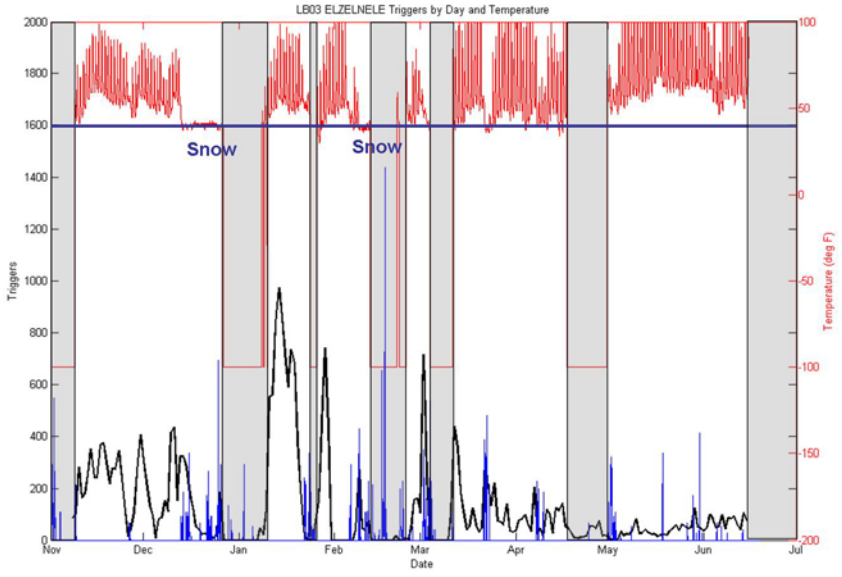

Figure 50. LB03 triggers per day compared with temperature (red) and precipitation (blue). Station shutdowns shown as gray boxes.

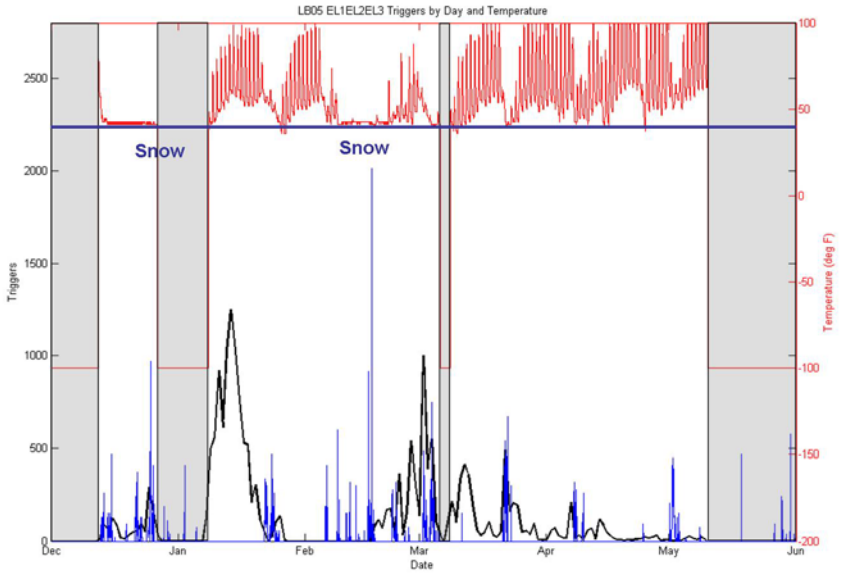

Figure 51. LB05 triggers per day compared with temperature (red) and precipitation (blue). Station shutdowns shown as gray boxes.

5.2.2 Michael's Ledge, Shaded

An accelerometer (MB04) and a geophone (MB06) were located on another part of Michael's Ledge in a shady, tree-covered spot. The accelerometer was very quiet for the duration of the project, recording only ten triggers, too small of a dataset to draw any conclusions. The geophone recorded a medium average triggering rate of 1.5 triggers per hour, four times less than the geophones in the warm, sunny location on Michael's Ledge. This station experienced serious intermittent power issues, and thus, there are large gaps of time when the station was not running. Nevertheless, there were 2583 station triggers, most of which occur during then hours when the sun is shining on the east-facing ledge, 9am to 3pm (Figure 52). Given the power issues, it is important to examine whether this daytime bias is due the station running at more hours when the solar panel was working. However, the station was running for 75 days at 7am, and 69 days between 7pm and midnight, a 7% change that is inadequate to explain the difference in the number of triggers. More triggers occur during winter storms, but it is difficult to assess the triggering rate following a snowstorm since the station was typically not running due to the solar panel being covered (Figure 53). Thus, it appears that winter storms do produce higher than average triggers, but the freeze-thaw effect at this location is unknown due to power supply problems. The lack of power during the freeze-thaw period may also account for some of the discrepancy in triggering rate between this geophone and the other two geophones located on Michael's Ledge, although it is impossible to quantify the amount without more data.

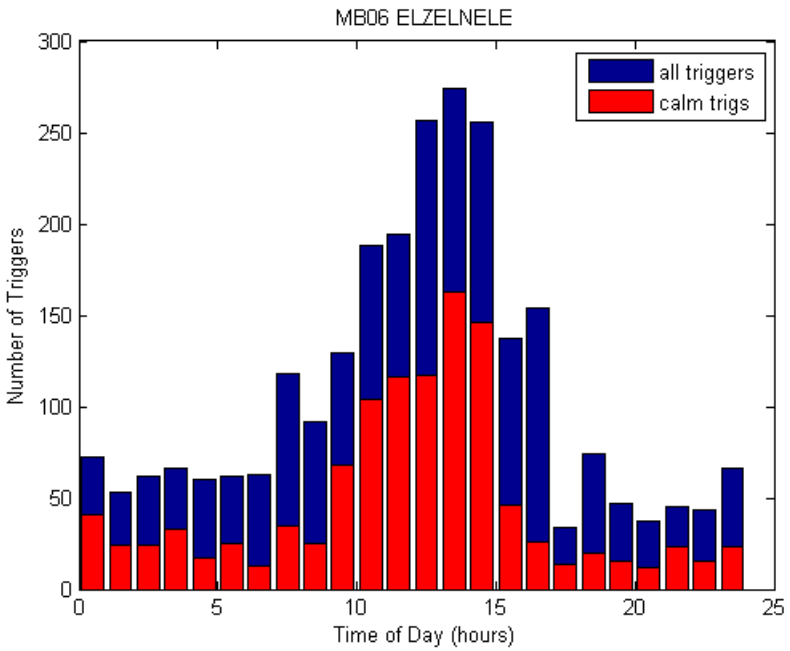

Figure 52. Station triggers at MB06, located high on Michael's Ledge.

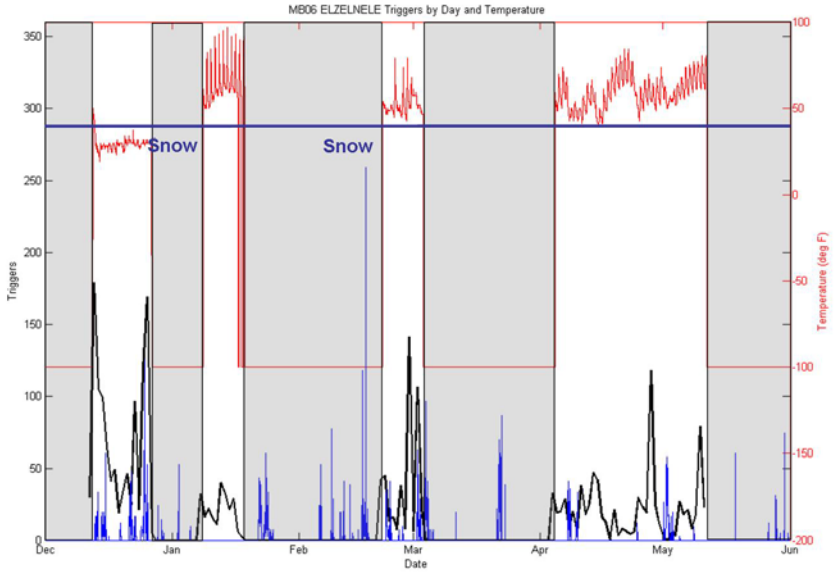

Figure 53. MB06 triggers per day compared with temperature (red) and precipitation (blue). Station shutdowns shown as gray boxes.

5.2.3 Talus near Rock Wall, Partially Shaded

Two geophones (MB02 and MB07) were placed at a low point between two talus piles very near the rock wall. Both stations suffered from severe instrumentation noise, especially MB07, of which of 64% of its initial triggers were due to internal noise. The average triggering rate at MB02 is 1.5 triggers per hour, which is four times lower than the hot sun Michael's Ledge location, but the same as the shady Michael's Ledge geophone. However, at MB07 the average rate is only 0.4 triggers per hour, which might be partially due to bad data issues during the most active part of the season. The triggers at this location appear to be correlated with sun exposure between 7am and 3pm (Figure 54). There is a correlation with winter storms as well, with most triggers happening during, but not necessarily after large storms (Figure 55 and Figure 56). The lack of triggering post-storm is consistent with observations that the valley floor stays colder than the cliffs due to tree coverage and a winter temperature inversion that develops when cold air sinks and pools in the valley. Thus, the lack of freeze-thaw triggers may reflect a lack of thawing inside cracks that are kept cool by surrounding rock and snow.

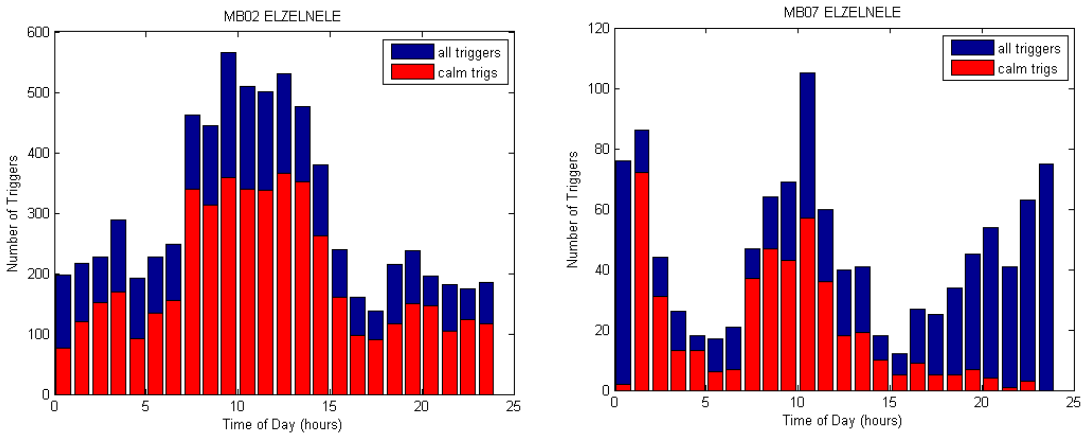

Figure 54. Station triggers at MB02 (left) and MB07 (right), which are located on a talus slope.

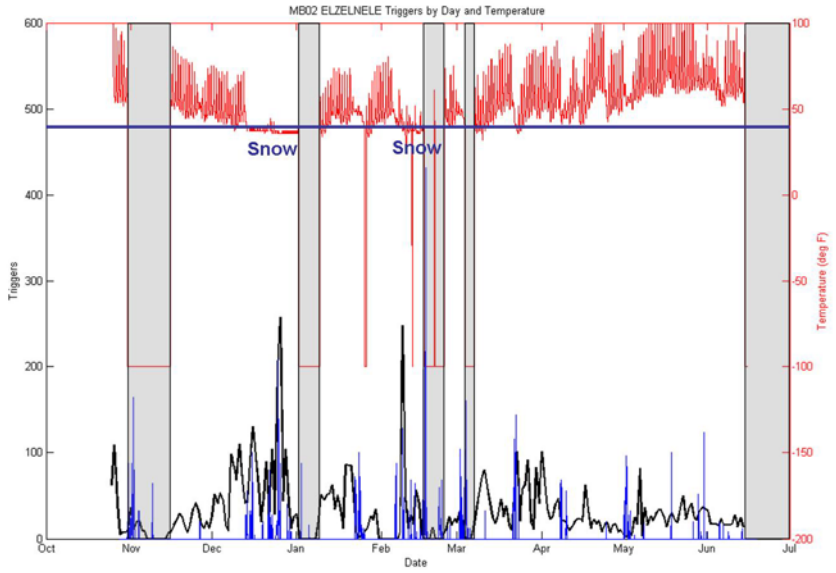

Figure 55. MB02 triggers per day compared with temperature (red) and precipitation (blue). Station shutdowns shown as gray boxes.

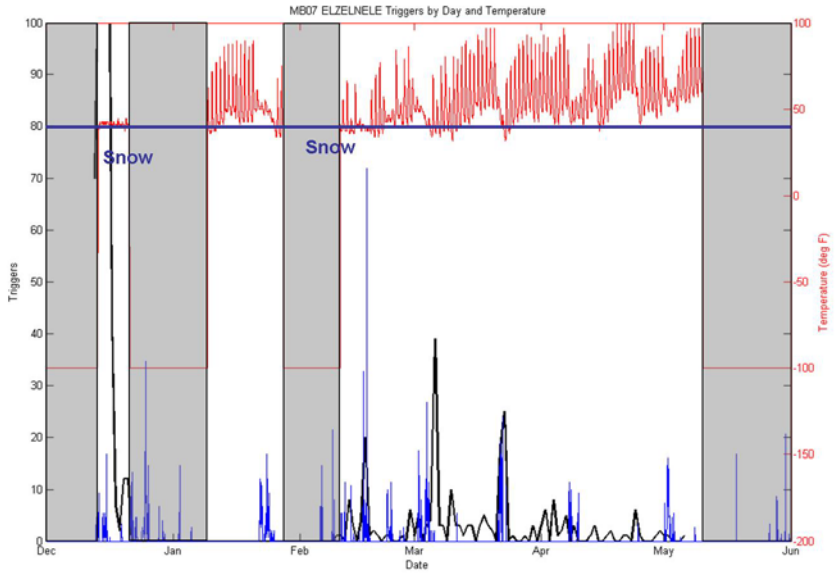

Figure 56. MB07 triggers per day compared with temperature (red) and precipitation (blue). Station shutdowns shown as gray boxes.

5.2.4 Yosemite Valley Away from Cliff, Partially Shaded

Station GH08, located in Yosemite Valley away several hundred meters from the nearest cliff, was equipped throughout the winter and the spring with an accelerometer and three barometric microphones. In the late spring the accelerometer was switched for a geophone. Batteries supplied the power and there was no solar panel until the late spring, thus power outages at this station have nothing to do with cloud and snow cover. This station experienced some instrumentation noise. The accelerometer, like the one on Michael's Ledge, was quieter than the geophone, recording only 0.1 triggers per hour or 142 total triggers. This instrument, especially, seems to be strongly correlated with time of day (Figure 57), but less so with snow events (Figure 58).

The geophone, installed in May, had no instrumentation noise and a low number of triggers (190) and triggers per hour (0.26) for the month in which it was running. This geophone does not show good correlation with daytime hours (Figure 59), and none with precipitation events (Figure 60). The low triggering rate and lack of temporal correlation is not surprising, considered that the main drivers for triggers at other geophones appear to be winter storms and a freeze-thaw cycle, which would be nonexistent in May.

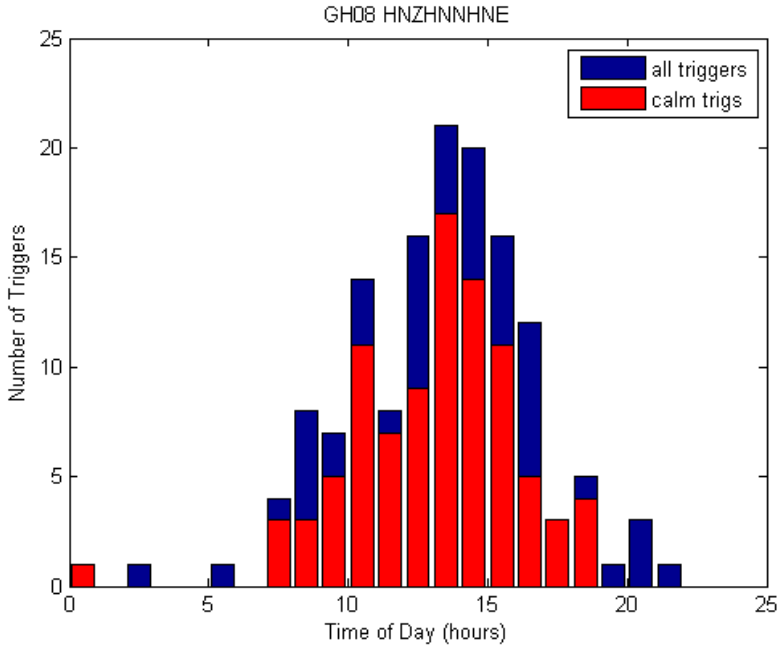

Figure 57. Station triggers at GH08.HNZHNNHNE, located in Yosemite Valley.

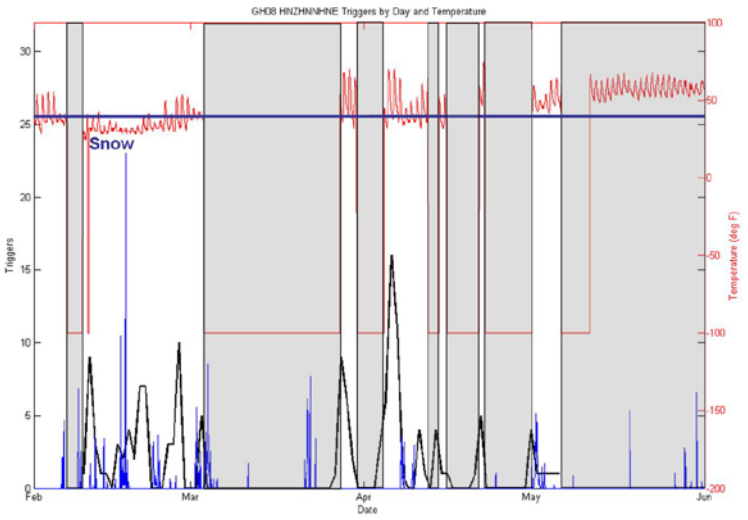

Figure 58. GH08.HNZHNNHNE triggers per day compared with temperature (red) and precipitation (blue). Station shutdowns shown as gray boxes.

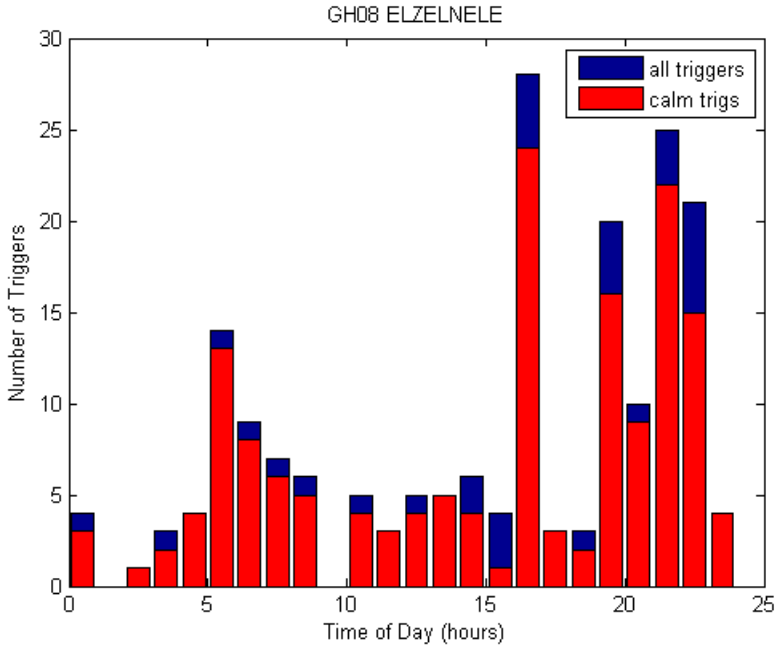

Figure 59. Station triggers at GH08.ELZELNELE, located in Yosemite Valley.

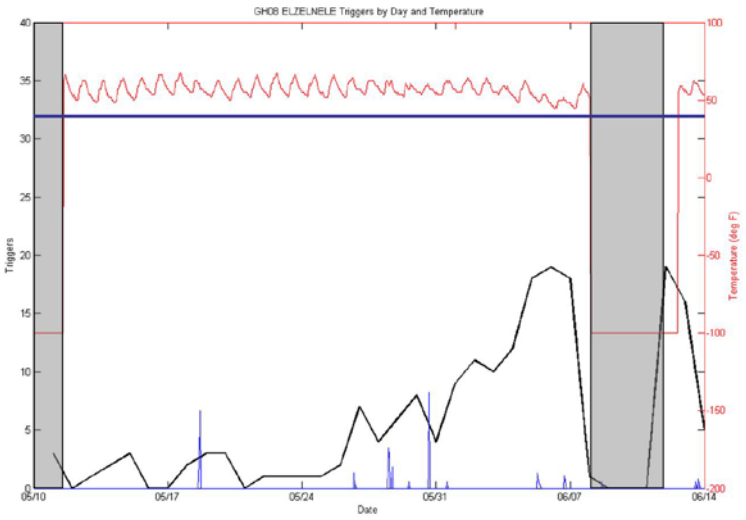

Figure 60. GH08.ELZELNELE triggers per day compared with temperature (red) and precipitation (blue). Station shutdowns shown as gray boxes.

The barometric microphones were attached to the station for the duration, but at times only two of the three microphones were working. The number of operational hours for two or more microphones is roughly double the number for all three microphones. However, the number and rate of two microphone triggers (5731 and 2.7 trigs/hr.) is eight times greater than three microphone triggers (702 and 0.64 trigs/hr.). Neither set shows a correlation with time of day (Figure 61), but both show a correlation with winter storms. This implies that the source of most triggers is winter weather, and not the other known infrasound sources such as larger waterfalls.

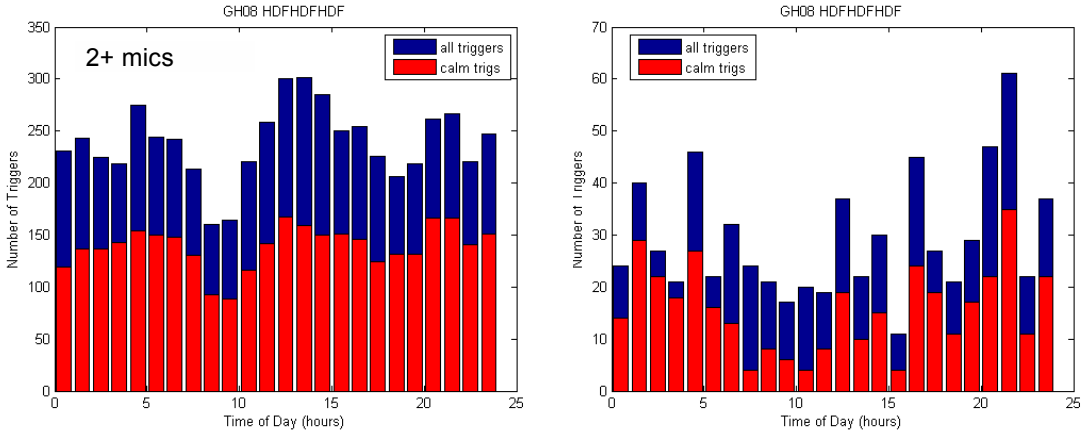

Figure 61. Station triggers at GH08.HDF, located in Yosemite Valley, for two or more microphones (left) and for three microphones (right).

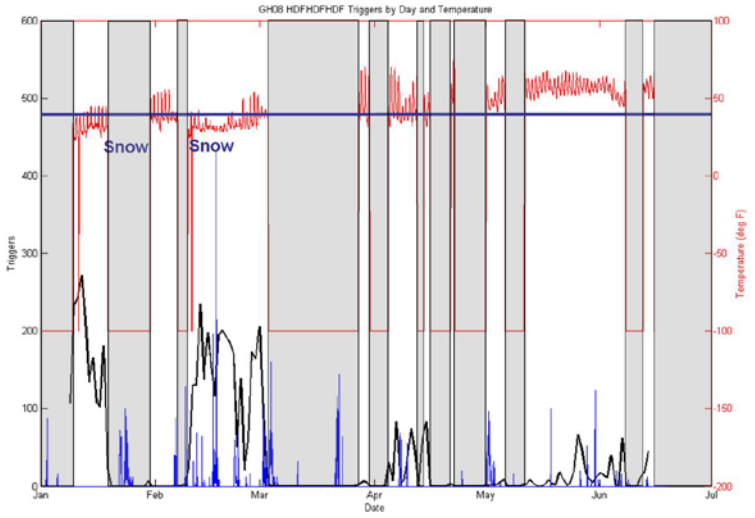

Figure 62. GH08.HDF triggers per day, for two to three HDF sensors, compared with temperature (red) and precipitation (blue). Station shutdowns shown as gray boxes.

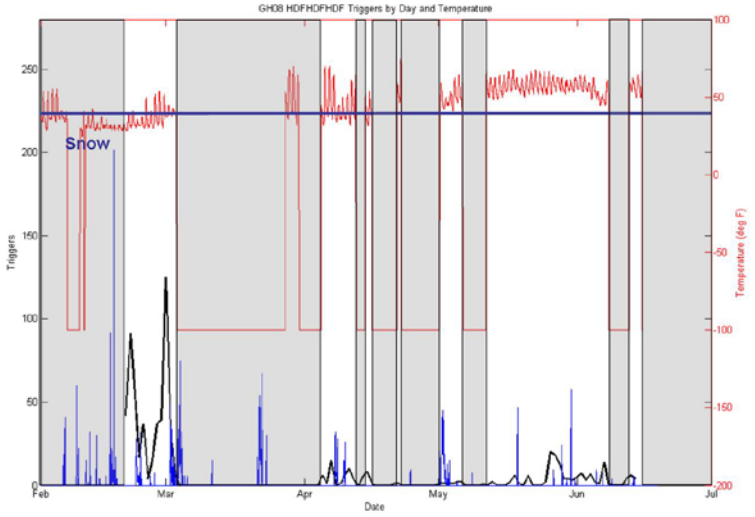

Figure 63. GH08.HDF triggers per day, for three HDF sensors, compared with temperature (red) and precipitation (blue). Station shutdowns shown as gray boxes.

5.2.5 Summary

All stations and sensors (geophones, accelerometers, and barometric microphones) with the exception of the very quiet and well-protected accelerometer at MB04 show significant correlation between triggering rates and winter storms. The two geophones at the warmest location recorded four or more times as many triggers as the others, and most of the triggers occurred at night following a winter storm. Therefore, most of the triggers at warm, sun-exposed locations are correlated with refreezing of snow and ice on warm days following a winter storm. In contrast, the other geophones in shady locations recorded the highest rates of triggering during the storms and also during the warmest hours of the days. These driving factors appear to be storm activity in the form of precipitation or wind and then snow avalanches caused by daytime melting.

A third possible explanation for some of the triggers is thermal deformation of the rock itself. If this is the case, then more events should be recorded on days with a greater thermal gradient. Data plotted in Figure 64 show the opposite pattern; the only days recording an above normal number of triggers are winter days with average or even low temperature differentials; in contrast, summer days with higher temperature differentials have relatively few triggers. The source of the seismic anomalies is not thermally driven rock deformation and instead is due to winter storms and the subsequent melting and freezing of snow and ice.

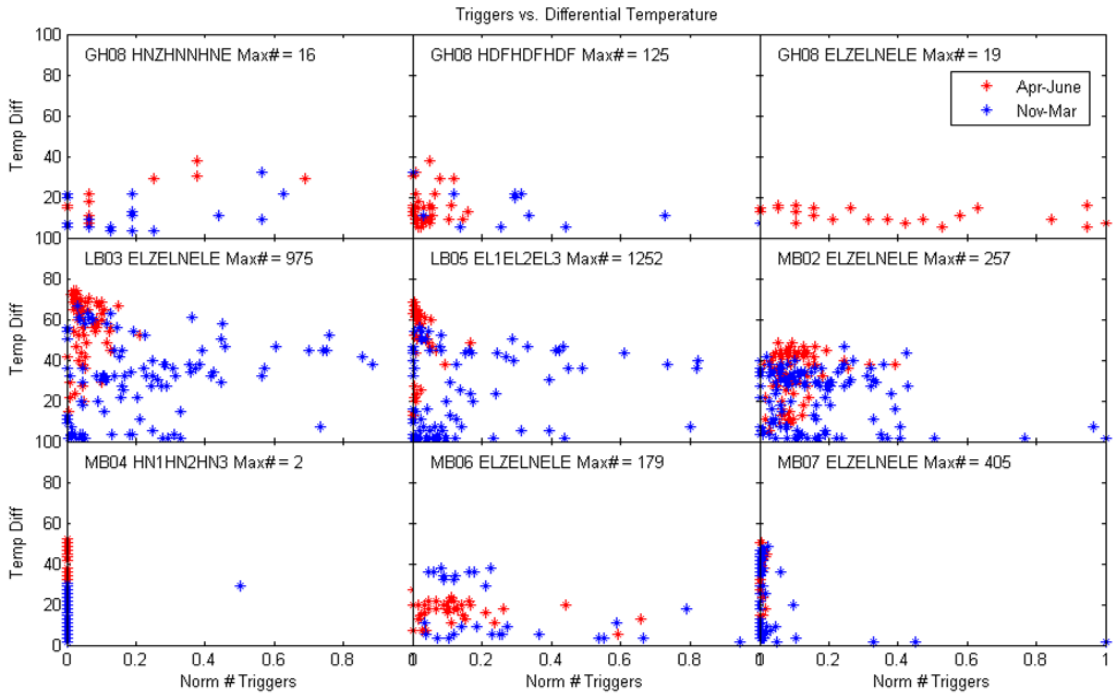

Figure 64. Normalized number of triggers per day vs. differential temperature recorded in the datalogger. The maximum number of triggers per day is listed for each station. Blue stars are days winter months (November – March) and red stars are summer months (April-June).

5.3 Conclusions on Instrument Response to Daily Changes

The purpose of this chapter is to document anomalous instrument response over time and determine whether or not that instrument response is related to rock falls. The two types of anomalous instrument response are daily drift, which we hypothesized might be tilt due to rock deformation, and changes in the number of triggers. The three main sources of triggering rate changes are refreezing of snow and ice that melting in the days following a storm, triggers generated from precipitation and wind during a winter storm, and daytime warming leading to small avalanches of snow and ice. The changes in triggering rate do not appear to be related to rock deformation unless that deformation is occurring due to freezing inside cracks, which can cause of rock falls. Thus, cliffs that collect snow and ice and are then exposed to warm sun have a strong freeze-thaw pattern that can be detected by nearby seismic sensors.

The daily instrument drift is certainly correlated with thermal changes, but whether the record reflects thermal changes in the rock or in the instrument itself is difficult to distinguish. The accelerometer affixed directly to the rock wall in a shady location presents the strongest case that thermally driven rock deformation is causing the instrument to tilt early in the morning when sun rises. However, the evidence is far from conclusive since there are geophones on sandy ledges, also in shade, that do not have this pattern. The difference in instrument type or placement, attached directly to the rock instead of placed on a sandy ledge, may be responsible for this difference. For further study of the daily drift, it is recommended that control stations be installed directly to the rock face in both cool and warm locations on the same cliff face with temperature and light-detection equipment at the sensor (rather than datalogger).

6 Detected and Reported Rock Falls

Rock falls recorded by the local seismic network are discovered either by searching for and finding an event reported by eyewitnesses, or through manual review of data selected by a triggering algorithm. The reported events are especially important since they provide valuable data that can be used to design processing methods and the triggering algorithm. It is unknown what percentage of rock falls over a certain minimum size goes unreported. There are, however, more reported rock falls near Yosemite and Curry Village, which happen to be highly populated areas with a larger number of potential witnesses. It follows that there are likely to be rock falls occurring in sparsely populated areas and in the middle of the night that go unreported. A seismic network was installed at the unpopulated but historically active Three Brothers area for the purpose of rock fall monitoring. The goal of the study was to learn as much as possible by monitoring rock falls at close range. The first step was to identify rock fall signals out of the thousands of seismic events that triggered.

6.1 Trigger Review Process

The triggering algorithm is intended to highlight times when a seismic event occurs that may be caused by a rock fall. In order to make a final determination of the seismic source, the full waveform data must be reviewed manually and compared to known rock fall and noise events, which is impractical to do for the entire dataset. Thus, only data picked by the triggering algorithm are candidates for full waveform review.

The total number of recorded triggers is large, even after elimination of single station triggers, instrumentation noise, and known earthquakes. There still remain 30 “network” (e.g. both instruments) and 539 geophone-only triggers from Phase 1, and 989 wide-network (e.g. more than one location) triggers from Phase 2. However, not all of these triggers are equally likely to be rock falls. There is variability in the total number of stations and the overall percentage of stations detecting each trigger. Furthermore, many are known to be occurring during heavy rain and winter storm events. Triggers with a high total number or high percentage of stations triggering were marked for full waveform review. With discretion, additional triggers were also reviewed, such as those occurring during otherwise quiet periods. Slightly different criteria were applied during Phase 1 and Phase 2 due to network configuration differences.

6.1.1 Phase 1

The instrumentation during Phase 1 consisted of one station with two instruments. If both instruments triggered, it was categorized as a "network" trigger. Overall, there were 121 recorded network triggers and 592 geophone-only triggers. Earthquakes were responsible for one network trigger and 53 geophone-only triggers. Instrumentation noise was responsible for 91 network triggers, suggesting that having two sensors on a single datalogger may not be the ideal situation since both instruments will record the same datalogger-noise events and thus, trigger. Three triggers were known to be associated with December 18th, 2007 Middle Brother rock fall, leaving 26 remaining network triggers to be investigated. The reported December 19th, 2007 Middle Brother rock fall was not picked up by the accelerometer and therefore did not trigger the network, suggesting that some of the 539 remaining geophone-only triggers ought to be reviewed. All of the network triggers were either eliminated as known events or reviewed (Table 8), and 85 of the 539 remaining geophone-only triggers were also reviewed, with discretion, usually during periods of calm weather or when rock falls were known to have occurred.

Table 8. Triggers during Phase 1 LB01 installment.

Sensor	**Accelerometer**	**Geophone**	**Network**	**Triggers**
Z / 1	838	1856	**Total**	121
N / 2	344	1887		
E / 3	340	1504		
All 3	**178**	**713**	MB Rock Fall	3
Non-Network	57	592	Instr. Noise	91
Inst. Noise/EQ	NA	53	Earthquakes	1
Remaining	NA	**539**	**Remaining**	**29**
Checked	**31**	**85**	**Checked**	**31**

6.1.2 Phase 2

The seismic network in operation during Phase 2 recorded 989 wide-network, non-earthquake triggers. This is still too high of a number to review all, but some triggers are more likely to be scientifically interesting than others. The total number of stations in operation at any given time is variable due to staggered installation and removal of stations, and power outage problems during snowstorms. Details about station operation for Phase 2 can be found in Appendix A. In summary, there were stations in operation in at least two different locations for 201 out of 230 days (87% of the time) and at three different locations for 127 (55% of the time) days. Thus, for the majority of the time of the deployment, large seismic events would have been captured as a wide-network trigger and the rock fall search efforts were focused on these events. Even so, there remained a large number of triggers to review, and criteria were needed to decide which triggers have priority for review. The applied criteria are listed as follows:

1. All triggers recorded at four or more stations (57).

2. All triggers recorded at three stations if 100% of stations triggered, unless the 3rd station was co-located with another high quality station (17).
3. All triggers recorded at two or three stations and with durations greater than 8 seconds.
4. Any triggers proximal to other (previously reviewed) triggers and thus, quick to review.
5. A few additional points, with discretion. For example triggers known to have occurred during times of calm weather were often reviewed.

In the end, a total of 181 of the 989 network triggers (18%) were reviewed manually, with the breakdown shown in Table 9.

Table 9. Breakdown of triggers recorded and reviewed.

Number of Stations Triggering		**4+**	**3**	**2**	**Total**
Total	Triggers	57	229	703	989
	Reviewed	57	34	88	181
100% triggering	Triggers	57	51	183	291
	Reviewed	57	17	73	147

6.2 General Discussion of Triggered Event Classification and Rock Fall Detection

The differentiation of rock falls from other events is an iterative process, starting with an examination of seismic data generated by known events such as reported rock falls, wind, rain, snowstorms, earthquakes, and small rock tossing experiments. During this process, it was discovered that rock falls strongly excite frequencies in the 1-20 Hz range, have strong, short duration impacts, and an overall duration that can last many tens of seconds. Furthermore, some rock falls have an initial weak low frequency (< 40 Hz) signal followed by the impacts with frequency response up to 200 Hz at close range. This signature helps to distinguish rock falls from other events. For example, rain primarily excites high frequencies (>100 Hz) and has a very short duration. Wind resonates in many different frequency bands, mostly greater than 20 Hz and has an emergent onset. Earthquakes excite the lower (< 20 Hz) frequency band, do not have strong individual impacts, and have a distinct, two-part P and S-wave signal where both parts are remarkably similar in their spectral response strength, especially on the Z component. Anthropogenic noise is usually accompanied by engine vibration and tends to have strong but narrowband frequency response over many hours.

After review, the events were classified as one of the following: rock fall, possible rock fall, coincidental noise (usually rain), anthropogenic noise, probable wind, earthquake, weak Low Frequency Event (weak LFE), strong Low Frequency Event (LFE), impact pulse, and miscellaneous unknown events. The LFEs are of unknown origin, but are common events repeated in similar scenarios that deserve a closer look. The typical LFE has a five to ten second duration and a frequency response from 4.5 Hz (the geophone corner) to 20 Hz. In contrast, nearby rock falls have a more broadband frequency response, and more distant rock falls that are detectable are larger and thus have a longer duration. Although it is not suspected that rock falls are responsible for the LFEs, this data is included since a definite source has not yet been attributed to these events. The following sections present some of the rock fall and LFE events. Other seismic sources, such as earthquakes and rain, are discussed in Chapter 7.

6.3 Detected Rock Falls of High Certainty

Rock falls recorded by the local seismic network are discovered either by searching for and finding an event reported by eyewitnesses, or through manual review of data selected by a triggering algorithm. The successful (or unsuccessful) capture of a reported rock fall helps to assess the probability of seismic detection in terms of rock fall size, distance to the event, and instrument type. In general, only rock falls in the very near vicinity of the station (< 1 km) are detectable unless the rock fall is exceptionally large. On average, rock falls occur approximately once a week in Yosemite Valley (Stock et al, 2011b, in prep.) but most of those rock falls are very small events in locations far from the seismic network, with variability in the reliability of the witnesses and estimated time. Therefore the seismic data was searched only for very large or very near rock falls.

Fortuitously, the first significant series of at least five Middle Brother rock fall events occurred just a few hundred meters away and started one week after the Phase 1 station (LB01) was installed. In addition, there were two Phase 1 and three Phase 2 small rock falls reported at Cathedral Rocks approximately 2.5 km to the south and across the valley. Also reported during Phase 2 were one additional Three Brothers rock fall, three Yosemite Village rock falls 2.5 to 4 km away, and one very large rock fall accompanied by at least five medium rock falls at Ahwiyah Point 4.5 – 6.7 km away.

After reviewing hundreds of triggers deemed have a high probability of being attributed to a rock fall, four to nine unreported rock falls and five more reported rock falls which had previously not been noticed in the dataset were discovered. In addition to the rock falls, several low frequency events (LFE) of unknown origin were found that do not resemble the known rock falls, but which are known to be local, Yosemite Valley events. The reported and discovered rock falls are listed in Table 10 for Phase 1 and Table 11 for Phase 2. Black lettering designates detected events, red lettering reported but undetected events, and blue lettering detected, unexplained events. Previously reported detected rock falls are colored blue, unreported detected rock falls yellow, and unreported possible rock falls orange.

Table 10. Rock falls and other events detected by sensor network and reported by eyewitness during Phase 1.

Reported RF, not detected		Detected RF, unreported	Possible rock fall	
Reported RF, detected		Anomalous, unexplained origin		
Event Type	**Date/Time, Local**	**Location**	**Reported?**	**Detected?**
Phase1				
Rock fall, medium	12/18/07 16:00	Middle Brother	Yes	Yes
Rock fall, small	12/18/07 16:20	Middle Brother	Y, in pm	Yes
Rock fall, small	12/18/07 17:42	Middle Brother	Y, in pm	Yes
Rock fall, small	12/19/07 15:28	Middle Brother/Camp 4 Wall	Y (15:32)	Yes
Rock fall, small	12/25/07, after dark	West of Camp 4	Y, after dark	No
Rock fall, small	1/4/08 18:33	Middle Brother	Y (19:00)	Yes
Rock fall, small	1/8/08 10:17	Middle Brother	Yes	Yes
Rock fall, small	1/27/08 7:30	Middle Brother?	Yes	Maybe (1539)
Rock fall, small	2/28/08 15:55	Middle Brother?		Yes
Possible rock fall	3/10/08 13:26	??		Yes
Possible rock fall	3/11/08 15:38	Middle Brother		Yes
Rock fall, small	3/13/08 15:30	Cathedrals	Yes	No
Pulse -> unknown	4/1/08 17:17	Middle Brother?		Yes
Possible rock fall	4/3/08 15:07	Middle Brother?		Yes
Possible rock fall	4/6/08 0:28	Middle Brother		Yes
Possible rock fall	4/7/08 12:12	Middle Brother		Yes
Rock fall, small	4/23/08 9:00	Lower Cathedral	Yes	No

Table 11. Rock falls and other events detected by sensor network and reported by eyewitness during Phase 2.

Event Type	Date/Time, Local	Location	Reported?	Detected?
Phase2				
Rock fall, small	10/26/08 8:00	Cathedrals?	Yes	No
Rock fall, small	10/31/2008 14-14:30	Middle Cathedral	Yes	No
Rock fall, small	11/1/2008 15-16:30	Middle Cathedral	Yes	No
Rock fall, medium	12/15/08 2:24	Middle Brother?		Yes
Rock fall, v. small	12/20/08 21:33	Middle Brother		Yes
LFE-> snow/ice (STORM)	12/26/2008 2:27-05:16	Middle Brother?		Yes, many
Probable rock fall	1/14/09 21:21	Middle Brother		Yes
Rock fall, medium	1/17/09 13:54	Three Brothers - Eagle Creek	Yes	Yes
LFE-> snow/ice (3-day post storm)	1/28/09 10:21	?		Yes
Rock fall, medium	1/29/09 17:15	Ahwahnee Superslide	Yes	No
LFE-> snow/ice (STORM)	3/3/09 6:49	?		Yes
Rock or snow?	3/4/09 5:20	Yosemite Village	Yes	No
Rock fall, small	3/28/09 0:15	Ahwiyah Point	Yes	No
Rock fall, v. large	3/28/09 5:26	Ahwiyah Point	Yes	Yes
Rock fall, medium	3/28-29/09 multiple	Ahwiyah Point	Yes	No
Rock fall, medium	3/29/09 14:00	Ahwiyah Point	Yes	No
LFE-> human?	4/6/09 21:20 - 22:13	?		Yes, many
LFE-> human?	4/7/2009 9:05-12:28	?		Yes, many
LFE -> unknown	4/15/09 14:25	?		Yes, many
Rock fall, medium	4/18/09 10:40	Ahwiyah Point	Yes	No
Rock fall, small	5/3/09 0:00	Glacier?	Yes	No
Rock fall, small	05/3/09 11-13:00	Ahwiyah Point	Yes	No

The fact that no rock falls at locations other than the Three Brothers were detected, except for the very large Ahwiyah Point event, helps to understand the limits of seismic monitoring. At least five events at Cathedral rocks were not detected only 2.5 km away but across the valley. The farthest detected rock fall, other than Ahwiyah Point, is the Eagle Canyon event less than 1 km away but on the other side of the Three Brothers. This rock fall was described as being loud and lasting many tens of seconds, which may indicate that it is a medium-sized event, but it does not stand out from closer, smaller events and may not have been detectable at twice the distance. However, this dataset is too small to derive any significant statistical result.

Spectrogram plots can help to show the similarities and differences between different rocks falls and between rock falls and other events. Seismic data were manipulated in Matlab using the waveform suite to produce the spectrogram plots (Reyes and West, 2011). Six examples of rock falls from different source areas, of different sizes, and distances ranging from a few hundred meters to nearly seven kilometers have been chosen in order to compare their spectral responses. The first example chosen is the Ahwiyah Point rock fall, a very large (46,000 m^3) rock fall recorded at a distance of 6.5 km. The spectrogram record reveals a distinct two-part signal. The detachment/falling part of the record (25 s on Figure 65) starts ten seconds before the main impact (35 s) with a strong frequency response from 5–12 Hz. The frequency response of the impact signal is much stronger and bleeds into higher frequencies, up to 50 Hz, but is similar to the detachment in that the dominant part of the response is in the same 5 - 12 Hz band. The duration of this signal is well over one minute, an indicator of both the size and the fall distance of the rock fall.

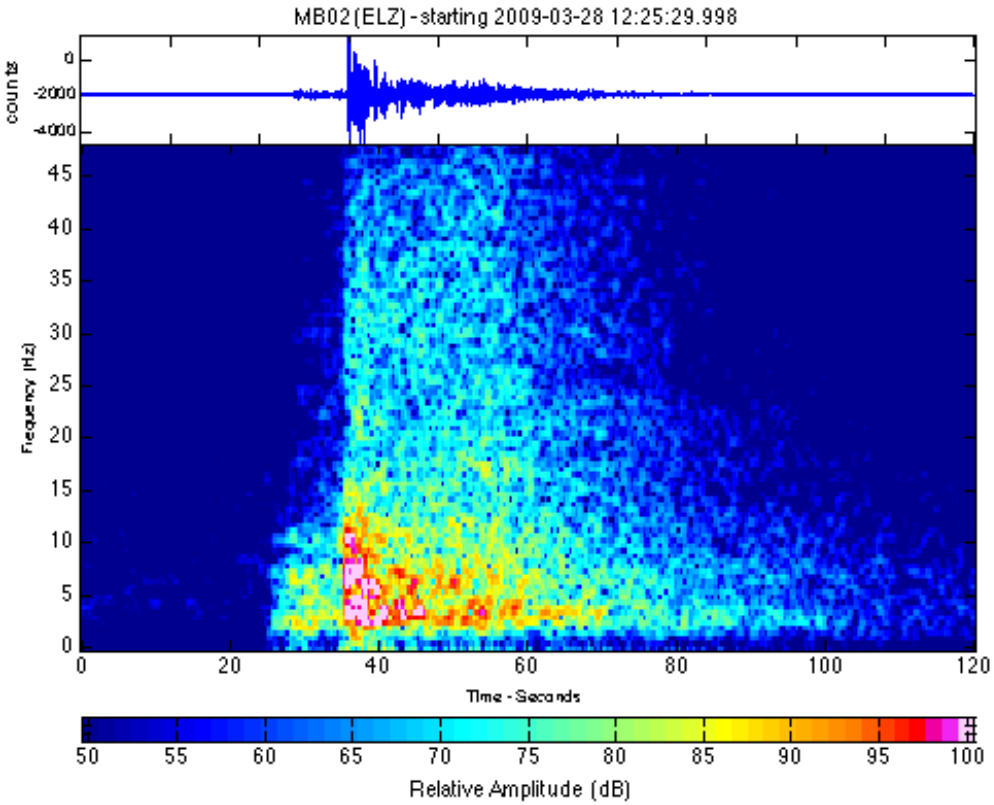

Figure 65. Reported very large Ahwiyah Point rock fall on March 28th, 2009, showing detachment (25 s) and impact (35 s) signals.

The Ahwiyah Point event is the only recorded rock fall known to be originating from a source area other than the Three Brothers, a testament to the size of the event. When the Ahwiyah Point rock fall (Figure 66, 1) is compared to events at the Three Brothers (Figure 66, 2-6), it is evident that frequencies greater than 40 Hz have been profoundly attenuated at a distance of only six kilometers, even for this very large rock fall.

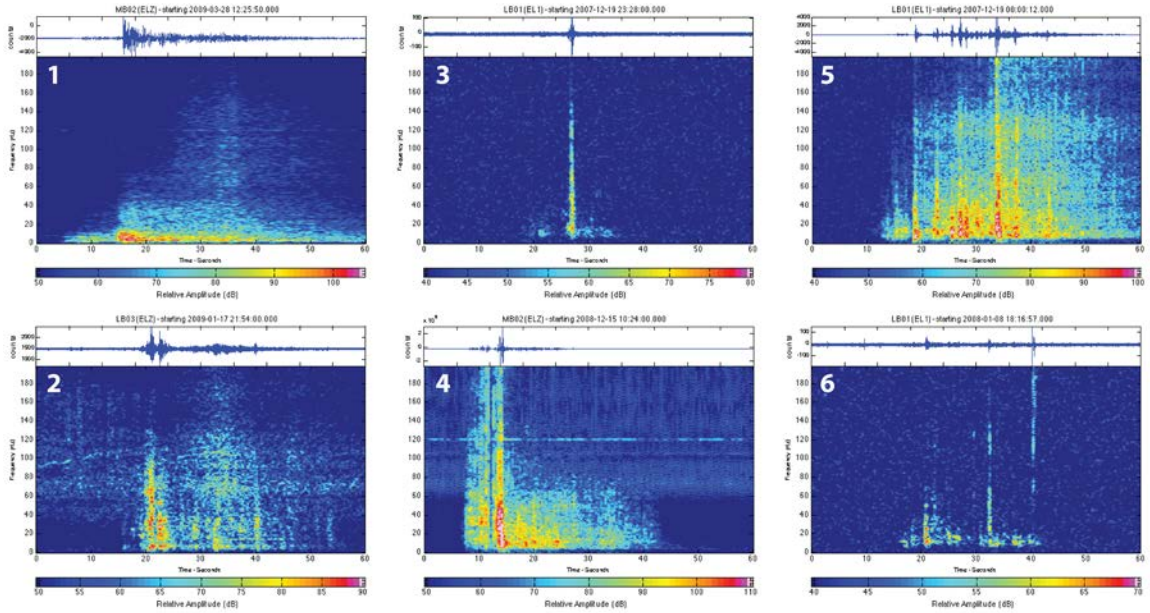

Figure 66. Six examples for rock falls. 1 – Ahwiyah Point rock fall, very large, at 6.5 km. 2 – Eagle Canyon rock fall, medium, opposite side and west of the Three Brothers at < 1 km. 3 – Middle Brother/Camp 4 wall rock fall, small, from far east source area, 800 m. 4 – Middle Brother rock fall, small-medium, from far west source area, 300 m. 5 – Middle Brother rock fall, medium, from central source area, 600 m. 6 – Middle Brother rock fall, small, from central source area, 600 m.

The Eagle Canyon rock fall (Figure 66, 2) is the second-farthest detected event. Although this rock fall is less than one kilometer from the nearest seismic station, it is on the opposite side and west of the Three Brothers. It occurred after dark, but was reportedly heard as a loud event that lasted many tens of seconds, which may indicate that the rock fall is medium in size. This rock fall shows several distinct impact events with a strong spectral response up to 100 Hz. However, in comparison with closer rock falls (Figure 66, 4-5), a dampening of the higher spectral frequencies is noticeable. There may also be a very weak pre-impact signal, although it is not distinct or certain.

The Middle Brother/Camp 4 wall rock fall (Figure 66, 3) was witnessed as a small rock fall originating from the far eastern Middle Brother source area. This rock fall had a single impact with a strong spectral response up to 150 Hz, and a distinct but weak pre-impact signal starting seven seconds before the impact. Also interesting is that the pre-impact signal is followed by a few seismically quiescent seconds before impact, possibly indicating a ballistic trajectory.

The Middle Brother rock fall on December 15th, 2008 (Figure 66, 4) is the only rock fall of the six that was not reported. However, it was detected at three different locations on both seismic and acoustic sensors, and the time difference between the seismic and acoustic arrivals indicates an impact 300 meters away, which is consistent with the top of the talus pile below the largest and most western Middle Brother source area. This event is therefore the closest rock fall of the six, and the strong spectral response below 60 Hz with some energy up to and probably greater than 200 Hz is a result of the lack of geometric seismic attenuation at such close range. The event shows a gradual increase in energy before the very strong impact, and then thirty seconds of lower energy impacts before coming to a rest.

The next two rock falls (Figure 66, 5-6) were both witnessed originating from the central Middle Brother source area 600 meters from the seismic station. The first event (Figure 66, 5) is a medium-sized rock fall that damaged the road and was the first and largest rock fall in a two and a half month series of rock falls from the same source area. This event starts with a six second, lower energy, lower frequency (< 40 Hz) signal associated with detachment and falling, followed by twenty-five seconds of several larger impacts with response up to 200 Hz, and an eventual decrease in energy as the rocks come to a rest. The second event (Figure 66, 6) occurred three weeks later and is a part of the same series of rock falls. There are some similarities to the larger event, including a few seconds of lower energy pre-impact signal followed by a few larger impacts with strong, higher frequency spectral response. This rock fall has a very similar spacing in time to the first event in the series (Figure 66, 5), but a very different character from the other four rock falls (Figure 66, 1-4). The similarity is spectral character between two events known to have originated from the same source area suggests that their trajectories were also similar, and that additional, unreported rock falls from that source area may be identified using spectral character.

There are additional rock falls that were discovered and are listed in Table 10 and Table 11, but are not presented in detail here. Detailed analysis of rock fall events, including additional spectrogram plots and commentary, can be found in later chapters.

6.4 Impact Pulses and Low Frequency Events (LFE)

The seismic network recorded several strong unknown events at multiple stations during the course of the project. The unknown seismic events fall roughly into two categories that are described as Impact Pulses (IPs) and Low Frequency Events (LFEs). These events, when compared with rock falls, tend to share some characteristics with rock falls but are also clearly different. Yet, they do not resemble any other known seismic sources either. In addition, broadband seismic stations outside of Yosemite Valley did not detect any of them, indicating that they are local to Yosemite Valley. It may turn out that some of these events are indeed rock fall related, and in fact, most of the Impact Pulses are categorized as "Possible Rock Fall" in Table 10 and Table 11. Other proposed sources of these unknown events are icefall, snow avalanches, very small local rock impacts, and anthropogenic events resulting from nearby road construction activities.

6.4.1 Impact Pulses

There were two afternoon events on March 10th and 11th, 2008. The weather was calm and stable during this time and had been for at least a week prior. The March 10th event (Figure 67) shows a strong response lasting less than two seconds in the 5 - 50 Hz range, accompanied by two narrow band 50 and 90 Hz signals that run ten seconds before and after the pulse event. The narrow band signal may be a gust of wind, an acoustic wave, or even an engine, but it is hard to pinpoint a definitive origin. The March 11th event (Figure 68) is a short one-second duration pulse with a high frequency (up to 200 Hz) response that somewhat resembles a rock fall impact. The accelerometer weakly picked up the March 10th event but not the March 11th event.

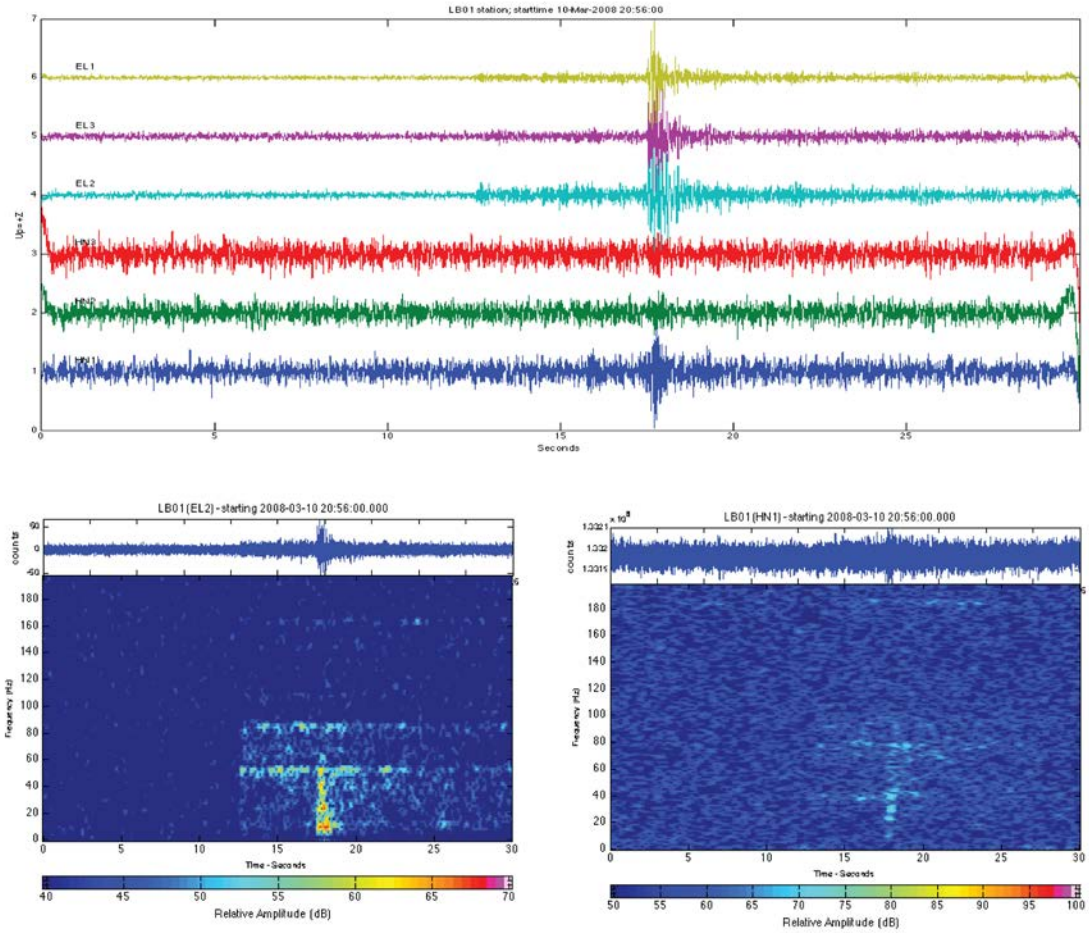

Figure 67. Possible rock fall recorded during the early afternoon on March 10th, 2008 in early afternoon, during a period of stable weather. Top, all of the geophone (top three) and accelerometer components (bottom three). Spectrogram of the geophone (bottom left) and accelerometer (bottom right).

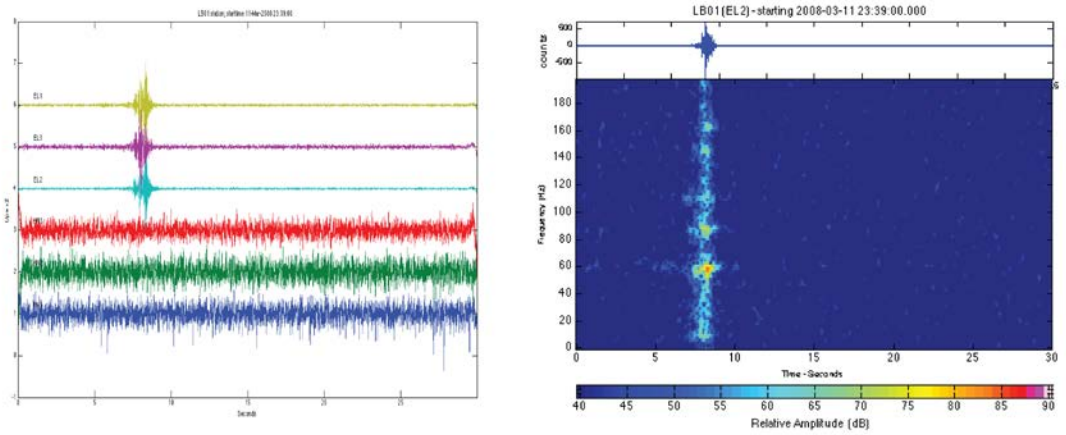

Figure 68. Possible rock fall recorded during the afternoon on March 11th, 2008 showing bleeding into higher frequencies, during a period of stable weather. Left, all of the geophone (top three) and accelerometer components (bottom three). Spectrogram of the geophone (right).

The next four events occur over a six-day period in April 2008. All occurred during the afternoon in clear weather, and none were detected by the accelerometer. These events all have several individual pulses, some of which strongly resemble the March 11th, 2008 event (Figure 69). The strongest event on April 6th starts with a large pulse with strong spectral response below 60 Hz but medium spectral response below 100 Hz and above 140 Hz, followed by several weaker pulses. (Figure 69, top right). The strong pulse somewhat resembles the strongest impact from a small rock fall originating at the closest Middle Brother source area (Figure 66, 4), but the lack of activity preceding and the spectral response following are very different.

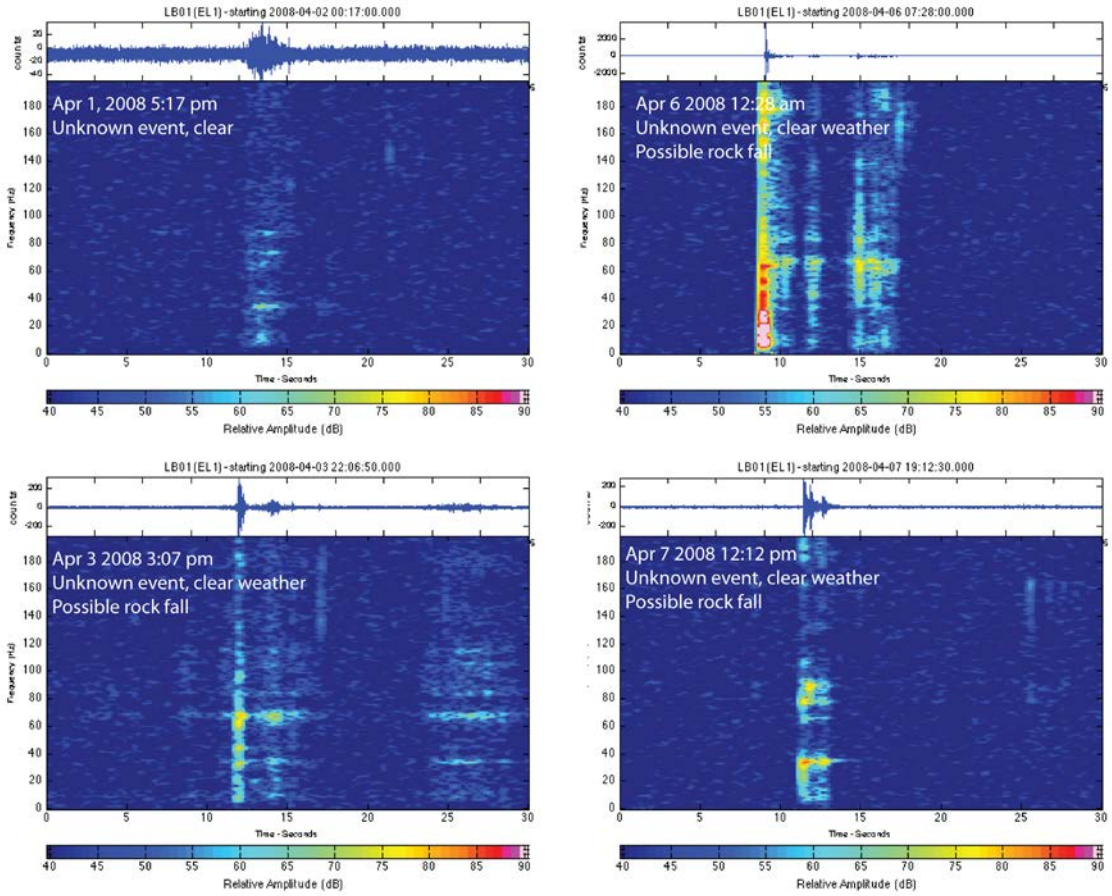

Figure 69. Impact pulses over a six-day period in April 2008. All are showing the geophone record from station LB01.

The impact pulses are the most similar to rock falls out of all the unknown events, and the event with the highest likelihood of being a rock fall is January 14th, 2009 event. In many ways, it strongly resembles Middle Brother rock falls from the central source area (Figure 66, 4-5), but 2-D location analysis places it nearer to station MB02 and the eastern source area. However, it is possible that a 3-D analysis may result in a change in the calculated location.

The other six impact pulses all occurred in mid-afternoon while the weather was clear, yet there were no reports of rock falls. Two of them occurred during a two-day period in March, and four over a six-day period in early April. None of these events strongly resemble any of the other confirmed rock falls, but their proximity in time to each another, and a lack of good alternate explanation may indicate that they are related to one another. The April events are remarkably similar to the second March event. The accelerometer did not pick up any of the five similar events, which may indicate that they are local to the geophone, although accelerometers often do not pick up weaker events. Since there is only one station operating, it is impossible to tell if these events are very small and local to the geophone or farther but still weak events. However, the lack of witnesses to any of the six mid-afternoon, good weather events leads to the conclusion that they are either not rock falls, or are very small rock falls in the near vicinity of the station.

6.4.2 Low Frequency Events

Several, strong Low Frequency Events (LFEs) occurred and were recorded at multiple stations in the local seismic network. These events do not resemble rock falls or other known seismic sources. Spectrally, they are similar to earthquakes except that they lack the two-part P and S-wave signal and are not recorded on regional seismic stations. Many of these events occur during or just after precipitation events, which may indicate that snow avalanches and icefall are the cause of at least some LFEs.

The first set of LFEs occurred on December 26th, 2008 on the fifth day of a winter storm. They typically have an initial strong, sudden 5 – 15 Hz pulse followed by gradual, ten-second tapering off of energy and higher frequencies. The 2:27 am (local PST) event is easily detected at the talus slope station (Figure 70, left) and a cliff station 300 m above and 500 m southeast (Figure 70, right). Evidence of the heavy rain and snow can be seen as higher frequency short pulses following the event (Figure 70, left). The 4:49 am event also shows evidence of precipitation (Figure 71, left) and a late-arriving higher frequency signal on the cliff station that may be an acoustic wave recorded by the geophone (Figure 71, right). The 5:16 am event appears to have two initial strong pulses in the beginning of the LFE (Figure 72).

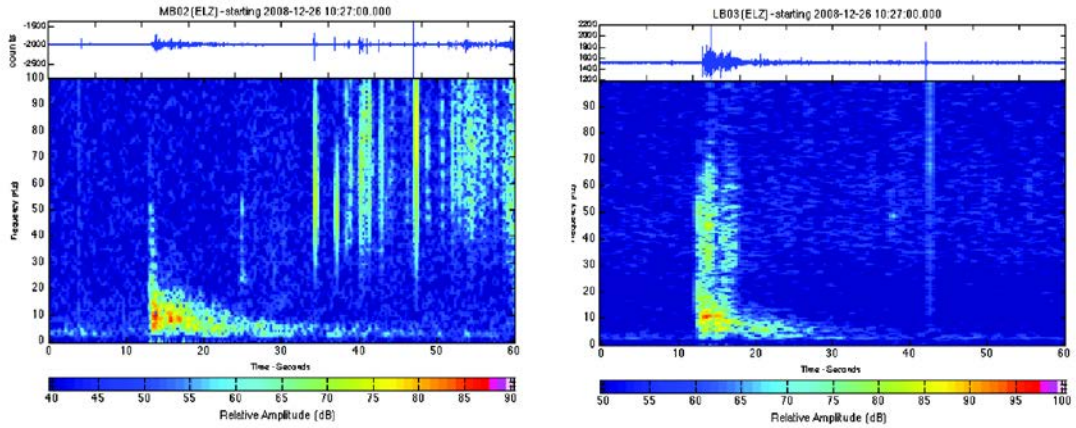

Figure 70. First strong LFE recorded during the night on December 26th, 2008 at 2:27 am local PST, during a week of stormy weather with heavy precipitation and wind from station MB02 east and on the talus (left) and station LB03 600 m southwest and 300 m high on Michael's Ledge (right).

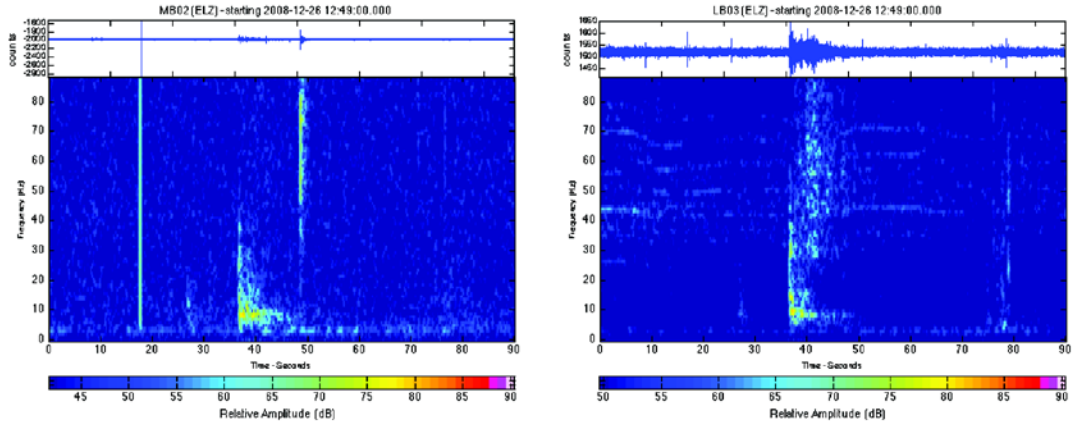

Figure 71. Second strong LFE recorded during the night on December 26th, 2008 at 4:49 am PST (38 sec), during a week of stormy weather with heavy precipitation and wind at station MB02 on the floor of Yosemite Valley (left) and station LB03 600 m southwest on a cliff 300 m high (right). Short duration, high frequency events at MB02 (left, 18 s and 50 s) are likely to be direct rain impacts on the sensor or nearby very small icefall. The higher frequency LB03 arrival (right, 40 s) may correspond to an acoustic wave arrival recorded by a geophone.

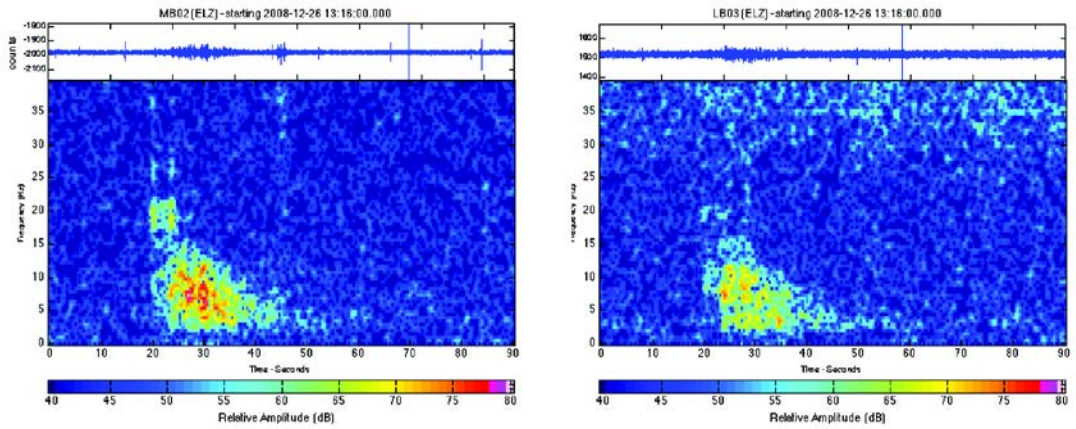

Figure 72. Third strong LFE recorded during the early morning on December 26th, 2008 at 5:16 am local PST, during a week of stormy weather with heavy precipitation and wind, from station MB02 east and on the talus (left) and station LB03 600 m southwest and 270 m high on Michael's Ledge (right).

A strong LFE with very similar character to the 5:16 am event on December 26th, 2008 occurred during the morning hours of March 3rd, 2009. This event also had two higher frequency pulses in the beginning of a strong LFE that gradually tapers off in energy over the next 10-15 seconds (Figure 73). Like the December LFEs, this event occurs during a winter storm which started at least two days prior and in the middle of a month of stormy weather. This LFE is preceded by a 5 - 10 Hz signal approximately five seconds before the first strong pulse, but it is difficult to ascertain whether this early signal is associated with the LFE or not.

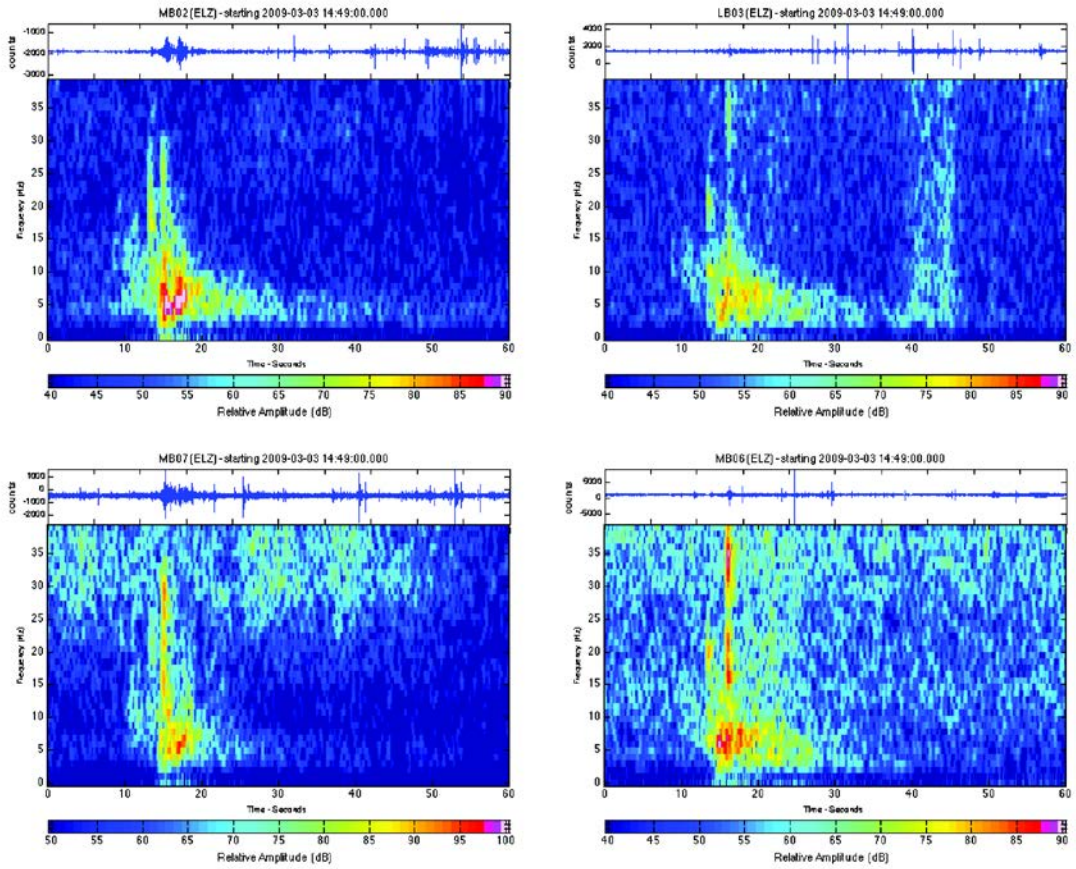

Figure 73. LFE recorded during the morning (6:49 am local PST) on March 3rd, 2009 showing response from stations on the valley floor (MB02, top left and MB07, bottom left) as well as two different cliff locations at LB03 (top right) and MB06 (bottom right).

There are LFEs with more emergent onsets and less well-defined spectral character. One example is the January 28th, 2009 LFE at 10:21 am (local PST) (Figure 74). This event occurred during calm weather, although it was only three days following the last storm cycle. Furthermore, the event at the talus station (MB02) is much stronger than at the cliff station (LB03), but the cliff station records a strong continuous signal in the 65 Hz and 90 Hz band, which may be engine noise. It is difficult, however, to say whether these two signals are related. Another example of an emergent onset LFE is the one on April 15th, 2009 at 2:25 pm (local PDT) (Figure 83). This event also occurred during a period of calm weather, although there had been a storm a week prior. There is some evidence that this event was detected two kilometers away at station GH08, although it is hard to state with certainty that the near and far detected events are one and the same.

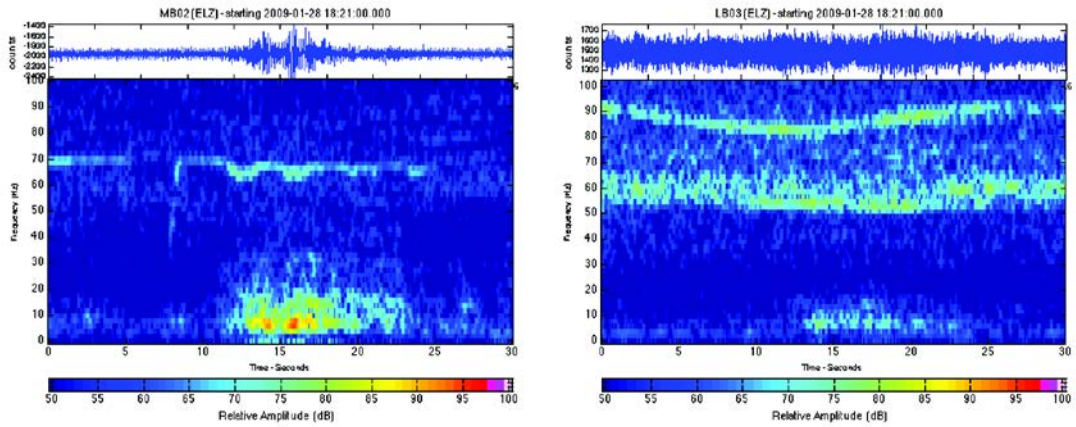

Figure 74. LFE recorded during the morning of January 28th, 2009 (10:21 am local PST) showing a strong response (11-20 s, > 20 Hz) at the MB02 station located on the valley floor (left), and a weaker response 300 m high on the cliff and 600 m southwest at station LB03 (right).

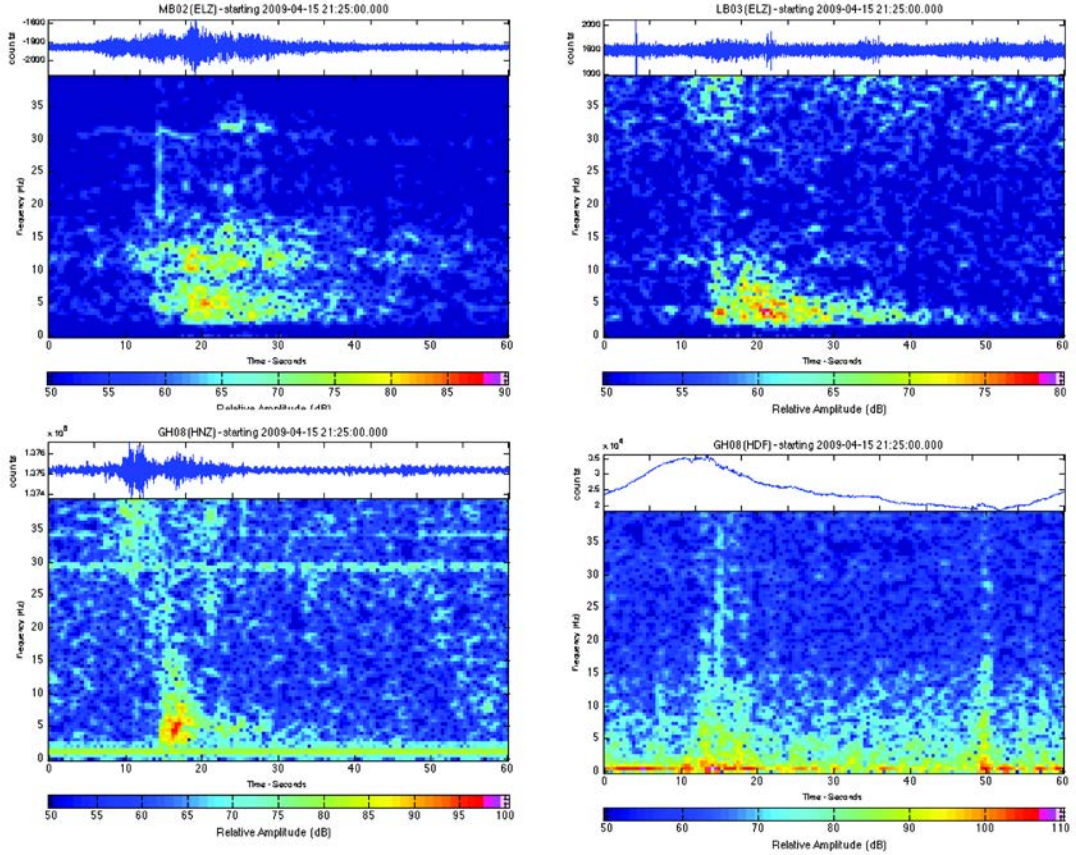

Figure 75. LFE recorded during the afternoon (2:25 pm local PDT) on April 15th, 2009 showing response from stations on the valley floor (MB02, top left and GH08 accelerometer 2 km away, bottom left), at a cliff location at LB03 (top right), and from an infrasound acoustic sensor at GH08 2 km away (bottom right).

There was a series of similar LFEs that occurred over a two-hour afternoon period on April 6th, 2009, and then another series the following day during the late morning and early afternoon. There were five geophones and two accelerometers at four different locations operating during this time. None of April 6th events were detected by either accelerometer (Figure 76), but two of the April 7th events might have been very weakly detected by the GH08 accelerometer two kilometers away. The weather was calm had had been that way for two weeks on April 6th, but a storm arrived on April 7th and the spectral records are correspondingly noisier with evidence of wind and rain.

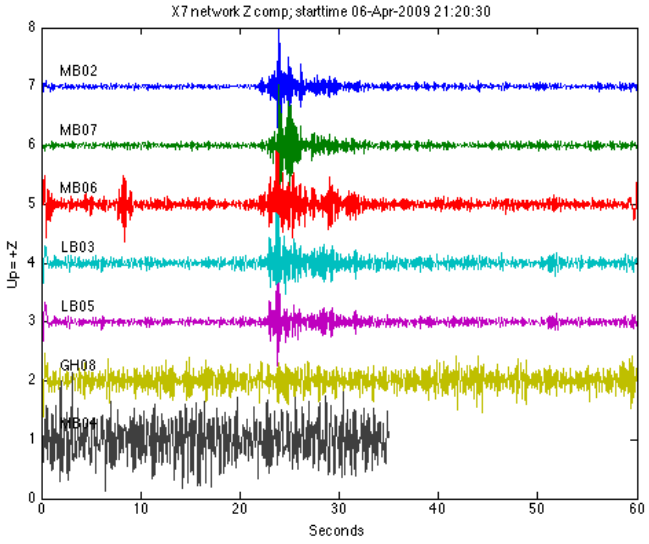

Figure 76. Filtered 2-8 Hz record showing LFE detected at five geophone stations (top five records) but not the two accelerometers (bottom two records).

The first strong LFE occurs at 2:20 pm (local PST) on April 6th, 2009. This event shares a similar spectral character to many other LFEs in that it has a strong, sudden onset in the 5 – 20 Hz band and a gradual tapering of energy over the next fifteen seconds (Figure 77). In addition, there appears to be a higher frequency arrival one second after the start of the LFE, and a constant spectral emitter at 14 Hz and higher resonant frequencies that likely correspond to a nearby engine. These characteristics are shared by the second LFE at 14:28 (Figure 78), the third LFE at 14:52 (Figure 79), and the fourth LFE at 15:13 (Figure 80). There are some other sources of noise in higher frequency bands, most likely wind associated with the approaching storm.

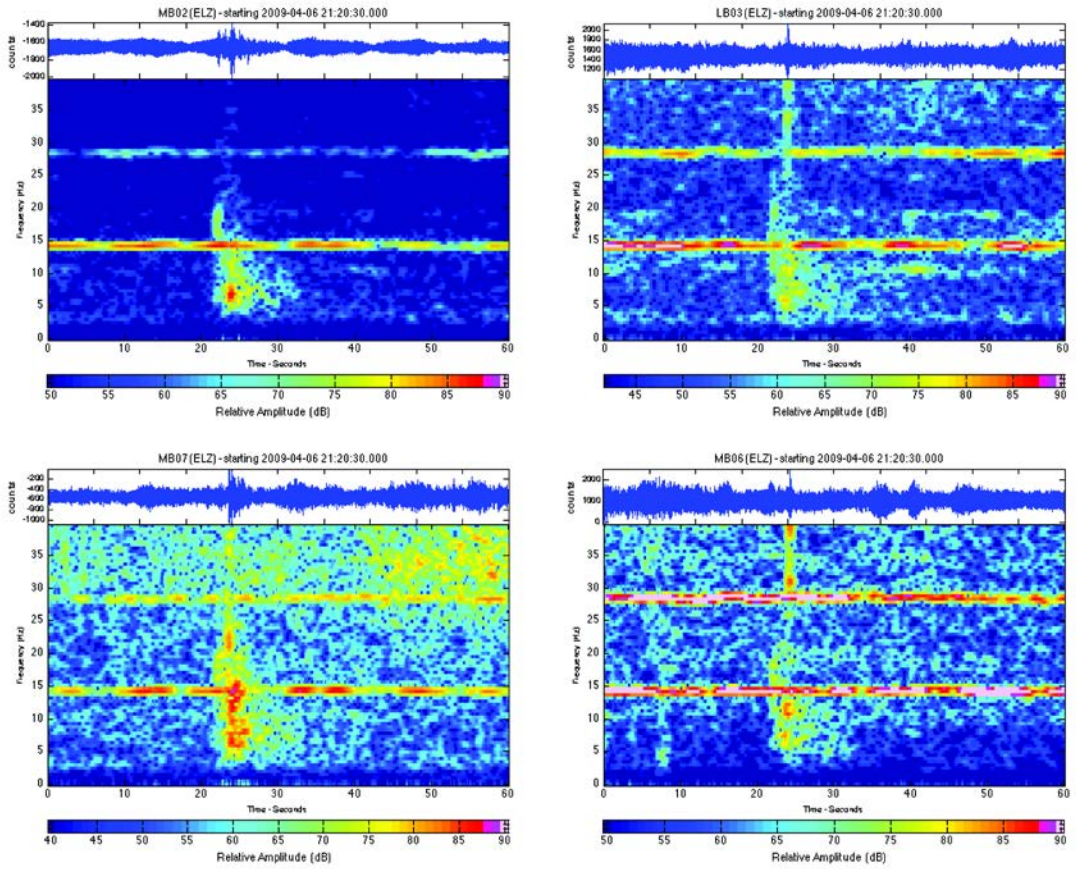

Figure 77. LFE recorded during the afternoon (2:20 pm local PDT) on April 6th, 2009 showing response from stations on the valley floor (MB02, top left and MB07, bottom left) as well as two different cliff locations at LB03 (top right) and MB06 (bottom right).

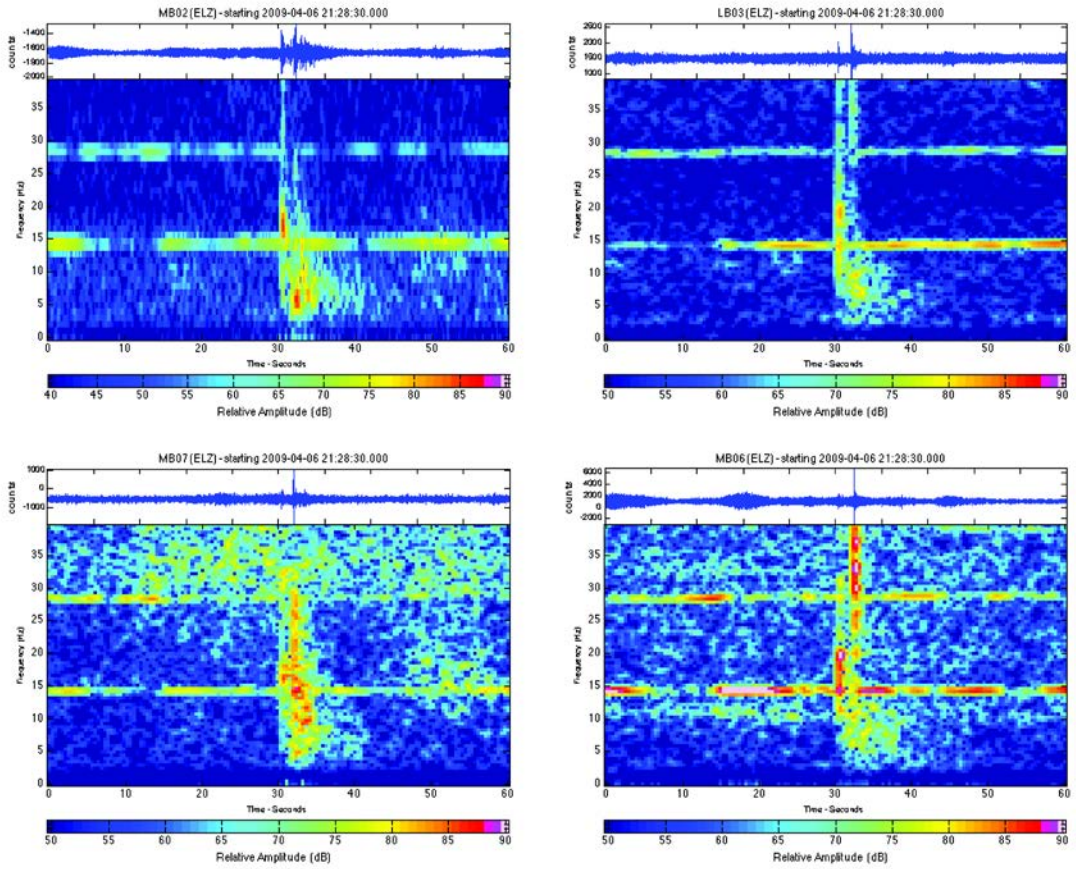

Figure 78. LFE recorded during the afternoon (2:28 pm local PDT) on April 6th, 2009 showing response from stations on the valley floor (MB02, top left and MB07, bottom left) as well as two different cliff locations at LB03 (top right) and MB06 (bottom right).

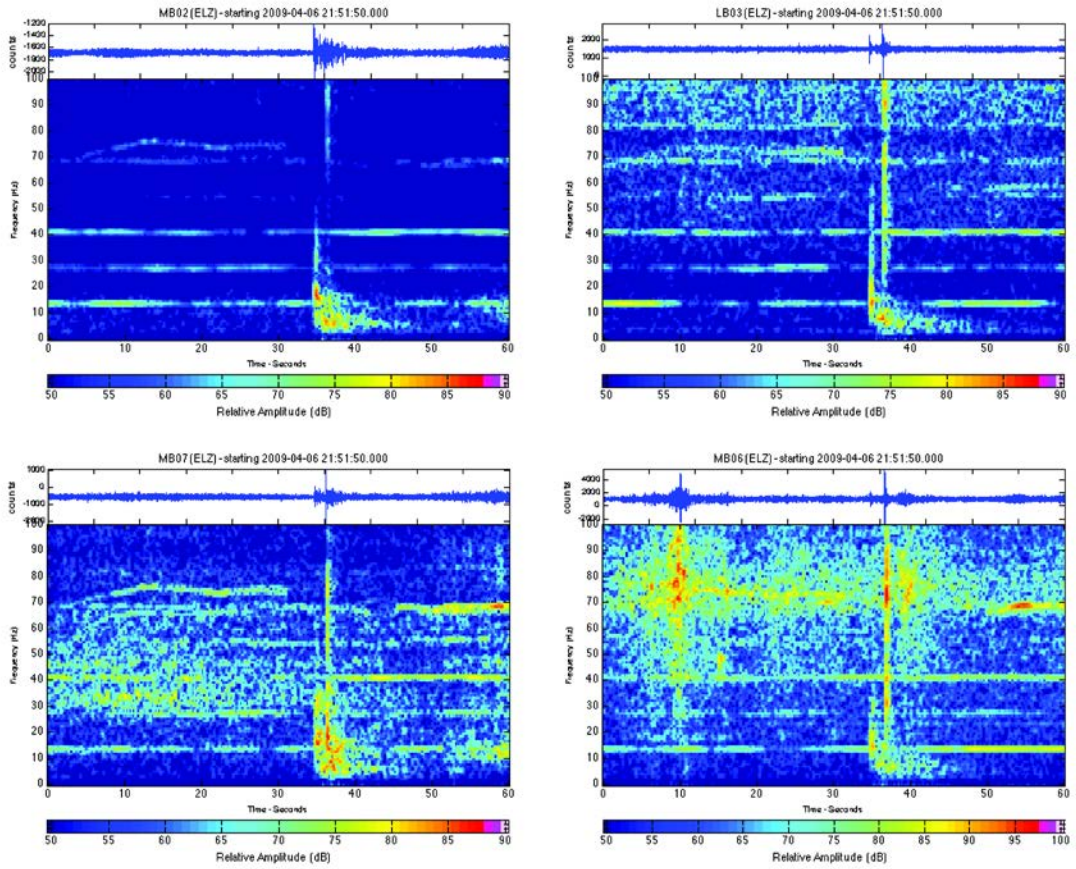

Figure 79. LFE recorded during the afternoon (2:52 pm local PDT) on April 6th, 2009 showing response from stations on the valley floor (MB02, top left and MB07, bottom left) as well as two different cliff locations at LB03 (top right) and MB06 (bottom right).

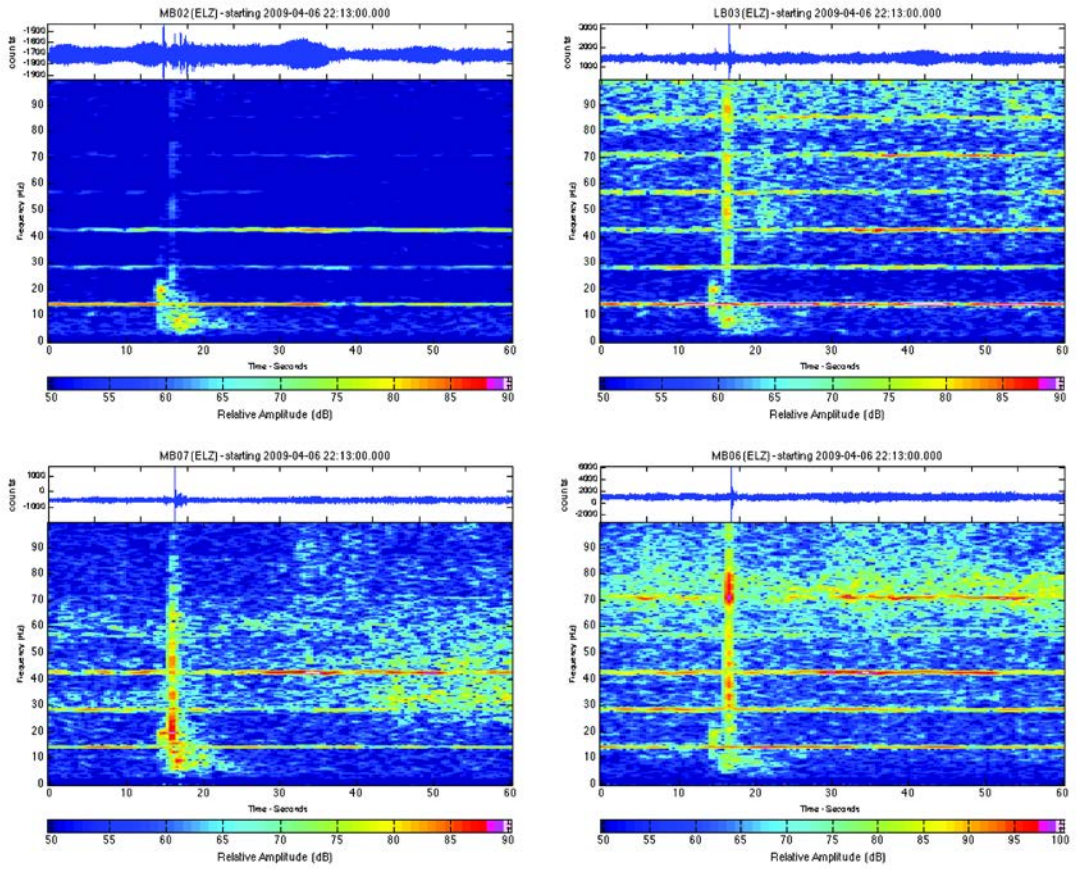

Figure 80. LFE recorded during the afternoon (3:13 pm local PDT) on April 6th, 2009 showing response from stations on the valley floor (MB02, top left and MB07, bottom left) as well as two different cliff locations at LB03 (top right) and MB06 (bottom right).

LFEs continued occurring the next day, on April 7th, 2009, starting with an event of similar spectral character to the April 6th events, at 9:27 am local PDT (Figure 81) that may have been weakly detected at the accelerometer two kilometers distant (bottom right). There is a strange, most likely human-caused spectral signal recorded at the valley floor station (top right), and evidence of rain and wind high on the cliffs. The next strong LFE occurs at 10:23 am and nearby engine vibration shows up as a steady narrow band signal (Figure 82). Finally, the last two strong LFEs on April 7th occur at 2:28 pm and appear similar to an earthquake in that there are two distinct events, although no evidence for an earthquake exists at regional seismic stations (Figure 83). In addition, the late-arriving high frequency pulse and engine vibration is noticeably absent from these records and it looks like these last two events are picked up at the accelerometer two kilometers away (bottom right), a deviation from the other LFEs. Unfortunately, these events are too emergent and weak to try and locate the source.

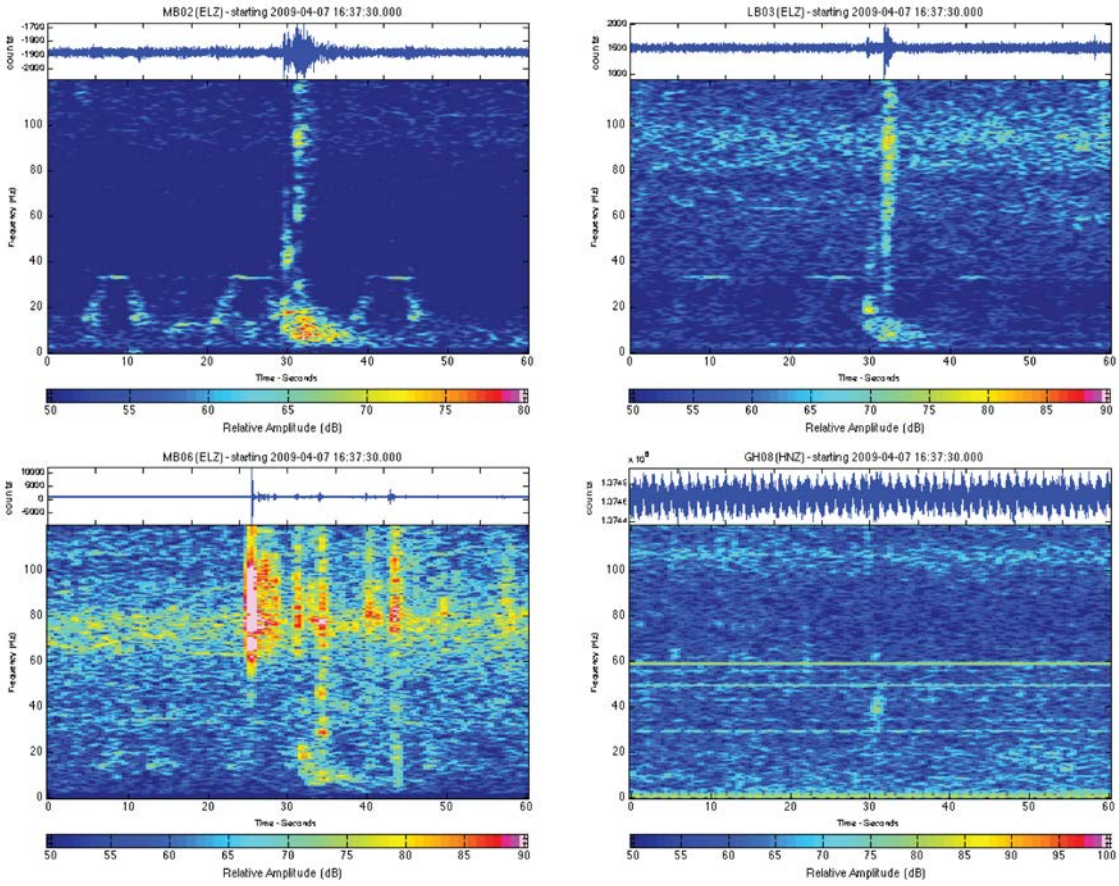

Figure 81. LFE recorded during the morning (9:27 am local PDT) on April 7th, 2009 showing response from stations on the valley floor (MB02, top left and GH08 accelerometer 2 km away, bottom right), and at on different cliff locations at LB03 (top right) and MB06 (bottom left).

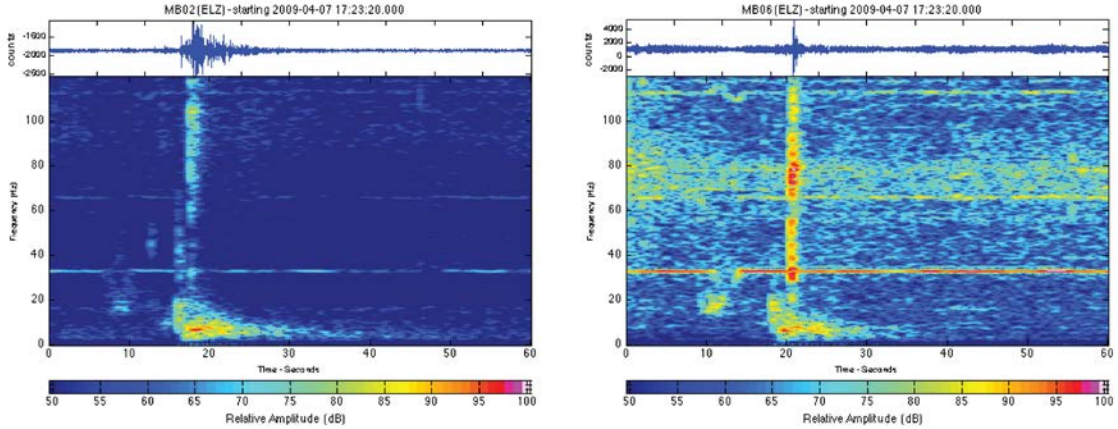

Figure 82. LFE recorded during the morning (10:23 am local PDT) on April 7th, 2009 showing response from stations on the valley floor (MB02, left) as well as 400 m high on the cliff at MB06 (right).

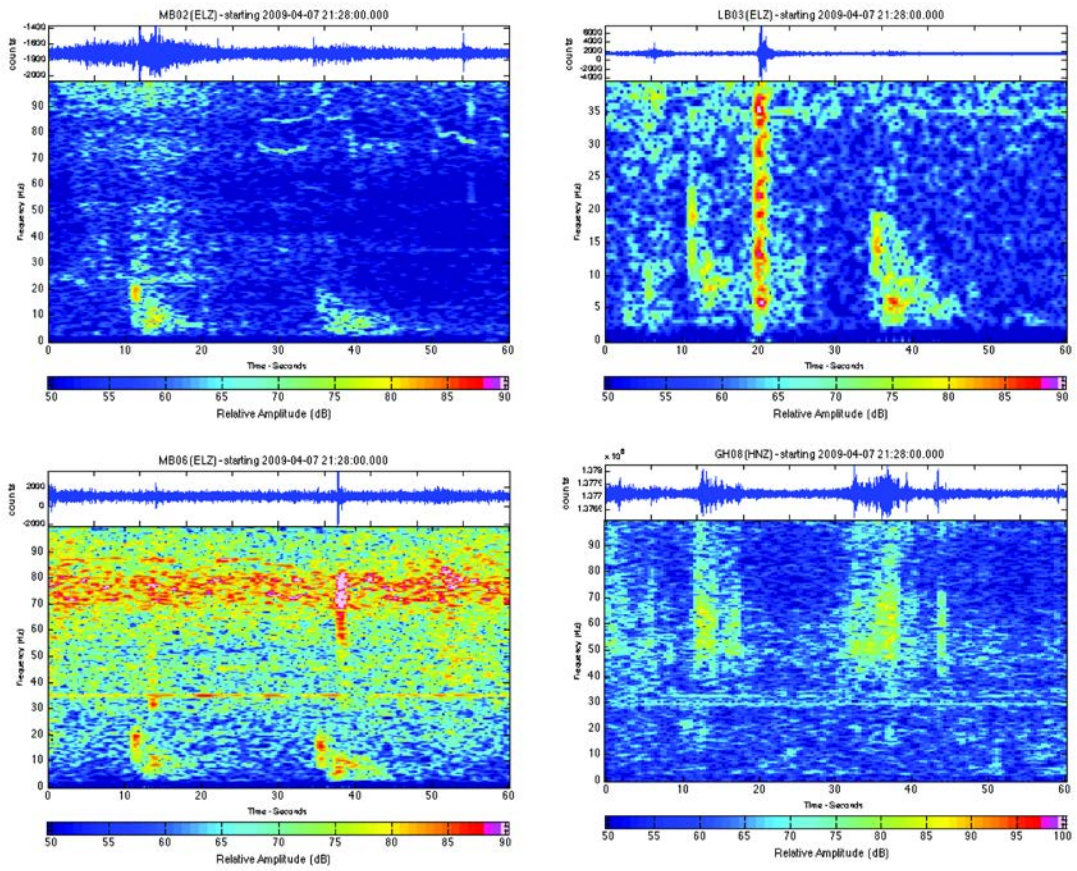

Figure 83. Two LFEs recorded during the afternoon (2:28 pm local PDT) on April 15th, 2009 showing response from stations on the valley floor (MB02, top left and GH08 2 km away, bottom right), and at on different cliff locations at LB03 (top right) and MB06 (bottom left). This event was checked on regional stations to eliminate the possibility of it being an earthquake.

There are three basic types of Low Frequency Events cataloged. Two of the three types have an initial strong, sudden 5 – 15 Hz pulse followed by gradual, ten-second tapering off of energy and higher frequencies, while the third type is more emergent and less well defined. Several of the sudden-onset LFEs occur in the middle of a winter storm and may be snow avalanches. The rest of the sudden-onset LFEs occur in the spring between late morning and early afternoon, and are accompanied by steady engine noise and a late-arriving high frequency pulse. These events are probably vibrations from nearby construction activities. The emergent events, one of which is detected over at least two kilometers, are difficult to attribute to any known source. Therefore, at this time, LFEs are not considered highly probable to be rock fall events, but they are local to Yosemite Valley, and may turn out to be related to rock falls in the future.

6.5 Reported Rock Falls Not Detected

There are several reported rock falls that were not found in the seismic record. These unsuccessful monitoring attempts are important to document since they help to bound the rock fall detection limit in terms of size and distance. Some important things to consider are that accelerometers are less responsive to rock falls than geophones, and that events across the valley are likely to attenuate more than events on the same side at similar distances.

The only detected event not from the vicinity of Middle Brother is the very large Ahwiyah Point rock fall, 4.5 – 7 km away, which generated detectable seismic waves out to 350 km. This event was preceded and followed by numerous medium-sized rock falls, none of which were detected at any of the local seismic stations. Other notable events that were not detected are the Ahwahnee Superslide event, a small rock fall notable for damaging cars at the Ahwahnee Hotel parking lot, and a small rock fall near Glacier Point (1.5 km away for an accelerometer and 3 km away for a geophone). None of the five small Cathedral Rocks events at 2.5 km northwest and across the valley were captured, although there were some triggers worth reviewing.

Three of the Cathedral Rocks rock falls were reported during a six-day period in late October and early November 2008. The first event occurred on the morning of October 26th, on a warm, calm day, but all triggers recorded that morning were from continuous low frequency noise that does not resemble a rock fall. By October 30th it had starting raining and continued raining heavily through the next few days with an inch reported on October 31st and nearly two inches on November 1st. The next event occurred during the early afternoon of October 31st, and there were no recorded triggers during that time. The last event occurred on November 1st in the afternoon when it was raining heavily. There were four recorded triggers during the correct time period, but two of them turned out to be small earthquakes located well outside of Yosemite Valley. The strongest trigger, at 2:59 (local PDT) occurs in the midst of a squall, as evidenced by all of the high frequency excitation (Figure 84, left) but is distinct from any rain signal. A closer look shows that the trigger excites frequencies in the 10-20 Hz range for about one second (Figure 84, right). Unfiltered, this event is completely hidden in rain noise (blue, Figure 84, bottom) and easily visible after 1 -20 Hz filtering and uncorrelated with rain spikes (red, Figure 84, bottom). This event and the other triggers not presented here look more similar to Low Frequency Events than they do a rock fall, and thus, are probably not rock falls.

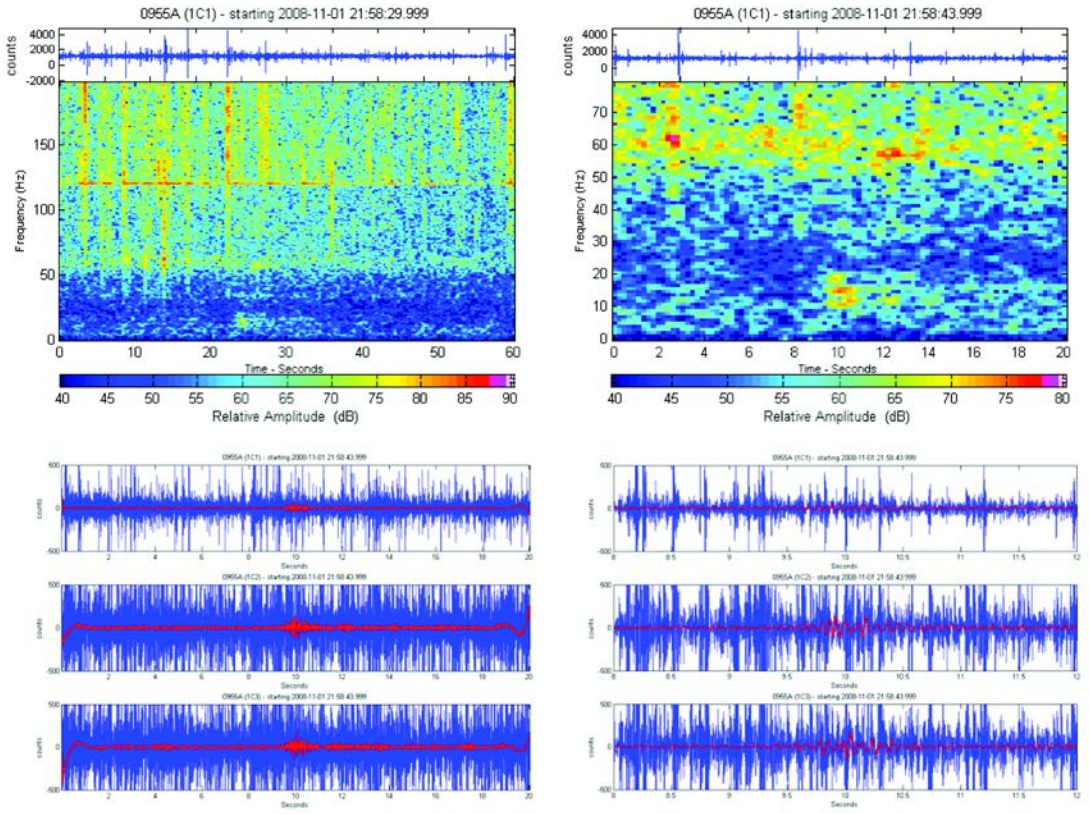

Figure 84. LFE at 2:59 local PDT on November 1st, 2008 during rainy period. 60 s record with multiple rain drops (top left), 20 s close-up spectrogram (top left), and time domain records with unfiltered noisy data in blue, and 1 - 20 Hz filtered data in red (20 s bottom left and 12 s bottom right).

Finally, there were two events that were heard and reported to be coming from the direction of Middle Brother, but neither the location nor the exact time can be pinpointed with any accuracy (Table 10). There were no triggers recorded during the reported time on December 25th, 2007. On the morning of January 27th, 2008, during a snowstorm, a loud rock fall noise was heard to the west of Yosemite Village. There is one geophone-triggered event that somewhat resembles an impact pulse at 7:39 am local PST (Figure 85, right), but nothing detected by the accelerometer (Figure 85, left). There also appears to be some weak, storm-related noise, so it not likely that this seismic event is a rock fall.

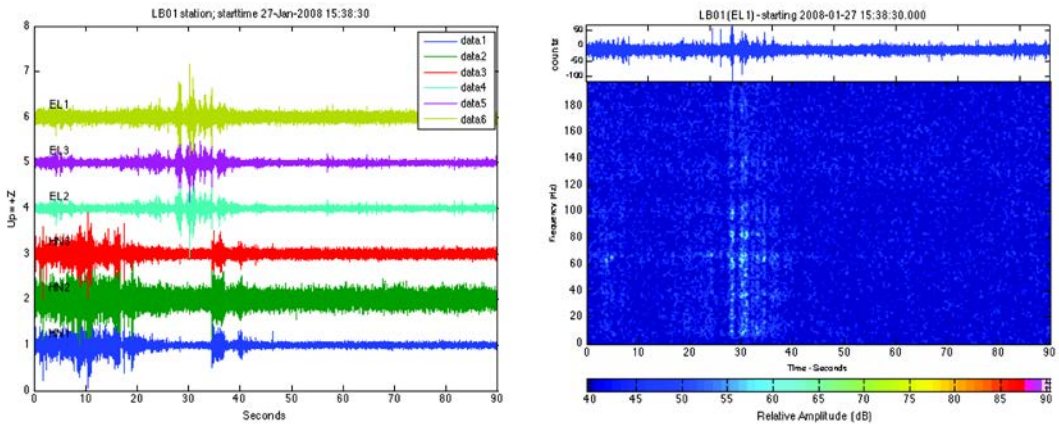

Figure 85. Triggered seismic events shown near the time of a reported rock fall.

In summary, none of the reported rock falls away from the vicinity of the Three Brother were detected by the seismic instruments, except for the exceptionally large Ahwiyah Point event. The closest non Three Brothers events were at Cathedral rocks only 2.5 km away, although it was across the valley and seismic waves likely attenuate more traveling across the valley. However, one event that occurred in Eagle Canyon was detected, although this location is technically on the other side of the same rock formation and was less than one kilometer away.

6.6 Summary

The search for rock fall events encompassed both a thorough review of high probability triggered data, and a targeted search for known events. In the end, twelve rock falls, and five possible rock falls were identified. Eight of the twelve identified rock falls had been reported. In addition, there were two unreliable reports of Middle Brother rock falls that were not recorded seismically, and no events were recorded away from Middle Brother, except Ahwiyah Point. The Eagle Canyon rock fall, which may be a medium-sized event, is the only Three Brothers rock fall recorded from a source area on the other side of the formation, and it is still only less than one kilometer away.

In addition to rock falls, other sources of seismic activity were characterized. Some unknown events were classified as impact pulses and low frequency events. Most of the impact pulses are thought to be possibly rock falls, but the evidence is not strong. The low frequency events are not suspected to be rock falls and are correlated with either winter storms or engine noise. Some of the winter storm low frequency events are probably snow avalanches or ice falls.

7 Waterfalls, Wind, Rain, Earthquakes, Humans: The Melange of Sounds and Vibrations from Non-Rock Fall Events

A melange of seismic and acoustic sources were discovered while reviewing data from the rock fall monitoring network. Common sources of seismic and acoustic in Yosemite Valley, other than rock and icefalls, are weather (e.g. rain, snow and wind), humans (e.g. engine, impacts, or electrical noise), and earthquakes. The instruments were placed on the surface for several months, only protected in some cases by sandbags or overhangs. The exposure of the instruments to the elements meant that a great deal of seismic noise from snow, rain, and wind was recorded. In addition, the Yosemite Valley is populated with visitors and workers all year round. Human beings create detectable seismic noise while constructing roads, performing maintenance, and driving vehicles. Finally, there are numerous active faults as well as the nearby volcano, Mammoth Mountain, which generate earthquakes on a frequent basis. All of these sources were identified by their spectral characteristics and confirmed, when possible, with other publically available data. A catalog of Yosemite Valley recorded seismic and acoustic data from several of these sources is presented in this chapter with the objective of providing a handy reference for future studies.

7.1 Precipitation

Winter storms bring heavy amounts of snow, rain, ice, and wind to Yosemite Valley, and can persist for days. Snow and ice accumulate on the cliffs during these storms (Figure 86) and break off when the load becomes too great or when it begins to melt after the storm during the typically warm, sunny days that follow.

Figure 86. Snow and ice accumulation on Yosemite cliffs from a recent storm.

Precipitation tends to cause a strong, short-duration spectral response exclusively in the upper frequencies (> 100 Hz) unless a raindrop or ice strikes directly on the sensor, in which case the response is extremely strong and broadband (Figure 87, 70.65s). Geophones usually record precipitation well, often showing many nearby raindrop or ice impacts during storms (Figure 88). Sometimes associated with the storm is low frequency noise (Figure 88, right), which is probably wind and nearby tree movement. Accelerometers are less sensitive to the precipitation and in fact, an accelerometer protected under an overhang at MB04 recorded no discernable rain or ice impact signal during the entire winter season. More exposed accelerometers do respond to precipitation (Figure 89), including direct strikes (Figure 89, top left, 16s), although sometimes the response is weak (Figure 89, top right). The precipitation can occur in strong bursts (Figure 89, bottom left), or be accompanied by wind (Figure 89, bottom right).

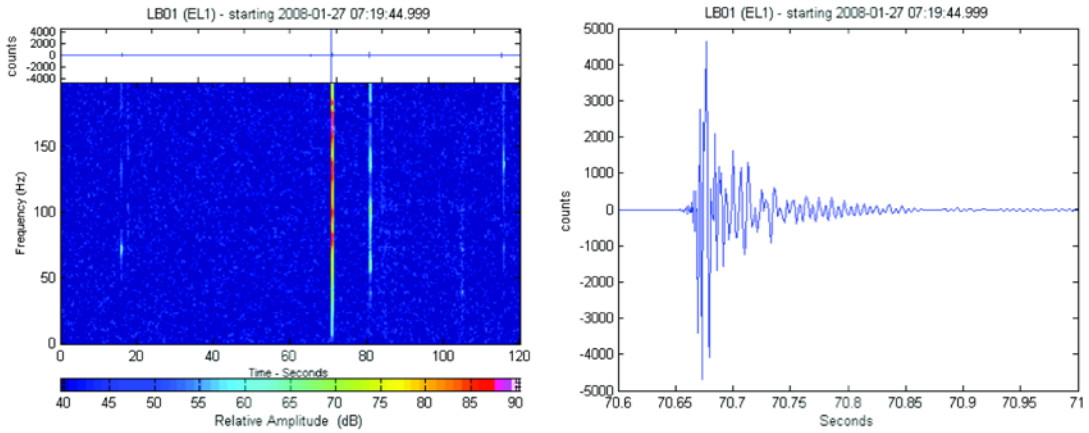

Figure 87. Spectrogram showing geophone (8 Hz) response during a winter storm, with a direct raindrop or ice impact of the sensor at 71 seconds (left). Time domain plot of the same impact (right).

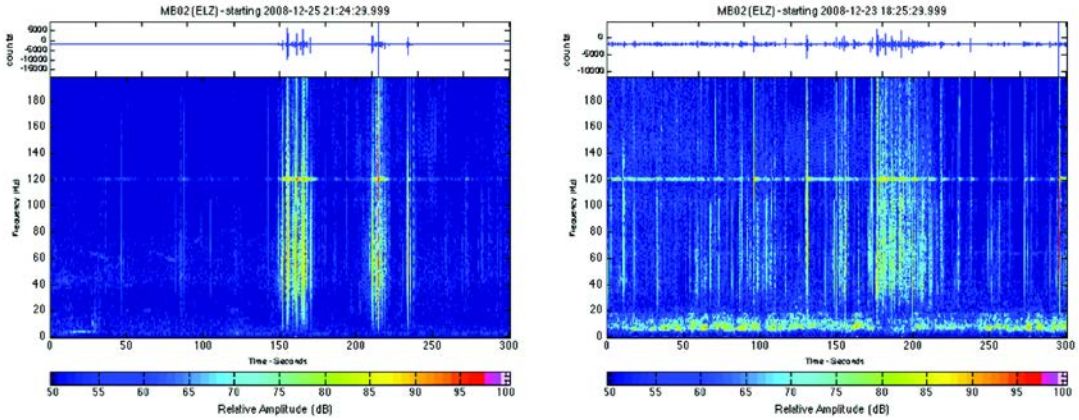

Figure 88. Geophone (4.5 Hz) spectrograms showing precipitation noise. The low frequency (~8 Hz) signal (right) is unknown in source, but is likely related to the winter storm and may be wind or tree movement.

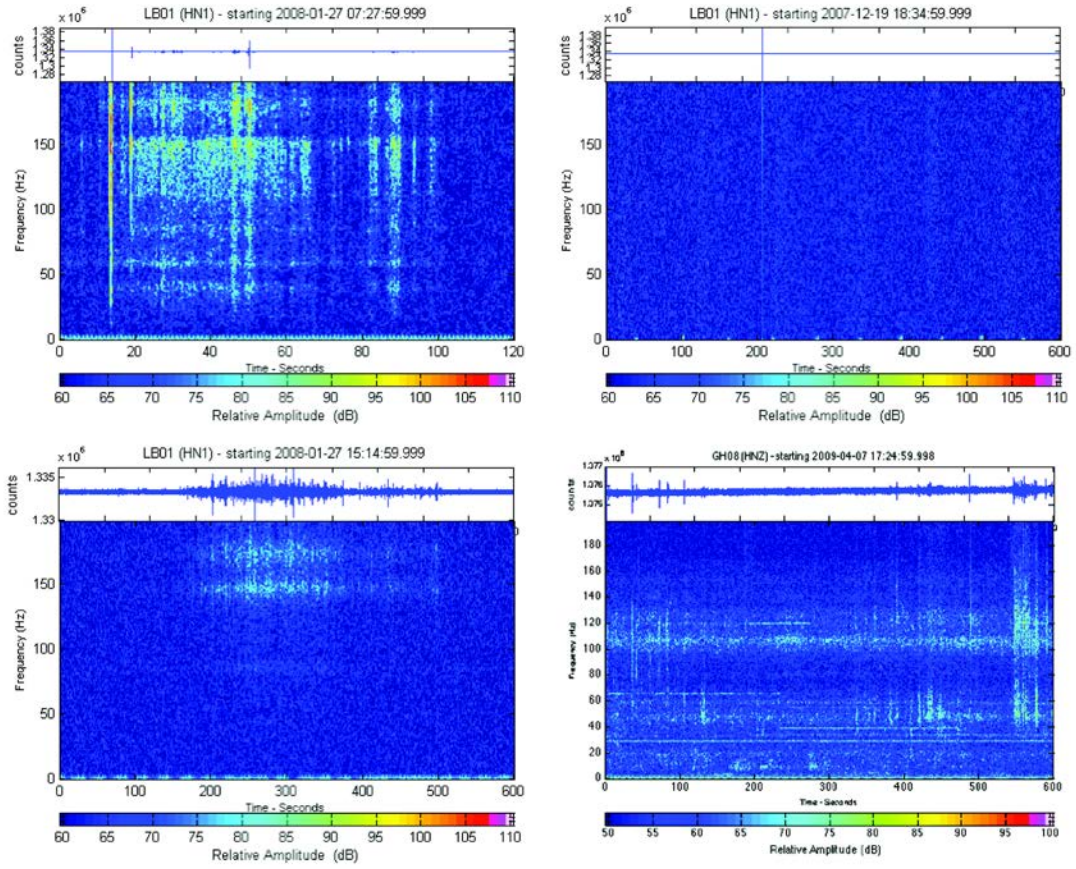

Figure 89. Accelerometer spectrograms during winter storms. Accelerometers typically respond less to precipitation than geophones. The strong response at 15 seconds (upper left) is likely a raindrop impacting directly on the sensor.

7.2 Wind

Wind often accompanies the winter storms, but can also occur during days with no precipitation, especially before storms. In some cases, site visits occurred on windy days, providing direct confirmation that certain noise signal observed on the spectrograms was due to wind alone. Wind comes in bursts lasting a second to several seconds, and can cause a response in several different, sometimes resonant frequency bands. Wind excites geophones in frequencies from 8 Hz to >150 Hz (Figure 90 and Figure 91) with the strongest excitations occurring at 80 Hz, 60 Hz, 40 Hz, 150 Hz, and 10 Hz, in order of strength. Thus, wind is likely to produce false triggers when filtering from 1-20 Hz (Figure 92), but has a very different spectral character from rock falls, and thus can be eliminated easily when triggered. Accelerometers record wind as noisy bursts in several frequency bands (Figure 93), although it can be hard to distinguish the wind from other sources of noise.

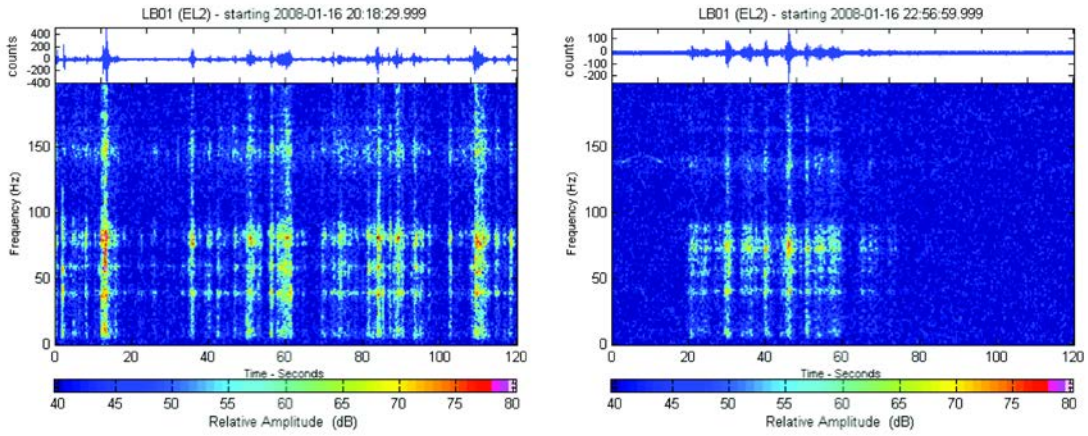

Figure 90. Geophone (8 Hz) spectrograms showing wind on a day when site maintenance was performed, thus verifying windy conditions.

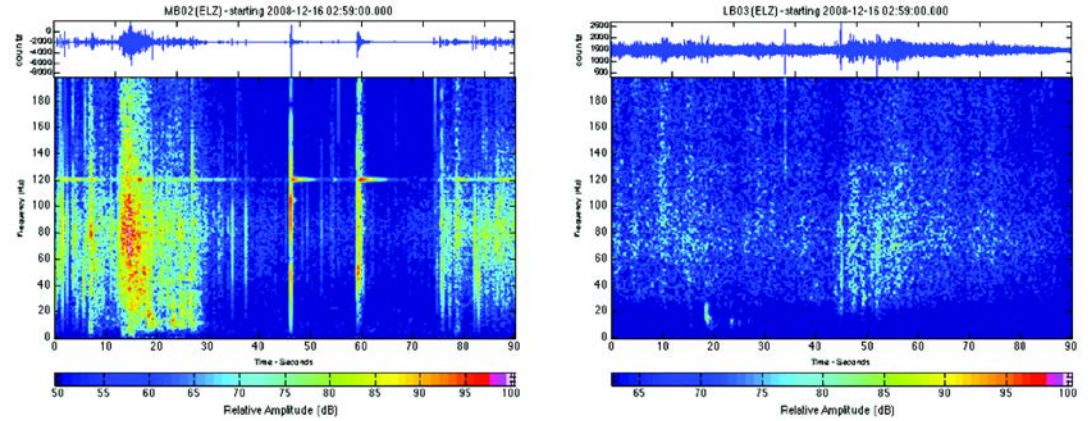

Figure 91. Geophone (4.5 Hz) spectrograms showing wind mixed with precipitation.

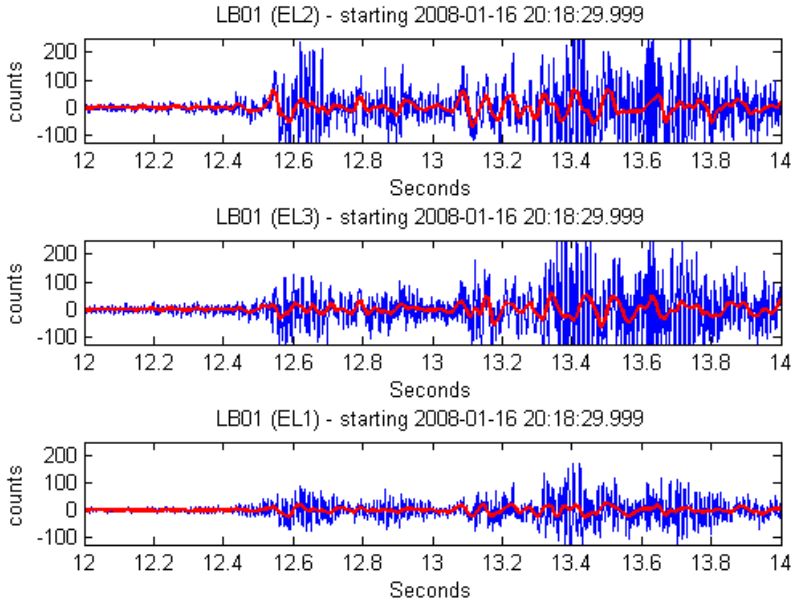

Figure 92. Wind recorded seismically showing unfiltered (blue) and filtered 1-20 Hz (red) data.

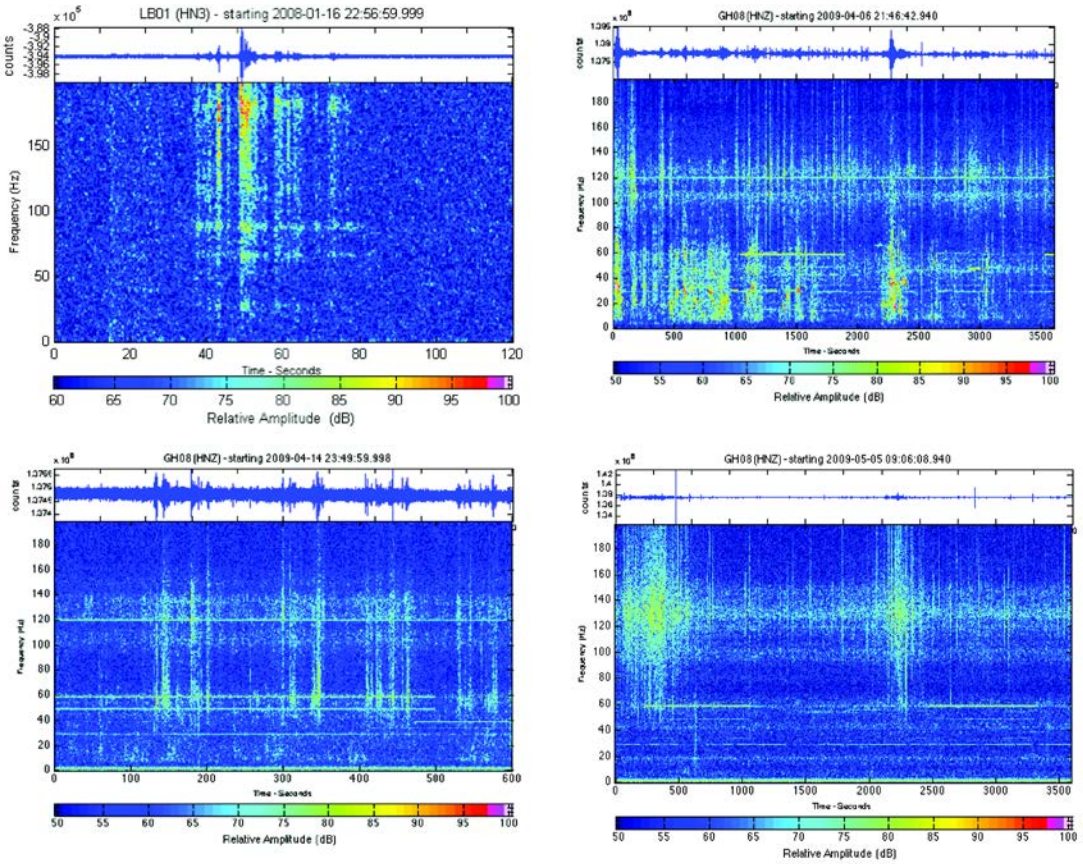

Figure 93. Accelerometer (RT131A-2/3) spectrograms showing wind and human noise (all but the top left). It was not raining in Yosemite Valley during any of these times, except perhaps a negligible amount on May 5th, 2009 (bottom right).

7.3 Small rock and ice impacts

Small rocks and ice fall off from exposed ledges and occasionally impact near the seismic stations. During a site visit on January 16th, 2008, the wind was sufficiently gusty to cause a baseball-sized rock to blow off from above, fall, and crash through nearby trees. The wind and the small rock impact can be seen clearly in the seismic record from the geophone (Figure 94, left) but only weakly from the accelerometer (Figure 94, right). Since the rock impact excitation is well above 20 Hz and of very short duration (~0.1 s), it and most of the wind disappears when the seismic record is filtered from 1-20 Hz (Figure 95).

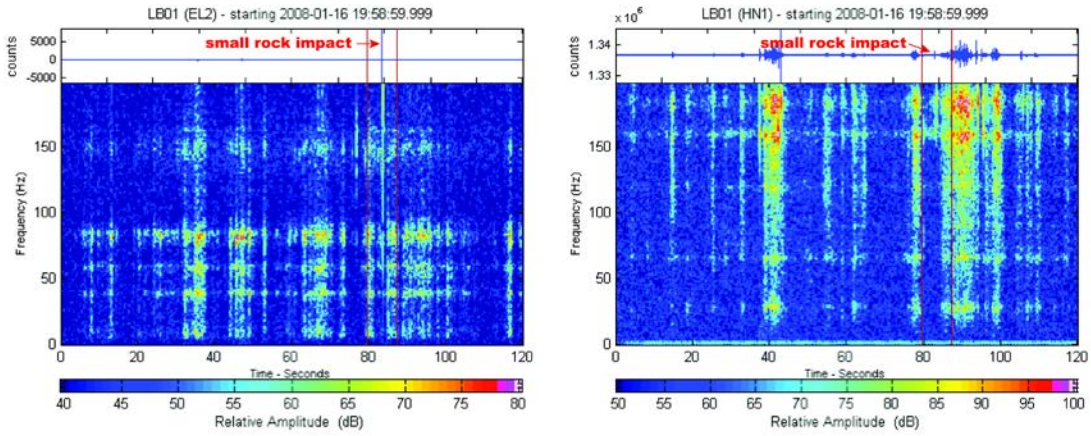

Figure 94. Windy records showing small rock impact at 83 seconds, easily visible on the geophone (left), less visible on the accelerometer (right).

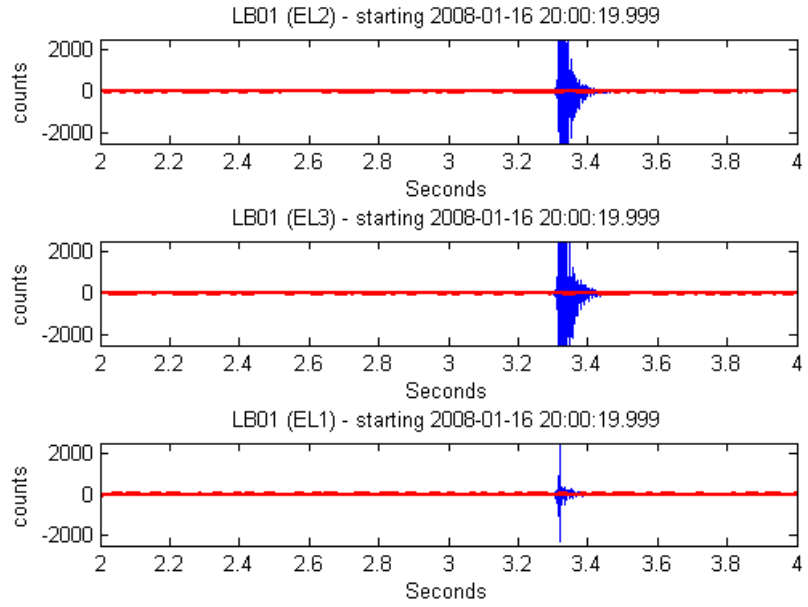

Figure 95. Two second time record of a very small rock landing near an SM-6 geophone on a windy day at 3.3 seconds. Comparisons between the unfiltered (blue) and filtered 1-20 Hz (red) data show that the impact does not excite lower frequencies.

7.4 Earthquakes

The Northern California seismic network detects thousands of regional earthquakes yearly. Earthquakes produce significant response in the same band, 1-20 Hz as rock falls and thus induce triggers. They also look remarkably similar to local Yosemite Valley non-earthquake, low frequency events of unknown origin that were described in the Chapter 5. All of the earthquakes reviewed have distinct P and S wave arrivals, which are remarkably to each other in spectral character and strength.

Matching the earthquake-induced triggers with the earthquake catalog eliminated most of them. However, some earthquakes were not eliminated using this method because they were too small to have been included in the catalog. When two low frequency events occurred a few seconds with similar spectral character to each other, they were marked as suspected earthquakes. These suspected earthquakes were then checked by downloading full waveform data from strong motion stations to confirm that they were regional and thus, not rock falls in Yosemite Valley.

Earthquakes of different sizes and distances to the seismic network had slightly different spectral character, as might be expected due to seismic attenuation. A M4.5 earthquake 271 km north has strong P and S wave response in frequencies less than 20 Hz (Figure 96). A M2.2 earthquake 217 km south has weaker spectral response, but still shows distinct P and S waves in frequencies less than 15 Hz (Figure 97). A M2.1 earthquake 59 km west has a more broadband but a surprisingly weak response, possibly due to rock type and seismic wave penetration depth (Figure 98), especially when compared to a similarly sized but more distant earthquake to the south (Figure 97). Finally, the magnitude 7.3 Sea of Okhotsk, Russia earthquake on November 24th, 2008 shows up with a strong signal with a nearly five minute duration, but only in frequencies less than 5 Hz (Figure 99).

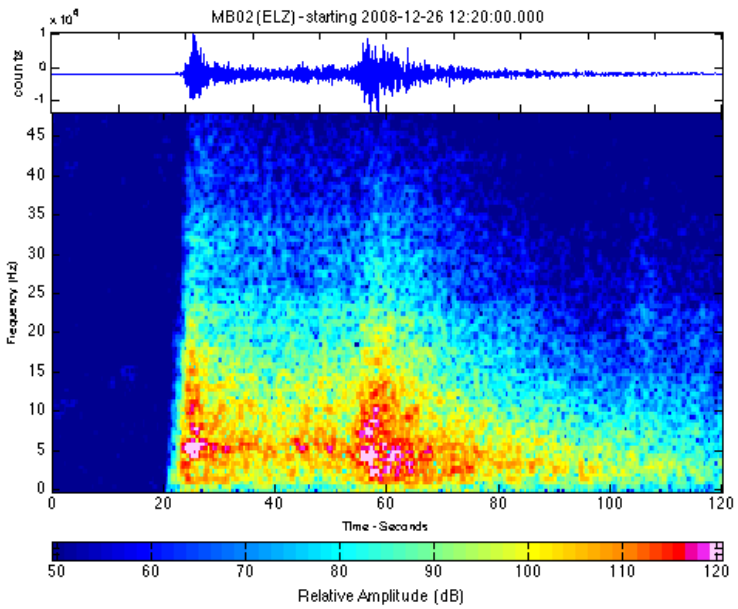

Figure 96. Magnitude 4.5 earthquake at Quincy, CA, 271 km north of Yosemite Valley.

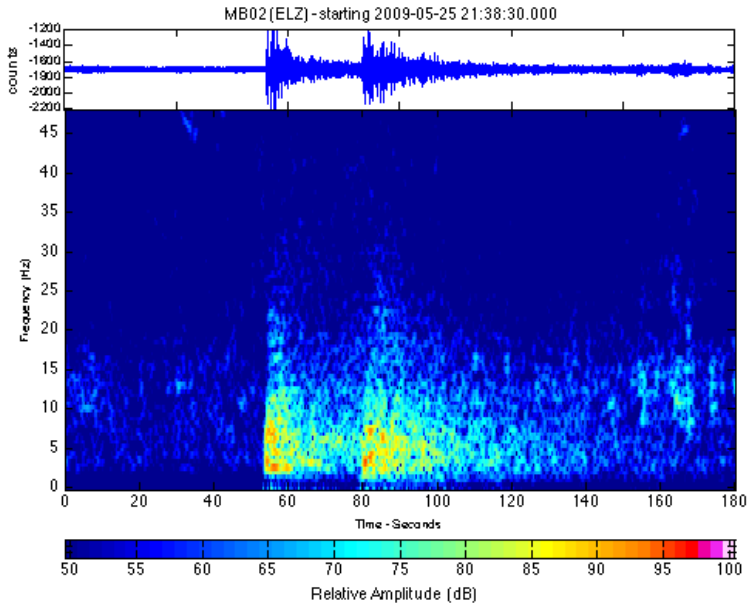

Figure 97. Magnitude 2.2 earthquake at Owens Lake, CA, 217 km south of Yosemite Valley.

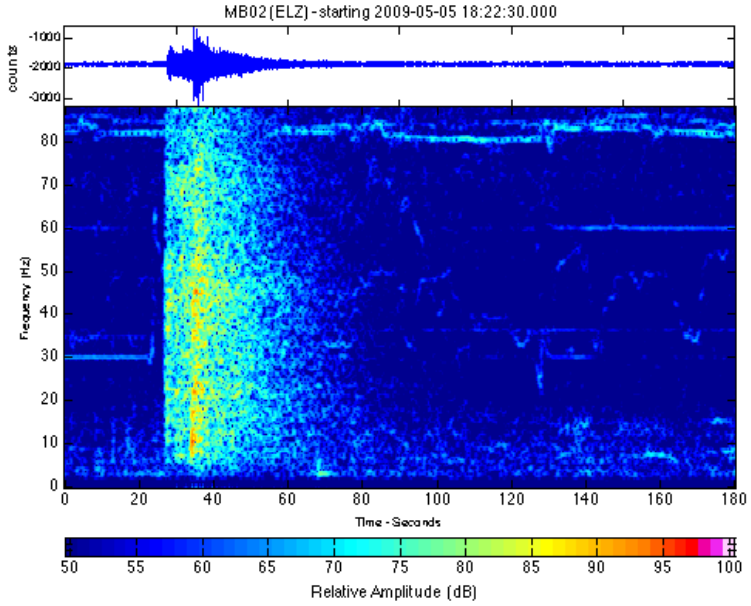

Figure 98. Magnitude 2.1 earthquake at Mariposa, CA, 59 km west of Yosemite Valley.

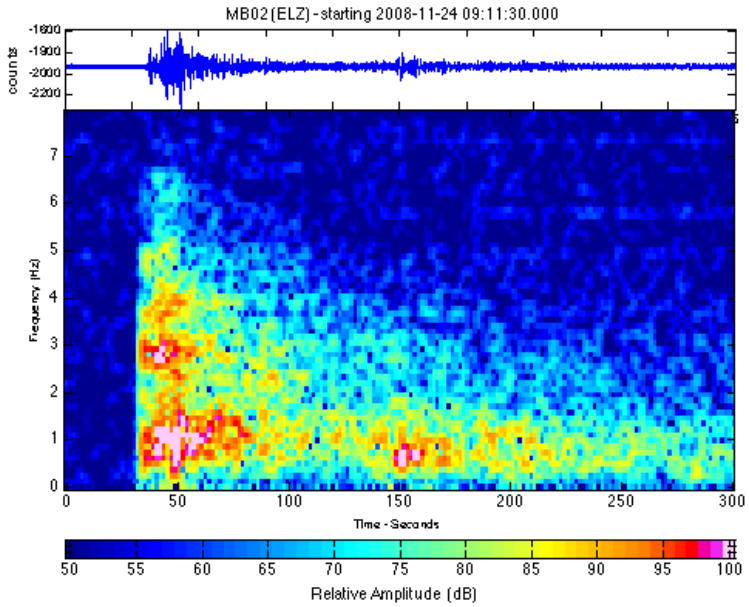

Figure 99. Magnitude 7.3 earthquake in Russia recorded in Yosemite Valley.

7.5 Anthropogenic Noise

Several human activities cause seismic signals (or noise) that can be detected by the instrumentation in Yosemite Valley. The most common sources of noise are road construction, maintenance (e.g. the garbage truck), vehicles driving in the road, engines, and electrical. Anthropogenic noise is most often identified by unusual frequency content. For example, engines vibrate in constant, narrow frequency bands and associated resonances. Time of day can also be helpful in identifying anthropogenic noise: i.e. construction only occurs between 8am and 5pm. In Figure 100, an idling engine produces a steady frequency that shifts, then stops abruptly at 3:30 pm, which is a reasonably time for construction crews to shut down. In Figure 101, there is a steady state engine vibration punctuating by odd, recurrent shifts in frequency.

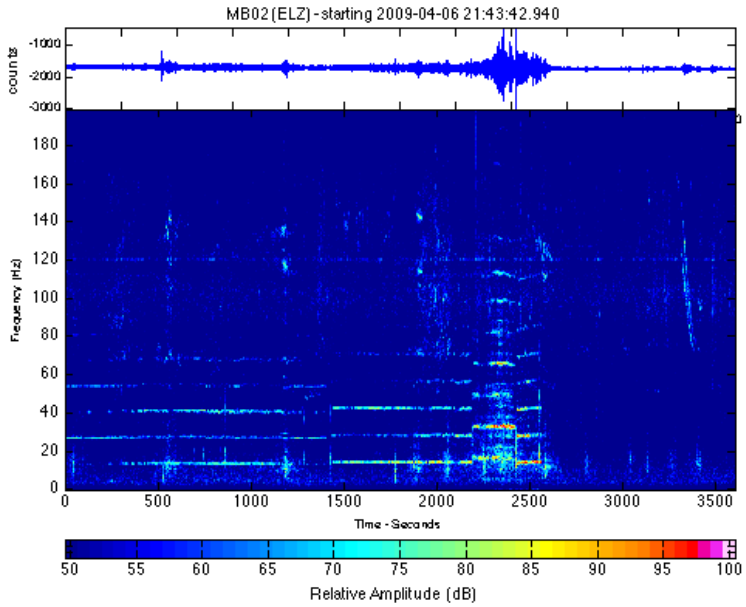

Figure 100. Anthropogenic engine noise showing concurrent frequency changes, then abruptly stopping at 3:30pm (local PDT).

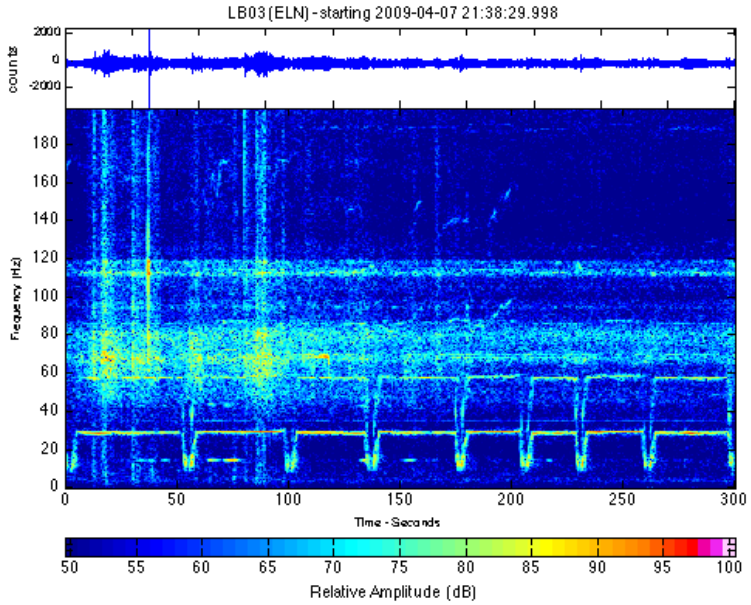

Figure 101. Anthropogenic noise manifesting as single frequency bands and regular, recurrent shifts. Wind and rain can also be seen in this figure in the higher frequencies.

In Figure 102, steady state engine noise consisting of several resonant frequencies is detected at two stations spaced 610 meters apart. The station on the left, MB02, is located below the cliffs near the road, while the station on the right, LB03, sits 270 m above the valley floor. Interestingly, it is the higher station (right) that more strongly detects this noise. In addition, there is an unexplained low frequency event at 105 seconds, accompanied by a high frequency pulse one second later. Several of these low frequency events were detected accompanying engine noise on April 6-7, 2008, suggesting that they may also be anthropogenic in nature.

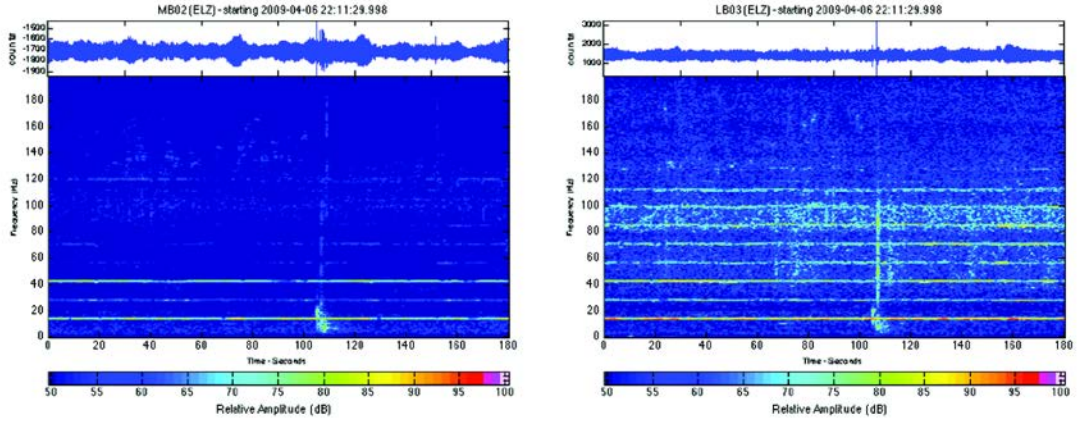

Figure 102. Anthropogenic engine noise is recorded at two stations 610 meters apart, with one (left) located on the valley floor and the other (right) sitting 270 m above on a cliff to the west. The engine noise is the constant, narrowband frequency. Also visible is an unexplained low frequency event at 105 seconds that may also be anthropogenic.

7.6 Acoustic and infrasound events

Three microphones installed in Yosemite Village monitored infrasound signals in Yosemite Valley. These three infrasound microphones were spaced a few meters apart, which takes advantage of the relatively slow speed of sound to calculate of the azimuth of the incoming wave. The infrasound signal came in two basic forms. The first type was an obvious short duration signal. The second type was continuously generated acoustic noise with no obvious onset that was sometimes difficult to identify without advanced signal processing. The microphones, being sensitive to pressure, pick up non-acoustic pressure changes as well.

For the short duration event signal, first arrivals were picked manually and then, the time difference in arrival was used to calculate the azimuth of an incoming wavefront. Some of the short duration, distinct events are due to anthropogenic activities, such as construction, maintenance, and road noise (e.g. the garbage truck). For example, in Figure 103, there were ten events in the span of six minutes, in the low-audible frequency band (30-100 Hz). The source of these events was determined to be moving around to the north of the microphones, on a road in a residential area, and may be a garbage truck. There is also a constant response in the 30 and 60 Hz bands, which is the AC electrical transmission band.

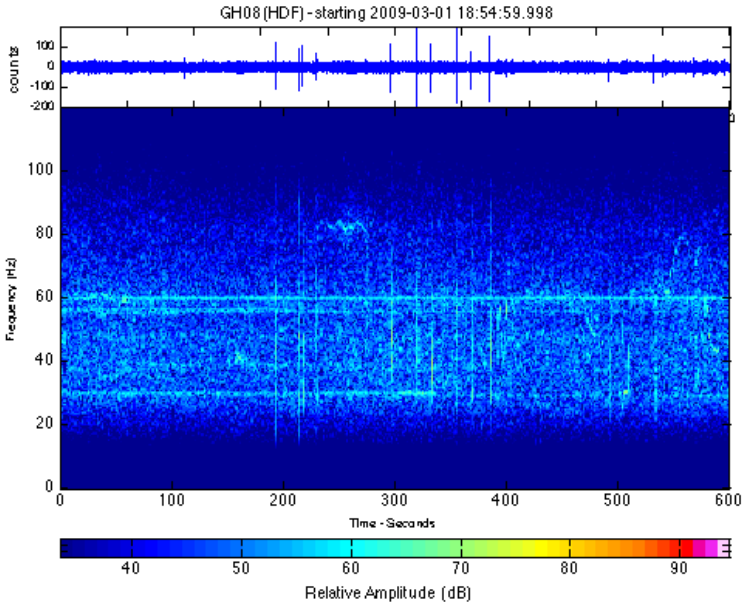

Figure 103. High frequency, short duration spikes are calculated to be originating in the direction of a residential area, and may be a garbage truck. Continuous 30 and 60 Hz noise is likely related to nearby electrical power transmission lines.

Continuous low frequency emitters, which the lack of obvious signal onset, can still be located using cross-correlation to calculate an accurate time lag between microphones. Barometric pulses due to wind are the dominant signal on the infrasound for the duration of the project, but are low enough frequency (0.001 – 0.01 Hz) to easily be filtered out. The signal shown in Figure 104 has a time lag of about seven seconds, from west to east. This barometric pressure pulse is calculated to be moving at 2.7 m/s (6 mph) and is coming roughly from the west, a reasonable speed and direction for wind in Yosemite Valley.

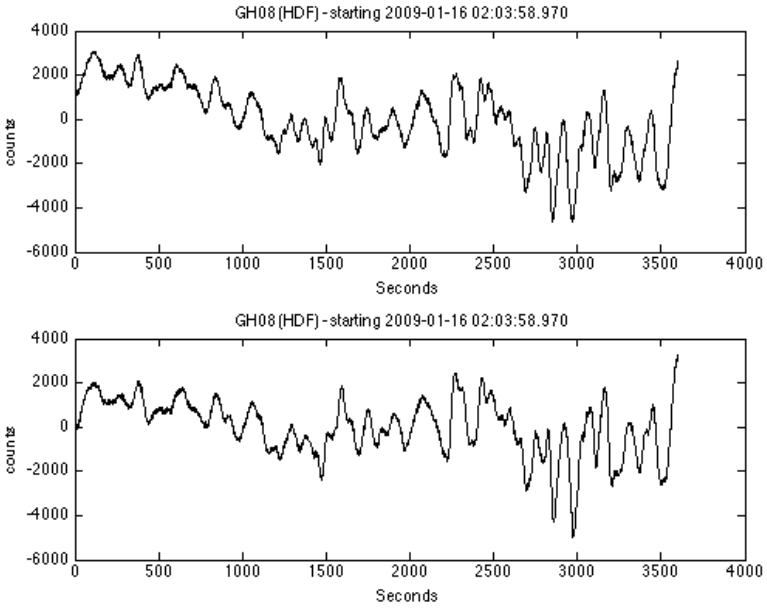

Figure 104. Infrasound records for one hour, showing pressure changes related to wind and mass air movements.

Yosemite Falls is located only 0.5 km from the microphone array, and can be a source of infrasound noise due to water as well as snow and ice falls during the winter. In 2009, the peak flow on the Merced River in Yosemite Valley occurred from occurred from May 16-18 and was calculated at 2600 cubic feet per second (cfs), driven by high country snowmelt. Infrasound records from that time show a strong continuous infrasound emitter in the 2-5 Hz band (Figure 105) that is absent at times when the river flow is very low. Cross-correlation shows that the source is located near the base of Lower Yosemite Falls at an azimuth of 280° and that the velocity of the signal is acoustic.

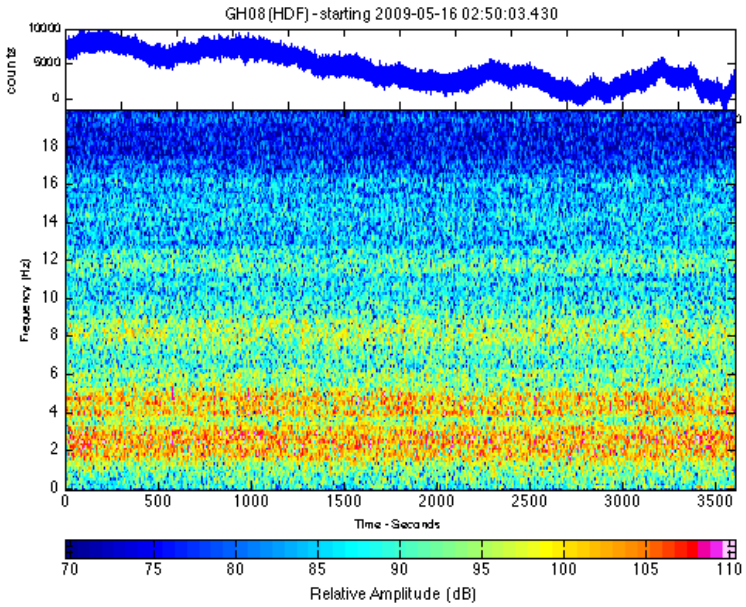

Figure 105. Infrasound records for May 16th, 2009 when the Merced River flow was estimated at 2600 cfs, showing strong waterfall signal from 2 – 5 Hz.

7.7 Summary

There are many sources of seismic and acoustic signals in Yosemite Valley that are interesting by themselves and important to understand in the context of rock fall monitoring. The biggest source of false rock fall triggers is the weather. Rain and wind were detected during storm cycles, and wind generates a low frequency pressure pulse on the infrasound microphones that has much higher amplitude than all acoustic sources. Even Yosemite Falls can be considered a weather phenomenon given that the acoustic noise it generates is driven by snowmelt. Earthquakes, while largely eliminated using the earthquake catalog, are common and trigger in the same band as rock falls. Finally, there is a high amount of human activity in the form of driving, construction, and maintenance, which generates seismic and acoustic noise. Understanding these common sources, classified as noise, can help to differentiate rock falls from other all other phenomena when sorting through large amounts of data.

8 Middle Brother Rock Falls

A number of rock falls at the historically active Middle Brother formation were seismically recorded at close range during the winters of 2007-08 and 2008-09. Witnesses reported additional details about some of these rock falls, such as the size and location of the source area. Many of the rock falls occurred during winter storms, suggesting that the immediate trigger may be related to precipitation or freezing and expansion of water in cracks. The first rock fall seismic monitoring station was installed only seven days prior to the first recorded rock fall. This station, consisting of an accelerometer and a geophone, was placed high on a mid-cliff ledge in the hopes of catching a rock fall at close range. In total, eleven to sixteen rock falls were recorded at Middle Brother during the two winter seasons of operation, out of which witnesses had reported only seven. Six of the eleven rock falls came from the same source area over a ten-week period. Thus, seismic instruments were able to detect rock falls, determine the source location, and monitor an instability that persisted for months.

8.1 Middle Brother Geologic Setting and Rock Fall History

Middle Brother is an 800 m tall, south-facing rock formation that juts out on the north side of Yosemite Valley. It sits just east of Eagle Creek, one kilometer east of the east buttress of El Capitan, about one kilometer west of Camp 4, and three kilometers west of Yosemite Village (Figure 106). The Merced River abuts the talus piles on the southeast-facing wall, squeezing Northside Drive (the Yosemite Valley exit road) between the large talus boulders and the riverbank. The rock formation has three major rock fall source areas, identified by prominent talus piles below light-colored, highly fractured fresh rock surfaces that contrast with the grey, weathered surrounding cliffs (Figure 107). The largest source area, identified a “A” in Figure 107, is more than 300 m wide and 300 m tall, and sits perched above a section of Michael’s Ledge that is notorious for rock falls among climbers, who use the ledge to access and descend climbs. Two additional major source areas, “B” and “C”, sit to the east of “A”, above and to the east of Rixon’s Pinnacle.

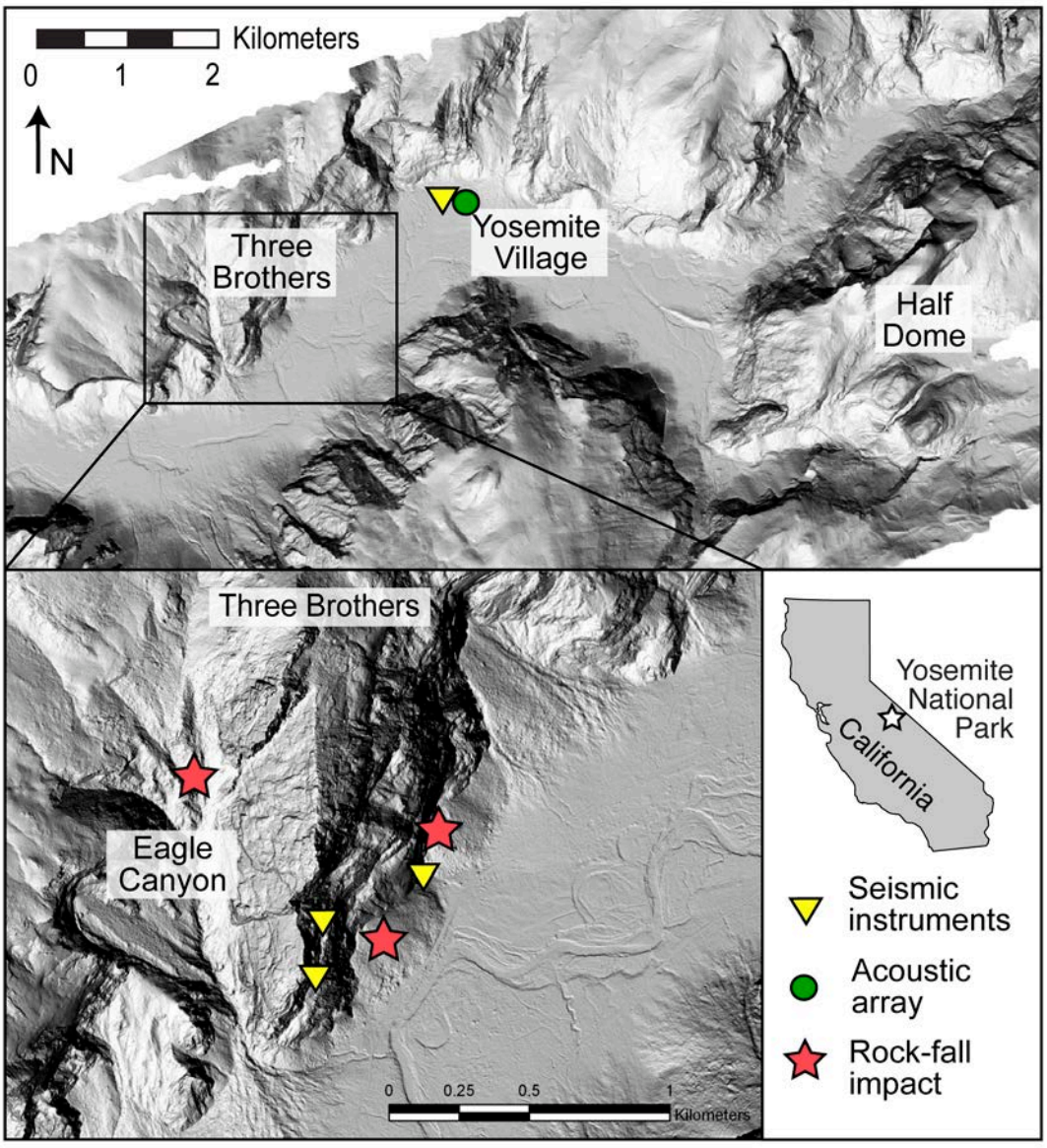

Figure 106. Middle Brother formation, seismic instruments, and known rock fall impacts at Middle Brother.

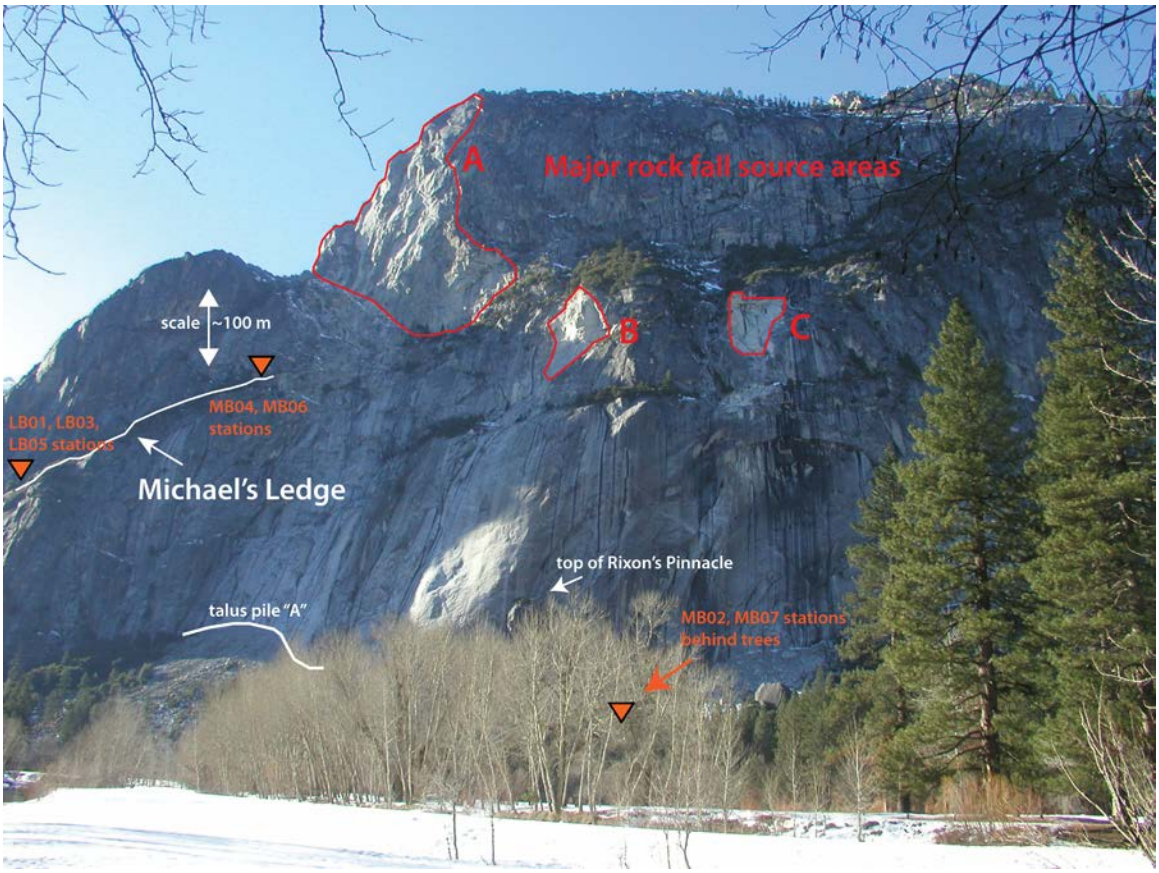

Figure 107. Middle Brother major rock fall source areas (A, B, C) and Rixon's Pinnacle. Also showing winter 2007-08 seismic station LB01 and winter 2008-09 stations LB03, LB05, MB04, MB06, MB02, and MB07.

The southeast exposure of Middle Brother means that the cliff is subject to an intense freeze-thaw cycle during the winter months. Frequent storms blow into Yosemite Valley during the winter, depositing large amounts of snow and/or rain. The valley floor, at 1215 m (4000 ft.), is low enough to receive a mixture of rain and snow during many of these storms, but the rims of the valley, at 2450 m (8000 ft.), are well above the typical Sierra Nevada snow line. While it might be tempting to characterize the rims as "cold" and the valley as "warm", this would be incorrect. The valley floor tends to be colder than cliff areas a few hundred feet above, owing to an atmospheric inversion that develops during the winter months where cold, dense air sinks and is trapped by the steep valley walls. The cliffs, especially those with sunny exposure such as Middle Brother, can vacillate from below freezing to well above freezing temperatures during a single day, while the valley remains cold. Thus, at Middle Brother, winter storms bring prolonged freezing temperatures and high amounts of precipitation, and afterward, sunny days bring rapid melting and drying of the cliff.

Explorers described the first reported rock fall in 1851 as rocks, called “We-ack”, blocking the old northside trail. It was understood that these named rocks had fallen in recent memory onto the old trail (Bunnell, 1911; Wieczorek; 1992). The old trail likely hugged the riverbank below the talus cone, meaning that debris from that pre-1851 rock fall must have traveled a distance that has only been observed recently during extremely large rock falls (> 500,000 m^3) (Wieczorek; 1992).

John Muir wrote meticulous and poetic descriptions of natural phenomena in the Sierra Nevada, including several rock falls he witnessed in Yosemite Valley. It is only fitting that he also witnessed Middle Brother rock fall. "On the 12th of March, 1873, I witnessed a magnificent avalanche in Yosemite Valley from the base of the second of the Three Brothers. A massive stream of blocks bounded from ledge to ledge and plunged into the talus below with a display of energy inexpressibly wild and exciting. Fine gray foam-dust boiled and swirled along its path, and gradually rose above the top of the cliff, appearing as a dusky cloud on the calm sky. Unmistakable traces of similar avalanches are visible here, probably caused by the decomposition of the feldspathic veins with which the granite is interlaced" (Muir 1960; Wieczorek, 1992). The event described by Muir is probably a very large rock fall with a very approximate volume of 20,000 m^3.

A very large rock fall happened again in January 1923, with a reported fall distance exceeding 300 m and volume great enough to block the road for a distance of 100 m and destroy hundreds of trees with thick trunks, up to 2.5 feet in diameter. An airblast was observed with this event that uprooted and blew the tree tops off, scattered them across the road, and knocked out 150 m of a high voltage power line (Wieczorek, 1992).

In 1987, small rock falls and cracking noises at Middle Brother started occurring with enough frequency over a two-day period that the National Park Service closed Northside Drive, the Yosemite Park exit road (Wieczorek and Snyder, 2004; Wieczorek, 2002; Wieczorek et al., 1995; Wieczorek et al, 1992; Yosemite Association, 1987). This closure was followed two hours later by the largest rock fall in recording history on March 10, 1987 at 2:47pm, when 600,000 m^3 of rock detached and buried Northside Drive to a depth of four meters

Rock fall events at the Three Brothers have been reported, on average, every ten years between 1873 and 1999 (13 rock falls), but more than twice a year from 2000 to 2010 (24 rock falls). More than half of the events occurred during the winter months of December through March, when the cliff is subject to both high amounts of precipitation but also a strong freeze-thaw cycle that repeats with every storm and subsequent sunny weather that follows. In that tally are five events, including those described above, that are classified as very large (~5,000 m^3 and greater). Very large rock falls often scatter debris across the northside trail or road and damage equipment in the narrow corridor between the talus and the river. All of the known very large Middle Brother rock falls occurred during the winter months.

In Yosemite Valley, tallying all locations, very large events have been reported every five to ten years. Middle Brother accounts for nearly a quarter of these very large events, a disproportionate amount, but only a small fraction (< 5%) of the over 800 rock falls reported in Yosemite Valley. We know now that rock fall reporting is biased toward areas in which people happen to be around to witness them. We also know that rock falls are currently reported to occur around once a week in Yosemite Valley, but that even with this greater diligence, we are still missing many events and still have a bias toward populated areas (Stock, personal communication, 2011). This is not meant to suggest that Middle Brother is likely to account for 25% of all rock falls, since there are many small source areas that are unlikely to produce very large rock falls. It does suggest, however, that rock falls at Middle Brother, like many other rock formations in Yosemite Valley, have been grossly under-reported, a postulation that is supported by the tenfold increase in reported rock fall at Middle Brother in the past decade when compared to the previous three decades, which may have been prompted by a greater awareness following two high profile rock falls in the 1990s. The disproportionately high percentage of very large events at Middle Brother may be due to the size of the unstable rock fall source areas there. In other words, Middle Brother may still be very likely to produce very large rock fall events in the future.

8.2 Winter 2007-08 Middle Brother rock fall series

A series of rock falls from a single unstable Middle Brother source area during the winter of 2007-08 was recorded by a single station equipped with a geophone and an accelerometer. Witnesses reported at least four rock falls and the seismic monitoring picked up at least six. We know that instabilities from rock fall events can persist for months, but in the absence of unbiased observation, we do not know for how long. In this case, three events occurred within two hours of each other and the last event occurred ten weeks later (Table 12). Seismic stations were in place for seven weeks after the last recorded rock fall, then dismantled for the summer season.

Table 12. Rock fall series from single source area at Middle Brother in winter, 2007-08.

Date/Time, Local	Location, suspected	Reported?	Weather	Comment
12/18/07 16:00	Middle Brother area "B"	Yes, reliable	Rain and snow	Medium rock fall observed
12/18/07 16:20	Middle Brother area "B"	Maybe, time specified "pm"	Rain and snow	Very similar to first event
12/18/07 17:42	Middle Brother area "B"	Maybe, time specified "pm"	Rain and snow	Weak event, some similarities to first event
1/4/08 18:33	Middle Brother area "B"	Yes, reliable	Rain and snow	Reported from SA "B", seismic character matches first event
1/8/08 10:17	Middle Brother area "B"	Yes, reliable	Approaching storm	Weak event, some similarities to first event
2/28/08 15:55	Middle Brother area "B"	No	Clear	Very similar to first event

The first in the series was reported on December 18th, 2007 at 4pm (local Pacific Standard Time (PST)). Witnesses driving along the road, Northside Drive, reported that large boulders crashed down the talus slope and onto the road. One boulder came to a rest on the road itself (Figure 108), and there were several locations on the roadbed with rock fragments and small impact craters (Figure 109, Figure 110, and Figure 111). One tree in the path of the rock fall was freshly splintered (Figure 112). Although it is difficult to assign a size with any certainty, this first event is thought to be a medium-sized event (> 50 m^3) based on the travel distance and size of some of the observed boulders. According to eyewitness reports, the rocks came from the near the top of a well-established source area ("B" in Figure 107 and Figure 113) and ricocheted south off a prominent ledge just below the source area, before impacting the talus slope and rolling onto the road.

Figure 108. Boulder found sitting in road (Northside Drive) following December 2007 Middle Brother rock falls.

Figure 109. Location of rock fragments and small impact craters on Northside Drive after the December 2007 Middle Brother rock falls. The road was closely immediately and was not plowed until spring.

Figure 110. Small crater from rock impact on Northside Drive.

Figure 111. Rock fragments and small craters from rock impacts on Northside Drive.

Figure 112. Freshly broken tree (center) visible in path of rock fall. The boulder resting on the roadbed can be seen on the far right side. Photo taken from Michael's Ledge.

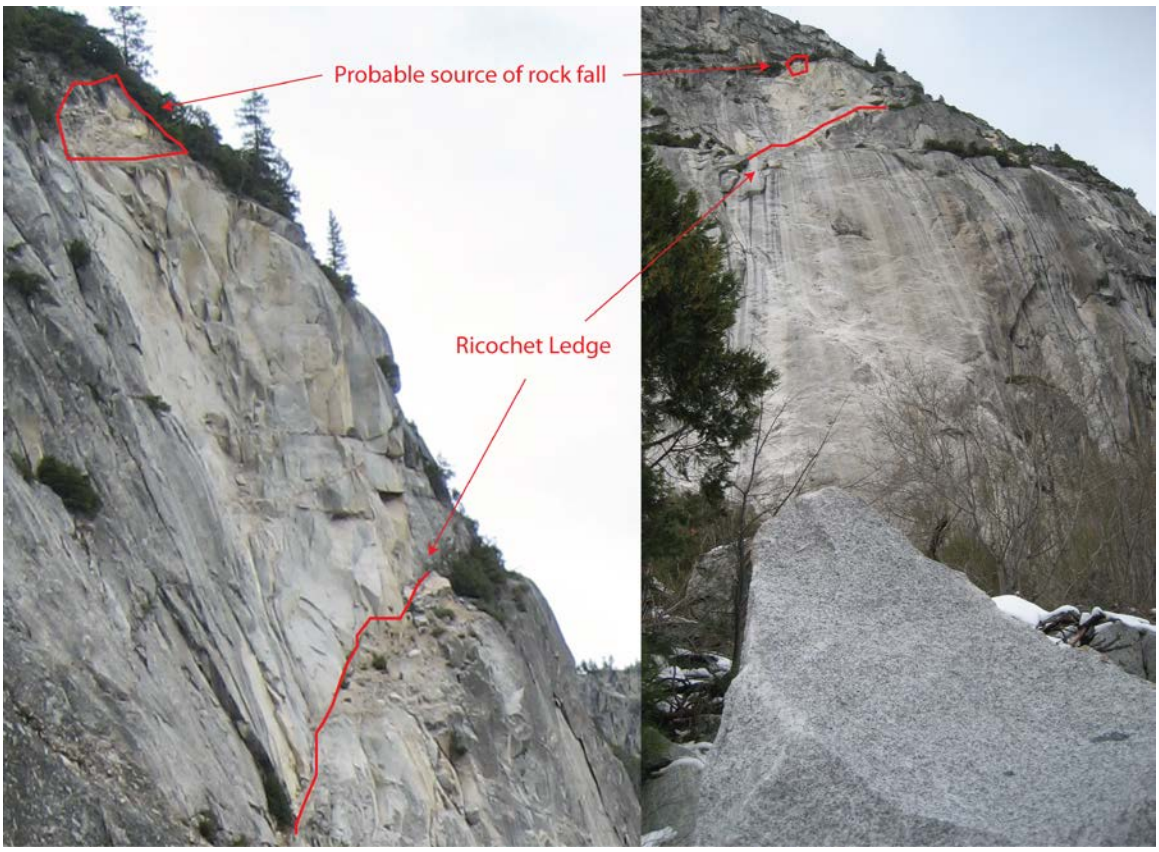

Figure 113. Source area of the December 18th, 2007 rock fall from Michael's Ledge (left). The source area can be seen above the boulder found on the road (right). The rocks ricocheted south (left in the photo) off the prominent ledge just below the source area.

This first event occurred only one week after the seismic station was installed. There are no known rock falls preceding this event, although the possibility still exists that small rock falls did occur before the seismic station was in place. Nevertheless, in the absence of evidence to the contrary, this event is believed to be the first in the series of rock falls from Middle Brother source area "B" during the winter of 2007-08.

The seismic station, over 600 m from the source area, picked up this first rock fall with a high signal to noise ratio. Seismic data show that the event lasted approximately fifty seconds with what appear to be seven to ten rock impacts over a twenty-five second period (Figure 114). The geophone had a strong response from 8 Hz (the corner frequency of the instrument) to approximately 50 Hz, with some individual impacts responding well above 100 Hz (Figure 115). The accelerometer had a good response from a few Hz to about 100 Hz, with the strongest impact generating recordable seismic waves at frequencies well above 100 Hz.

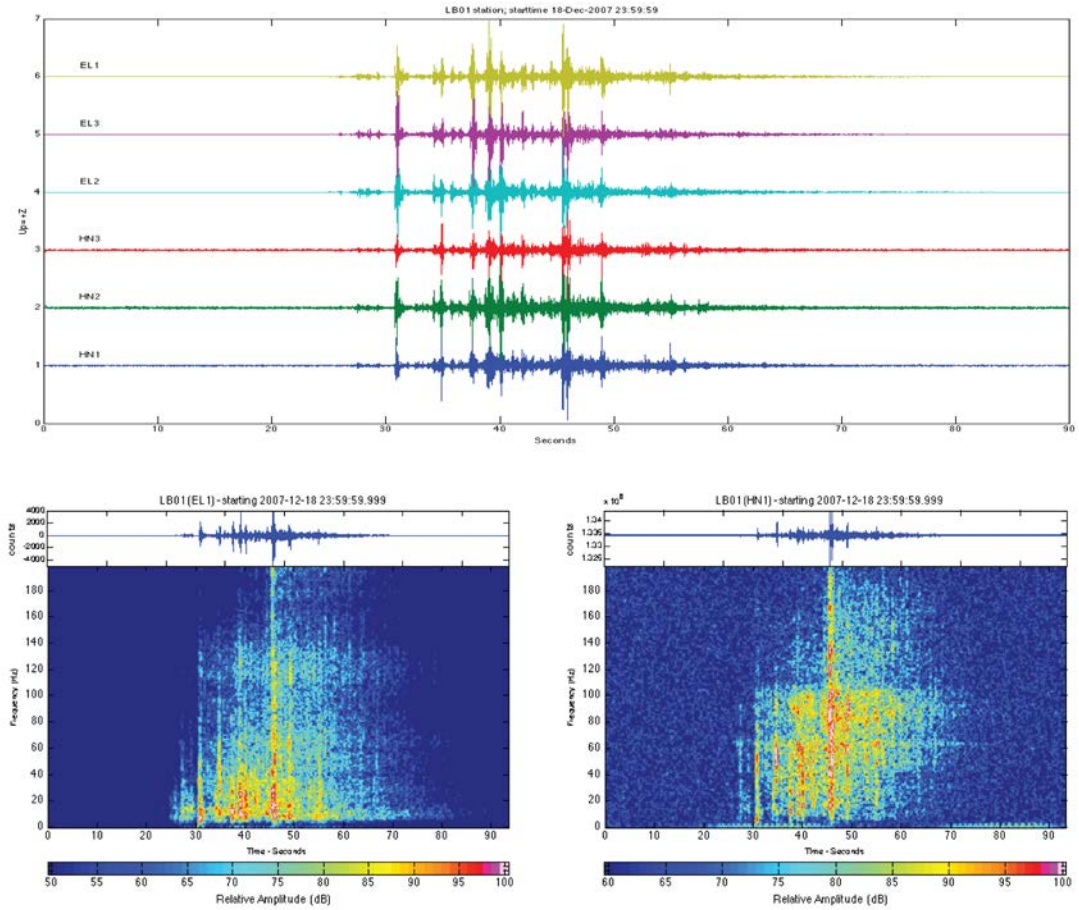

Figure 114. Seismic records (top) and spectrogram Z-component records (bottom) of the December 18th, 2007 Middle Brother rock fall at station LB01 600 m away (geophone, left, accelerometer, right, all times in GMT).

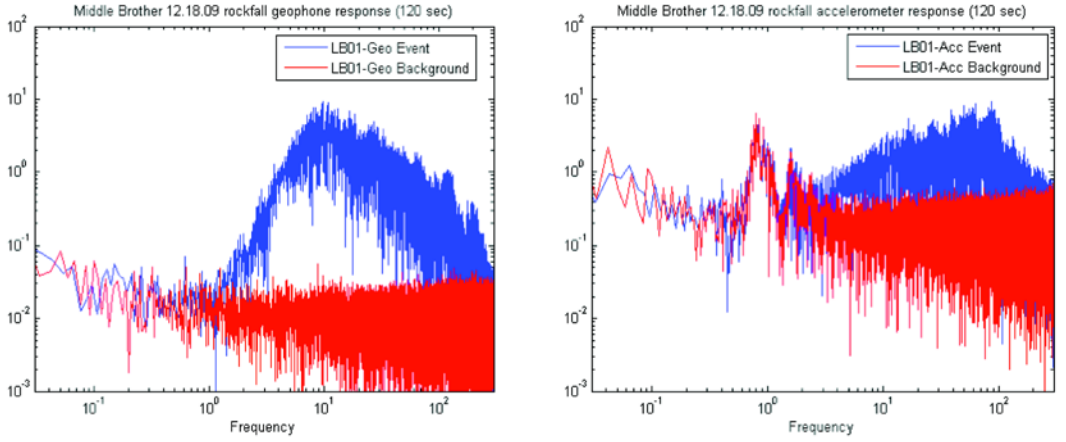

Figure 115. Geophone (left) and accelerometer (right) spectral response to the December 18th, 2007 Middle Brother rock fall (blue), compared with background noise level on the same day (red).

Closer examination of the seismic data reveals that there is a signal arriving at least six seconds prior to the first strong impact pulse (Figure 116). This pre-impact signal is certainly associated with the rock fall in progress prior to impact, and may be a record of the initial detachment. A detachment signal, if it exists, would be particularly interesting as it may help to determine the initial failure mechanics. Normally, such a calculation requires several stations, but this data was collected during a single station feasibility study, precluding this type of analysis. However, this data may help to determine future potential for failure mechanics studies based on first motions. In order for first motion analysis to be a possibility, the signal-to-noise ratio must be high enough to determine orientation. The signal initiation can be seen on a zoomed in view, but the amplitude is very near the amplitude of noise arriving prior to (what appears to be) the first motion (Figure 117), thus picking out first motions with any certainty in orientation is difficult.

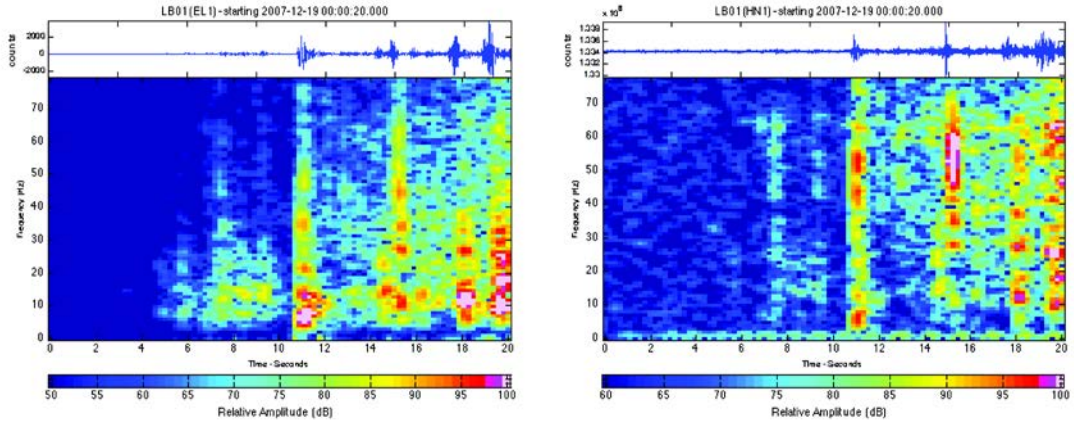

Figure 116. Close up of the initiation of the rock fall. The main rock fall signal starts at 10.5 seconds, but there is a signal arriving more than 6 seconds earlier on the geophone (left) and accelerometer (right).

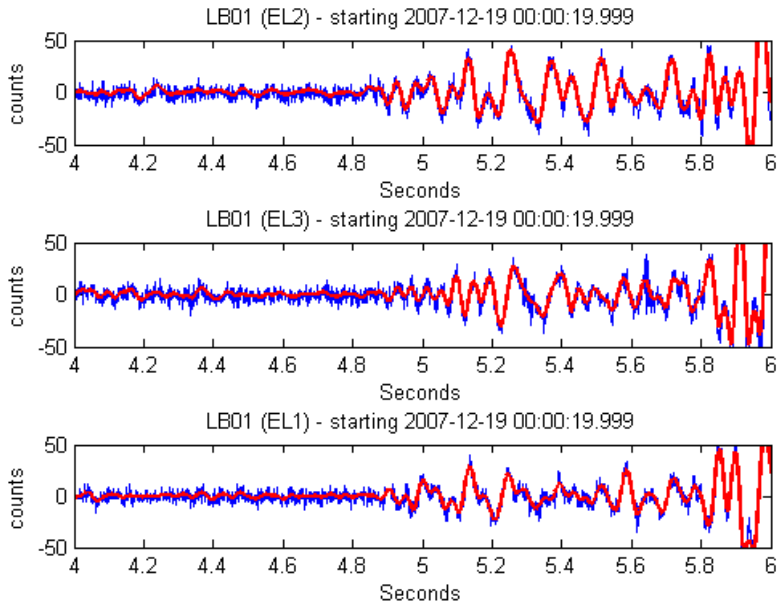

Figure 117. Two-second view showing the initial signal of the December 18th, 2007 rock fall. Filtered 1-20 Hz data is shown in red and unfiltered data in blue.

The Middle Brother cliff was put under intermittent observation and the road closed immediately following the first observed rock fall during the winter of 2007-08. It was reported that rock falls continued that evening, but no specific times were recorded until the following afternoon, when a small rock fall was reported at around 3:30 pm (local PST) from source area "C". The difference in seismic characteristics between this rock fall and all of the others supports the hypothesis that both source areas "B" and "C" were simultaneously producing rock falls. Thus, the next day's rock fall is not part of the series and is discussed in detail in later sections.

Using the information from eyewitnesses and the results from the triggering algorithm, additional rock falls were found. There are two more rock falls during the next two hours, at 4:20 pm and 5:42 pm. The 4:20 pm rock fall (Figure 118) has an overall weaker spectral response than the original record but a very similar seven to ten individual impacts spread out over a forty second period. No initiation or detachment signal is visible. The 5:42 pm rock fall (Figure 119) is even weaker, barely registering on the accelerometer, and shows only three to four impacts over a twenty second period.

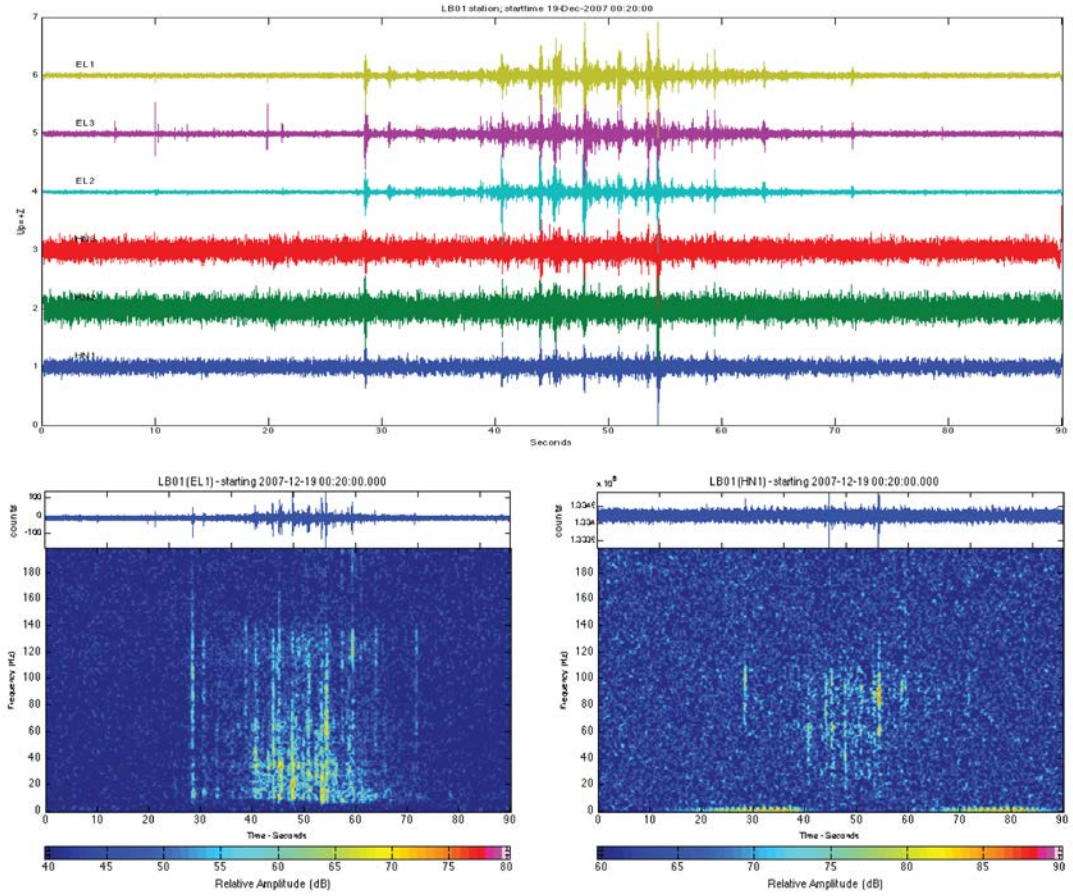

Figure 118. Middle Brother rock fall on December 18th, 2007 at 4:20 pm local PST. Seismic data is indexed to GMT.

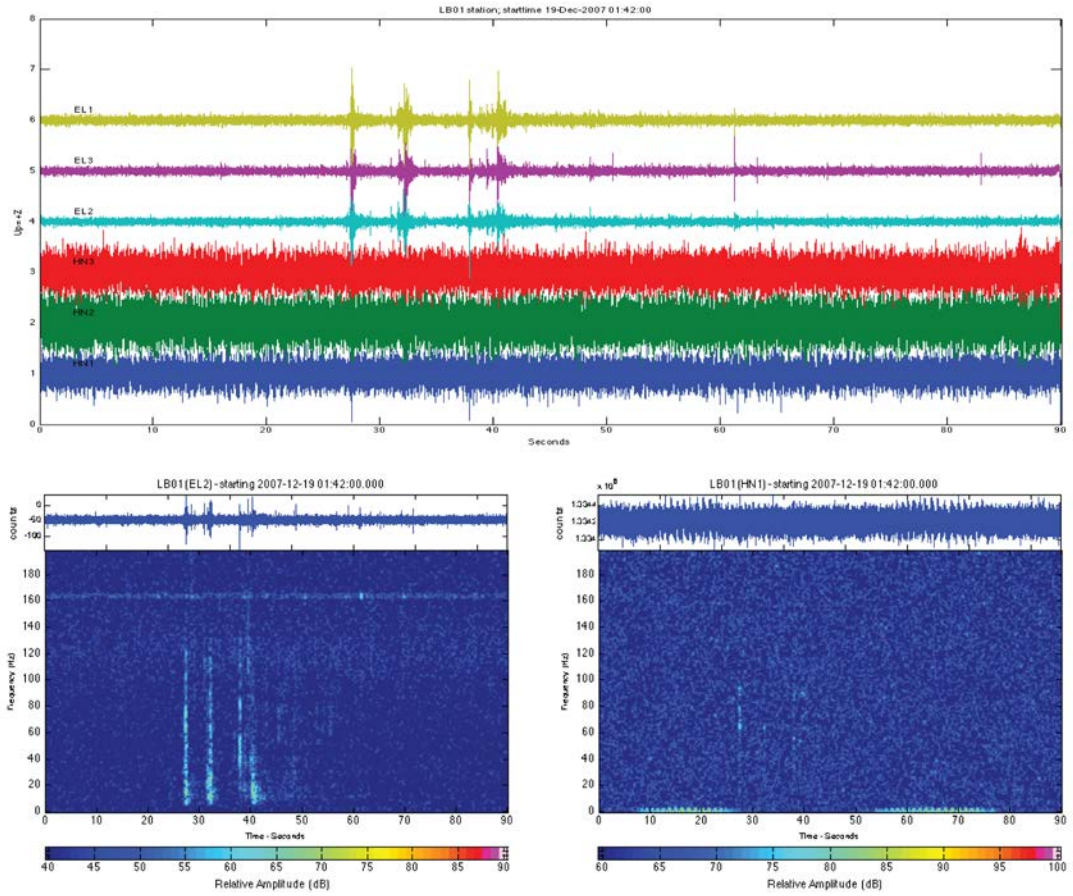

Figure 119. Middle Brother rock fall on December 18th, 2007 at 5:42 pm local PST. Seismic data is indexed to GMT.

One more rock fall was witnessed and reported from the same site on January 4th, 2008. In addition, there were at least three additional instances of rock fall noise heard from the direction of Middle Brother, on December 25th, 2007 after dark, on January 8th, 2008 at around 7pm, and on January 27th, 2008 in the morning. Of those, the rock falls on January 4th and 8th, 2008 triggered the seismic network. There was no sign of any rock fall activity on the evening of December 25th. There were triggers on the morning of January 27th, including one weak event at 7:39 am but it does not strongly resemble a rock fall. Finally, on February 28th, 2008 at 3:55 pm (local PST) a seismic event triggered and was determined to have a high likelihood of being a rock fall from source area "B" due to the similarity in seismic characteristics. This rock fall was not witnessed, although the weather was clear.

The January 4th event, at 6:33 pm (local PST), lasts forty seconds and has seven to ten impact pulses, and possibly some activity before the first large impact (Figure 120). The seismic character of this event suggests that it too originated from source area "B". The January 8th event, at 10:17 am, was reported to originate from source area "B". It is a weaker event with three to five distinct pulses over twenty-five seconds and more activity in the lower frequency band. It was also not recorded by the accelerometer (Figure 121). In fact, if not for a reliable eyewitness report, this event would not be considered a high certainty rock fall event.

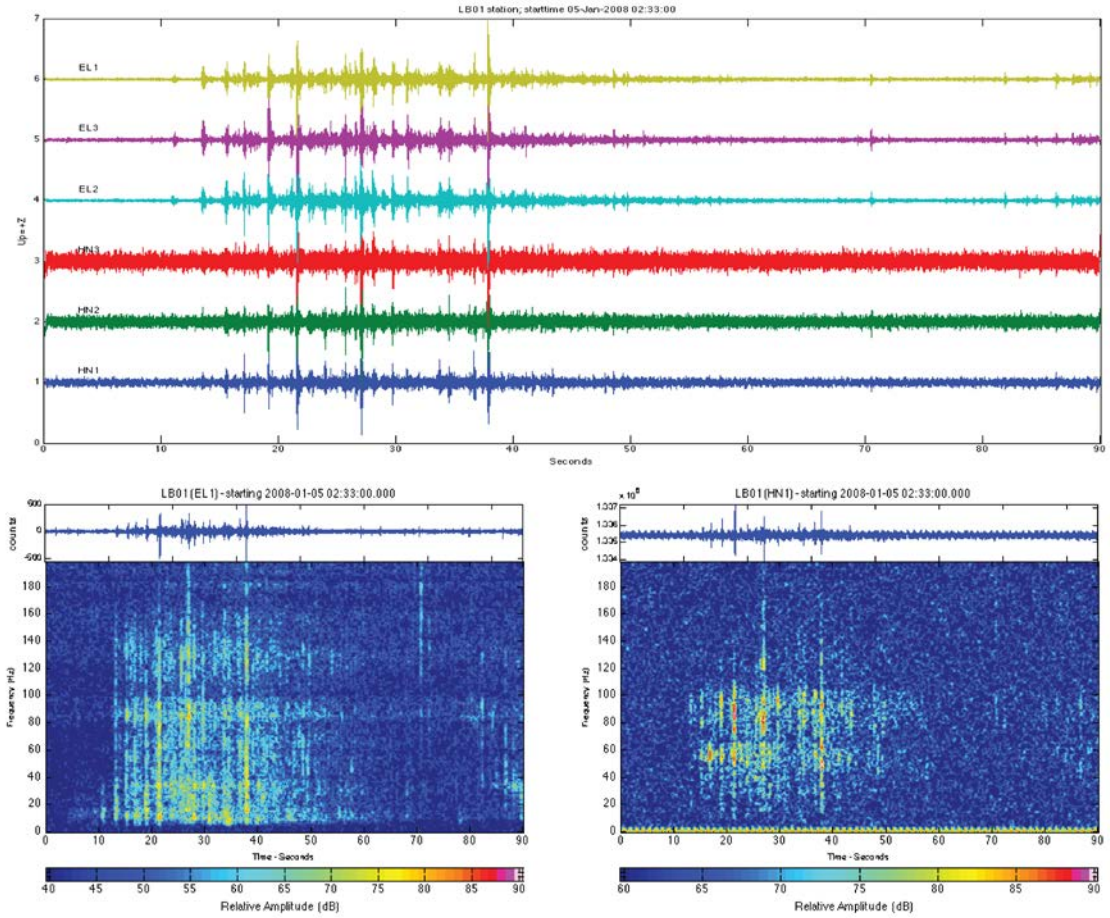

Figure 120. Middle Brother rock fall on January 4th, 2008 at 6:33 pm (local PST). Seismic data is indexed to GMT.

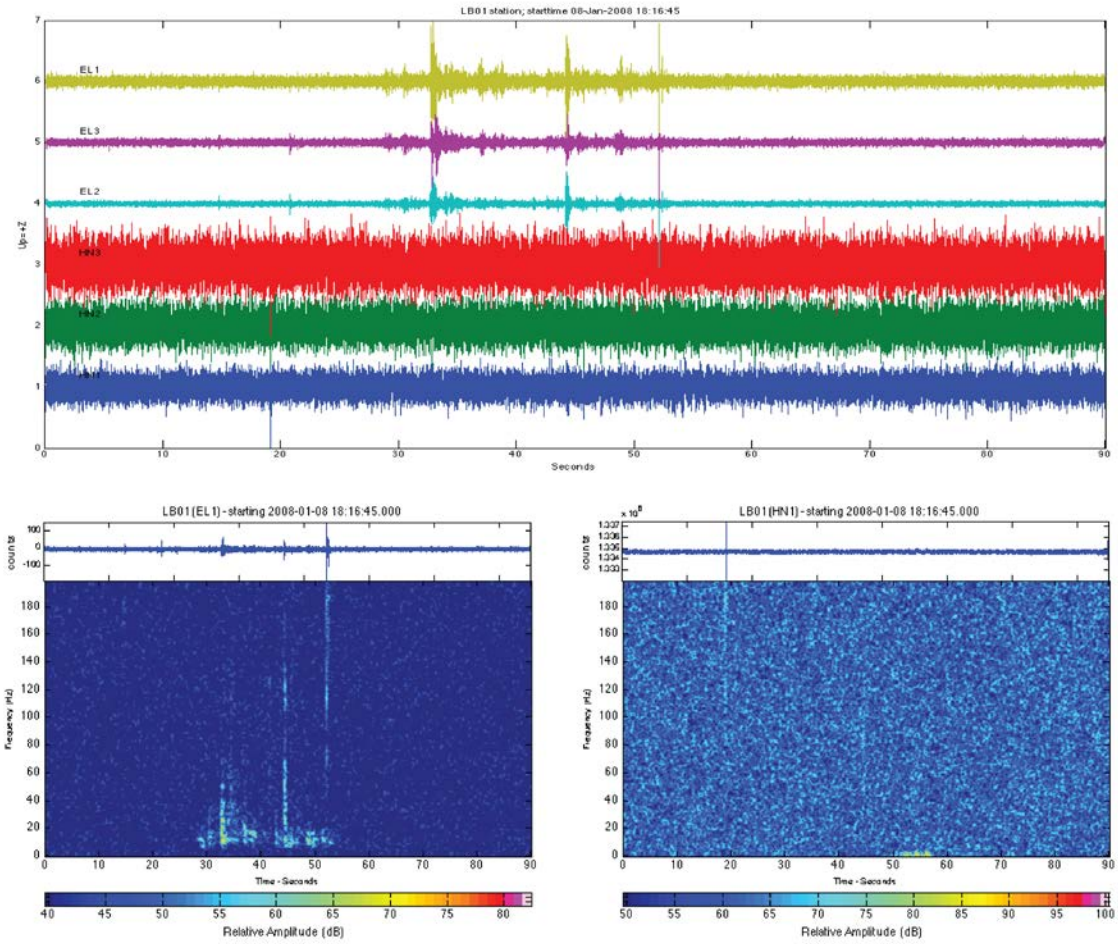

Figure 121. Middle Brother rock fall on January 8th, 2008 at 10:17 am (local PST). Seismic data is indexed to GMT.

Finally, two months after the initial event, a seismic event highly resembling a Middle Brother source area "B" rock fall was discovered on February 28th, 2008 at 3:55 pm (local PST). It was not reported even though the weather was clear, but is considered a high certainty event due to its seismic character. This rock fall, like many previous events, has ten to twelve distinct impacts over a thirty-second period (Figure 122).

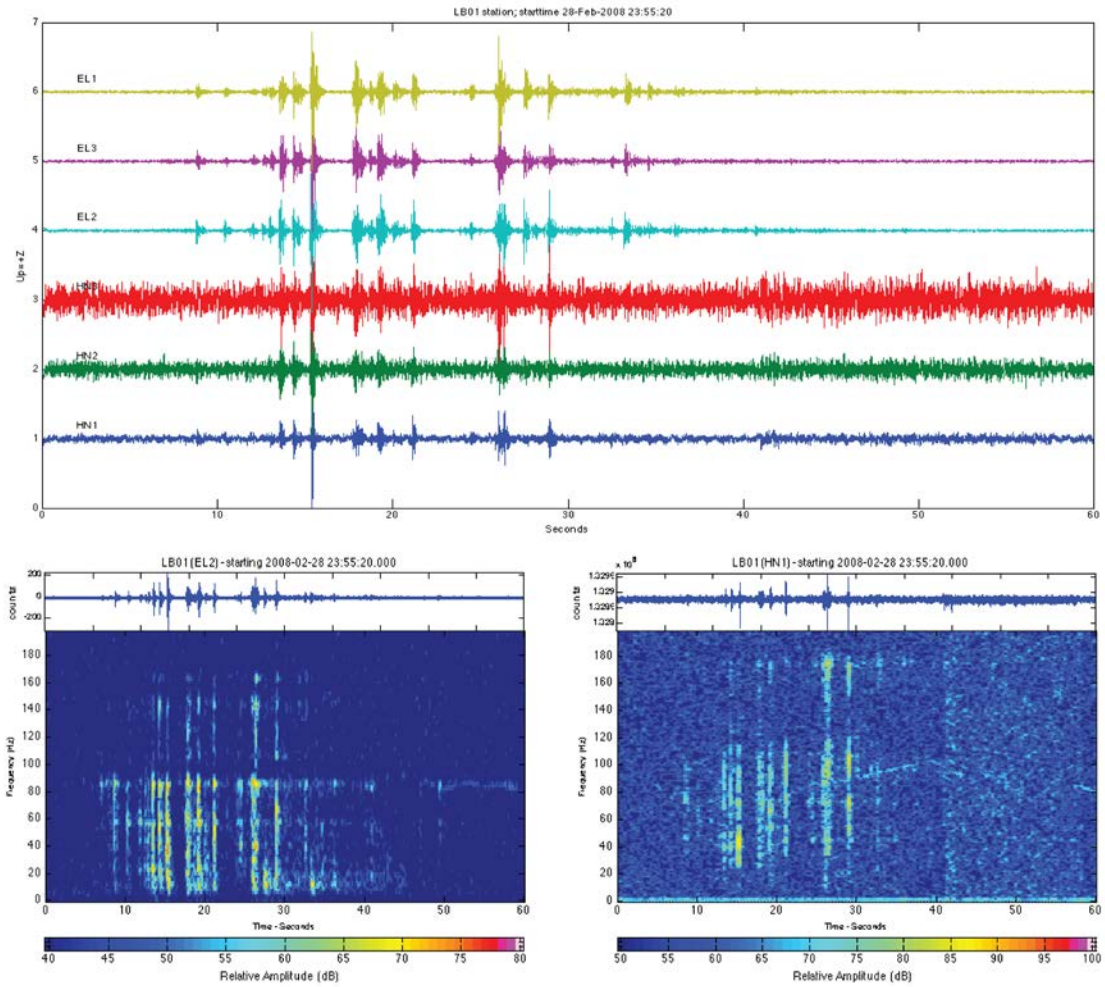

Figure 122. Middle Brother rock fall on February 28th, 2008 at 3:55 pm (local PST). Seismic data is indexed to GMT.

The similarity in spectral character and timing of these six rock falls was the key to grouping all of them together as coming from a single source area. At least two, and possibly four of these rock falls were actually witnessed as coming from Middle Brother source area "B". The similarity in timing of the individual impacts over a 30 to 40 second duration is indicative of a similar trajectory and fall height (Figure 123). These features also stand out in spectrograms, especially when grouped in order of similarity and when using the same color scale (Figure 124). Brighter colors indicate stronger amplitudes, and thus, larger impacts caused by bigger blocks. The largest event is also the first event (upper left corner, Figure 124). The presence or lack of higher frequencies is a clue to the distance to the rock fall. Higher frequencies rapidly attenuate, even for very large rock falls. The fact that all six events have at least one impact with a spectral response of at least 150 Hz indicates both that these rock falls are close, and that they are all a similar distance away. The two smallest rock falls (ride side, Figure 124) are dissimilar enough from the others that, if not for a reliable eyewitness placing one of them at source area "B", they might not have been included as a definite part of this rock fall series. Conservatively, they might not even have been classified as rock falls with highly certainty. Thus, these two weakest rock falls are especially important case studies that are used to assess other unknown seismic events.

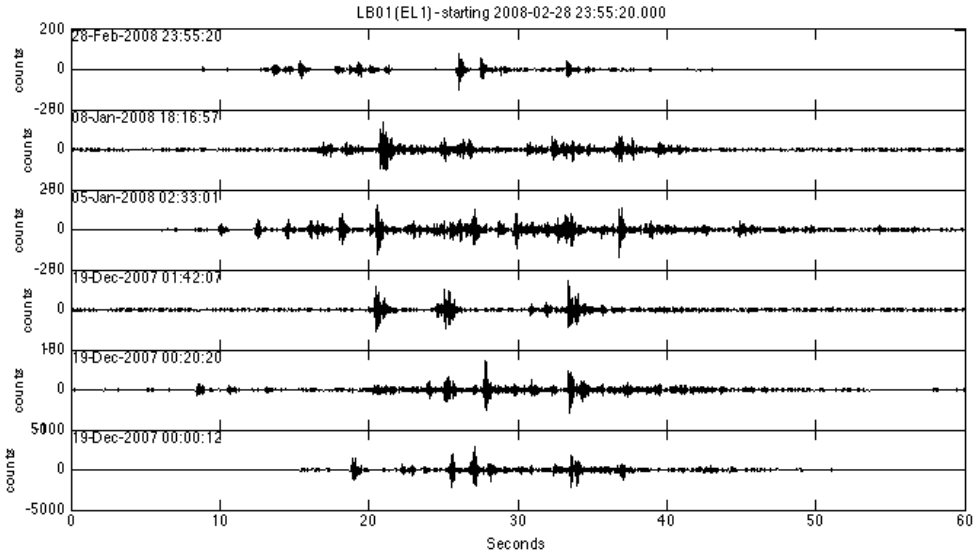

Figure 123. Six rock falls originating at Middle Brother source area "B" during the winter of 2007-08, showing Z-component seismic records recorded by an 8 Hz geophone.

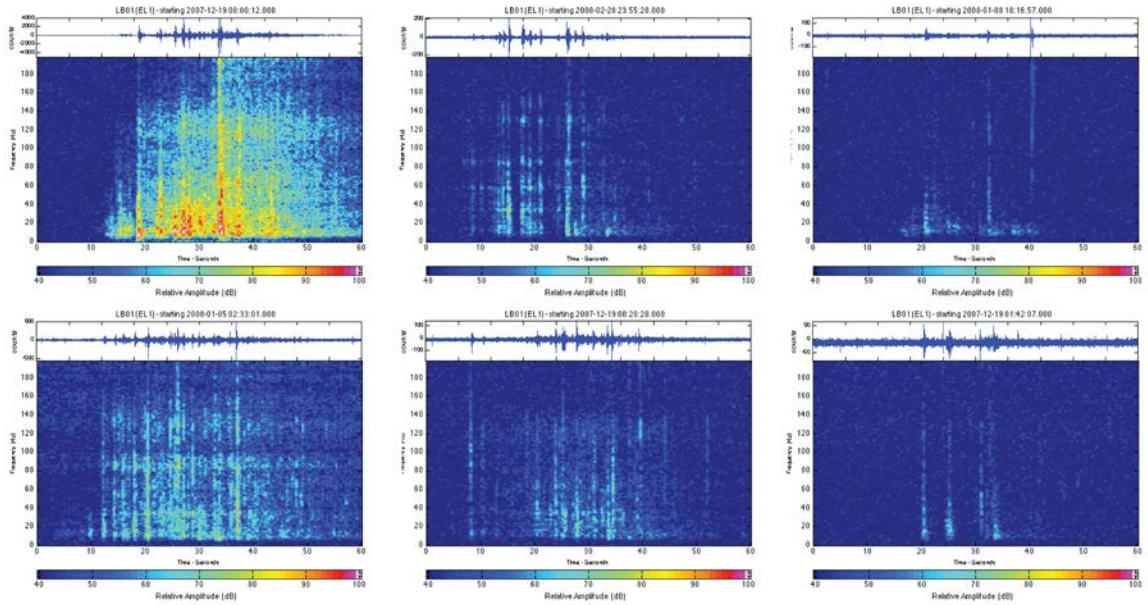

Figure 124. Rock fall spectrograms showing 60 seconds of data and the same color scaling for the six Middle Brother source area "B" rock falls in winter 2007-08.

8.3 Rock falls near Middle Brother unrelated to the series

Five additional rock falls in the vicinity of the Three Brothers were recorded that do not appear to be part of any known rock fall series (Table 13). The rock falls described in this section span two different winter monitoring seasons, but there were no instruments in place during the summer. During the winter of 2007-08, there was a single station on Lower Brother with a geophone and an accelerometer, which was removed in April 2008. During the winter of 2008-09, six seismic stations at three different locations were installed at the Three Brothers, including two infrasound microphones for a short period of time.

Table 13. Rock falls in the vicinity of Middle Brother not part of a known series.

Date/Time, Local	Location, suspected	Reported?	Weather	Comment
12/19/07 15:28	Middle Brother area "C"	Yes, reliable	Rain and snow	Reported from SA "C", dissimilar to all previous events
12/15/08 2:24	Middle Brother area "A"	No	Rain and snow	Response on infrasound acoustic
12/20/08 21:33	Middle Brother area "A"	No	Storm cycle lull	Small event that was discovered when rock fall cut a cable
1/14/09 21:21	Middle Brother area "B" or "C"?	No	Clear	Somewhat uncertain, impact east of seismic stations
1/17/09 13:54	West of Lower Brother	Yes, location unknown	Clear	Large rock fall reported, location unspecified, seismic waves arriving from the west of LB

On December 19th, 2007, a reliable witness observed a small (a few m^3) rock fall at 3:30 pm that originated from Middle Brother source area "C" (Figure 107). This event occurred within 24 hours of three rock fall events from Middle Brother source area "B". Source areas "B" and "C" look very similar, so the possibility was considered that the witness was mistaken on the source location. The seismic character of this rock fall, however, is very different from the other rock falls from source area "B". This rock fall consisted of a single, sharp impact with response over 150 Hz preceded and followed by low frequency signals. Only the geophone recorded signal below 20 Hz and triggered the event detection algorithm. The accelerometer, although not triggering, did register this event between 50 and 100 Hz (Figure 125). The pre-impact signal starts eight seconds earlier than the impact pulse and appears to last about four seconds. The early pre-impact period and the seismically quiescent four seconds leads to the hypothesis that the pre-impact signal is related to the detachment and that the rock went ballistic prior to a single large impact. The seismic character of this event is different from the other rock falls from source area "B" in the following ways: it has an earlier initiation signal, a seismic quiescent period, and a single impact. These differences lend credibility to the idea that this rock fall is not part of the rock fall series from source area "B", and thus, the location, source area "C", was correctly observed by the eyewitness. In addition, the simplicity of this record, e.g. a detachment signal followed by a single impact, makes it a good candidate for testing the feasibility of other types of analysis.

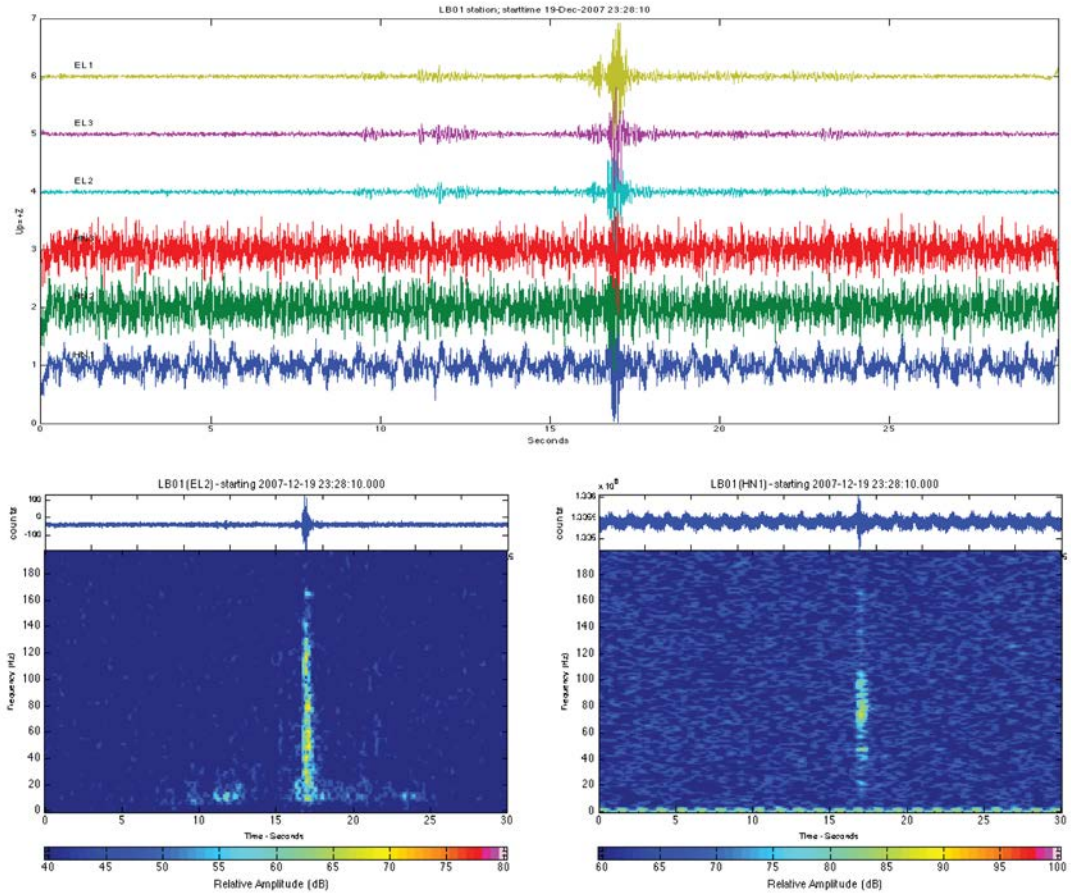

Figure 125. Middle Brother rock fall on December 19th, 2007 at 3:28 pm. Seismic data is indexed to GMT.

The next few rock falls occurred during the winter of 2008-09, when there were stations several hundred meters apart in place. On December 15th, 2008 at 2:28 am, an unreported rock fall occurred during a winter storm. Precipitation noise can be seen on some spectrograms in the form of higher frequency spikes (Figure 126). This rock fall consists of several large impacts over a thirty second period and a six second pre-impact signal, but one of the early impacts is dominant over the others, which is different than previously-recorded events. Given that this event was detected at seismic stations in three different locations, there in an opportunity to locate the event. The seismic waves arrive at stations MB02 and MB07, at the base of the cliff between source areas "A" and "B" before they arrive at stations LB03 and LB05, on Michael's Ledge west of Middle Brother (Figure 107). The location of the seismic source can be estimated with a third location, but the timing at station MB06 is unreliable due to a malfunctioning GPS unit. It has been determined, however, that the seismic waves are not arriving on a direct path between the MB02/7 and LB03/5 locations since the back-calculated velocities are too high. Therefore the seismic waves are either originating at a location between or oblique to the two locations. The third station, MB06, has both seismic and infrasound sensors (Figure 127). The velocity difference between seismic and acoustic waves is used calculate an event distance to station MB06. Although the absolute timing is incorrect, the internal timing is consistent, allowing the calculation. This event occurred between 270 and 320 meters from station MB06 and since the infrasound wave arrives earlier at the east-most microphone, the source is also east. All of the Middle Brother source areas are east of station MB06, but only the top of the talus pile from source area "A" is 300 meters away, while other talus piles and source areas "B" and "C" are significantly further. Therefore, this is a rock fall that originates from source area "A" and is large enough to produce seismic waves recorded at three locations and infrasound picked by the microphones.

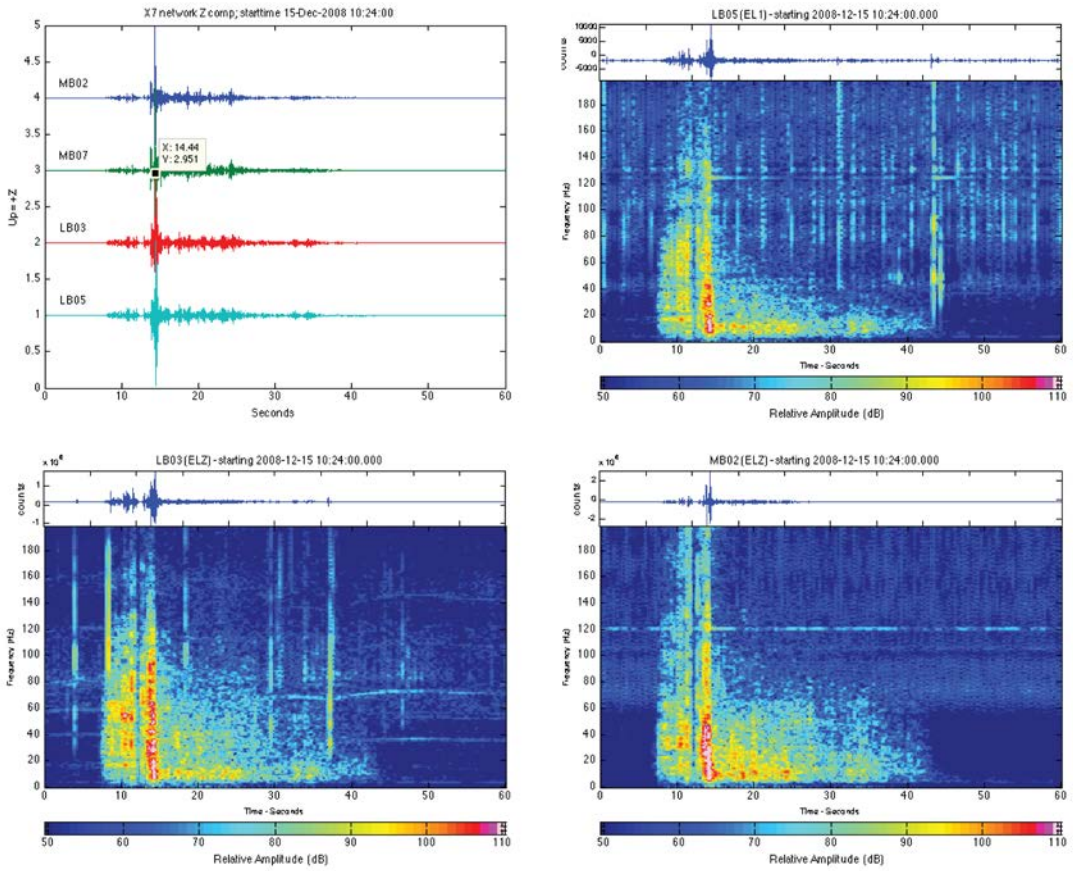

Figure 126. Middle Brother rock fall on December 15th, 2008 at 2:24 am (local PST). Seismic data is indexed to GMT. Two stations, LB03 and LB05 (top right and bottom) left are located on a ledge 270 m above the valley floor and MB02 (bottom right) is located between the cliff between two talus piles.

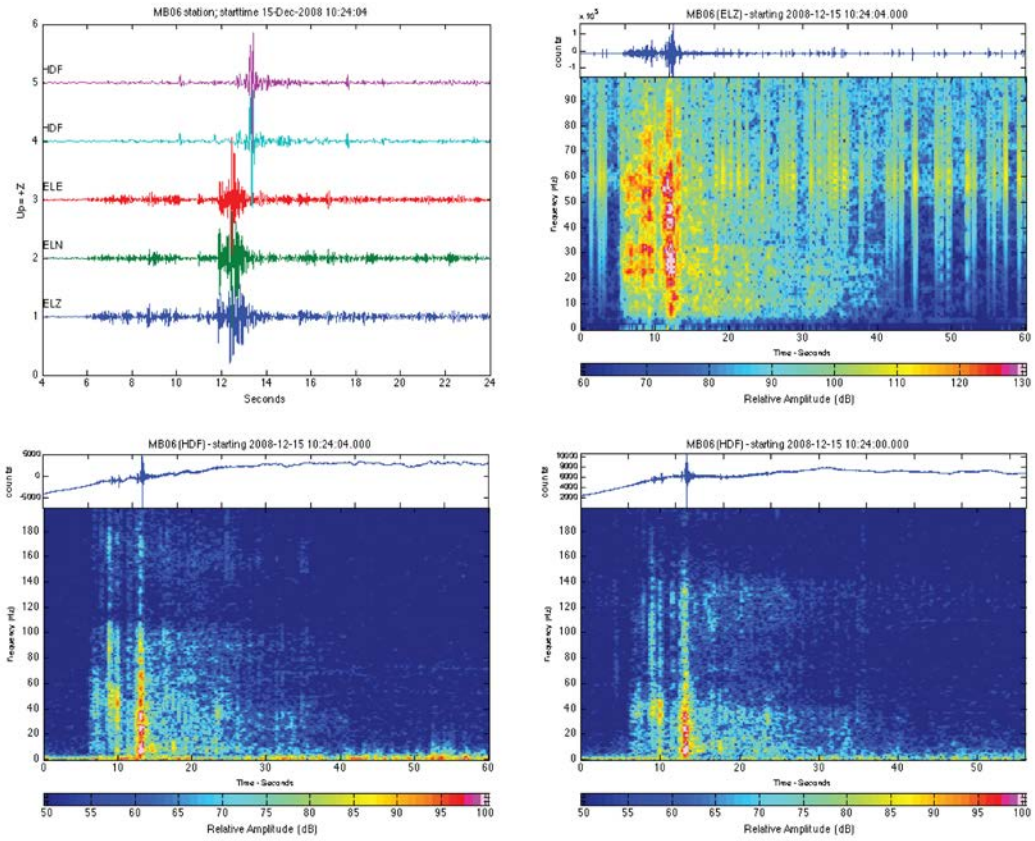

Figure 127. Middle Brother rock fall on December 15th, 2008 showing records from station MB06 400 m above the valley floor. The seismic signals are shown as records ELE, ELN, and ELZ in the top left and the ELZ spectrogram in the top right. Infrasound signals, HDF, are shown in the top left and also in both spectrograms on the bottom.

The next rock fall occurred on December 20th, 2008 at 9:33 pm (local PST) during a short lull in a storm cycle. This event severed a cable connecting a datalogger and an infrasound acoustic microphone placed in an exposed location below source area "A". Although there were five geophone stations running, only the geophone a few meters from the severed cable recorded any seismic activity. Based on the lack of widespread detection, this is a very small event. The signals recorded by the two infrasound sensors and the three-component geophone are shown in Figure 128 (top left). The sensor with the severed cable is the second record from the top, and after 18 seconds, the entire signal is electronic noise. A close up of the two infrasound sensors is shown in Figure 128 (top right) with the severed cable sensor as the top record. The bottom half of Figure 128 shows spectrograms from the geophone (bottom left) and the undamaged infrasound sensor (bottom right). Since this rock fall was only recorded at one station, it did not cause a network trigger and was only discovered by looking for the moment when the cable severed. The infrasound microphones were moved into Yosemite Valley for the remainder of the season after this incident.

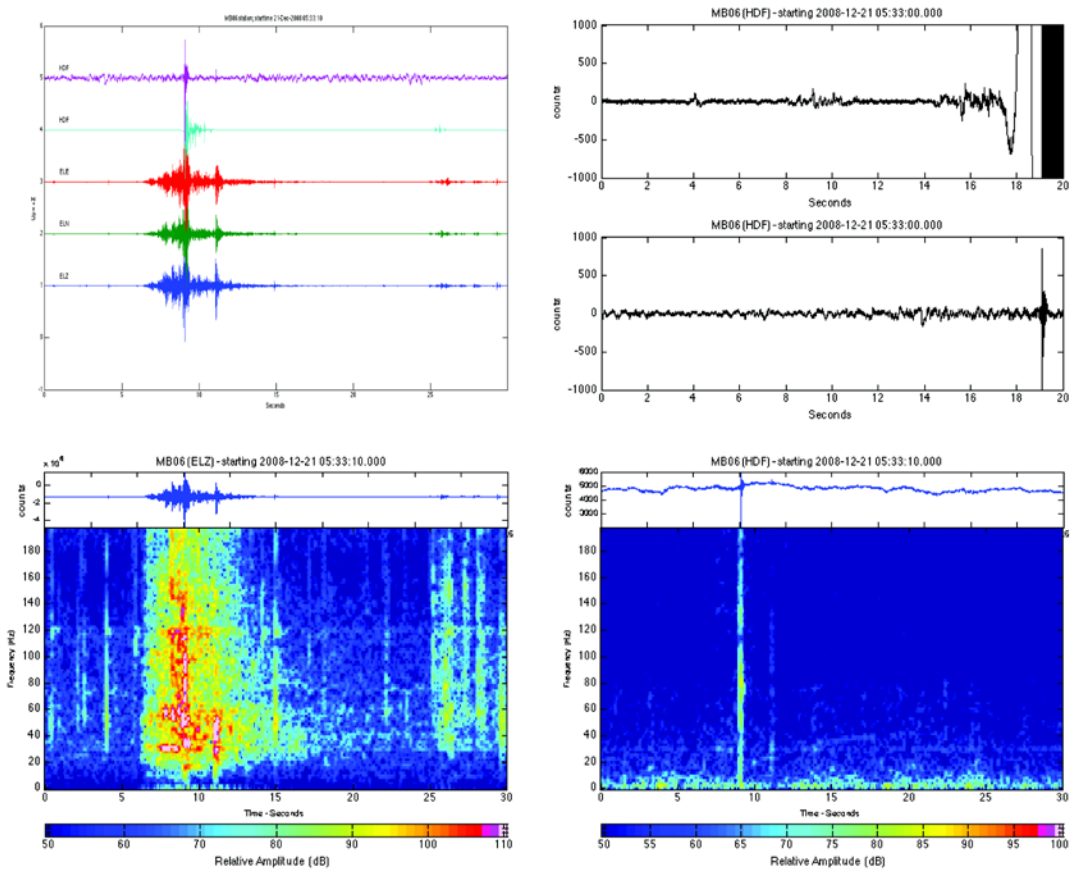

Figure 128. Middle Brother rock fall on December 20th, 2008 at 9:33 pm (local PST). This rock fall severed one of the cables to the infrasound acoustic sensor. Top left shows the two infrasound signals and the three-component geophone: the second record from the top is the infrasound sensor with the cut cable, at 18 seconds (top left). A closer look at the two infrasound channels (top right) reveals that the signal on the top sensor looks normal and then gets very noisy, and corresponds with a spike on the bottom sensor. Spectrograms of the intact infrasound sensor (bottom right) and the geophone (bottom left) are shown.

On January 14th, 2009 a probable rock fall was detected at three different locations during a period of clear weather, but occurred at 9:21 pm (local PST), which contributes to it being an unreported event. There are four individual impacts over a twenty-second period with some seismic activity preceding the first impact by five seconds (Figure 129). The strongest impulse was recorded at the easternmost station near the base of the cliff (MB02). The seismic waves arrive at the MB02 station first as well, and a rough 2-D analysis of the location of the seismic source puts it very near to or east of MB02 (Figure 130).

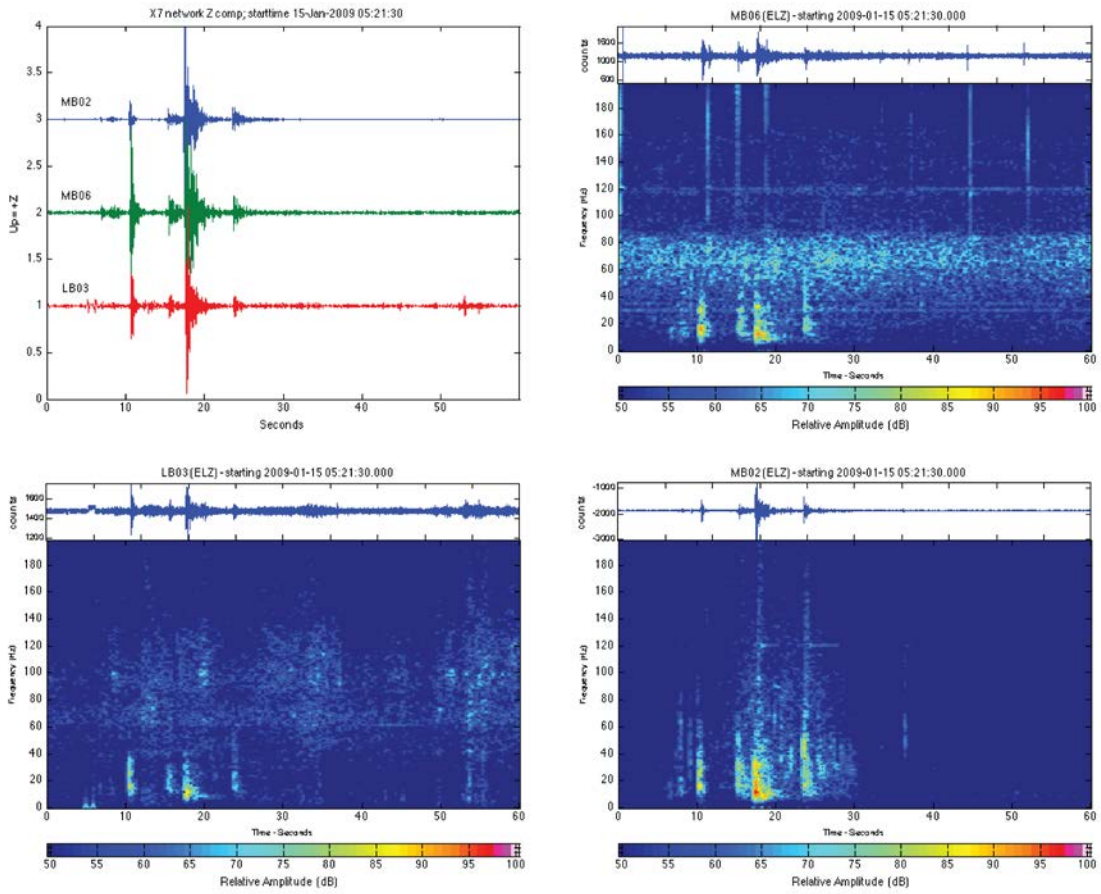

Figure 129. Middle Brother probable rock fall on January 14th, 2009 at 9:21 pm (local PST), showing three stations (top left), station MB06 high and east on Michael's Ledge (top right), station LB03 lower and west on Michael's Ledge (bottom left), and station MB02 east on and on the talus pile (bottom right).

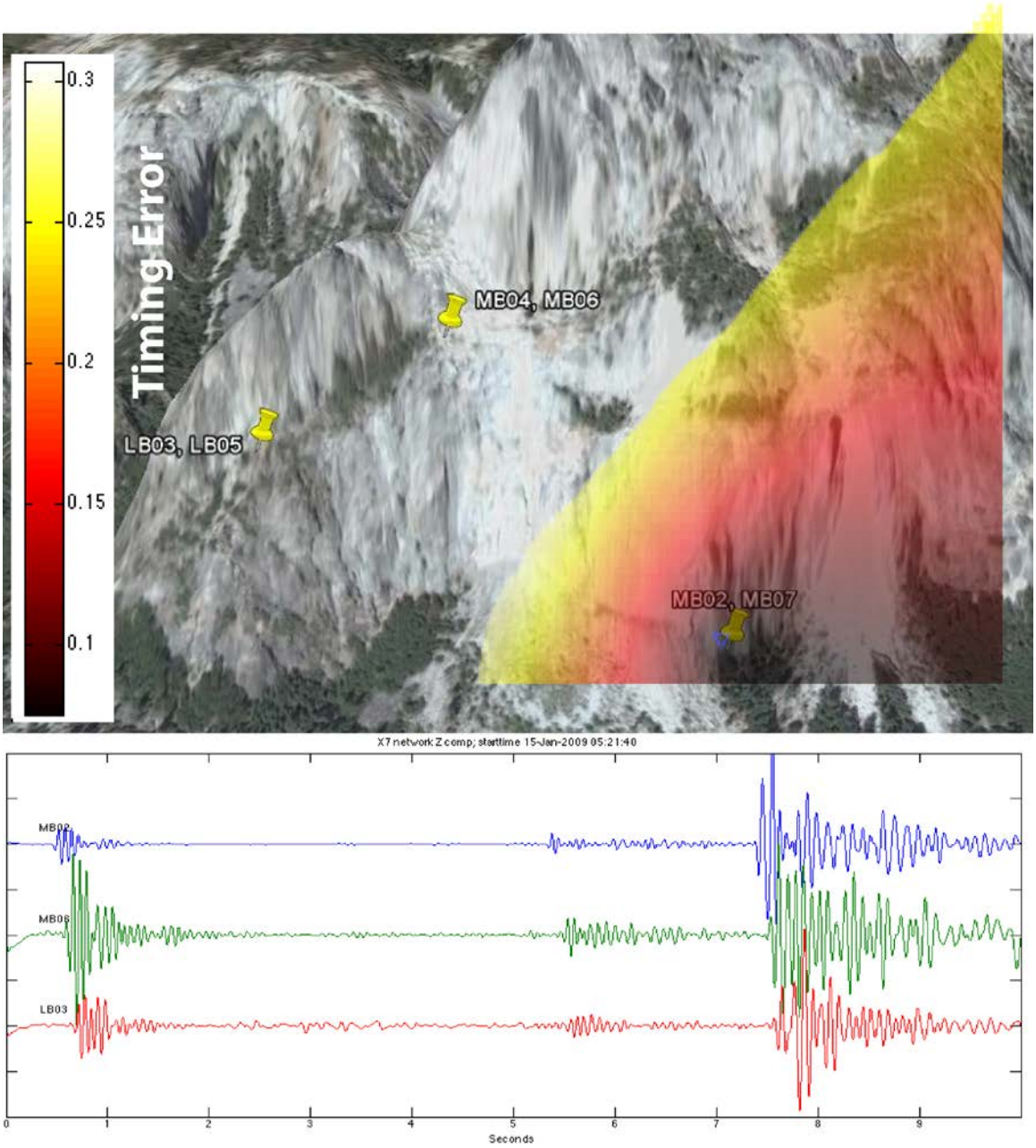

Figure 130. Map showing the roughly calculated 2-D source location to the near MB02. The colors represent the sum of the difference in seconds of the measured and calculated arrival times (top). Lower numbers represent a better model fit to the data. A 10-second seismic record shows that that waves arrive at MB02, then MB06, and last at LB03 (bottom).

On January 17th, 2009 at 1:54 pm (local PST) a rock fall was reportedly heard somewhere between Middle Brother and El Capitan on a clear day. The seismic record looks very similar to other rock fall events in that it has higher frequency content in the form of five or more individual impacts over a forty second period, and some pre-impact signal (Figure 131), but the spectral energy dissipates rapidly above 40 Hz. The fact that spectral energy is confined to the lower frequencies is a sign that this rock fall is farther away than other Middle Brother rock falls. Since there are stations at three locations in operation, it is possible to locate the source of the incoming seismic waves. First of all, the waves arrive first at the westernmost station, LB03, indicating, at minimum, that this is the closest station. A rough model inversion of the location of the incoming waves places them to the directly west of LB03 (not oblique to or between LB03 and the other stations) and that they are travelling horizontally along the face of the cliff (Figure 132). Therefore, according to the seismic data, this event originated at a location on the north side of Yosemite Valley, west of Lower Brother, and is probably a medium to large rock fall near to the seismic network but farther than any of the Middle Brother source areas. This is consistent with the eyewitness account, which reported tens of seconds of rock fall activity someplace between the East Buttress of El Capitan and Middle Brother. It is also consistent with the lack of talus pile evidence at Middle Brother and the hypothesis that this event may have occurred in the difficult-to-reach Eagle Canyon on the west side of the Three Brothers (Stock, 2011).

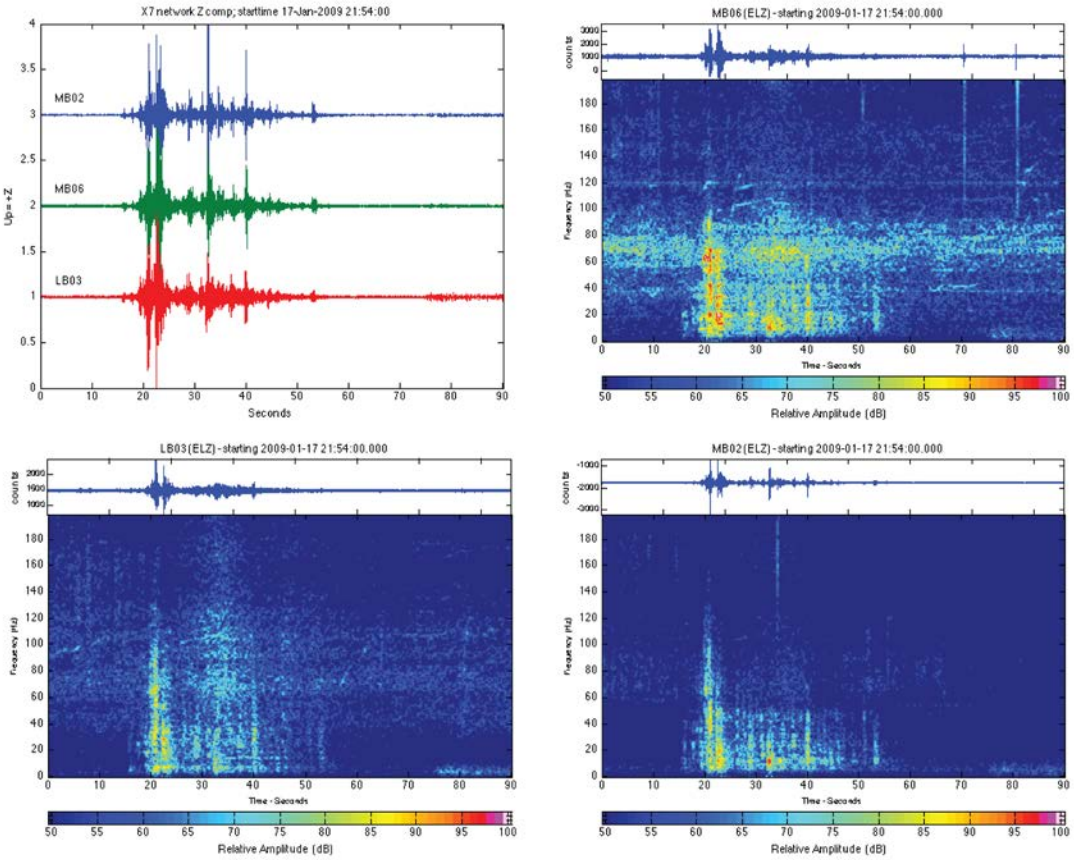

Figure 131. Middle Brother rock fall on January 17th, 2009 at 1:54 pm (local PST).

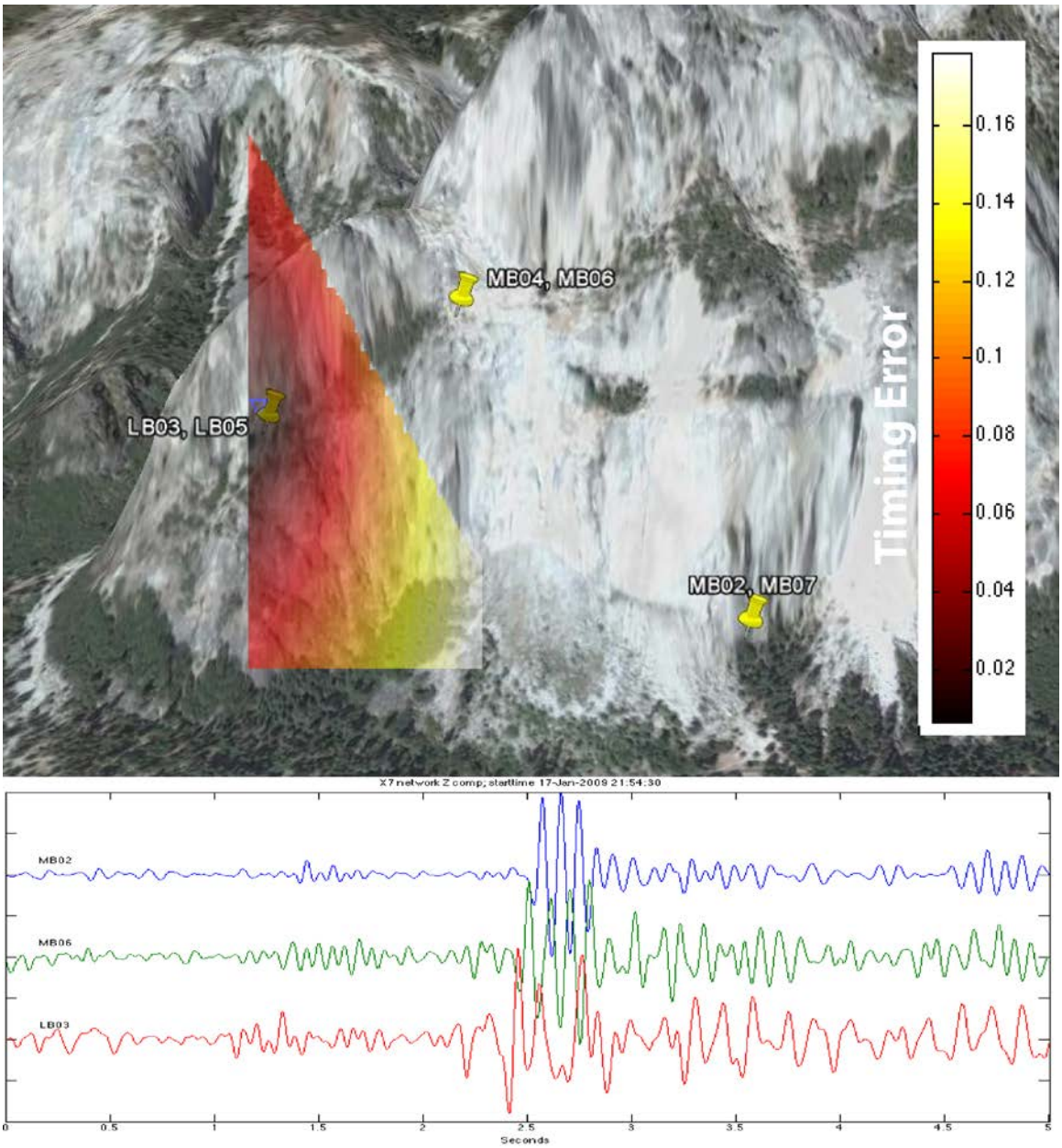

Figure 132. Map showing the simplified two-dimensional source location to the west of LB03, LB05. The colors represent the sum of the difference in seconds of the measured and calculated arrival times (top). Lower numbers represent a better model fit to the data. A 5-second seismic record shows that that waves arrive at LB03, then MB06, and last at MB02 (bottom).

8.4 Discussion of uncertainty in designating seismic events as rock falls

Eleven seismic events have been declared rock falls with high certainty. Deciding that a particular seismic event is, or might be a rock fall is a multi-step, iterative process that is deserving of explanation. For three of the eleven high certainty rock falls, highly reliable witnesses corroborated the time and location. In two cases, the rock falls were heard at a particular time, but not seen. In two more cases, the rock fall locations were seen but the time was not reported reliably. In another case, the equipment was damaged in a location known to be exposed to rock fall and the seismic record of this event was found by searching the data for the moment when the instrument was damaged. Thus, eight out of the eleven rock falls discovered in the seismic data were supported by other evidence and provided a valuable set of examples from which other unknown seismic events could be assessed. In the end, another three events were also determined to be rock falls due to their similarity in spectral character to the other rock falls and/or their widespread detection. This is, however, a conservative number. There are an additional five seismic events that share some characteristics with rock falls and have not been attributed to any other seismic source. There is not enough data to be highly certain that they are, or are not rock fall records. Instead, these five events have been declared "possible rock falls".

The five possible rock falls are compared to similar rock falls and other non rock fall seismic events in order to show some of the similarities and differences. The least certain of the declared rock falls (e.g. probable)(Figure 133, 3) and one of the possible rock falls (Figure 133, 4) are presented next to two known rock falls (Figure 133, 1-2) and two low frequency events that are believed to be snow avalanches during winter storms (Figure 133, 5-6). Both of the possible rock falls have a strong spectral response below 40 Hz like the snow avalanches, but the duration of each individual event is much shorter and more similar in length to a rock fall impact. Furthermore, the January 14th, 2009 event has several bursts that bleed into higher frequencies like a rock fall (Figure 133, 3). The January 14th event was detected at three different locations at Middle Brother and 2-D source location analysis places this event near or to the east of station MB02, with a high amount of timing error. Nevertheless, the similarities of this event make it likely to be a rock fall.

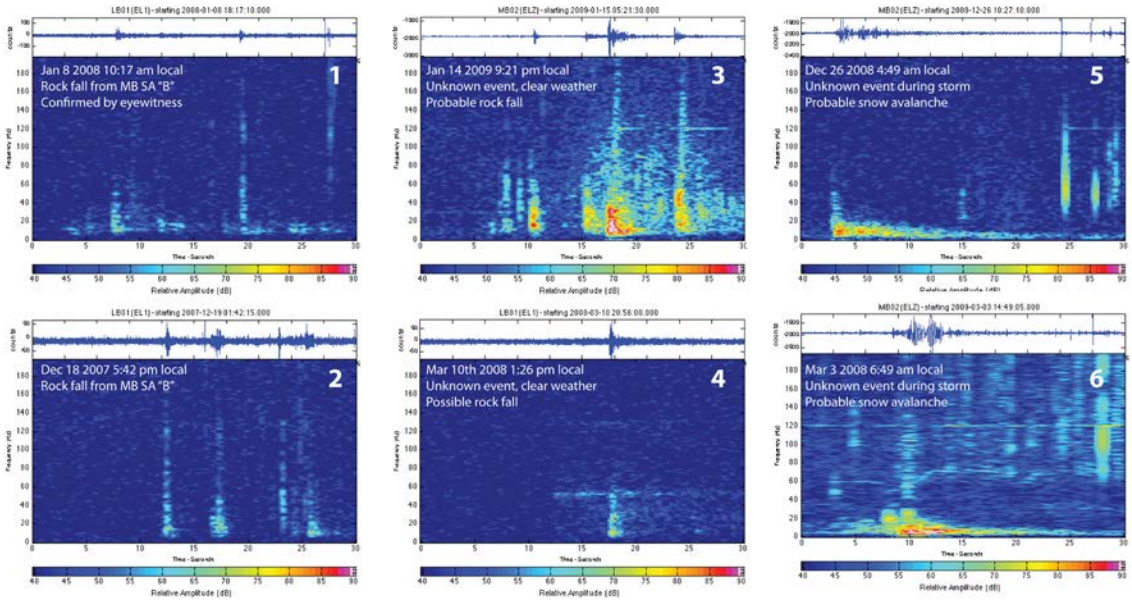

Figure 133. Confirmed rock falls (left), suspected rock falls (center), and suspected snow avalanches (right).

Seismic characteristics of four more suspected rock falls show a broadband impulse-like character reminiscent of strong individual impacts (Figure 134 3-6). In comparison, two rock falls with one and several individual impacts are also shown (Figure 134 1-2), but they have a gradual increase in energy with decreasing frequency, a trait that is not shared by the four possible rock falls. Furthermore, three of the four possible rock falls occurred during clear weather in mid-afternoon, and none were reported. These events might instead be small impacts local to the one station in operation.

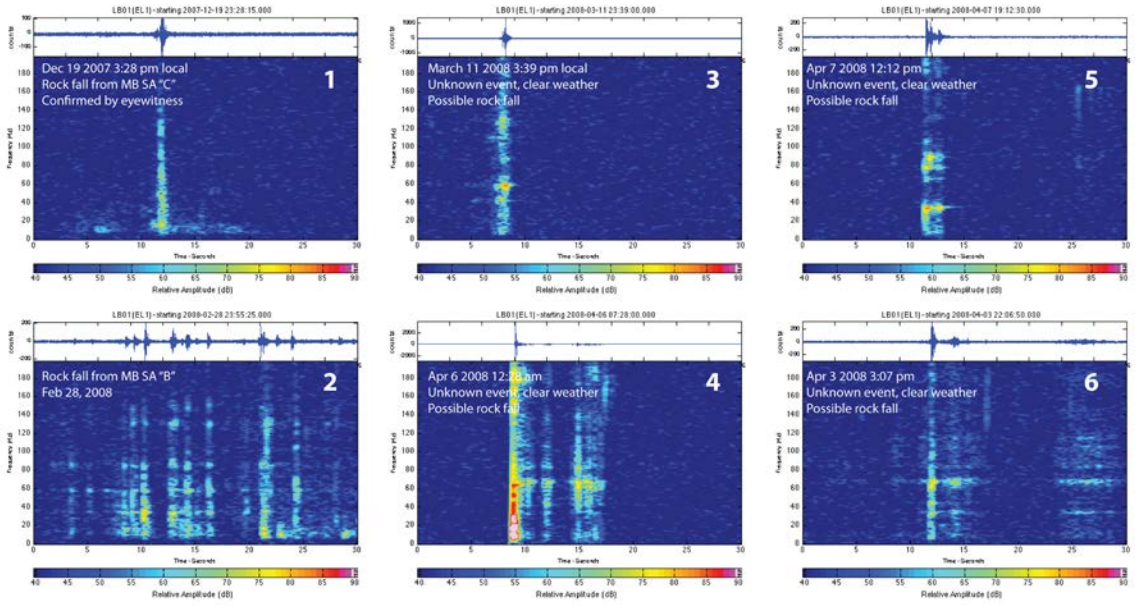

Figure 134. Confirmed rock falls (left) and suspected rock falls (center, right).

8.5 Analysis

Advanced analysis of the rock fall seismic signal has the potential to determine the initial mechanics of failure, locate impacts, and quantify the physical characteristics of rock falls. Many of these techniques require isolation of particular events, for example, detachment and impact, in order to study them. Analysis efforts were concentrated on two events, both with pre-impact signals: the largest rock fall in the source area "B" series on December 18th, 2007 (4pm) and the December 19th, 2007 single impact rock fall from source area "C".

The first step was to isolate the pre-impact and first impact signals in order to calculate the fall distance. The separation in time between the pre-impact signal and the first impact is approximately 5.7 seconds for the December 18th rock fall. If it is assumed that the some of the falling blocks went ballistic, the impact location is calculated at 160 meters below the source. This is approximately the location of the ledge below source area "B" from which the rocks impacted and ricocheted to the south (Figure 113). The separation in time between the pre-impact signal and the first impact for the December 19th rock fall is 7.4 seconds, leading to a calculated impact location 270 meters below the source, which is approximately the distance between the bottom of source area "C" and the top of the talus pile. Therefore the observed separation in time supports the hypothesis that the initial signal is associated with the first movements of the rocks away from the cliff while subsequent larger signals are associated with impacts.

Next, a search is conducted for P, S, and Rayleigh waves. These different wave types, if they can be identified, may allow application of more advanced analysis methods to determine source mechanics. It is known from other rock falls that the timing of the first arrivals is consistent with P-waves traveling in granite, as would be expected. It is also know that these impacts are 600 to 1000 meters away. This means, approximately, that the P waves would arrive in 0.2 seconds and S waves in 0.3 seconds. The theoretical lack of separation in arrival time of P and S-waves at this close distance makes them difficult to identify.

There are no distinguishable S-waves for either signal of the (larger) December 18th rock fall (Figure 135). The very first motion of the pre-impact signal is extremely hard to pick out in terms of timing and orientation on the geophone (top three records, Figure 135), and is completely lost in the noise on the accelerometer (bottom three records, Figure 135). However, the orientation of the first large impact of the rock fall can be seen clearly and is positive in the up, east, and south directions. The location of this impact is believed to be at approximately the same elevation as the station along the cliff face, which runs to the northwest and dips approximately 70 degrees to the southeast.

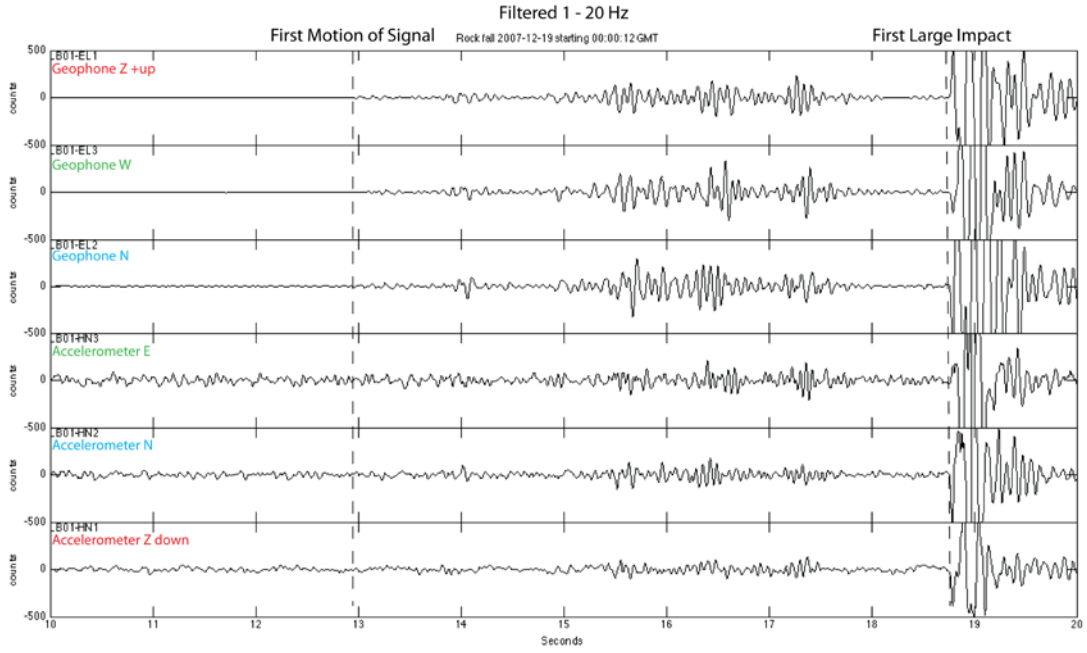

Figure 135. First motions of the pre-impact signal and the first large impact picked out for the December 18th, 2007 Middle Brother rock fall at 4pm local PST.

The smaller, single impact rock fall from December 19th, 2007 has indistinguishable pre-impact motion on the accelerometer record, and for the geophone, is barely detectable (Figure 136). It is difficult to assign an orientation to either pre-impact signal or first large impact. Even zooming in on the impact signal does not help to clarify the situation since the impact is obscured by some earlier-arriving signal or noise (Figure 137).

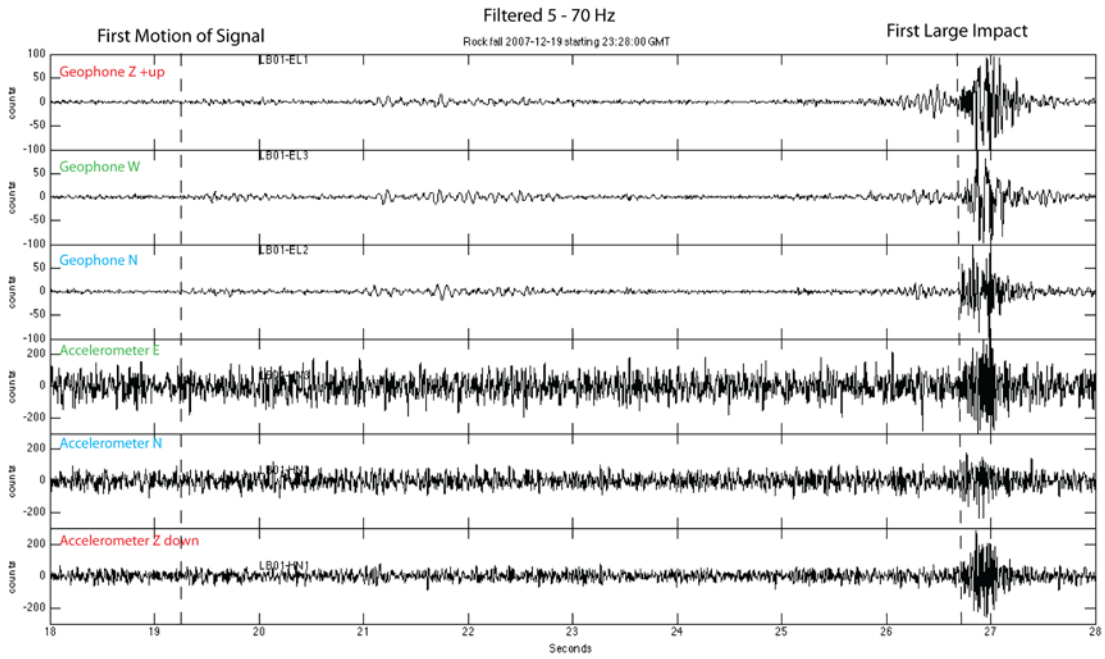

Figure 136. Pre-impact signal and the first large impact picked out for the December 19th, 2007 Middle Brother rock fall at 3:28 pm local PST.

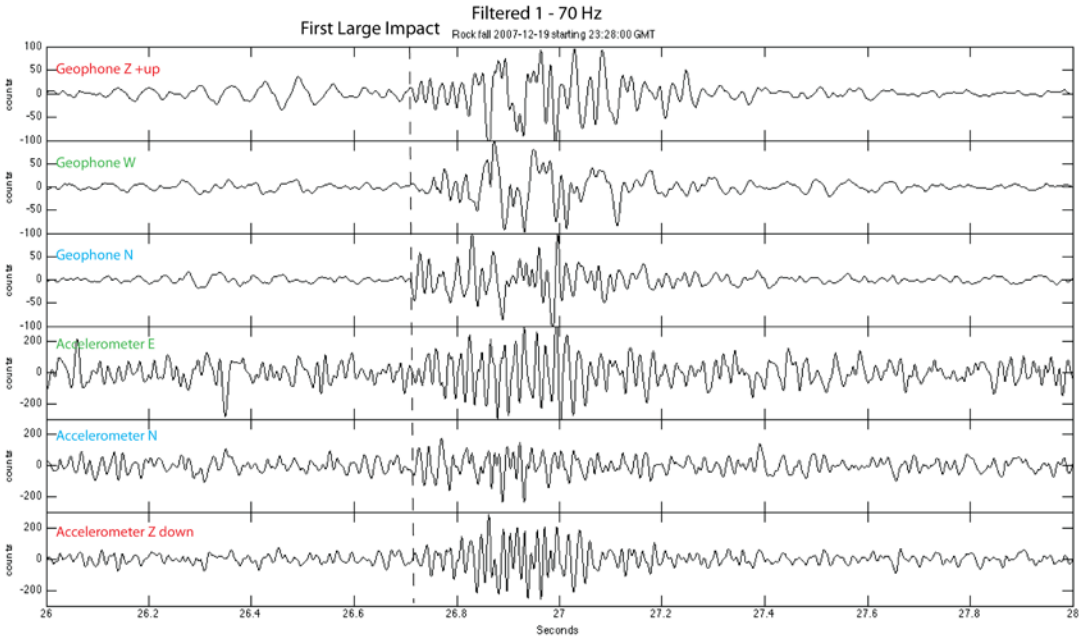

Figure 137. First motion of the first large impact picked out for the December 19th, 2007 Middle Brother rock fall at 3:28 pm local PST.

The December 19th rock fall is still the best candidate for a Rayleigh wave search since it is a single large impact. First, the components were rotated to radial and transverse directions, low pass filtered at 10 Hz, and bracketed around the expected Rayleigh wave arrival time (Figure 139). The results are interesting, showing that the Rayleigh wave appears to be oriented in the radial-transverse direction rather than the radial-z direction. This means that Rayleigh waves are traveling along the cliff surface. It follows that Rayleigh waves would always be rotated on a cliff in the near vicinity of a surface event that occurs on the same cliff. It is not known if this holds true for rock fall events that occur on other cliffs farther away.

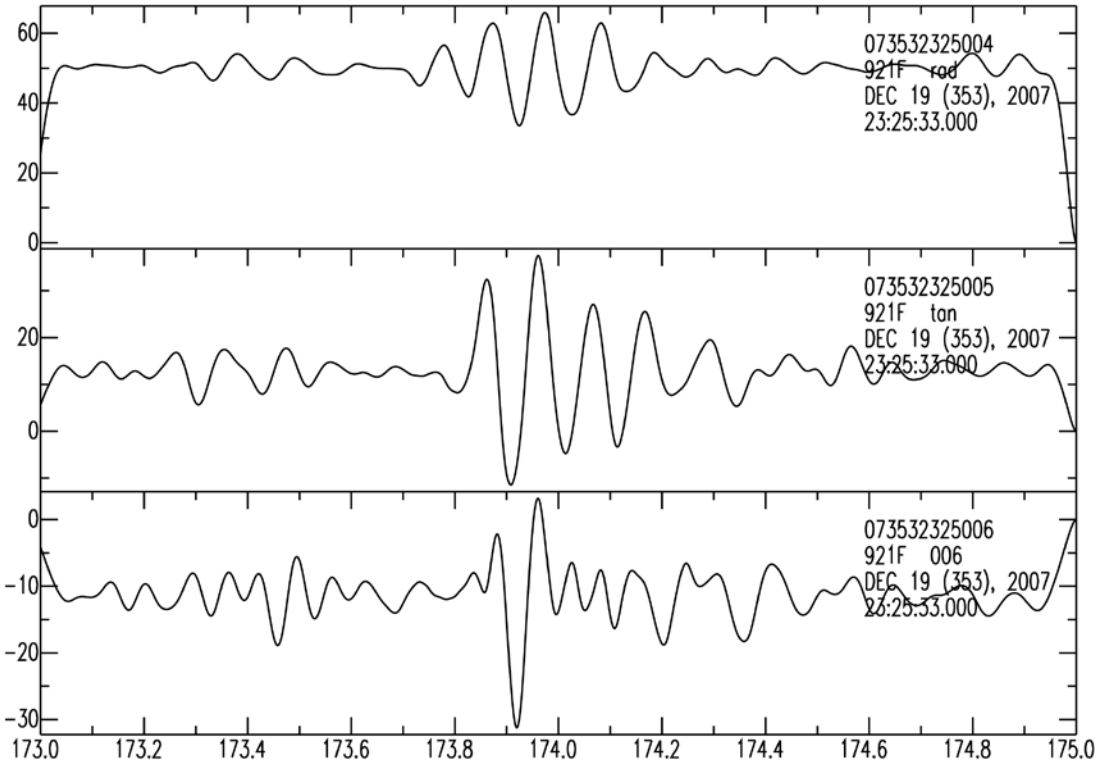

Figure 138. December 19th, 2007 rock fall low pass filtered at 10 Hz.

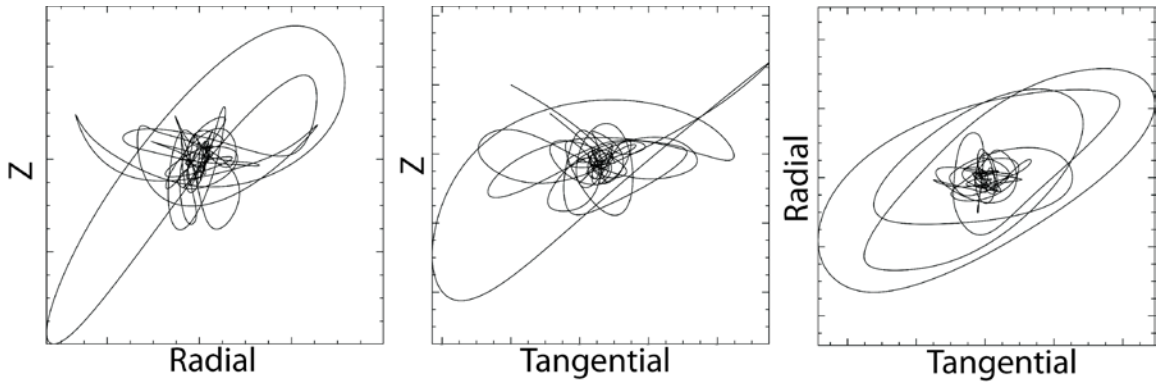

Figure 139. Particle motions of the December 19th, 2007 rock fall low pass filtered at 10 Hz.

In summary, pre-impact signals can be picked out and appear, based on their timing, to be related to the initiation of the rock fall. However, the pre-impact signals are too weak to allow identification of the orientation of their first motions to or distinguish S or Rayleigh waves. Large impacts motions do have distinguishable orientations, but still no identifiable S-waves. However, there appears to be prominent Rayleigh wave generation even on smaller impacts and these Rayleigh waves are rotated from their normal orientation and traveling along the surface of the cliff in the near vicinity of the rock fall.

8.6 Discussion

The detection of at least eleven rock falls in the vicinity of Middle Brother with both seismic and acoustic instruments indicates that monitoring does have the capability of monitoring and locating rock fall events. Out of those eleven rock falls, seven were witnessed visually or audibly, but three were unknown until seismic records were checked. There were five possible rock falls but more data is needed to be certain as to the origin of these six events. One of the three unreported rock falls damaged an equipment cable and would not have been discovered otherwise since it is a very small event that was detected at only one station. Another unreported rock fall was a fairly substantial event that occurred in the middle of the night during a winter storm, so it is no surprise that there were no reporting witnesses. The last event was also fairly substantial and occurred during a clear afternoon, but was still not reported.

All but three of the eleven rock falls occurred during or just after winter storms, and the remaining three occurred in January and February when snow and ice still covered parts of the cliffs. None of these eleven rock falls were recorded in the vicinity of Middle Brother during the months of November, March, April, May, or June, even though seismic instruments were in operation for all or part of those months. Although this is a small dataset covering a very short amount of time, this data is consistent with historically reported rock falls at Middle Brother, of which over half occurred in only the four winter months, from December through March.

The seismic character of the rock falls changes depending on the source location, fall distance, and distance to the instruments. In general the source locations are 400 to 800 meters high and thus, the rocks fall for many seconds and gain enough velocity to produce large, energetic impacts on the talus. Rock falls from source areas “B” and “C” sit above steep cliffs and likely have a ballistic phase before impact, judging by the pre-impact seismic signal and the presence of large impacts later in the seismic record. Rock falls from source area “A” travel down a less steep cliff and have a more gradual build up of seismic energy as the rocks bounce down the face of the cliff.

The large impacts are, in general, the source of the rock fall signal, generating strong seismic waves in a broadband frequency range that dissipate rapidly with distance. Most impacts recorded at a distance of 600 meters on the same cliff produce strong spectral frequencies to 100 Hz, with the largest impacts up to 200 Hz. In contrast, the large Eagle Canyon rock fall on the opposite side of the buttress but less than one kilometer away produced spectral frequencies to only 40 Hz, with the largest impacts up to only 100 Hz.

The pre-impact signal, although not seen on all records, provide clues to the initiation and trajectory of the rock before impact. This signal appears to be related to the first motion of the block as it fails and begins to fall, and the timing between the pre-impact signal and the impact is consistent with fall distances between source area and impact zone. The pre-impact signal may also hold clues to the detachment of the block, but most likely, detachment emits a very weak seismic signal that dissipates rapidly, and thus requires very close instrumentation in order to measure.

In order to explore source mechanics, pre-impact first motions of rock falls were analyzed. In all cases, the orientations of first motions are difficult to identify. S-waves were not detectable on the simplest records, and if they exist, they are buried in signal from additional impacts and movement of the rocks on the talus after impact. The weakness of the pre-impact signal, lack of S-waves, lack of distributed stations, and lack of good models for steep three-dimensional topography such as Yosemite Valley preclude using established source mechanics analysis methods, although this may be an area for future research.

Rayleigh waves, however, were quite easy to find after low pass filtering of the data and windowing the seismic records in the time when Rayleigh waves would be expected. Not surprisingly, Rayleigh waves travel along the surface of the cliff face when the rock fall originates from the same cliff.

The lessons learned from this project can be applied to future monitoring efforts. In general, the higher sampling rates are not required to detect rock falls, but they can help to differentiate rock falls from other seismic events and estimate the distance and location. A network of stations is required to estimate the location of the seismic event, and infrasound sensors provided invaluable data in order to determine distance to the seismic event in the absence of S-waves. Finally, geophones were far more successful at recording rock falls than accelerometers. Out of the eleven rock falls detected, the accelerometers picked up less than half, and often in higher frequencies than the geophones. Therefore, accelerometers will miss more events, require higher sampling rates for detection, and a different triggering algorithm based on higher frequency events.

8.7 Conclusion

Seismic, and for a short time, acoustic sensors were installed at Middle Brother during the winters of 2007-08 and 2008-09 for the purpose of rock fall monitoring. eleven events were recorded and have been assessed, with high certainty, as rock falls. Five additional unknown events were also recorded. The rock falls that are considered to be high certainty were declared so because they were witnessed, heard, matched very closely other confirmed events, were widely detected, and/or damaged monitoring equipment. Of the eleven rock falls, all occurred during the months of December, January, and February, although stations were in operation December through April during the first winter and November through June during the second winter. In fact, seven rock falls occurred during winter storm activity, and six of them occurred in December, during what might reasonably be considered the first winter storm of the season. Interestingly, all of the five unknown events occurred during March and April, which may be a clue as to their origin. These events do not resemble other low frequency unknown events which are believed to be snow avalanches during storms.

The rock falls are believed to have originated from all three source areas at Middle Brother as well as one event that discovered on the other side of Middle Brother in Eagle Canyon. One week after installation of the first station, a rock fall occurred at Middle Brother from source area "B", damaging the nearby road. A total of six rock falls were recorded seismically from that same source area over the next two and a half months, of which four to five were witnessed. Rock falls from the same source area have similar seismic signatures in terms of frequency content, duration, and spacing of the individual impacts. These rock falls fell and ricocheted off a south dipping ledge about 150 below the source area according to eyewitness reports, the location of the debris and road damage, but also the timing between the first recorded motion and first impact.

One rock fall was witnessed originating from Middle Brother source area "C" less than 24 hours after the first recorded rock fall. The seismic signature of that event is different from the Middle Brother source area "B" rock falls in that it only has a single impact and a longer initiation to impact time. The timing of the initiation and the rock fall is consistent with the free fall distance between the bottom of the source area and the top of the talus pile. Thus, the seismic data is consistent with the eyewitness report.

Two more rock falls are believed to have initiated from source area "A". One rock fall damaged an infrasound cable and is believed to be a small event since it was only detected at one nearby station. The other was widely recorded at three locations as well as two infrasound microphones, and analysis of the seismic and acoustic waves indicates that the largest impact occurred at the top of talus pile "A".

The last event was reported to be a large rock fall lasting tens of seconds that was heard, but not seen, somewhere between El Capitan and Middle Brother. No geomorphological evidence for this event was found at Middle Brother, leading to the hypothesis that this rock fall occurred somewhere up the hard to reach Eagle Canyon, west of Middle Brother. The seismic records of this event confirm that it was indeed west of Middle Brother and that the frequency content was lower than closer rock falls but still reasonably high, indicating a rock fall that was reasonably close, but farther than the local Middle Brother events. Thus, the seismic data supports the initial hypothesis of an Eagle Canyon rock fall.

Detectable signals include the pre-impact motion, when it existed, and the impacts for larger events. Not successfully determined was the orientation of those pre-impact signals or the identification of S-waves. Rayleigh waves are strongly generated by impact events, and they travel along the surface of the cliff, rotated from their normal, flat ground orientation. There may be potential for advanced analysis based on P and Rayleigh waves, but additional stations, distributed over a wider area, would be required. Thus, the seismic and acoustic monitoring has shown to be effective at detecting and confirming eyewitness accounts, as well as locating the source areas and impacts when enough data is available, and has shown potential for other types of more advanced analysis.

9 The 2009 Ahwiyah Point rock fall

The 2009 Ahwiyah Point rock fall began with a series of small precursory rock falls during the night of March 28th, 2009 and cumulated with the largest event recorded in over 20 years in Yosemite Valley at 5:26 am PDT (Figure 140). Rock climbers camped across the valley on Washington Column reported being woken up several times during the night by loud rumbling and witnessed sparking as rocks impacted the cliff face on the way down. The southern portion of the Mirror Lake Loop Trail, a popular hiking route, was buried in up to 8 meters of rock debris for a distance of 290 meters (Collins and Stock, personal communication) (Figure 141). Smaller rock falls continued for months afterward, and were photographed on several occasions (Figure 142).

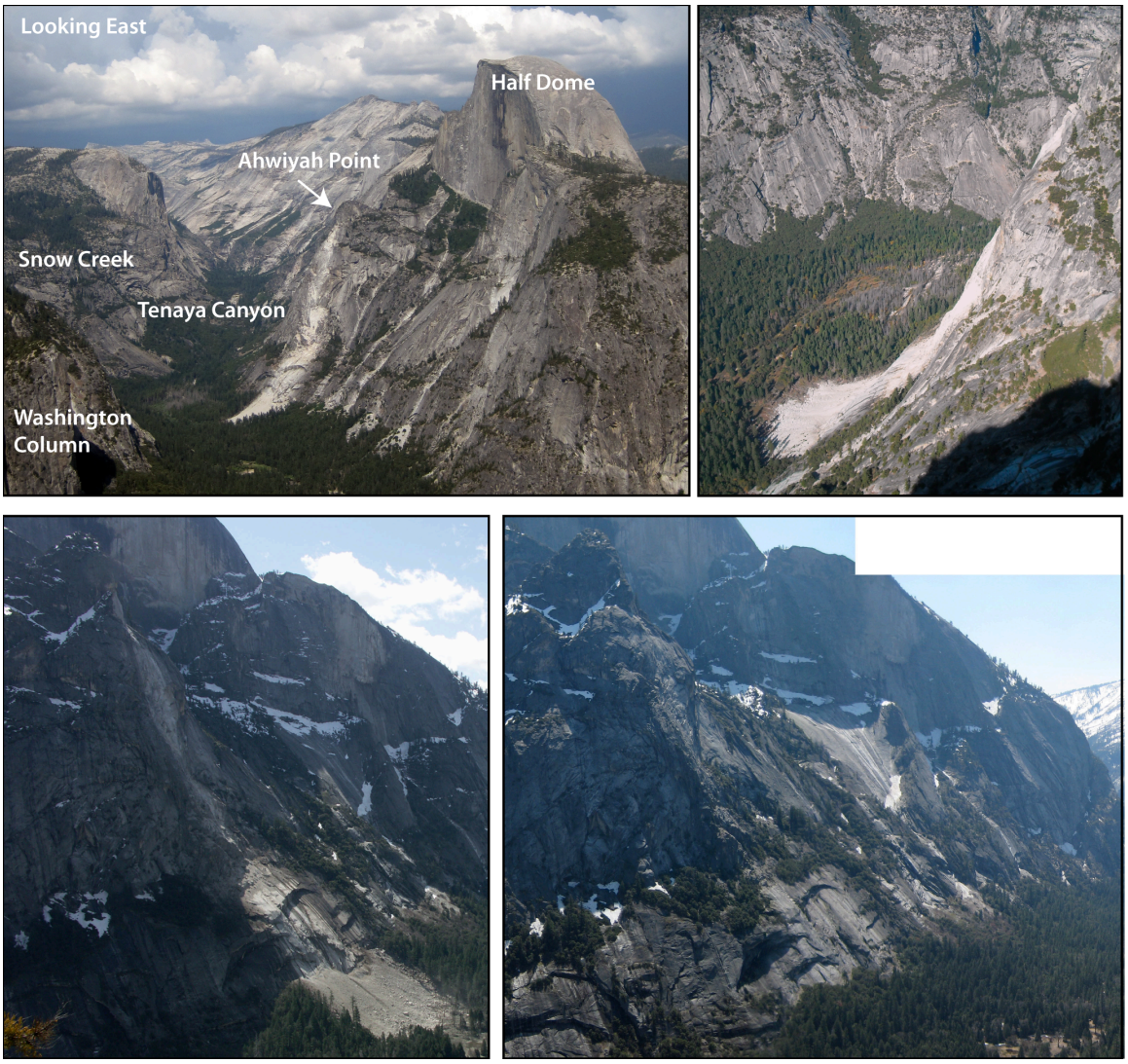

Figure 140. Views of the Ahwiyah Point rock fall. The white streak visible in the middle of the cliff face is the runout path. Ahwiyah Point is located in eastern Yosemite Valley just east of Half Dome (top left). View of the Ahwiyah Point rock fall runout zone from the northwest shoulder of Half Dome, showing the source area, travel path, and impact area on the floor of Tenaya Canyon (top right). Looking at Ahwiyah Point from the Snow Creek trail across the valley after (bottom left) and before (bottom right) the rock fall. (Photos courtesy NPS/Greg Stock except for bottom right photo, courtesy of Dan Kocevski).

Figure 141. The southern portion of the Mirror Lake trail was buried by the talus. The intersection of the trail with the new talus is shown on the left. On the right, the entire 290 meter wide new talus is shown (Photos courtesy NPS/Greg Stock and Bob Sas).

Figure 142. Ahwiyah Point after rock falls on March 29, 2009 (left) and April 18th, 2009 (right). These events were 100-1000 times smaller than the largest event on March 28th, 2009 at 5:26 am. (Photos courtesy Allyson Gunsallus (left) and Tony Rousmaniere (right)).

Ahwiyah Point is located about 800 meters northeast of Half Dome in eastern Yosemite Valley, about 4.4 to 6.7 km from the local Yosemite rock fall seismic network which was in place and recording data during the rock fall (Figure 143). The rock fall impact was large enough to be detected widely on strong motion seismic networks up to 350 km away and registered as a **M**2.4 earthquake, data that was retrieved and used to supplement the locally recorded seismic and infrasound data. In addition, this rock fall was well-documented with high resolution photography and field observations, airborne LiDAR before the rock fall in 2006 and after the rock fall in 2010, and post rock fall terrestrial LiDAR in 2009.

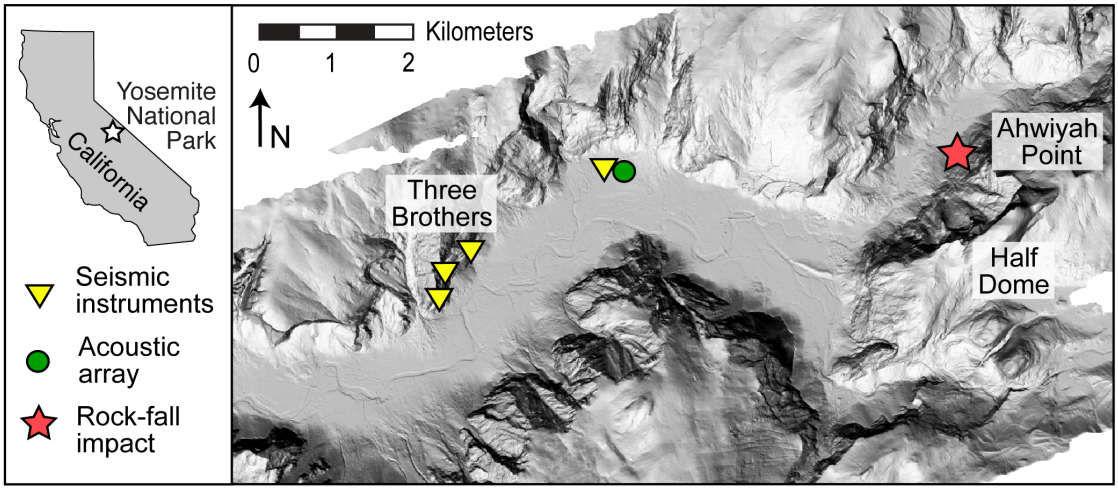

Figure 143. Map showing location of Ahwiyah Point rock fall and sites of seismic and acoustic instrumentation. Inset shows location of Yosemite National Park in California, USA.

9.1 LiDAR, photography, and field observations

Field observations, LiDAR, and high resolution photography were methods employed to document the geomorphological changes to the cliff and talus, measure the volume and dimensions of the rock fall block that initially detached, and map out the locations of impacts and areas where additional rocks were knocked loose en-route to the talus. The results from these research efforts were then used to tie in the physical parameters of the rock fall with the seismic observations and calculate the rock fall trajectory.

Pre rock fall high-resolution (gigapixel) photographs of the Ahwiyah Point area were acquired as part of the National Park Service Yosemite xRes project (http://www.xrez.com/case-studies/national-parks/yosemite-extreme-panoramic-imaging-project/). The Yosemite xRes project photographed cliffs throughout Yosemite Valley in 2008 and stitched together hundreds of images to create panoramic images from 20 different vantage points (Stock et al., 2011a). Ahwiyah Point was photographed from three locations on the rim of Yosemite Valley and Tenaya Canyon. After the rock fall, photographs were acquired from the same vantage points in lighting conditions as similar as possible to the original photographs, in order to compare pre and post rock fall cliff geometry.

Airborne LiDAR data were collected by NCALM in 2006 before the Ahwiyah Point rock falls, and then again in 2010 following the rock falls. Collins and Stock (personal communication, 2011) collected terrestrial LiDAR data in May 2009 from two scan positions on the floor of Tenaya Canyon. The post-failure geometry, including the talus slope, was reconstructed using data from all three data sets by Collins (personal communication) using a standard suite of filtering algorithms to remove vegetation, obtain a homogenously dense set of point clouds, and construct spherical surface triangulation models specifically intended for steep, overhanging terrain (Maptek, 2011).

The total volume of the Ahwiyah Point rock fall was calculated at 46,700 m^3 of intact rock from LiDAR and photographic data. The vast majority mobilized during the largest event on March 28th, 2009, at 5:26 am (PDT). This total volume includes 25,400 m^3 from the rock-fall source area (Figure 144), 2,000 m^3 from intermediate blocks dislodged as the rock mass traveled downwards along the upper cliff face, and 19,300 m^3 from the initial mid-cliff impact of the rock fall on the lower promontory (Figure 145) (Collins and Stock, personal communication). A minor additional amount of rock, estimated to be less than 1,000 m^3, was detached below this point and prior to final impact on the talus. The block from the initial source area measured, at maximum dimensions, 80 meters long by 50 meters wide by 26 meters thick (Figure 144). Prior to failure, this block was resting on a 46° inclined, west dipping surface with a dip direction of 262°, slightly oblique to the normal of the cliff face of 285° along the rock fall runout path. The block slid off the ramp and fell approximately 350 meters before impacting a prominent ledge mid-cliff, dislodging the majority of the rest of the rock fall volume. The combined rock fall debris continued down the cliff an additional 300 meters before striking the top of the 80 meter tall talus slope, remobilizing a significant volume of the existing talus, and generated an airblast that knocked down hundreds of trees.

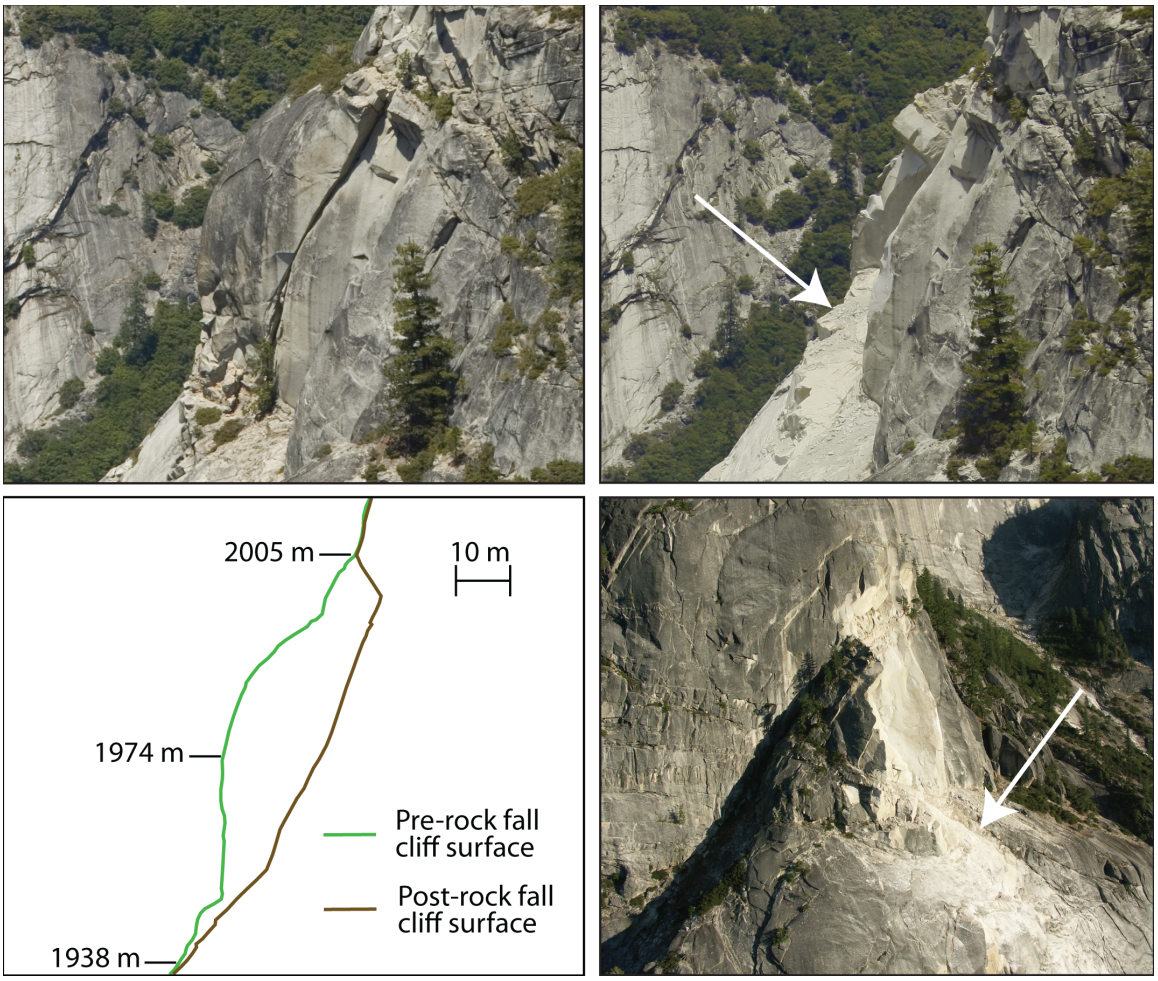

Figure 144. High-resolution photographs of the source area showing the before (top left) and after (top right) rock fall conditions, taking from the northwest shoulder of Half Dome, to the west. A cross-section of the source area block calculated from LiDAR (bottom left). A view of the source area from the east (bottom right). Arrows point to the 46° sliding surface. (Photographs courtesy NPS/Greg Stock, LiDAR cross-section from Stock and Collins (personal communication)).

Figure 145. High-resolution photographs of the mid-cliff impact area from across the valley (left) and from below in Tenaya Canyon (right). (Photographs courtesy NPS/Greg Stock).

9.2 Detailed Analysis of Seismic Data

Seismic and data were recorded locally as part of an ongoing rock fall monitoring study in Yosemite Valley and also acquired from regional strong motion seismic networks. The analysis of seismic data from this event focuses on three main areas: identifying the distinct events associated with the rock fall, discussing the proliferation of different seismic phases, and understanding how waves travel in and beyond Yosemite Valley.

9.2.1 Seismic detection of the Ahwiyah Point rock fall

The Ahwiyah Point rock fall produced distinct ground motion records on 107 seismic stations ranging from 4.4 kilometers to 353 kilometers. The event registered on the regional strong motion seismic network as a magnitude 2.4 earthquake with an event time of 12:26:04.53 GMT. Close examination of the seismic moveout (Figure 146) reveals that there are 3 distinguishable events associated with the rock fall. The first impact (I) is the largest, most distinct, and most easily identified part of the signal. Preceding the impact are two smaller events occurring at 9.6 seconds (D1) and 7.25 seconds (D2) prior to the main impact, +/- 0.3 seconds. The moveout of the three signals is constant in time separation and the moveout velocity is calculated at 5800 m/s. This velocity is consistent with P (compressional) waves in granite, as expected. The first arrivals of the three distinct events are labeled P_I, P_{D1}, and P_{D2} in order to differentiate the first arrival P-wave phases from other seismic phases that may exist from the same three events. There also appears to be a weak, less-distinct phase associated that has the impact with a moveout velocity of 3400 m/s, believed to be an S-wave (Figure 146, S_I).

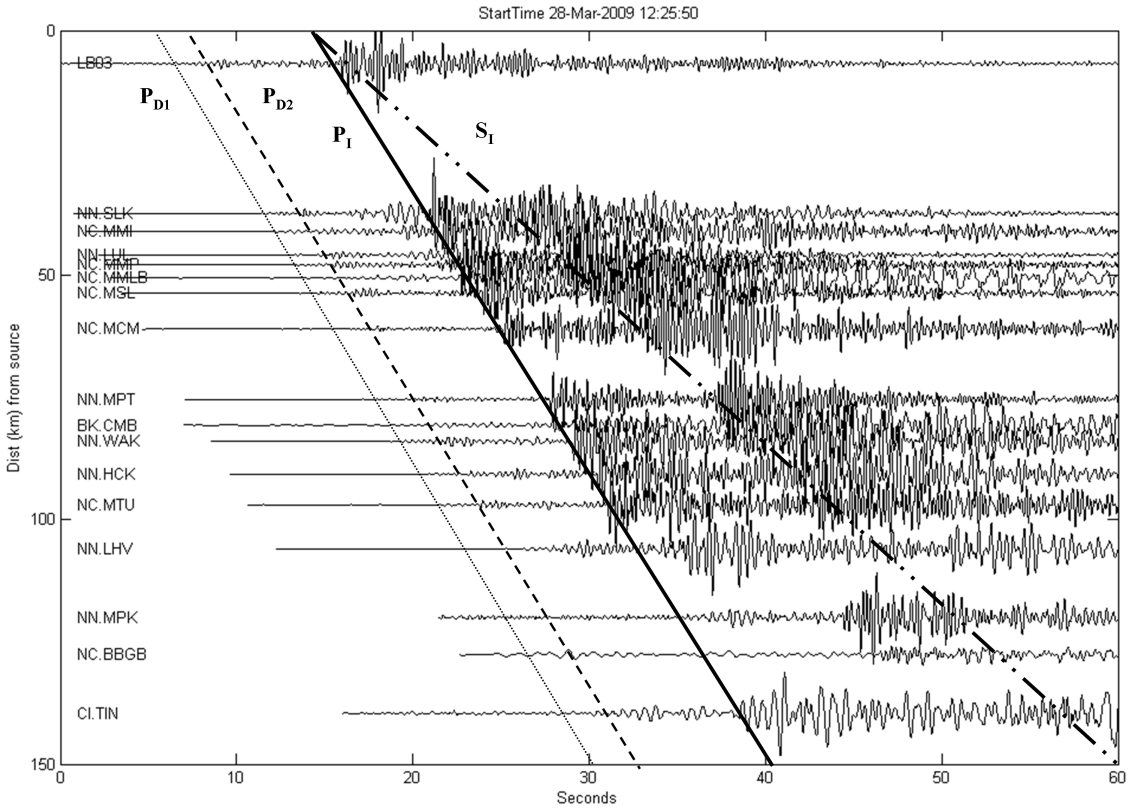

Figure 146. Ahwiyah Point rock fall as seen on seismic station from 0 to 150 km. The moveout velocity is 5800 m/s of the first three seismic signals, and 3400 m/s for the last one.

The two detachment signals are significantly weaker than the impact signal and buried in the noise before filtering. Thus, it is the impact that is detected by the strong motion seismic network and used to calculate event time, location, and magnitude. The detection rate of each of the three seismic signals for the local (X7), broadband triaxial, and broadband uniaxial networks is shown in Table 14. Only stations with a clear impact signal were included, thus, the impact detection rate is, by default, 100%. There are other regional stations that did not detect the rock fall but almost all of them are located more than 150 km away. In some cases, the signal-to-noise ratio was too high to produce a clear onset of the signal; these cases are designated low quality (LQ) resolution. The maximum distance for resolving each of these signals is included.

Table 14. Detection rates of various seismic networks for the Ahwiyah Point rock fall.

Network		Detachment 1		Detachment 2		Impact	
		Detecting	Dmax (km)	Detecting	Dmax (km)	Detecting	Dmax (km)
X7 Stations	All	5 (83%)	6.7	5 (83%)	6.7	6 (100%)	6.7
Strong Motion Triax	HQ	4 (15%)	81	9 (33%)	220	27 (100%)	353
	LQ	11 (41%)	234	21 (78%)	255		
Strong Motion Uniax	HQ	22 (30%)	187	61 (82%)	263	74 (100%)	263
	LQ	42 (57%)	220				

The D1 signal was detected on five of the functioning local (X7) stations, all except the vertically mounted accelerometer at 6.5 km. For the regional stations, the D1 signal was resolved with high quality at four (15%) of the triaxial stations and 22 (30%) of the uniaxial stations, out to 81 and 187 kilometers, respectively. When lower quality resolution data is included, 11 (41%) of the triaxial and 42 (57%) of the uniaxial stations detect the D1 signal, out to a maximum distance of 234 and 187 kilometers, respectively.

The second detachment signal (D2) was considerably stronger and was detected on the same five out of six functioning X7 network stations, as well as nine (33%) of the triaxial stations and sixty-one (82%) of the uniaxial station out to 220 and 263 kilometers, respectively. Including the lower quality resolution data increases the number of triaxial stations to 21 (78%) out to a maximum distance of 255 kilometers, but yields no increase in the number of uniaxial stations.

9.2.2 Calculated Seismic Velocity in the Sierra Nevada

Compressional (P-wave) seismic velocity ranges from 5500-6000 meters per second (m/s) in intact granitic rock. Given that the source of the seismic waves is on the surface, and that most of the seismic detectors are also on the surface, rock velocity can be approximated by dividing the azimuthal distance by the travel-time of the first arrival. This is only a rough approximation because the path of the first arriving seismic wave is usually not a straight line through a single rock type. At short distances, a higher proportion of the wavepath will include soil and fractured rock. Furthermore, waves traveling indirect paths (and thus greater distances) through high velocity granitic rock may precede direct arrivals. Thus, at short distances, calculated velocities are usually lower than expected. At long distances, the first arriving seismic waves will sample deeper (and presumably faster) layers, resulting in higher velocity calculations. The calculated P-wave seismic velocities range from 4300 to 5000 m/s at distances less than 10 km and 6000 to 6500 m/s for good data at distances greater than 150 km. The mean P-wave seismic velocity at distances of 40 to 120 km is 5770 m/s with a standard deviation of 130 m/s. The azimuth may also be a factor in seismic velocity since rock type changes with direction. Along the spine of the Sierra Nevada, all of the rock is granitic (roughly N-NW to S-SW), but varies greatly perpendicular to the Sierra Nevada, such that velocities in those directions may also vary. Figure 147 shows an interpolated velocity map for varying distance and azimuth with stations that detected the rock fall event. At distances greater than 150 km, more stations along the spine of the Sierra Nevada recorded the event than in other directions, despite the fact that there are far more stations outside the Sierra-Nevada (mostly along the San Andreas fault zone to the west), indicating that Sierra-Nevada granitic rock is a good transmitter of seismic waves.

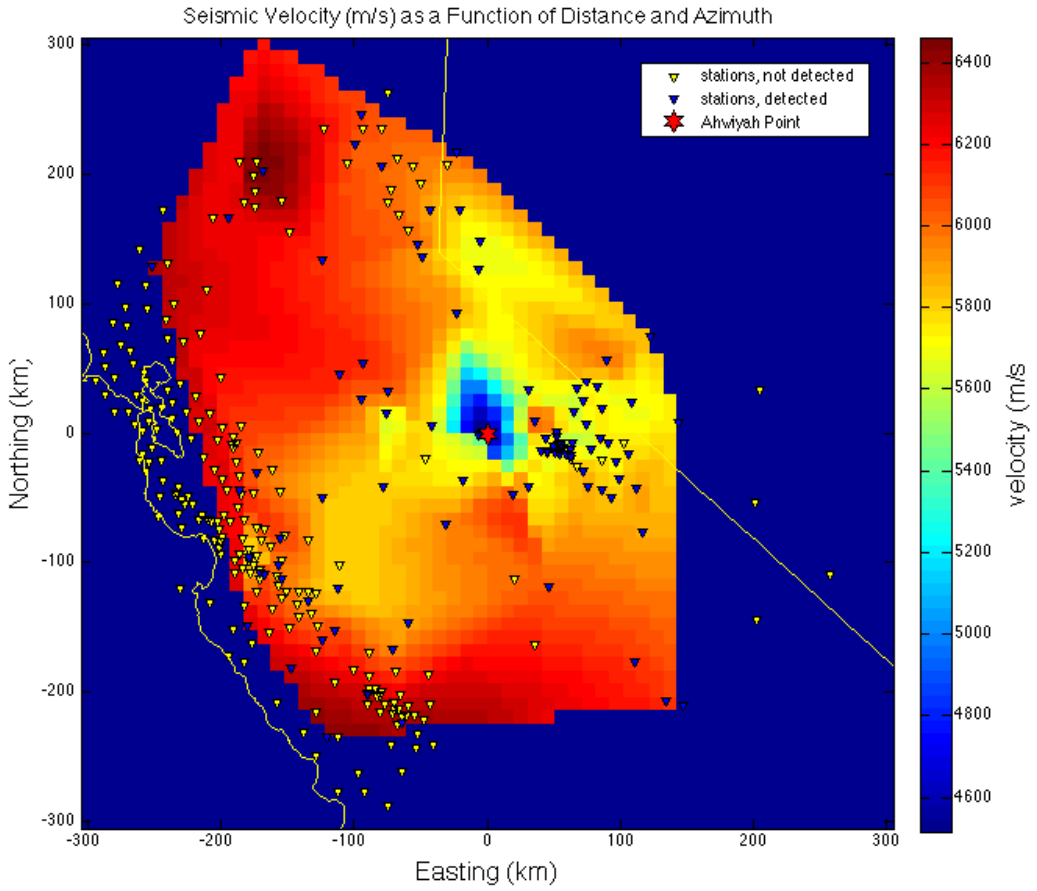

Figure 147. Seismic velocity of first arrivals as a function of distance and azimuth. Blue triangles are the stations that detected the rock fall, yellow triangles represent stations that did not detect the rock fall.

The apparent velocity of P-waves in Yosemite Valley was calculated as a unexpectedly low 3000 m/s. This calculation was done between two stations located midway up the same cliff face approximately 6.5 km from the rock fall. The azimuth between the two stations was oblique to the rock fall azimuth: thus, directly arriving seismic waves would be expected to produce abnormally high apparent velocities, not low ones. Therefore, it was determined both that the seismic waves are likely to be traveling along the cliff face rather than on azimuth through the valley sediments, and that the exfoliation and other jointing seen in granite near the surface lowers the average seismic velocity between two stations on the surface.

9.2.3 Seismic data recorded by local Yosemite rock fall network

The Ahwiyah Point rock fall was detected by five out of the six operating instruments in four different locations. An accelerometer and two infrasound microphones in Yosemite Village (GH08) were the closest instruments to the event, at 4.4 km away. All other instruments were located at Middle Brother, including two geophones on the talus at 6.2 km away (MB02 and MB07), one vertically-mounted accelerometer at the highest accessible point on Michael's Ledge 400 m off the valley floor at 6.5 km away (MB04), and two geophones at Lower Brother 270 m off the valley floor at 6.7 km away (LB03 and LB05). Unfortunately, one of the Yosemite Village microphones and one geophone station (MB06, co-located with MB04) were not operational. Thus, there were geophones in two Middle Brother locations, one accelerometer at a third location at Middle Brother, one accelerometer in Yosemite Village, and two infrasound microphones in Yosemite Village.

The geophones clearly show a pre-impact signal and then a main impact (Figure 148). The pre-impact period has a clear onset and spectral energy in frequencies less than 10 Hz. Spectrogram records reveal that the pre-impact signal starts off weak (5s in Figure 149), then increases in strength and frequency two seconds later (7s). The two-part pre-impact signal preceding the main impact is also detected on the wider seismic network (P_{D1} and P_{D2} in Figure 146). The main impact has higher spectral strength and amplitude and higher frequencies (Figure 149) than the pre-impact signal.

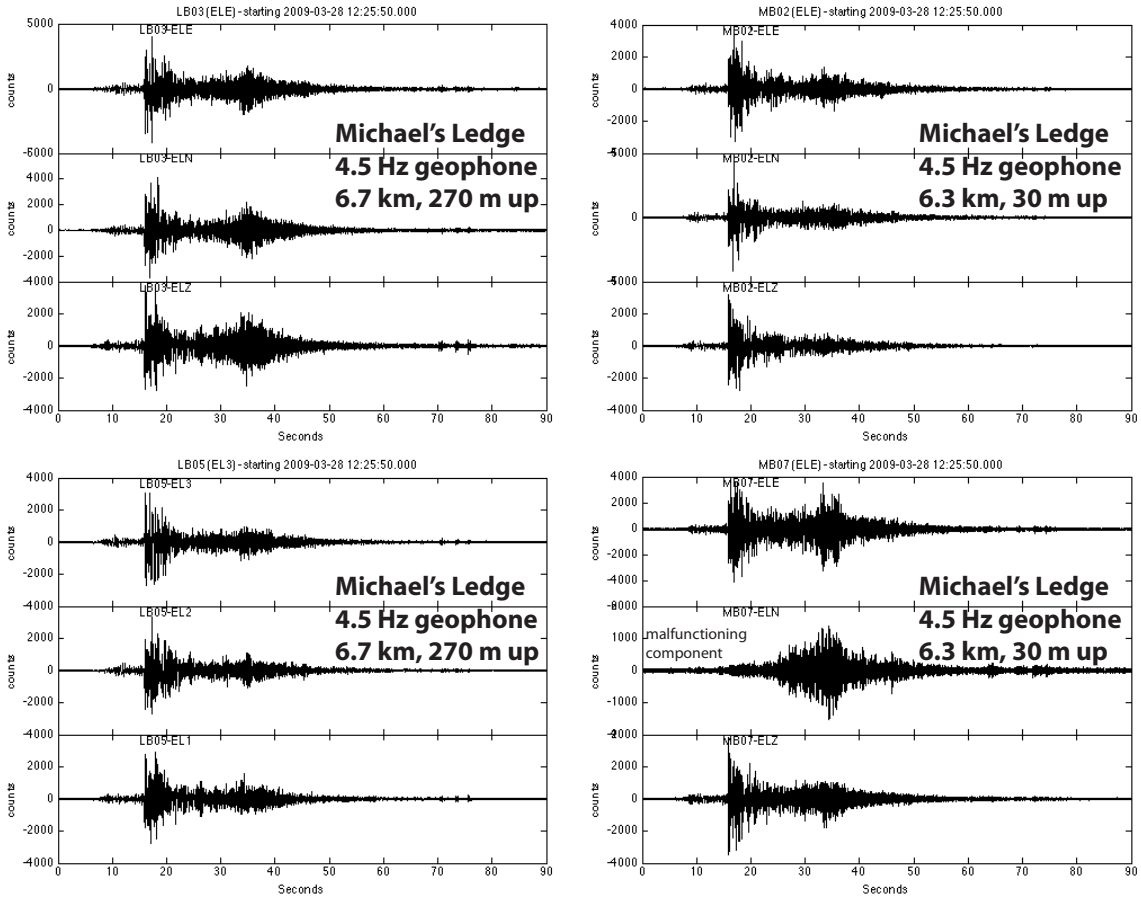

Figure 148. Geophone records of the 2009 Ahwiyah Point rock fall.

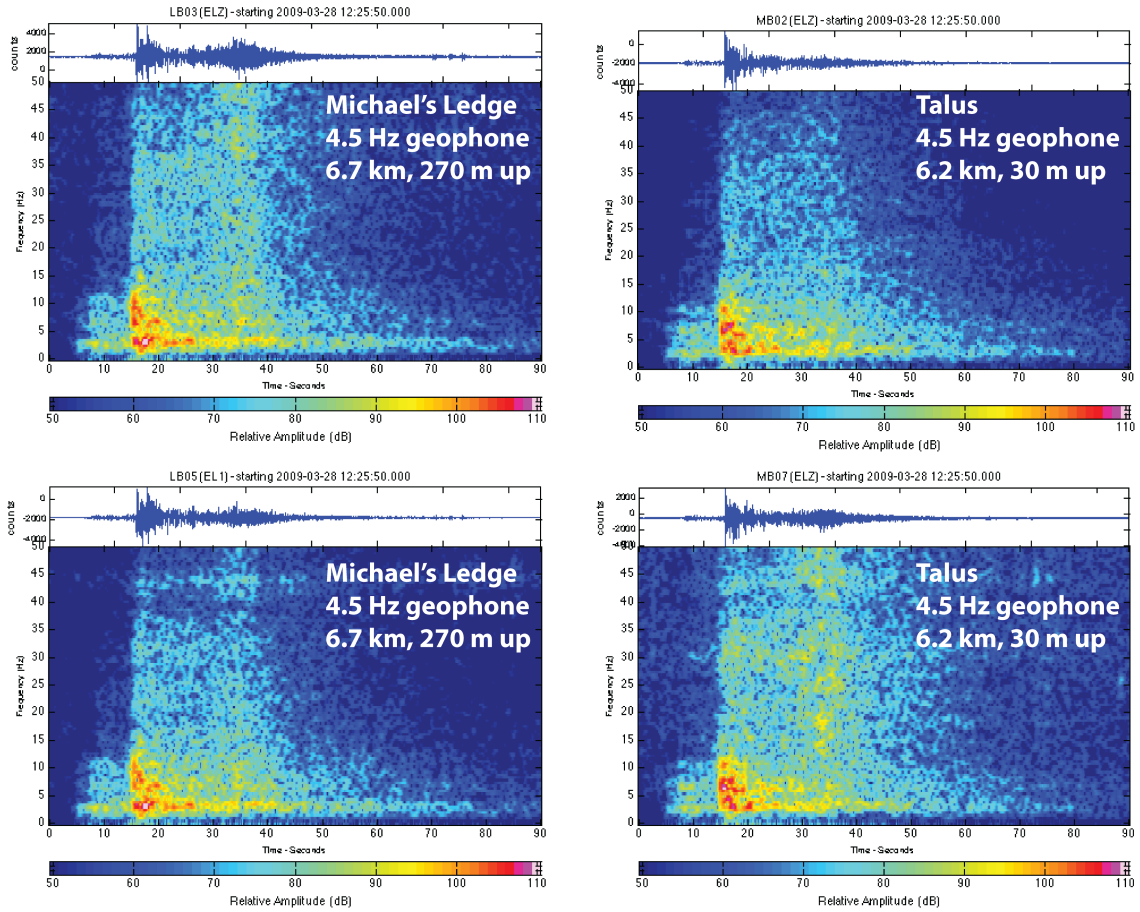

Figure 149. Geophone spectrograms of the 2009 Ahwiyah Point rock fall.

The accelerometers consistently do not record events as well as the geophones, as is the case with the Ahwiyah Point rock fall. The Yosemite Village accelerometer does not register a noticeable pre-impact signal in the time domain if unfiltered (Figure 150, left), but does pick it up between 1 and 9 Hz as shown on a spectrogram (Figure 151, top left). The accelerometer on Michael's Ledge does not even show a noticeable impact signal unless filtered (Figure 150, right) and still, it is only a weak, short signal (Figure 151, top right). The reason for the difference in sensitivity of the two accelerometers is at least partly attributed to distance, as one station is only 4.4 km away while the other is 6.5 km away. Part of the sensitivity difference might also be attributed to instrument type and placement: an RT131A 2/3 on deep sediment away from the rock walls (the closer instrument) versus a vertically rock-mounted Terratech SSA-320 on Michael's Ledge (the farther instrument). The peak response for the accelerometers is between 2 and 8 Hz (Figure 151, bottom).

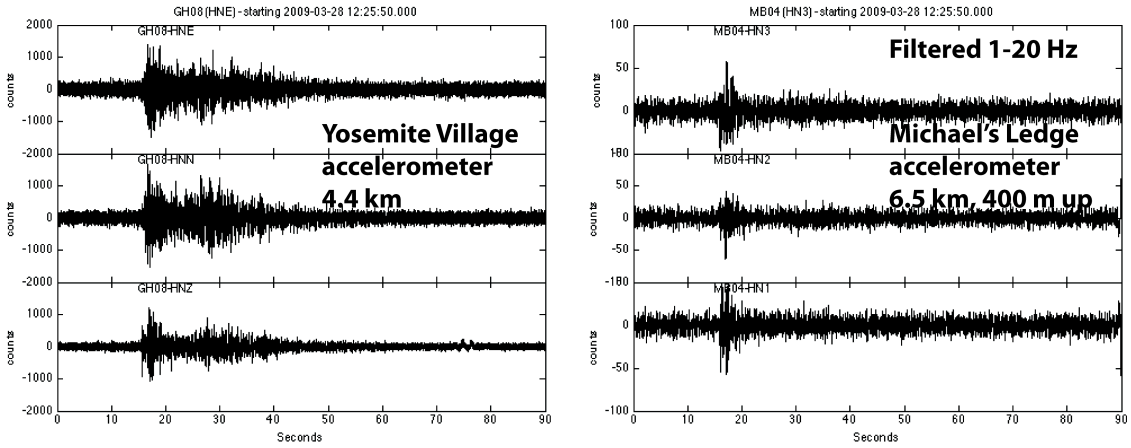

Figure 150. Accelerometer records of the 2009 Ahwiyah Point rock fall.

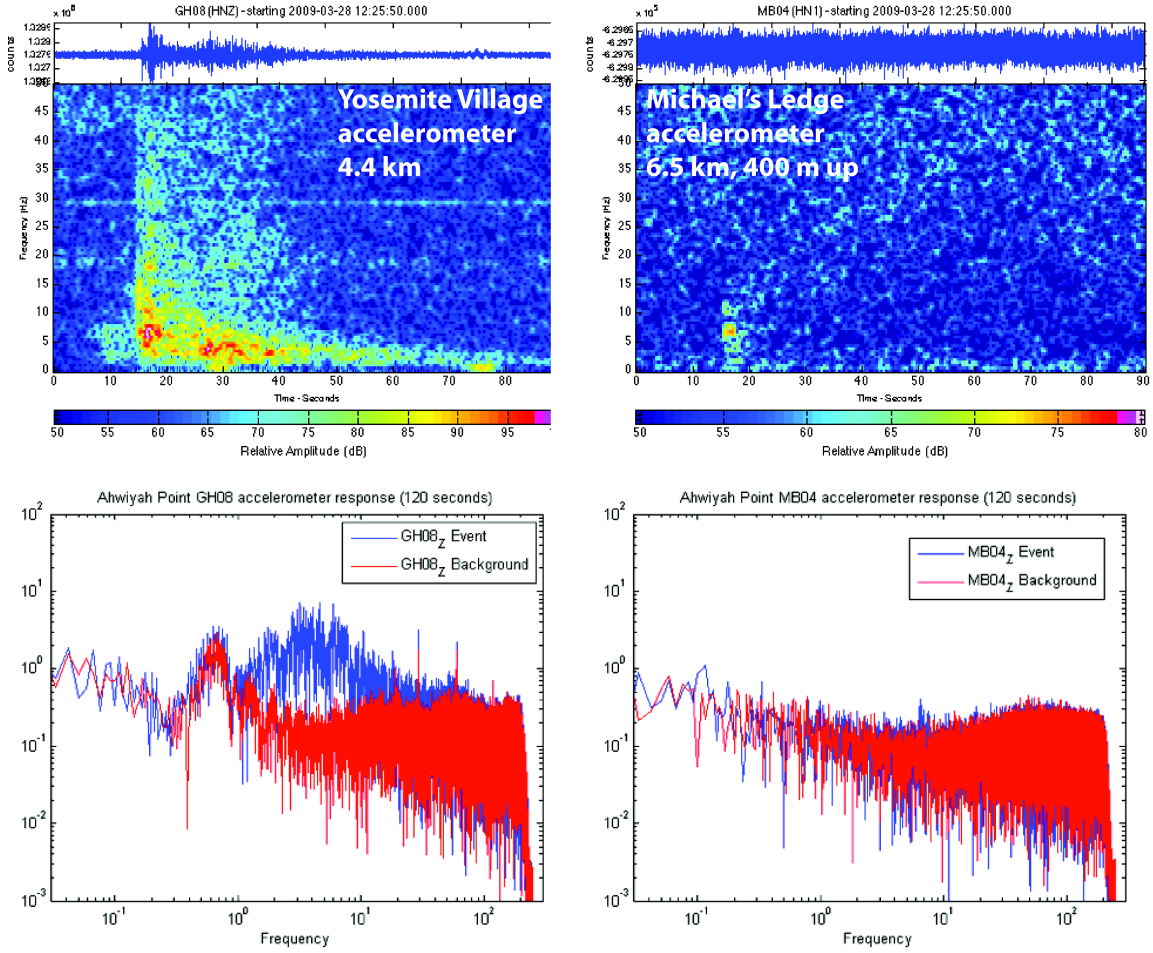

Figure 151. Accelerometer spectrograms (top) and spectral plots (bottom) of the 2009 Ahwiyah Point rock fall.

9.2.4 Analyses using polarity of first motion

The polarity of the first motion can be used for a significant number of seismic analyses. At a single triaxial station, the polarity and relative magnitude of the first motion can be used to locate the azimuth to an earthquake. An array of stations can help to identify the physical characteristics of the seismic event itself to help determine if the event is an earthquake or not, and if so, the type and orientation of the fault. In the case of a rock fall at a site with complex topography, like Yosemite Valley, the first motions can help to illuminate how seismic waves might travel in that topography. P-wave first motions for all three components were closely reviewed in order to determine the orientation of the incoming wavefront in the Yosemite Valley, and also to determine if it might be possible to extract information about the mechanics of the rock fall. For example, P-waves may have either a positive (compressional) or a negative (tensile) polarity, and that polarity is a function of the initial first motion and the wavepath from the event to the seismic station. Therefore, polarities usually change depending on the azimuth and sometimes distance to the event, and the geographic pattern of polarity at several stations is an indicator of source mechanics.

9.2.4.1 Direction of Incoming Wavefront

The azimuth of the incoming P-wave can be assessed by comparing the relative magnitudes of the three components. A P-wave can have either a positive or negative first motion, which leaves two theoretical directions for an incoming wave. However, usually the incoming seismic wave be safely assumed to be coming from below ground for a seismic station on the earth's surface. This may not hold true for stations installed on or near cliffs, where seismic waves may arrive from above. In order to make this calculation, the relative magnitudes of the east (E) and north (N) components are used to narrow down the direction of the incoming wavefront to two possibilities; one with a positive first motion, and the other with a negative first motion. The polarity of the Z-component is matched with the polarities and magnitudes of the two possibilities to assign the vertical dip of the incoming waves, with one possibility coming from above, and the other below. Figure 152 illustrates this concept at a Middle Brother cliff location.

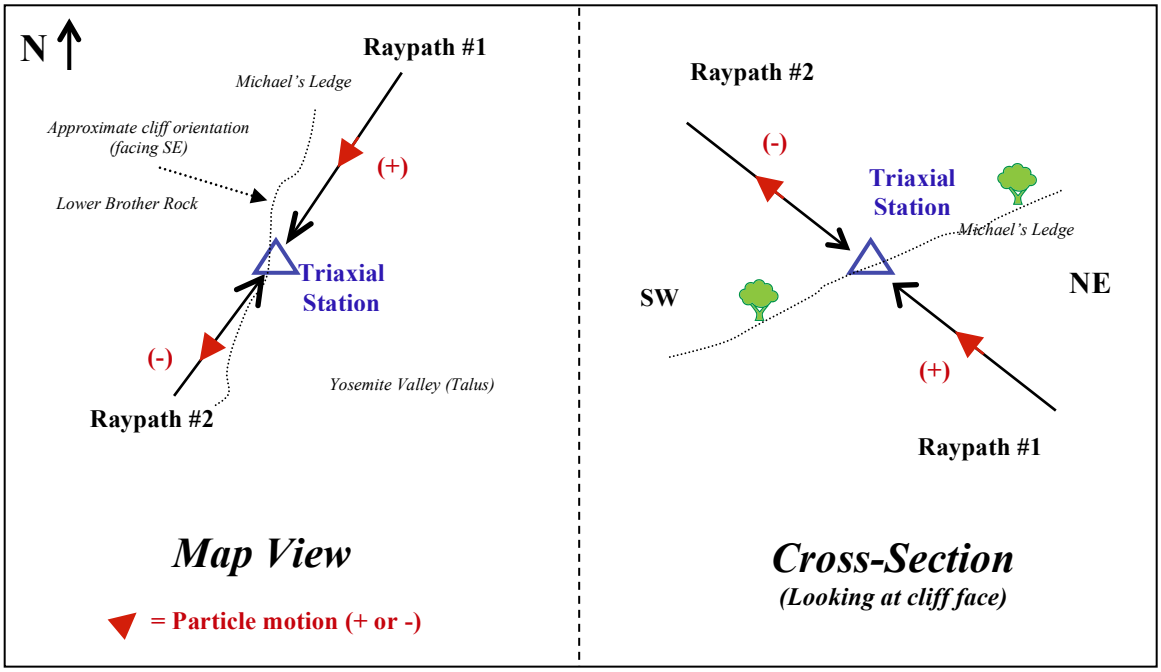

Figure 152. P-wave first motion polarity used to locate incoming seismic signal.

When this technique was applied at the three Middle Brother geophone stations, it was discovered that the wavefront arrives via the granitic cliff (Figure 153) instead of on azimuth directly from the rock fall, which passes through unconsolidated basin sediments. In addition, the apparent velocity between the two locations is less than the P-wave velocity in granite. If the waves were arriving obliquely to the cliff (e.g. on azimuth from the rock fall), one would expect to falsely high apparent velocity. Thus, the lack of a falsely high apparent velocity supports the result from the polarization analysis. This travel path variation is not a surprise since seismic velocities in granite are much higher than in unconsolidated sediments, and it is well-known that a high impedance contrast from mountain to basin rock causes most of the seismic energy to be reflected back into the soft basin instead of transmitted into the rock.

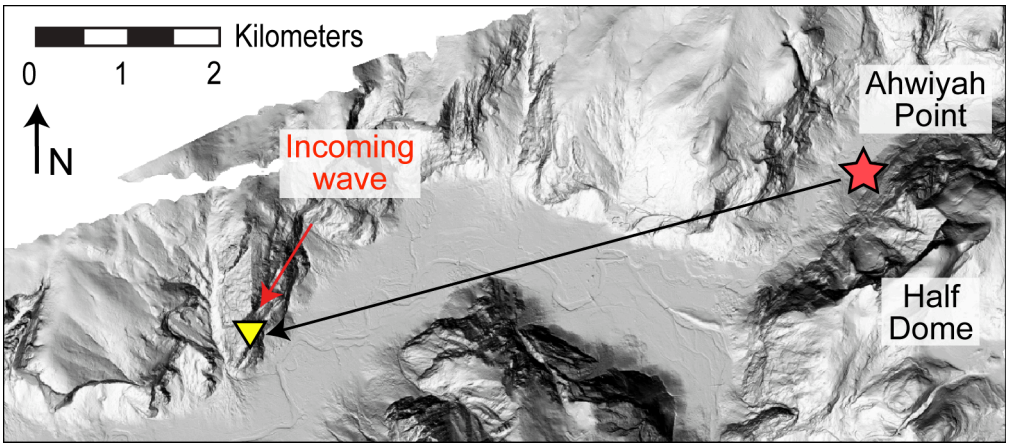

Figure 153. Azimuth of incoming wavefront compared to rock fall azimuth.

9.2.4.2 Polarity as an indicator of source mechanics

There are three incoming P-waves with semi-distinct onsets: an initial (weak) detachment signal (P_{D1}), a second detachment signal (P_{D2}), and an impact signal (P_I). Each of these signals corresponds to a different physical event during the course of the rock fall, which, in theory, can be characterized with an array of stations at different azimuths and distances. However, first motions can sometimes be difficult to identify if the event is emergent or the signal is weak.

The D1 and D2 events are associated with the movement of the rock block before impact, and thus, are highly interesting scientifically. However, these signals are also very weak and difficult to distinguish from background noise and interfering signals arriving earlier. Since the polarity can change with azimuth, the Z-component records showing P_{D1} and P_{D2} were sorted by azimuth and shifted to a common event time using known distances and a P-wave velocity of 5800 m/s (Figure 154). This figure illustrates that picking out the timing orientation of first motions is difficult. Even when one looks only at the closest stations (Figure 155), it is still difficult because the signal is weak and emergent, although P_{D1} is clearly down at cliff stations LB03 and LB05.

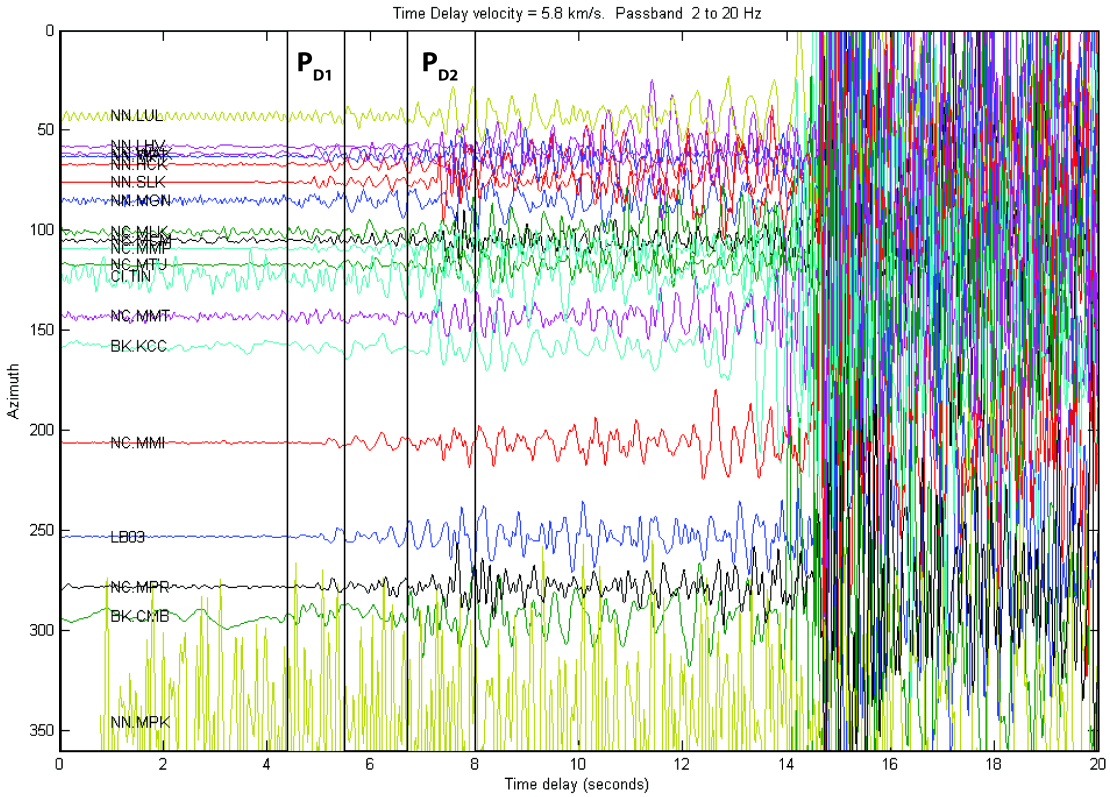

Figure 154. Detachment event first motion (Z) sorted by azimuth.

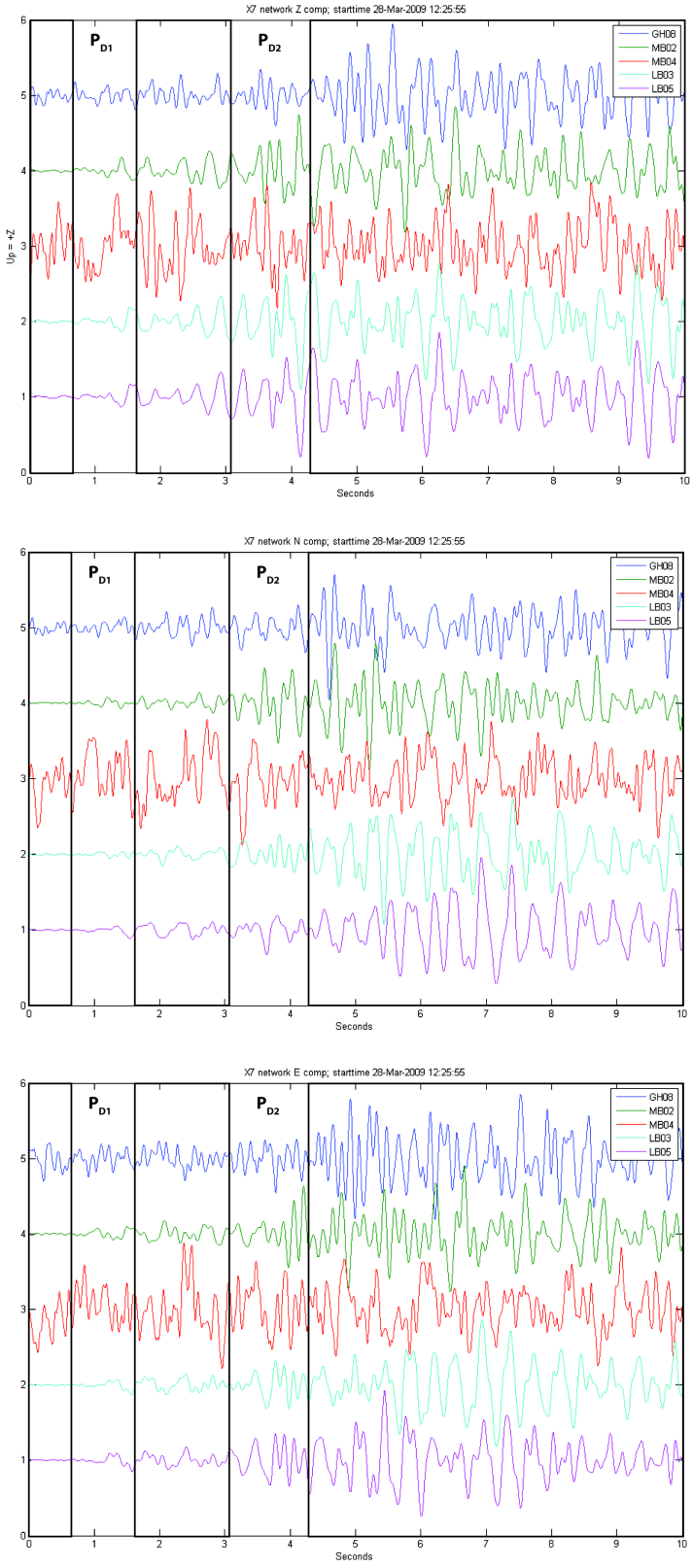

Figure 155. Detachment first motions for local (X7) network.

The impact is a stronger signal with a much higher signal to noise ratio. The Z-component impact P-wave is positive (up) at all azimuths (Figure 156), suggesting that this phenomenon is associated with the source mechanism and not with wave propagation in complex topography. Unfortunately, there are only four regional triaxial stations with a good record of the impact, too few to draw conclusions about first motions in the radial or transverse directions. The local seismic network, whose stations are all approximately on the same azimuth (west of the rock fall), also show a positive (up) P_I at all stations but the accelerometer at GH08, where it is unclear (Figure 157). The N-S and E-W components, which line up nearly perfectly in the transverse and radial directions, respectively, are less clear. The N-S component possibly shows a down (south) motion on the three geophones. The E-W component shows a west first motion at MB04 and LB05, an east first motion at MB02 and LB03, and an unclear emergent first motion at GH08.

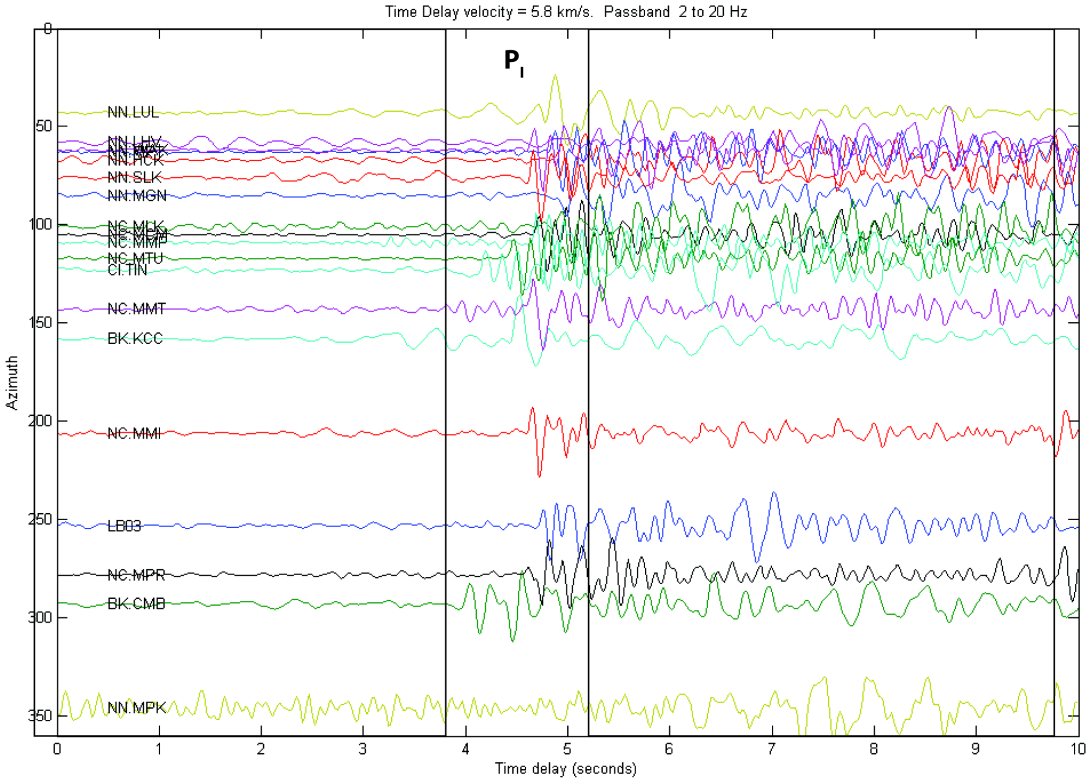

Figure 156. Impact event first motion (Z) sorted by azimuth for wider seismic networks.

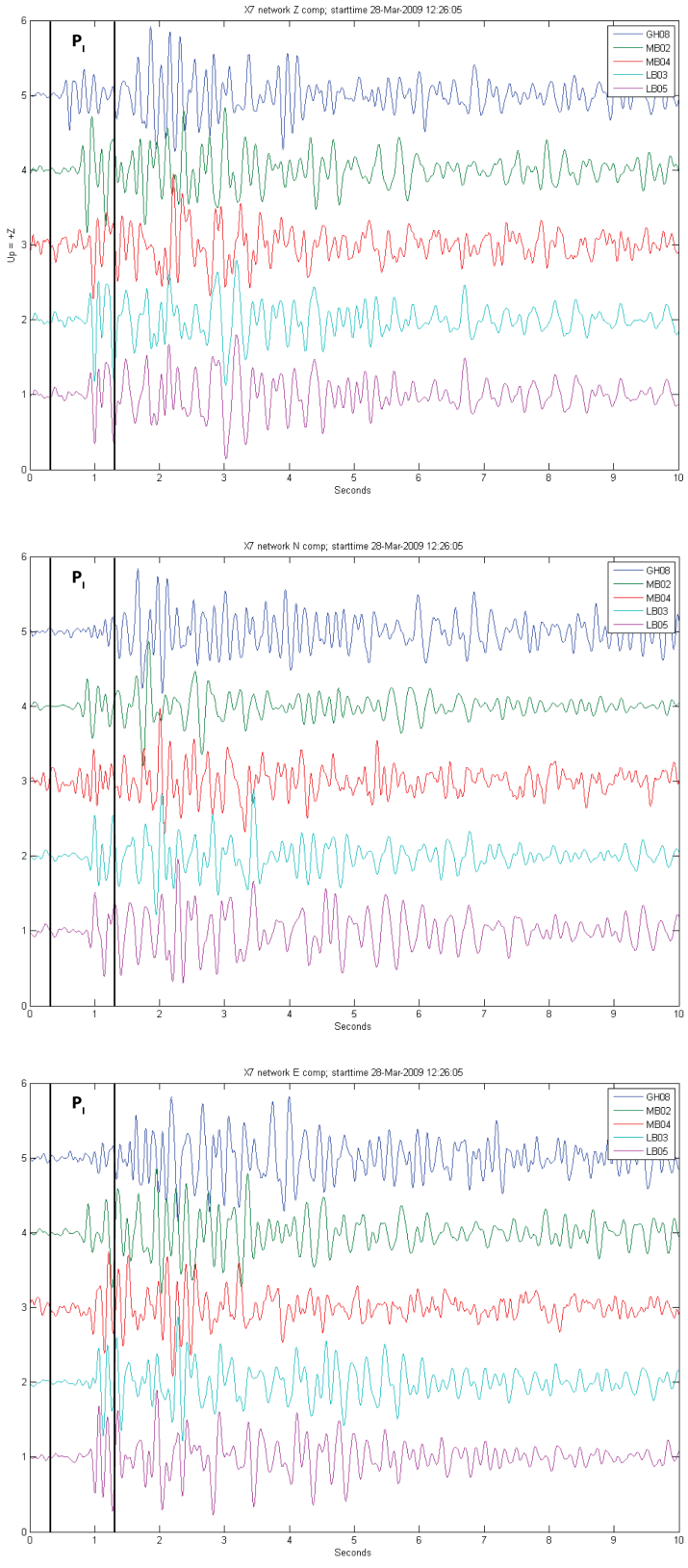

Figure 157. Impact first motions at local (X7) network.

In summary polarity can help to identify the physical characteristics of a rock fall, but there need to be several triaxial stations near to and distributed around the rock fall event. The number of broadband triaxial stations with a high enough signal-to-noise ratio was too low to draw any conclusions, and the signals were difficult to pick at even the local stations.

9.2.5 Identification of Seismic Phases

There are three main wave types expected for a seismic event: compressional (P), shear (S), and surface (Rayleigh) waves. The identification of distinct phases can be used to assess how waves are traveling through the ground at a site with complex topography, such as Yosemite Valley, and also to determine an initial source mechanism. Comparisons between the amplitude ratios of P, SH, and SV waves can be used to rule out double-couple (typical earthquake) solutions and resolve focal mechanisms even better than well-distributed polarity data (Julian and Foulger, 1996). Thus, comparison between the amplitudes of different phases, which may be easier to identify than polarity, may yield a focal mechanism solution for rock falls.

The differences in particle motion, frequency, and velocity are used to identify the different phases. The P-wave particle motion is radial to the direction the wave is traveling; the S-wave particle motion is transverse; the Rayleigh wave has a retrograde looping particle motion traveling on the surface. These wave types also have different velocities: for granite, P-wave velocity is 5500-6000 m/s; S-wave velocity 2800-3200 m/s; and Rayleigh wave velocity less than 3000 m/s. Rayleigh waves are also much lower frequency relative to P and S waves, usually less than 0.1 to 2 Hz at regional distances. P-waves are easy to identify since they arrive first and the moveout velocity can be matched to the rock type. S-waves can be identified by rotating the seismic components to radial and transverse directions, picking out a distinct arrival on the transverse component at several stations, and checking the moveout velocity to confirm it is in a reasonable range for S-waves. Rayleigh (surface) waves can be distinguished primarily using low-pass filtering to isolate the lower frequencies, plotting the moveout at different velocities, and calculating the phase velocity. Particle motion plots (radial-Z) can confirm the retrograde motion associated with Rayleigh waves.

It has been established already that there are three distinguishable seismic events associated with the Ahwiyah Point rock fall, and that these seismic events are all incoming P-waves with a positive (pushing) motion (P_{d1}, P_{d2}, and P_I). The unfiltered data do appear to show at least one more phase arriving, but, in contrast with a typical earthquake signal, it is difficult to identify distinct shear and surface waves phases since they travel at similar velocities and are buried in noise from emerging P-waves as the rock fall progresses.

It has also been established that the incoming P-waves are not from the radial (direct) direction, but rather appear to be arriving along the cliff faces for the X7 stations. Thus, establishing the true transverse component is difficult. There are four three-component broadband stations within 100 km of Yosemite Valley. These stations were rotated to radial and transverse directions and two of them show an emergent S-wave (S_I) as well as a Rayleigh wave (L_{rI}), which is better resolved in a lower frequency band (Figure 158 and Figure 159). There is no clear identification of S-waves at the other two broadband triaxial stations, nor at any of the six X7 stations, although there does appear to be a second weak arrival with a moveout velocity of 3400 m/s from the impact event, which is consistent with expected S-wave velocity (Figure 146, S_I).

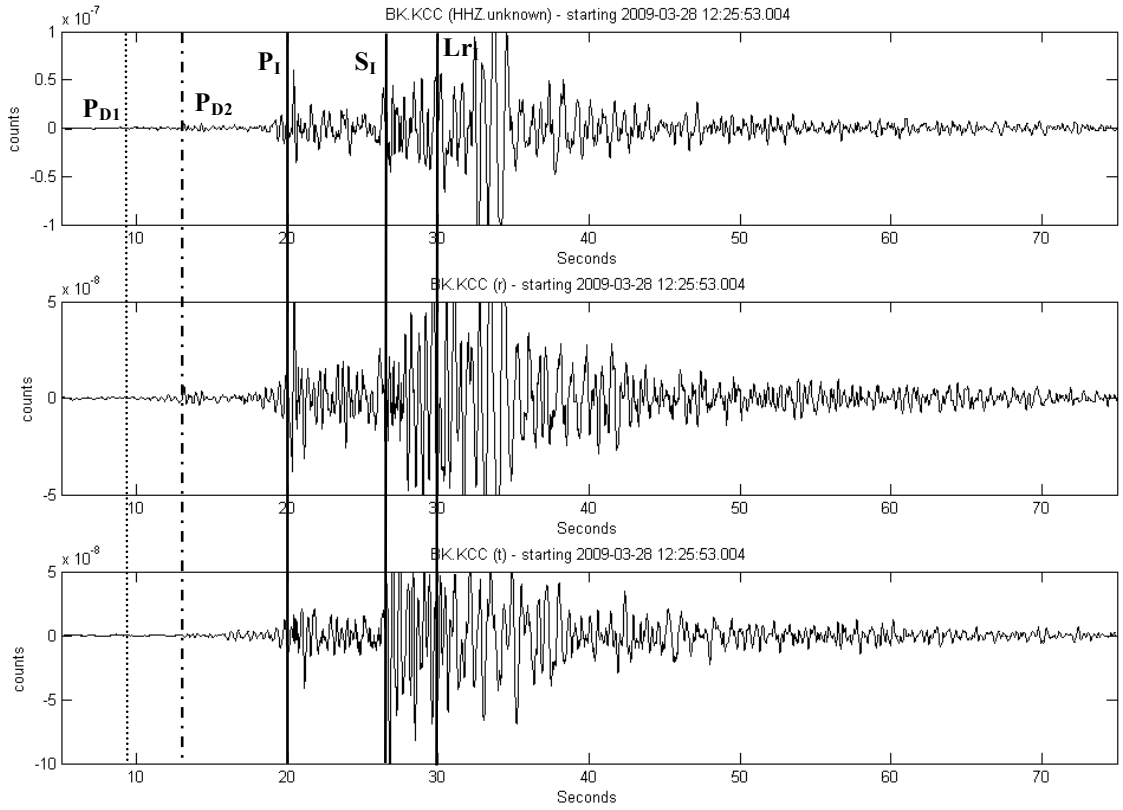

Figure 158. Broadband station KCC filtered 1-20 Hz, showing seismic phases.

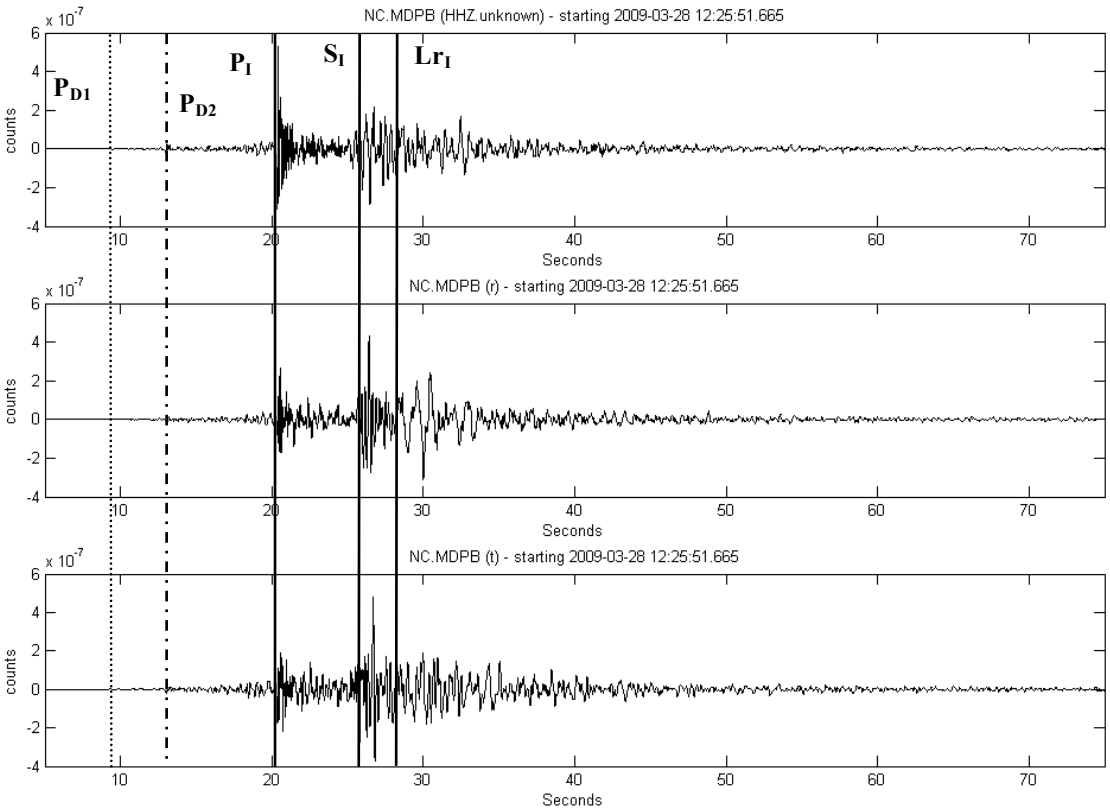

Figure 159. Broadband station MDPB filtered 1 – 20 Hz, showing seismic phases.

The moveout of Rayleigh waves can be seen by first filtering in the 0.3 to 0.5 Hz band, and then plotting either the radial or the Z-component of the recorded waveforms at twenty-five different stations sorted by distance (Figure 160). The moveout velocity is calculated to be about 2800 m/s, a reasonable velocity for Rayleigh waves in granite. Rayleigh waves are also identifiable by their retrograde circular motion along radial paths away from the event. In this case, it was found that it was difficult get good results, as the passband changed the particle motion results. This might be due to a change in the azimuth of the incoming wave depending on frequency and the fact that Rayleigh waves, traveling only on the surface, have different paths than P and S waves. It is therefore unknown if the Rayleigh waves are traveling along the cliffs like the P waves, or more directly on azimuth from the rock fall. Two examples of polarization analysis targeting Rayleigh waves are shown in Figure 161. In this case, the radial direction is the azimuth from the rock fall, and the waves were filtered in the 0.55 to 0.90 Hz band, which is the band that was used successfully for Rayleigh waves generated from other rock falls in Yosemite Valley (Uhrhammer, 1996; Wieczorek et al., 2000). However, this passband happens to be well below the corner frequency of the geophone. The Rayleigh wave at the cliff station, LB03, is easily identified arriving in on azimuth from the rock fall, indicating a more direct route than the P-waves. However, at the talus station, it is less obvious and the motion in that frequency band is dominated by Z (e.g. up and down) motion. The interaction of the waves at the junction between valley and cliff may account for this motion and the difficulty in identifying Rayleigh waves.

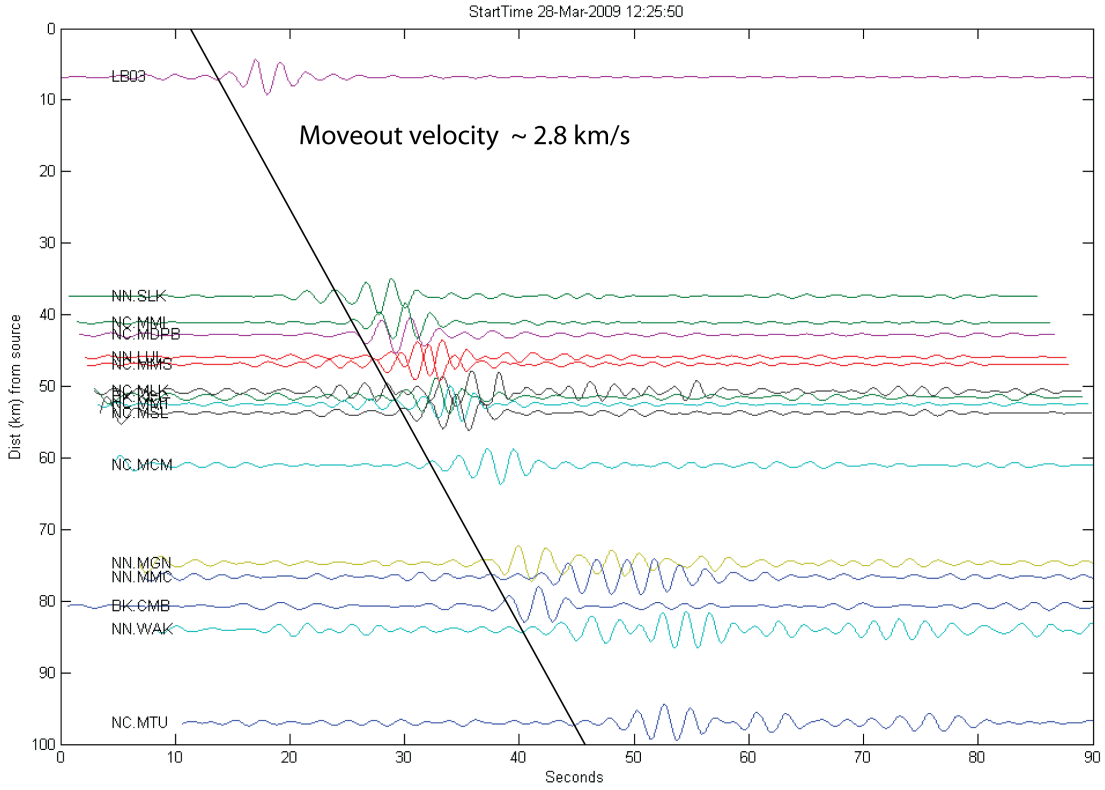

Figure 160. Rayleigh wave moveout for Z component. Moveout velocity is 2800 m/s.

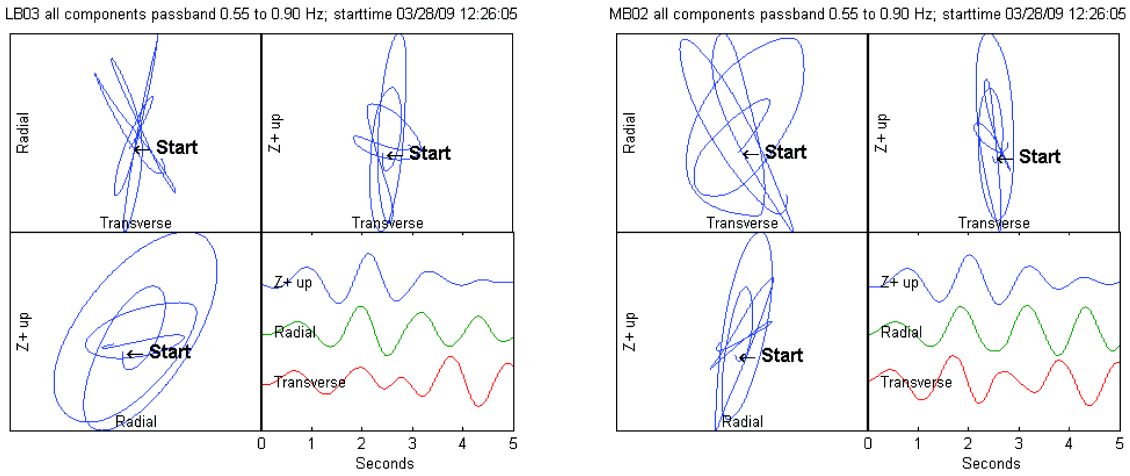

Figure 161. Rayleigh waves at station LB03 on Michael's Ledge, and MB02 at the base of the cliff.

In summary, there appear to be distinct compressional and Rayleigh (surface) wave phases at most stations. Rayleigh waves are strongest in frequencies that are well below the geophone corner used for the local seismic monitoring, but still detected. Shear waves are very difficult to distinguish, although some of broadband stations may have a weak S-wave arrival seen on a moveout plot (Figure 146). There are no distinguishable shear waves at the Yosemite Valley stations, which is partially due to the very short separation in time between P and S waves at close distances. However, the main reasons that S-waves are difficult to identity at the local stations is that they are believed to be weak if they exist and the complex, indirect wavepaths in Yosemite Valley make it difficult to identify S-waves using polarization analysis since radial and transverse directions are not easily determined.

9.3 Detailed Analysis of Acoustic Data

Rock falls are loud events that can often be heard as rumbling several kilometers away, as was the case with the Ahwiyah Point rock fall heard in Yosemite Village and beyond, over 4 km away. The primary acoustic source is blocks impacting the cliff, ledges, and talus. Acoustic monitoring can be used to detect the rock fall, record individual events associated with the rock fall, and locate the azimuth to the source of the acoustic waves. The feasibility of acoustic monitoring was explored during Phase 2 using barometric infrasound microphones compatible with the seismic dataloggers. These microphones are commonly used in volcano monitoring studies to record large pressure pulses associated with volcanic explosions and cone collapses (Johnson et al., 2004). Microphones sensitive to audible acoustic waves were not installed as part of the feasibility study since they are not compatible with the existing instrumentation.

9.3.1 Acoustic Waves Recorded By Geophones

Sometimes acoustic waves can also be picked up with geophones. Normally, it is impossible to distinguish an acoustic wave from a compressional seismic wave on a geophone, unless the time-zero and distance to the source is known. Thus, a large rock fall is one event in which a geophone-recording acoustic wave may be distinguished from other seismic waves. Indeed, the geophones appear to have picked up an acoustic signal arriving about twenty seconds after the rock fall initiation, distinguished by higher frequency (70 – 120 Hz) content (Figure 162). The acoustic velocity in air is 333 m/s at 3° C (the approximate temperature at the time of the rock fall). Using the distance and time zero of the Ahwiyah Point rock fall, the signal velocity is calculated as 335 m/s, providing strong supporting evidence that this later arriving signal is in fact acoustic. This signal is most strongly detected at stations on Michael's Ledge (Figure 162, right), which is not surprising since sound travels well to locations high on the cliff.

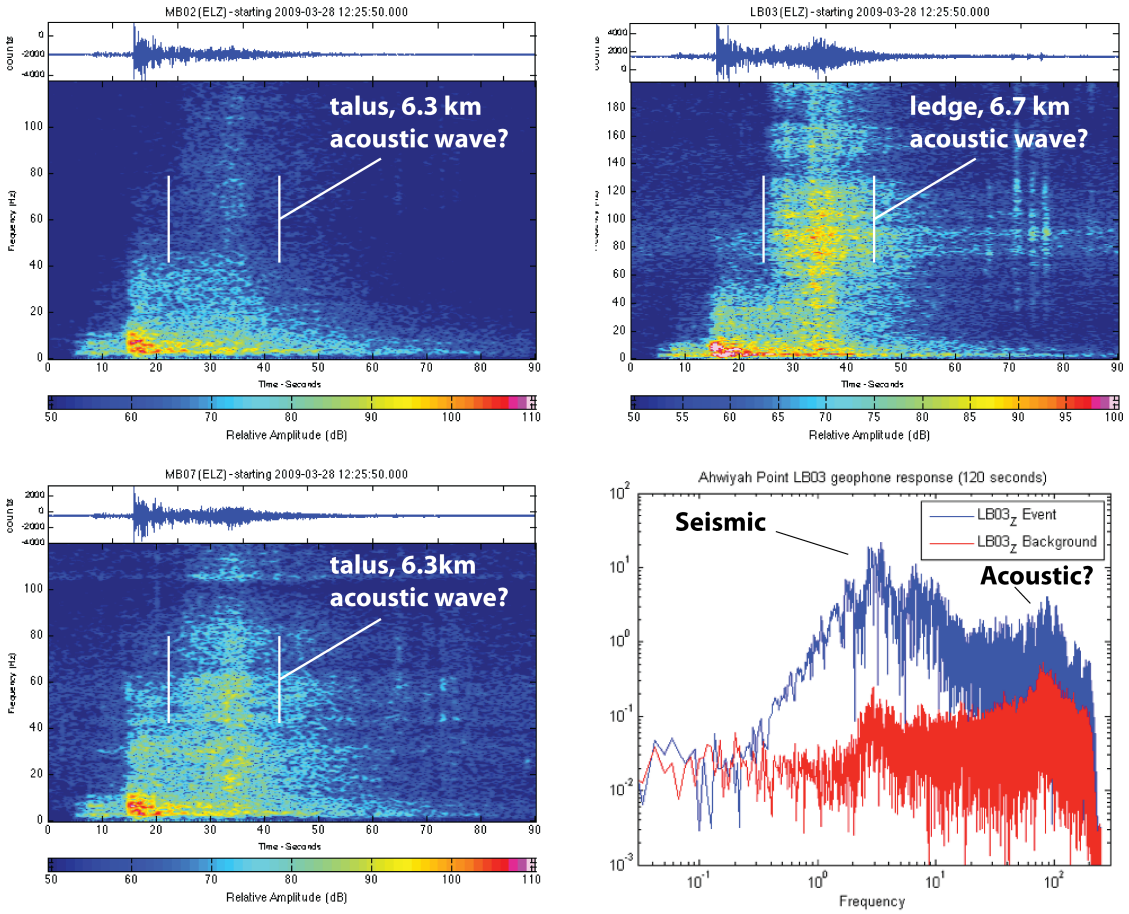

Figure 162. Spectrograms showing the late-arriving higher frequency wave that may be acoustic, and a spectral plot comparing the Ahwiyah Point rock fall to background (bottom right).

9.3.2 Infrasound Recorded By Barometric Microphones

Three barometric infrasound microphones were installed in Yosemite Village spaced approximately twenty meters apart from each other. The relative slowness of a sound wave means that the azimuth can be calculated with an array of microphones recording data with normal GPS precision in timing and a few meters separation of the microphones. Technically, four microphones are required to establish an azimuth in a three dimensional space, but if microphones are placed on flat ground and it is assumed that the acoustic signal is coming from the air (above), three microphones suffice to locate an incoming signal.

The data obtained from the microphones is first filtered to isolate the acoustic event of interest from other sources of acoustic noise. In this case, there are large, very low frequency signals associated with wind gust and mass air movement that can obscure the rock fall. The infrasound microphones picked up a strong rock fall signal in frequencies less than 10 Hz, but examination of the spectral response to the background noise (Figure 163, red) and the rock fall (blue) reveals a sharp drop-off in instrument sensitivity at frequencies greater than 10 Hz, thus indicating that the lack of higher frequency signal is at least partly a function of instrument response. The acoustic record lasts less than 30 seconds, thus the lowest observable frequency from the rock fall is 0.25 Hz, but the dominant low frequency signal is still present. High pass filtering at 0.1 Hz eliminates the lower frequency noise and allows the rock fall signal to stand out.

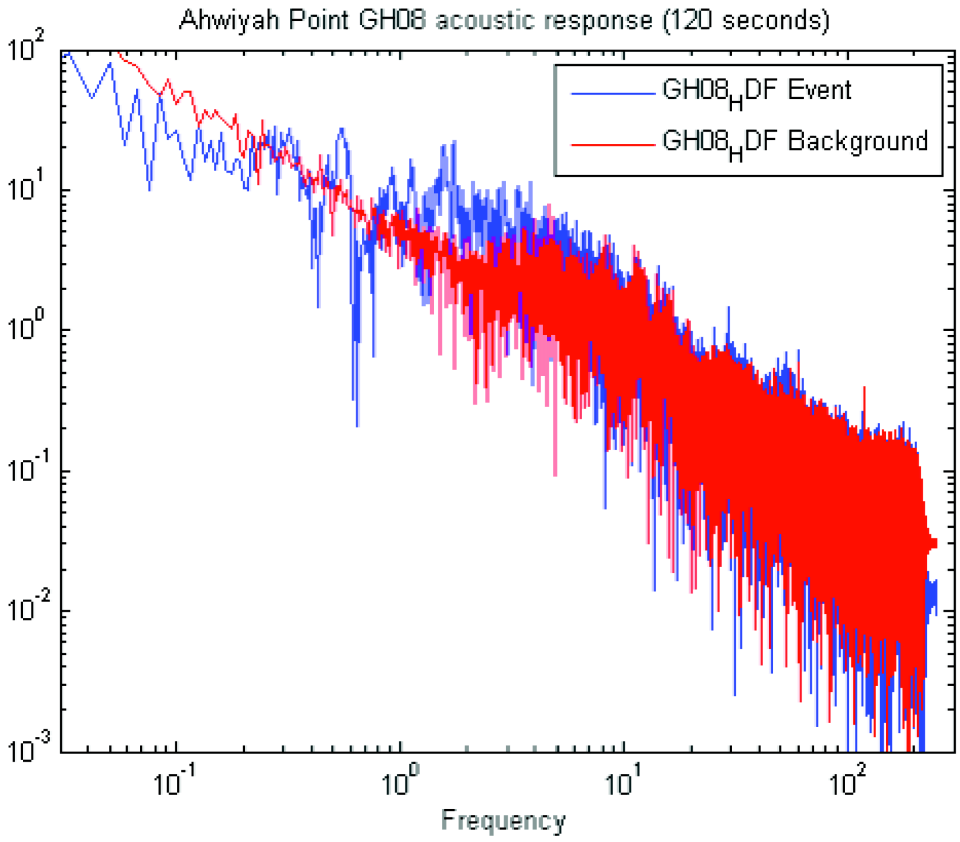

Figure 163. Acoustic spectral response of a rock fall compared to background acoustic noise.

Next, cross-correlation is used to calculate the timing delay between each of the microphones. Cross-correlation measures the similarity of two waveforms as a function of the time lag between them. The waveforms have maximum correlation at the time lag equivalent to the timing delay of the incoming waveform, which can be calculated with Equation 1.

$$(f \star g)(t) = \int_{-\infty}^{\infty} f(t) * g(t+\tau) d\tau \qquad (1)$$

This eliminates the need for precise and accurate time picks. Once the timing delay is known, the waveforms can be stacked, which magnifies the acoustic wave of interest while reducing noise and other signals through destructive interference. An accurate timing delay is also essential for calculating the azimuth of the incoming wave.

At the time of the Ahwiyah Point rock fall, one of the microphones was malfunctioning, which means that a single azimuth of the incoming plane wave cannot be determined and the possibilities can only be reduced to a cone of azimuths. For illustrative purpose, if it is assumed that the incoming plane wave is arriving parallel to the ground, then there are only two possibilities left (Figure 164). However, it is recognized that the acoustic waves may not be coming from a ground parallel direction, thus all directions between the two illustrated are still possible.

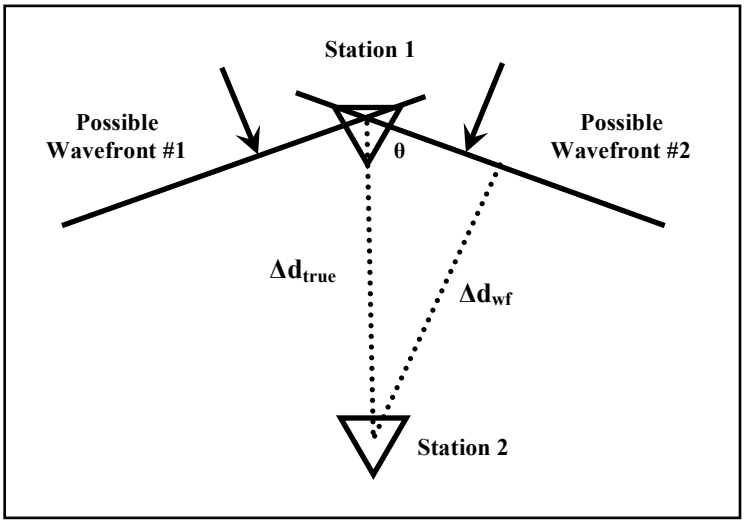

Figure 164. Illustration of how two stations can isolate the incoming wavefront azimuth to two possibilities assuming the wave is arriving nearly parallel to the ground.

The two microphones are spaced 18.6 meters apart and the spatial separation results in a temporal separation showing clearly that the wave arrives first at the east most microphone (Figure 165). Cross-correlation of the signals (Figure 166) pins the time delay between the two microphones at 0.042 seconds.

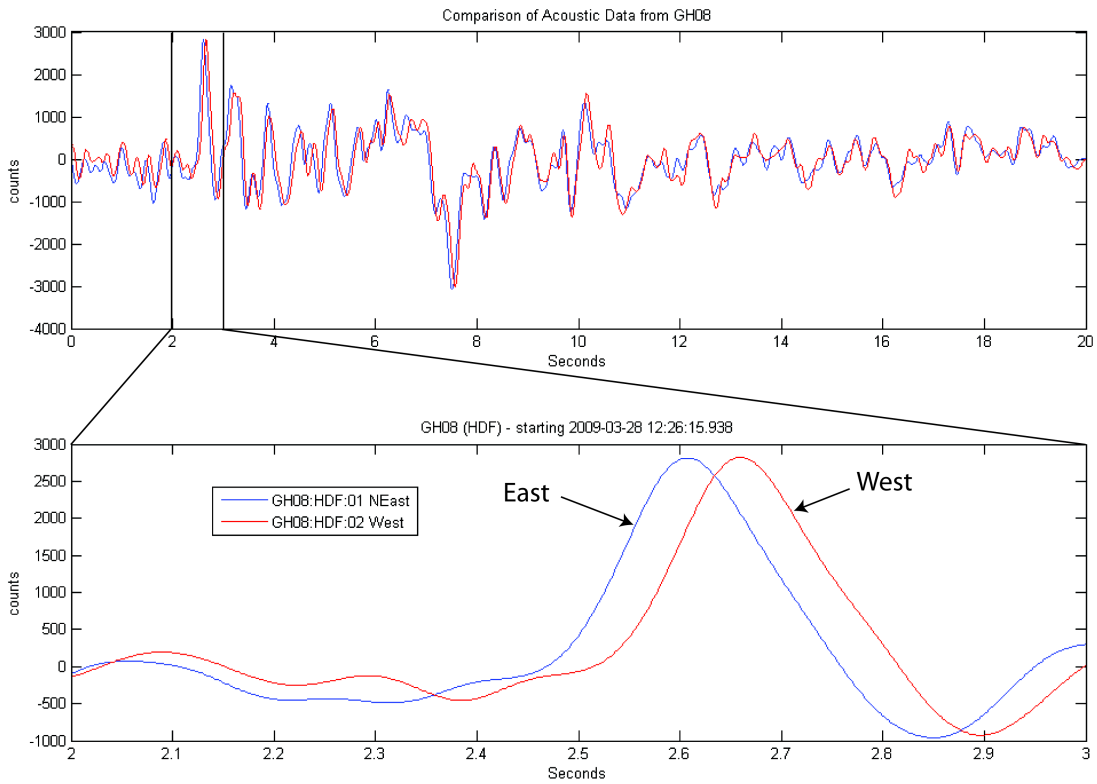

Figure 165. Barometric microphone records of the Ahwiyah Point rock fall. The separation in time helps to identify the direction of the incoming plane wave.

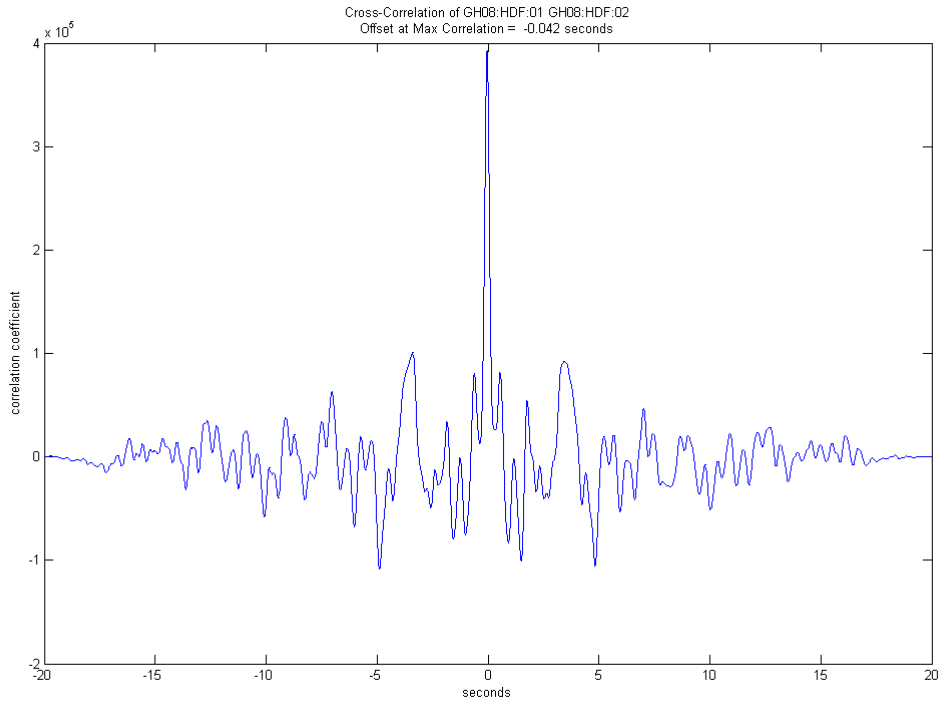

Figure 166. Cross-correlation of the two infrasound waveforms to determine the time delay.

The cone of potential azimuths for the incoming wavefront ranges from 239° to 315°, and the actual azimuth to the rock fall is 263°, but the line-of-sight path is blocked by a rock buttress (Figure 167 and Figure 168).

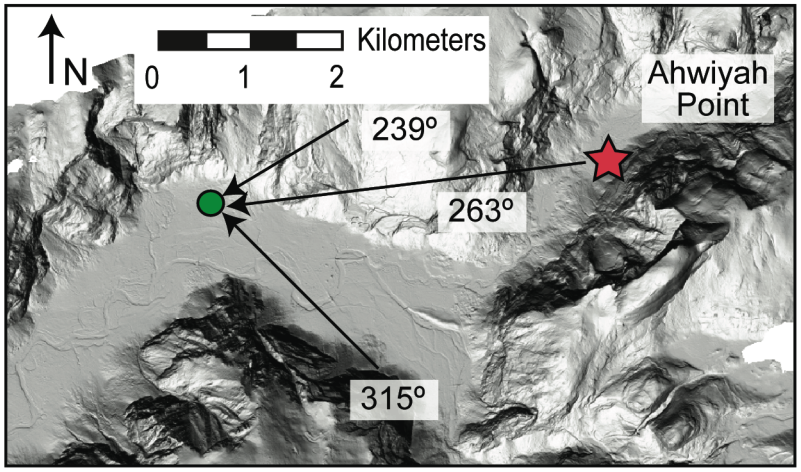

Figure 167. Range of possible azimuths for incoming acoustic wavefront between 239° and 315°. The direct azimuth to the rock fall is 263°, but a buttress blocks line of sight.

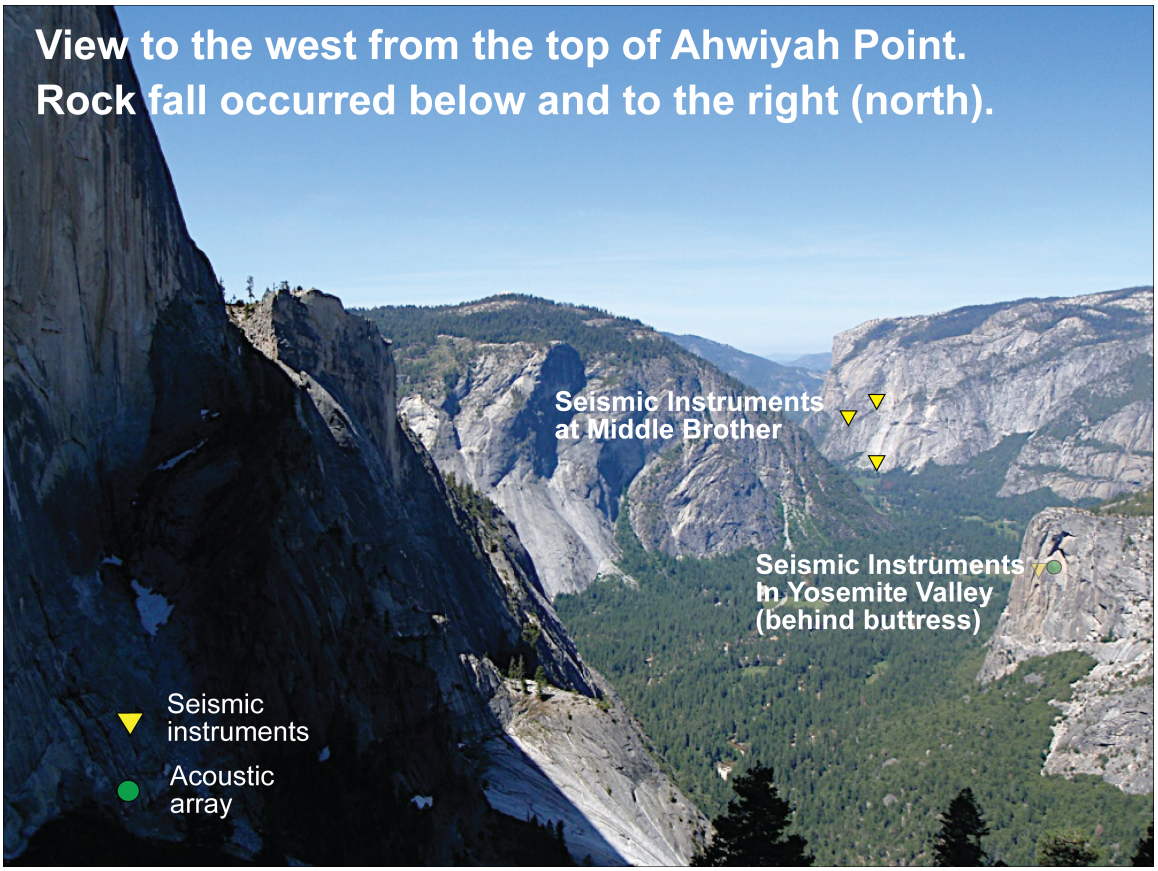

Figure 168. Location of seismic and acoustic instruments as seen from the summit of Ahwiyah Point (photo courtesy Mark Miller).

The calculation of the azimuth of the incoming wave supports but does not prove that the rock fall was the source of this acoustic wave. It must also be confirmed that the timing of the acoustic wave is consistent with the timing of the rock fall. In this case, the back-calculated acoustic velocity from signal onset to impact time is 325 m/s with an error of +/- 17 m/s, which is well within the estimated acoustic velocity at the time of the rock fall of 333 m/s. The error is due to a first-pick variation of 0.1 seconds and indirect (non line-of-sight) path length variation of 200 meters. What is also notable is that the first pick (e.g. this calculation) coincides with the impact and not with the detachment of the rock fall.

Stacking the two available waveforms using the calculated time delay enhances and helps to resolve additional features in the waveform, such as detachment. A stacked waveform spectrogram reveals that there is an early arriving signal at 2 Hz about seven seconds before the main impact (Figure 169, ~20s). This signal coincides with the timing of the seismic D2 event. Also visible on the spectrogram is a change in the dominant frequency of the rock fall from 2 Hz initially to less than 0.5 Hz after a few seconds, which may be related to the airblast (Figure 169, ~30s).

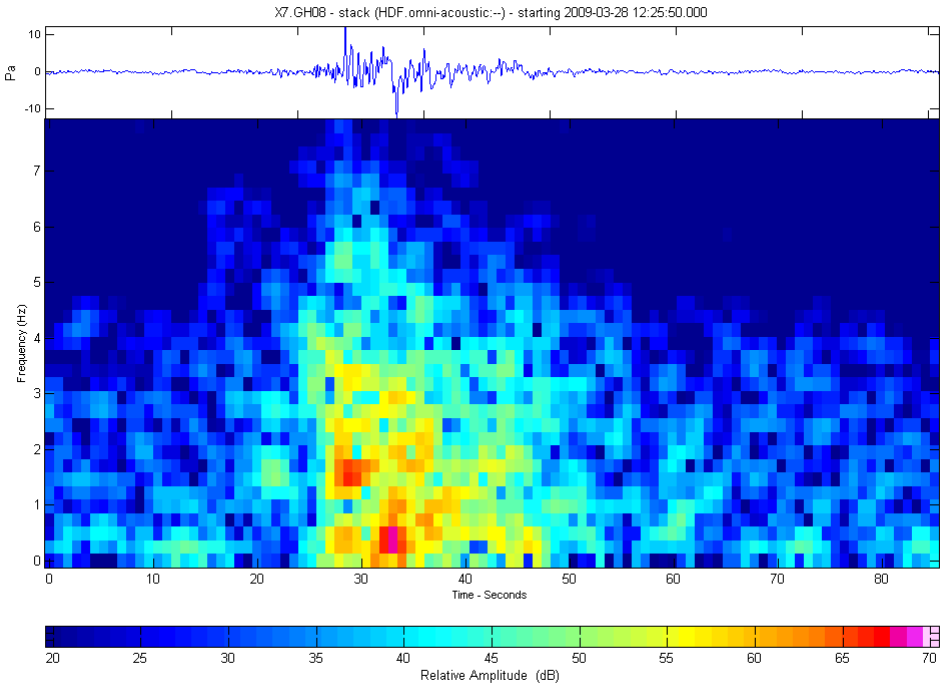

Figure 169. Spectrogram of stacked infrasound (left) and spectral response to event compared to background (right).

The D2 event also stands out on a simple time domain stacked waveform (Figure 170, top), but there is no acoustic signal corresponding to the seismic D1 event. However, the D1 event was both seismically weak and likely to be associated with a detachment or launch of the rock fall block from a ledge. Because of the sensitivity band of the instrument (infrasound, i.e., sensitive to high-velocity movement of air in front of a large block) and the nature of a signal likely to be emitted from an initial detachment (i.e., a faint, high frequency (audible) cracking sound), the D1 signal should not have been picked up by this instrumentation.

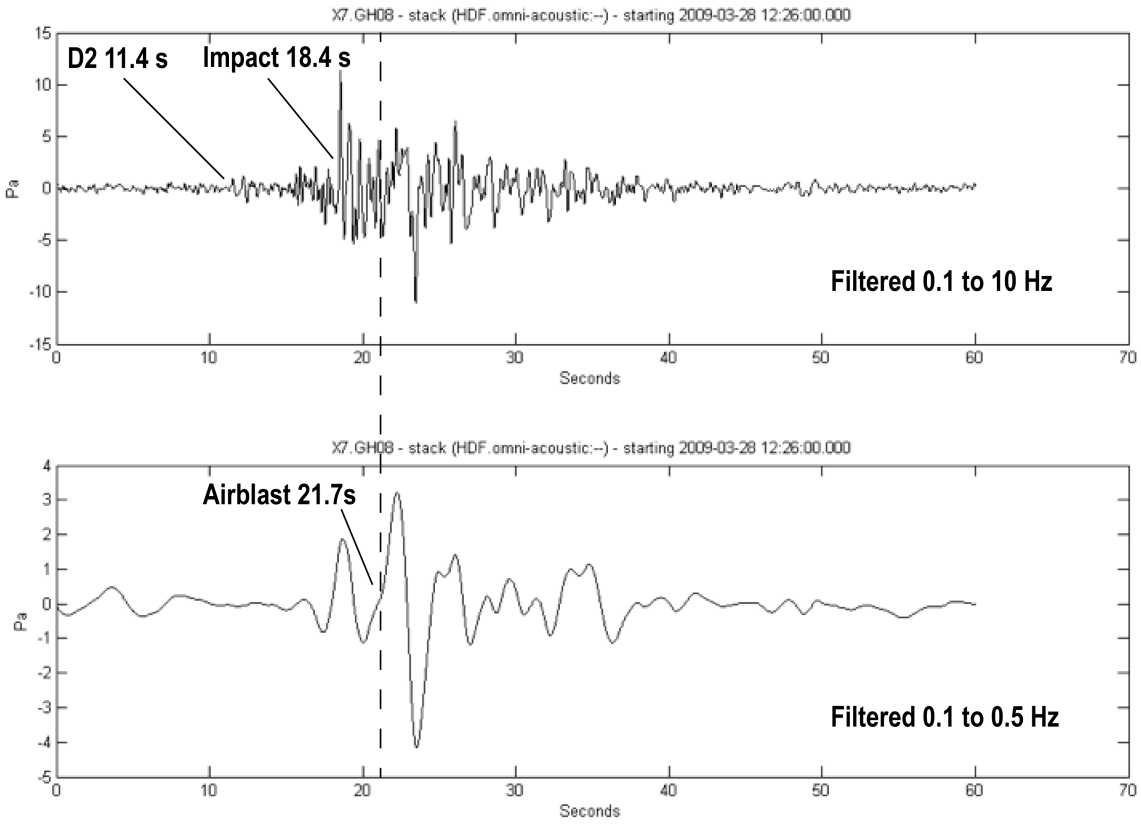

Figure 170. Stacked infrasound record of the Ahwiyah Point rock fall showing the second detachment event and the impact (top) as well as the lower frequency airblast signal that arrives 3.3 seconds later (bottom).

At the end of the infrasound acoustic record, bandpass filtering from 0.1 to 0.5 Hz shows the same strong low frequency acoustic wave as seen on the spectrogram, arriving 3.3 seconds after impact (Figure 170, bottom),. Ballistic calculations using LiDAR and seismic data indicate that the rock blocks were likely landing on the talus pile 3.3 seconds after the mid-cliff impact (the first major impact detected). Rock falls sometimes produce airblasts caused by a buildup of air beneath falling rock that gets squeezed out between the rock and the ground upon impact. There is evidence of an airblast at Ahwiyah Point in the form of toppled trees beyond the talus that were not impacted by falling rock (Figure 171), and shearing of tree trunks at heights greater than 3 meters, a result seen from other rock fall induced airblasts (Wieczorek et al., 2000). Therefore, the later arriving lower frequency signal is related to an airblast. Because airblasts are pressure phenomena caused by the rapid movement of a mass of air many tens of meters across, it is not surprising that the infrasound microphones picked it up.

Figure 171. Hundreds of trees were knocked over by an airblast (left), which typically shears trees several meters above the ground (right).

9.4 Trajectory Analysis

The combination of seismic data and the well-constrained rock fall dimensions and cliff geometry from LiDAR and photography data allows analysis of Ahwiyah Point rock dynamics. The initial mode of failure and the progression of the rock debris as it travels down the slope can both be evaluated using the available data.

The block that detached from the source area was tall relative to its thickness, suggesting that two modes of rock fall initiation are possible: toppling and sliding. The fractures bounding the back of the failed rock block are inclined obliquely to and away from the cliff face, and thus, the center of mass was well within the bottom footprint of the block (Figure 144). The block was resting on a 17 - 27 m wide ledge with downslope dip of 46°. Assuming a static friction angle for unpolished granite of between 42° and 51° (Goodman, 1989; Lajtai and Gadi, 1989) indicates that the detached block was, frictionally, barely stable when dry. This suggests that the mode of initial failure was sliding, not toppling.

The LiDAR-calculated mid-cliff impact distance is 330 m as measured from the bottom of the ramp, although there is material (2000 m^3) knocked out en-route approximately 130 m below the source (All distances are referenced from the bottom of the source block to the center of the impact zone). Using the two distinct detachment-related signals at 9.6 s (D1) and 7.3 s (D2) prior to the main impact (I) the impact distances for both ballistic and sliding trajectories down the face of the cliff can be back calculated. Differences in seismic and acoustic timing (t) of detachment, impact, and airblast events were used to constrain the sliding and freefall distance (d) using Equation 2.

$$d = \left(\frac{a * t^2}{2} \right) + v_0 * t \qquad (2)$$

where *a* is acceleration and *v* is velocity. The acceleration of rock sliding down a slope with inclination (β) can be related to the coefficient of friction (μ) of the rock mass by Equation 3 (Erismann and Abele, 2001).

$$a = g(\sin\beta - \mu\cos\beta) \tag{3}$$

where μ is equal to the tangent of the friction angle (θ), and *g* is the gravitational constant.

Seismic data can help to verify the initial mode of failure as sliding, not toppling. A sliding block would travel obliquely to the cliff face in the ledge dip direction whereas other modes, such as toppling, might instead fall directly. The calculated direct fall impact distance assuming a toppling mode would be 420 ± 60 m starting at time D1 and 240 ± 40 m starting at time D2. Because the fall distance from the bottom of the source area to the top of the impact zone is 330 m (i.e. not corresponding to either toppling scenario), the timing of D1 and D2 also supports a hypothesis of sliding before falling off, rather than toppling.

Thus, it is hypothesized that the source area block detached at time D1 and slid obliquely to the cliff face along on the dipping ledge until reaching the edge at time D2, at which point it launched ballistically for a short period of time. This is supported by a relatively steep launch velocity vector of 46° and steepening of the cliff to greater than 70° below the ledge (Collins, personal communication). Following launch, the trajectory is controlled by the launch velocity and its vector, which is a function of the dip and dip direction of the ledge, the distance slid, and the friction angle. Modeling of a range of initial parameters (e.g. friction and sliding distance) reveals that the trajectory is highly sensitive to small changes in the initial parameters. The ledge measures 17 to 27 meters wide (Collins and Stock, personal communication), and the 1996 Happy Isles rock fall slid down a 47° dipping ledge before going ballistic and clearing the entire cliff, which happens to only be possible if the initial sliding is nearly frictionless (Wieczorek, 2000; Uhrhammer, 1996). Thus, the sliding distance was bound from 17 to 27 m, and the dynamic friction angle bound from 0° to 15°.

At a 17 m distance, the block slides for 2.4 ± 0.2 seconds and falls 123 ± 7 m before contacting the cliff face. At a 27 m distance, the block slides for 3.0 ± 0.2 sec and falls 177 ± 10 m before contact. The results from the 17 m sliding scenario are a better match to both the distance to the material knocked off en-route (130 m) as well as the time difference between initiation at D1 and launching at D2 (2.3 sec), and is shown in Figure 172.

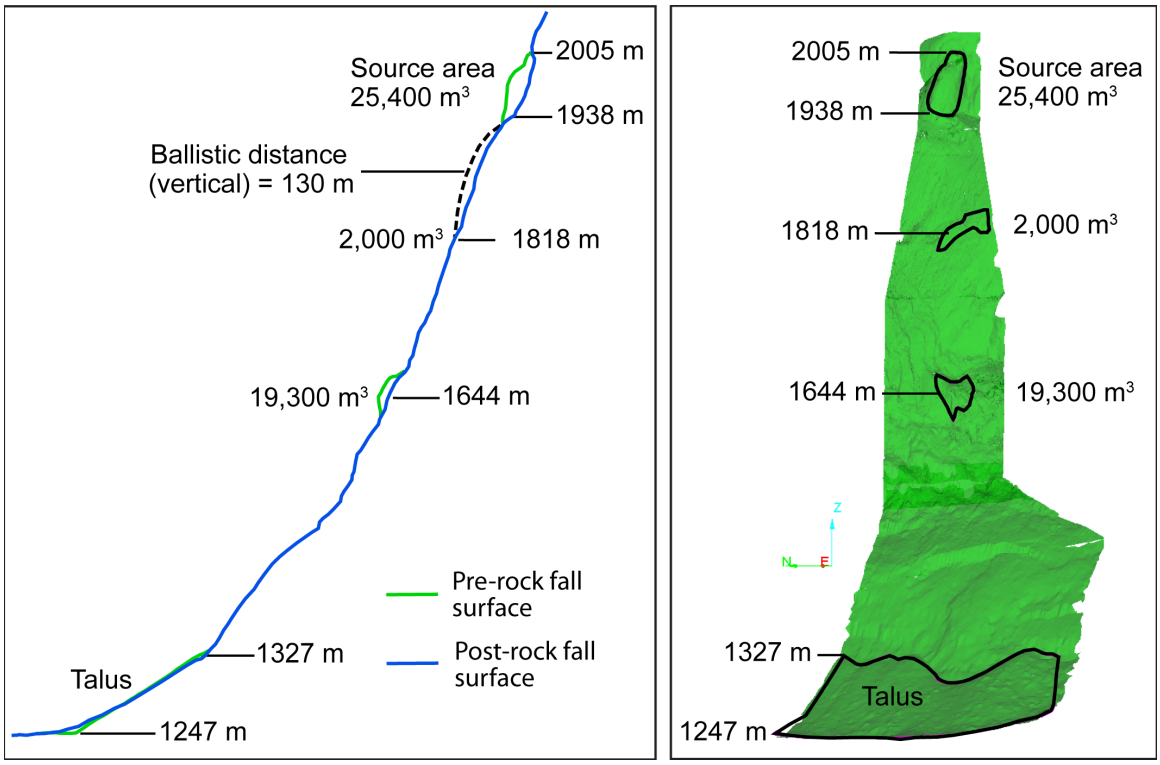

Figure 172. Cliff cross section (left) and frontal view (right) showing the locations, surfaces, and changes to the cliff profile of detached block, impacts, and talus. The calculated ballistic trajectory is also shown (Profile and volumes courtesy Collins and Stock, personal communication).

At the end of the ballistic phase, the rock fall debris continued to fall down the steep (~70°) cliff face before violently impacting a prominent ledge 330 m below the bottom of the source area. The high velocity of the falling rock (73 m/s ± 5 m/s) and the change in slope from approximately 70° to approximately 35° at the ledge is the reason for the energetic mid-cliff impact.

Following the mid-cliff impact, the combined rock fall debris continued down the flattening (53°) cliff face before impacting the talus slope and producing an airblast that knocked over hundreds of trees. A lower frequency infrasound acoustic wave arrived 3.3 seconds after the mid-cliff impact is likely due to the airblast. By using Equation 2 and plugging in the timing of the low frequency acoustic wave, the mid-cliff impact velocity (73 m/s ± 5 m/s), and an estimated vertical acceleration along a 53° cliff, the fall height below the mid-cliff impact is calculated to be between 270 m and 300 m. This distance, approximately 600 to 630 m below the rock fall source area, is consistent with the actual dimensions of the rock fall and cliff geometry, verifying that the low frequency signal originated at the talus pile impact zone and is due to the airblast.

9.5 Conclusion

The usefulness of seismic and acoustic monitoring of rock falls was put to the test by the Ahwiyah Point event. The very large main event was easily detected by both the local seismic and acoustic instruments as well as by broadband stations out to 350 km. However, none of the small or medium-sized rock falls that preceded or followed the event were detected by the local network, which helps to assess the detection range for seismic monitoring. The seismic instruments recorded predominantly compressional (P) waves and Rayleigh waves even though the geophone corner frequency of was well above the dominant Rayleigh wave frequency. S-waves may have been recorded by a few of the broadband stations, but the evidence is weak and inconclusive. The onset of seismic waves was too emergent and too weak to use polarization analysis to try and assess source mechanics at the small number (four) of regional triaxial seismic stations that were close enough to record a high signal-to-noise ratio. Locally, it might be possible for to assess the impact source mechanism if there were more stations at different azimuths, but the pre-impact events, which are arguably more interesting, are too weak to easily differentiate onset and polarity.

The acoustic sensors also showed promise in locating rock fall events using three microphones at each site to determine the azimuth of the incoming wavefront. In this case, one microphone was malfunctioning, and there was no direct line-of-sight to the rock fall, but the event was detected with a clear time separation between the two remaining microphones. The same method was tried with seismic stations a few hundred meters apart, but back calculation of velocity and polarization analysis of the first motions indicate that seismic waves follow the granite cliffs in Yosemite Valley instead of arriving directly on azimuth from the rock fall.

The details captured by the local seismic and acoustic instruments were used to conduct an analysis of the rock fall initiation and trajectory by comparing to results from LiDAR and photography. The LiDAR and photography data accurately pinpointed the dimensions of the source block, the size and orientation of the ramp off of which the block slide, and locations of impacts (Collins and Stock, personal communication). The seismic instruments picked up two distinct pre-impact events that were matched to sliding and launch of a block off a ledge, and the timing of the first major impact was consistent with a prominent mid-cliff impact that nearly doubled the size of the rock fall when additional rock was knocked loose. The acoustic data picked up one of the pre-impact events and the large impact, but it also recorded a low frequency later arriving pressure pulse that has been matched, timing-wise, to the top of the talus pile as calculated from the ballistic analysis. This low frequency pressure pulse is additional evidence for an airblast generated upon impact that knocked trees down beyond the edge of the talus.

Trajectory analyses using the LiDAR and seismic data suggest that the rock fall started when a block detached, slid down a steeply dipping ledge with little to no friction, and launched into a short ballistic trajectory before contacting the wall (and dislodging a relatively small amount of debris). The rock then tumbled until impacting a prominent ledge with such force that a volume of additional rock nearly equivalent to that launched from the source area was dislodged from the cliff face.

Thus seismic and acoustic monitoring, sometimes in combination with other available data, can be used to identify rock falls in the seismic record, differentiate rock falls from other seismic events based on phases and spectral character, locate the direction of incoming seismic and acoustic wavefronts, analyze the structural conditions that led to failure, and map the trajectory of the rock fall.

10 Conclusion and Discussion

The objective of this research was to monitor for rock falls with seismic and acoustic sensors placed as close as possible to a known rock fall source area. The first phase of the study was an initial feasibility study consisting of a single station. This station was equipped with a geophone and an accelerometer and placed high on a ledge, several hundred meters from three major rock fall source areas. Rock falls began occurring near this station within one week of installation and were easily detected by the instruments in frequencies ranging from a few Hz to over 200 Hz. The results from the initial feasibility study laid the groundwork for the second phase, in which five geophones, two accelerometers, and three infrasound sensors were installed in a four-station network. The specific objectives of the project, once it was determined that the study was feasible, were to characterize rock falls and other sources of seismic and acoustic activity, analyze the data for information about physical parameters and seismic wave transmission, and finally to search for precursory cracking and small rock falls.

10.1 Discussion of Equipment Design and Methodology

The original intent of the project was to place instruments close enough to a rock fall source area in order to capture acoustic emissions associated with rock fracture. However, in reality, the high number and large size of source areas meant that, even if efforts had been undertaken to install instruments via roped climbing, the likelihood of a rock fall occurring nearby while instruments were in place was extremely low. The Middle Brother rock formation offered an excellent compromise: with three major rock fall source areas situated just east of an accessible ledge system, instruments could be placed high on a cliff and nearer to source areas than anyplace in the valley. Middle Brother is also reasonably safe in winter, as snow and ice do not accumulate or avalanche except for a brief period following a storm, and has a strong winter freeze-thaw cycle that correlates well with historical rock falls. Three stations were spread over a 600 m footprint at Middle Brother, which turned out to be slightly larger than the dominant wavelength of signals emitted from rock falls, a favorable aperture for event monitoring. Ideally, it would have been better to install additional stations in the valley and on the rims, but most of the surrounding area is protected wilderness, and thus, instrument installations are highly restricted. There was was enough extra equipment for one additional station which was installed two kilometers away in Yosemite Valley at a non-wilderness site. The network was optimized for monitoring at Middle Brother except for the single outlying station.

The revised network configuration also meant that detecting high frequency acoustic emission events associated with small rock fracture was unlikely due to geometrical attenuation. However, detecting large rock fractures, rock movements, and rock fall impacts were still a reasonable monitoring objective from a few hundred meters away. Seismic signals from these types of events should be expected to range from a few Hz to hundreds of Hz. Given these expectations, 500 Hz is a high enough sampling rate to capture the entire expected rock fall signal and low enough to allow continuous (instead of triggered) recording with industry-standard field seismic equipment. The Reftek RT130 dataloggers borrowed from DTRA and PASSCAL have enough on-board memory for weeks of recording at these sampling rates, and consume power at a low enough rate to run through winter storm cycles with a reasonably small and portable solar panel and battery array. Thus, the revised monitoring objective facilitating the project by allowing more practical and more aesthetically acceptable (important in a National Park) instrumentation.

Geophones and two different types of accelerometers were tested for this project. The geophones, e.g. velocity sensors, were much better at recording the seismic events, especially weaker signals, than the accelerometers. The maximum seismic response of rock falls was around 8 Hz, which at the corner frequency of the geophone used during the feasibility study. During Phase 2, the 8 Hz geophone was replaced by 4.5 Hz geophones, and the lower frequency geophones proved adequate for detecting the first motions associated with rock falls. However, Rayleigh waves arrive in frequencies well under 4.5 Hz and were somewhat difficult to resolve. Furthermore, we know there were some medium-sized rock falls that were not detected seismically at a distance of a few kilometers, and that Rayleigh waves should be strongly generated by surface events such as rock falls. Therefore, it may be worthwhile in the future to test a lower frequency geophone (~1 Hz) to see if Rayleigh waves from medium-sized rock falls are sufficiently prominent to be detected at greater distances.

There was some concern about seismic wave transmission losses due to impedance contrasts and potentially poor contact between instruments sitting on but not affixed to the rock. National Park wilderness permits did not encourage any use of waveguides, bolts, or epoxy. However, the expected seismic waves are tens to hundreds of meters long and are thus, relatively unaffected by small openings. In addition, there are numerous and extensive open fractures between the source and receiver and these fractures are more likely to affect the seismic wave attenuation than rock contact at the receiver. The experiment showed that there was no noticeable difference between geophones placed in sand on the ledges and those placed directly on rock surfaces. In fact, an accelerometer affixed vertically and directly to the rock was the worst performing instrument of the entire network in terms of event detection, a result that is more a function of instrument type than rock contact. Thus, impedance and unaffixed instrumentation may not be a great concern from hundreds of meters away, but might affect close range acoustic emission monitoring should that type of project become a reality in the future.

10.2 Results Summary

The two winter seasons of seismic and acoustic monitoring produced a large dataset with at least three rock falls that were invaluable for developing processing methods and a customized rock fall triggering algorithm. After combing through the data, it was determined that a total of twelve to seventeen rock falls were captured, a variable number that reflects uncertainty in some events. Eight of the captured rock falls were reported by eyewitnesses and four more were supported by strong evidence. Having the seismic monitoring system in place increased the number known rock falls (8) by at least 50% (12), and possibly as much as 125% (17). On the other hand, some of these events are very small (if they are rock falls at all). Only three of the four highly certain but unreported rock falls are large enough to have been noticed and included in the database under normal circumstances. Thus, the real contribution of the seismic network is an estimated 38% increase in reporting rate over the project duration, still a significant number.

All but one of the detected rock falls came within one kilometer of the seismic stations, at the Three Brothers. All of the reliably reported events from that same area were detected, but two unreliably reported events were not. Thus, it is likely that those unreliably reported events did not actually occur at the Three Brothers. All eleven of those local (high certainty) rock falls occurred during the months of December, January, and February although stations were in operation for twice as many months. Seven of the eleven rock falls occurred during winter storm activity, and six of them occurred in December, during what might reasonably be considered the first large, cold winter storm of the season. This result is consistent with historical seasonal analysis of rock falls at the Three Brothers (Greg Stock, personal communication, 2011).

The differentiation of rock falls from other seismic sources was an iterative process. Processing, filtering and the triggering algorithm successfully eliminated the vast majority of data from consideration, but still left thousands of data segments to be considered for review. Those data were prioritized in order of decreasing probability of being a rock fall, which was determined primarily by the total number or percentage of stations triggering. Hundreds of high probability data segments were reviewed and classified as rock falls, earthquakes, probable snow avalanches, anthropogenic noise, rain, wind, or unknown. Classification of these events was often aided by other data, such as that retrieved from weather or regional seismic stations. For example, winter storms caused great deal of higher frequency seismic noise as well as a handful of widely detected low frequency events that are probably snow avalanches. Earthquakes were eliminated using the earthquake catalog unless unlisted, in which case they were easily identified by characteristic P and S wave arrivals and also by their appearance on regional (non-Yosemite) seismic records. The infrasound vibrated with continuous noise that was, at times, larger in amplitude than distinct events. Cross correlation of the low frequency (< 0.01 Hz) signal revealed the wind as a low velocity (non-acoustic) high amplitude pressure signal arriving from the west. In the spring, cross correlation of mid-frequency (2-5 Hz) infrasound reveals a strong continuous acoustic emitter to the north of Yosemite Village correlating perfectly with high flows on the Merced River: this is Yosemite Falls. Anthropogenic noise can be identified by unusual narrow-band frequency content. The strongest anthropogenic signals usually were recorded at stations high on the cliffs, where acoustic waves from the road beneath arrived unimpeded by energy-absorbing vegetation.

There were also two observed temporal patterns in the seismic data that appear to be related to the temperature, time of day, or relative aspect of the sun. The first was a noticeable daily periodic fluctuation in the mean of the data, e.g. a daily instrument drift. The second pattern is an apparent fluctuation in the number of triggers. One possible explanation for these phenomena is rock cracking and flexure in response to thermal fluxes, a potential rock fall trigger. Thus, the patterns were closely examined in the hopes of eliminating instrumentation noise and other possible (and less relevant to rock fall triggering) explanations. In the end, the higher instrumentation triggering rate was correlated with storm activity and is most likely due to snow and ice melting, sliding off, and impacting ledges below. The periodic drift of the seismic mean is clearly related to thermal changes associated with solar radiation, but it is difficult to conclusively eliminate internal instrumentation noise as the source. The evidence for detection of rock cracking and flexure is thus inconclusive, but monitoring the seismic mean drift should be kept in mind when designing future instrument configurations.

A representative signal from a rock fall might include pre-impact rumbling, several seismically distinguishable individual impacts, and an acoustically detected airblast. The time lag of between these different components of a rock fall and the frequency range of each is an indicator of the physical parameters, trajectory, distance to, or even a fingerprint from a particular source area. For example, the time lag between the pre-impact signal and the first impact is consistent with free-fall distances from source to first large impact at mid-cliff or on talus. Rock falls from the same source area have similar seismic signatures in terms of frequency content, duration, and spacing of the individual impacts because they are following similar trajectories. The seismic wave amplitude at any particular frequency, at the same source-to-receiver distance, is a function of the rock fall size. Thus, if several rock falls are identified as coming from the same source area (based on similarity in impact spacing), their relative sizes can be determined from amplitude. However, the frequency range is a function of source-to-receiver distance, with the upper frequencies bounded by geometric attenuation. For example, at 500 meters, large impacts resonant in frequencies greater than 200 Hz; at 800 meters, only up to 120 Hz; at 6 km, the frequencies do not exceed 50 Hz.

Precise location of rock falls using seismic data can done, roughly, in one of two ways. Single station event location is possible if there are clear P and S wave arrivals by calculating distance first and then azimuth to the event. Distance is normally calculated in strong motion seismology from the timing separation between P and S wave arrival, but there were no locally detectable S-waves. At some stations, infrasound and seismic sensors were co-located, which allowed the distance to be calculated from the time lag between P waves and acoustic waves instead. The azimuth can be found by looking at P waves alone since displacement occurs only in the radial direction. For stations at close range, the azimuths were always calculated toward particular talus slopes. For more distant rock falls, the incoming seismic waves were found to be traveling along the cliff face rather than directly from the event and through the valley. This result was supported by low apparent velocity calculations between two stations along the same cliff when high apparent velocities would be expected for seismic waves arriving obliquely to the cliff (and directly from the rock fall). The arrival of seismic waves via the cliff rather than directly through the valley is not a surprise given that seismic velocities in Yosemite granitic rock are much higher than in valley unconsolidated sediments. High impedance contrasts at the mountain-basin interface causes most of the seismic energy to be reflected back into the soft basin instead of transmitted forward into the rock. Furthermore, even without basin reflection, the velocity difference between each of the two travel paths may be large enough that seismic waves traveling a longer distance through the granite arrive first. Thus, locating rock falls with a single station is difficult for more distant events, but feasible for very near events.

The second way to locate rock falls is to use data from multiple stations. The rock fall location can be pinpointed with high-accuracy if stations are sufficiently well distributed and the topography is well modeled. Rough approximations of the rock fall locations were calculated by modeling the cliff face as a simple planar surface. The calculated locations for events at the same cliff were consistent with talus and known impacts, which may mean that simple 2-D modeling is sufficient to locate nearby rock falls. Individual impacts from a single rock fall, if sufficiently distinguishable, and non-rock fall events may also be located in the same way. In some cases, the azimuth was a key clue as to the origin of a signal. For example, slow, low frequency pressure pulses were consistent with westerly wind, steady infrasound vibration arrived from Yosemite Falls, and short-duration acoustic events came from the direction of a nearby residential area (with garbage collection). Locating rock falls at greater distances requires a more widely distributed network since P waves do not travel on-azimuth, preferentially arriving instead via nearby cliff faces. Complicated seismic wavepaths likely make it impossible to pinpoint individual impacts at distance, especially considering that the difference in azimuth between the impacts would only be a few degrees. Even acoustic waves can arrive off-azimuth in the narrow Yosemite Valley when rock buttresses block the line-of-sight between the source and receiver.

The timing, polarity, and relative amplitudes of the seismic waves contain information about the mechanical rock fall initiation and dynamical progression of rocks falling down the cliff face. These mechanics and dynamics can still be explored at distance even if precise locations cannot be pinpointed. Source mechanics refers to the physical movement of the rock that creates a particular seismic wave pattern. In the case of the rock fall, there are different physical movements associated with cracking, sliding, toppling, and impacts. In strong motion seismology, source mechanics are primarily calculated using inversion techniques and a good earth model, although such methods are difficult to apply accurately at close range with a surface event such as rock fall that occurs in complex topography. For the widely detected Ahwiyah Point rock fall, the regional strong motion seismic network automatically calculated the magnitude and located the event via this type of inversion. While the map location was quite good, the calculated event depth was a problematic 7 km, which may indicate that the current earth model used for regional earthquakes is not well tuned to a surface event in a steep valley such as a rock fall, although this is an area that deserves more research. There are alternate ways of calculating source mechanics by examining the polarity and relative amplitudes of different seismic phases. Of particular interest to rock fall research is the pre-impact (e.g. detachment) signal since they may help in understanding the conditions required for initiation and failure. Unfortunately, pre-impact signals were very weak and P wave polarity was often difficult to determine for all three components, even at close range. There was better polarity resolution of the impacts, but too few triaxial stations distributed in the near vicinity of Yosemite to analyze the data well. S waves were nearly non-existent and did not appear to be generated strongly at the source, if at all. Even Rayleigh waves were somewhat difficult to resolve due to their prevalent frequency being well under the geophone corner and complex valley-cliff boundary interactions. For near events, it was found that Rayleigh waves were rotated from their standard radial-Z orientation and traveled sideways up the cliff. For distant events this was not the case and stations located at the valley-cliff junctions had the worst Rayleigh wave resolution of any site. There may still be potential for source mechanics analysis based on P and Rayleigh waves, but this would be an area of new research and additional stations distributed over a wider area would be required.

Rock fall dynamics refers the progression of the rock fall starting with initial failure, sliding off a ledge, impacts on the way down, dislodging of additional material, talus impacts, airblast, and finally the rocks rolling and bouncing to a rest. The relative timing of the seismic and acoustic signals can be compared to the topographical profile and geomorphological evidence to back-calculate the trajectory and impact velocities. The dynamics of the Ahwiyah Point rock fall were explored with a combination of data from seismic, acoustic, high-resolution photography, and lidar, in collaboration with other researchers (Zimmer et al., 2012 in prep). Two distinct pre-impact events were matched to the start of sliding and subsequent launch of a block off a ledge before most of the rock mass went ballistic. A mid-cliff impact was sufficiently violent to knock out debris equivalent in volume to the initial rock mass, an event that is reflected seismically by a major impact signal whose timing correlates with the observed free-fall distance. The combined debris then traveled noisily down the face of the cliff before impacting the talus, sliding to a stop, and changing the morphology of the talus. An airblast that knocked over hundreds of trees was picked up by the infrasound and found, through its acoustically determined timing, to have been generated at the top of the talus.

Thus, the seismic and acoustic monitoring detected rock falls that were previously unknown and able to locate and distinguish rock falls from different source areas. In addition, the data contained information about trajectories and was analyzed with remote sensing data in order to resolve some rock fall dynamics. The records of rock falls from different source area and many non-rock fall events were cataloged and used to develop data processing techniques and triggering algorithms. While there were some analyses and hypotheses that were inconclusive, there were many successful results. Furthermore, there are clear ways to continue this project with new objectives, as will be discussed next.

10.3 Recommendations for future work

The work presented in this research should be continued to further explore some of the project objectives and build up the knowledge database. Three recommended future projects are: a) continued monitoring with a greater emphasis on acoustic, b) additional data analysis supplemented with the new data, and c) acoustic emission monitoring at sites with strong triggering mechanisms to record movement and rock fracture.

10.3.1 Rock fall monitoring future projects

Continuing rock fall monitoring in Yosemite Valley is recommended to increase the size of the rock fall database for further analysis and continue the search for triggers and precursors. Cliff monitoring at Middle Brother showed that it is possible to locate rock falls with a network of sensors, characterize events based on a spectral record, and analyze rock fall dynamics. Increasing the number of stations to include sites on the rims and at other cliffs is highly desirable to explore better detection, location, and possibly source mechanic studies. However, it is acknowledged that a larger, better-distributed network may not be allowed in a National Park due to issues related to aesthetics and wilderness impacts. Nevertheless, at a minimum, permission should be sought to increase the size of the network by adding instruments in developed areas.

Future monitoring should have an increased emphasis on acoustics, while still keeping geophones and infrasound at most sites. The three infrasound microphones proved to be valuable in identifying and locating at least two rock falls at Middle Brother, capable of picking up many of the same signals as the seismic data, and detected an airblast that was missed entirely by seismic instruments. However, audible acoustic waves reportedly heard in Yosemite Village from smaller rock falls preceding and following the Ahwiyah Point event were not captured. Infrasound and seismic instruments are also not likely to pick up precursory cracking noises or small rock falls that are of high interest for real-time hazard monitoring and assessment. Smaller, less clear rock falls and snow avalanches may be better resolved by adding acoustic monitoring component. Thus, continued monitoring with a greater emphasis on acoustics is recommended to increase the catalog of recorded events, permit additional analyses, increase the network size for better detection and locations, and continue the search for precursors.

10.3.2 Continued analysis of existing data and future data

There are some additional ideas that should be explored with the current dataset, however, in all cases, additional data is likely critical for the development of these ideas. The first idea is to compare seismic characteristics, such as energy and duration, with rock fall parameters, such as potential energy, runout, and freefall distance and compare the results from Yosemite with previous studies. Currently only two of the recorded rock falls are good candidates for this typed of analysis, although there may be one or two more from the historical record. Determining the radiated seismic energy would be the first step, either by developing a rock fall specific magnitude or integrating energy in a seismic velocity envelope. In either case, the magnitude would need to be adjusted for attenuation with distance and that calculation would likely be specific to Yosemite. For some rock falls, there is a calculated seismic moment magnitude, which is a good starting point but one that may not be the best reflection of radiated seismic energy in Yosemite. Once energy is well estimated, seismic and physical parameters can be compared.

Analysis of seismic data has shown that distinct arrivals can be traced to the physical trajectory of the rock fall and also that it is possible to locate rock fall impacts based on polarity and triangulation using a sensor network. 3-D site modeling may help to refine the calculated impact locations and trajectory and there may be opportunity to collaborate with 3-D block modelers. This first step for these projects would be to develop a good, useable model of the cliff using available high-resolution topographic maps, photography, and airborne lidar.

10.3.3 Acoustic Emission Monitoring of Rock Fracture

The original motivation behind this research was to capture acoustic emissions associated with rock fracture, a goal that should still be pursued. While it is suspected that seismic monitoring may be able to identify progressive failure and precursory cracking, it is unlikely that instruments could be installed in the right location as there is no way of knowing where and when rock falls are imminent. Nevertheless, rock cracking and movement may be detectable at many sites even without subsequent rock falls. There is evidence that rock flakes in Yosemite Valley are flexing in response to temperature changes and solar radiation. This phenomenon offers a possible explanation for rock falls that trigger in warm, dry conditions (Collins and Stock, 2010). Flexure and movement is likely accompanied by rock fracture that should be detectable and located using acoustic emission sensors. It is recommended that higher frequency acoustic emission sensors be installed at a location with a strong thermal flux due to solar radiation, and preferably installed at the same location as the crackmeters.

References

Aki K. and Richards P.G. (2002). *Quantitative Seismology 2nd Edition.* University Science Books.

Allen R. V. (1978). Automatic earthquake recognition and timing from single traces, *Bulletin of the Seismological Society of America* 68. 1521-1532.

Ambuter B. P. and Solomon S.C. (1974). An event-recording system for monitoring small earthquakes. *Bulletin Seismological Society of America* 64, 1181-1188.

Amitrano D., Grasso J.R., and Senfaute G. (2005). Seismic precursory patterns before a cliff collapse and critical point phenomena: *Geophysical Research Letters* 32: L08314.

Anderson J.A. and Wood H.O. (1925). Description and theory of the torsion seismometer. *Bulletin of the Seismological Society of America* 15: 1-72.

Archibald J.F., Calder P.F, Bullock K., and Madsen D. (1990). Development of in-situ rockburst precursor warning systems. *Mining Science & Technology,* 11(2), 129-152.

Arosio D., Longoni L., Papini M., Scaioni M., Zanzi L., and Alba M. (2009). Towards rockfall forecasting through observing deformations and listening to microseismic emissions. *Natural Hazards and Earth Systems Science* 9: 1119-1131.

Baltay A., Prieto G. and Beroza G.C. (2010). Radiated seismic energy from coda measurements and no scaling in apparent stress with seismic moment. *Journal of Geophysical Research* 115: B08314, doi:10.1029/2009JB006736.

Blake W. and Leighton F. (1970). Recent developments and applications of the microseismic method in deep mines, Ch. 23, *Rock Mechanics Theory & Practice-Proceedings of the 11th Symposium on Rock Mechanics,* 429-443.

Blake W., Leighton F., and Duvall W.I. (1974). Microseismic techniques for monitoring the behavior of rock structures. *U.S. Bureau of Mines Bulletin,* 665.

Blake W. (1978). Evaluating data from rock burst monitoring systems using the energy of microseismic events. *AE/MS Activity in Geologic Structures and Materials: Proceedings of the 2nd Conference.* 109-116.

Blake W. (1984). Evaluation of some rock burst precursor phenomena. *AE/MS Activity in Geologic Structures and Materials: Proceedings of the 3rd Conference,* 239-249.

Boler F.M. and Swanson P.L. (1992). Observation of heterogeneous stope convergence behavior & implications for induced seismicity. *Pure and Applied Geophysics.* 139: 639.

Bracewell R.N. (1999). *The Fourier Transform and its Applications*. McGraw-Hill Science/Engineering/Math 3rd edition.

Brady B.T., and Leighton F.W. (1977). Seismic anomaly prior to a moderate rock burst: A case study. *International Journal of Rock Mechanics, Mining Science, and Geomechanics Abstracts,* 14, 127-132.

Bunnell L.H. (1911). *Discovery of the Yosemite and the Indian War of 1851 which led to that event* (4th ed.): Los Angeles, G.W. Gerlicher, 355 p. (Reprinted 1990, Yosemite National Park, Yosemite Association, 315 p.)

Calder P.N., Archibald J.F, Madsen D., and Bullock K. (1990). High frequency precursor analysis prior to a rockburst. *Rockbursts and Seismicity in Mines: Proceedings of the 2nd International Symposium,* 177-182.

Chavan A.S., Raju N.M., and Srivastava S.B. (1993). Rock burst prediction: An empirical approach. *Rockbursts & Seismicity in Mines: Proceedings of the 3rd International Symposium,* 163-167.

Collins B.D. and Sitar N. (2005). Monitoring of coastal bluff stability using high resolution 3D laser scanning. *ASCE Geo-Frontiers Special Publication 138: Site Characterization and Modeling, Remote Sensing in Geotechnical Engineering*, E.M. Rathje, ed., ASCE, Austin, Texas, Jan 24-26, 2005.

Collins B.D. and Stock G.M. (2010). Correlation between thermal gradient and flexure-type deformation as a potential trigger for exfoliation-related rock falls. Abstract EP43A-0742 presented *at 2010 Fall Meeting, AGU*: San Francisco, Calif.,13-17 Dec.

Dammeier F. (2010). The seismic signature of rockslides: a review of events in the central Alps. Master of Science in Earth Science Thesis at ETH Zurich.

Dammeier F., Moore J.R., Haslinger F., and Loew, S. (2011). Characterization of alpine rockslides using statistical analysis of seismic signals. *Journal of Geophysical Research*, doi:10.1029/2011JF002037, in press.

Deparis J., Jongmans D., Cotton F., Baillet L., Thouvenot F., Hantz D. (2008). Analysis of rock-fall and rock-fall avalanche seismograms in the French Alps. *Bulletin of the Seismological Society of America* 98: 2: 1781-1796.

Dreger D. S. and Helmberger D.V. (1993), Determination of Source Parameters at Regional Distances with Single Station or Sparse Network Data. *Journal of Geophysical Research* 98, 8107-8125.

Dreger D. S. (2003) TDMT_INV: Time Domain Seismic Moment Tensor INVersion, *International Handbook of Earthquake and Engineering Seismology*, 81B, 1627.

Dziewonski A.M., Chou T.-A., and Woodhouse J.H. (1981). Determination of earthquake source parameters from waveform data for studies of global regional seismicity. *Journal of Geophysical Research* 86. 2825–2852.

Ebel J.E. and Bonjer K.P. (1990). Moment tensor inversion of small earthquakes in southwestern Germany for the fault plane solution. *Geophysical Journal International* 101: 133-146.

Ellenberger J.L., Heasley, K.A., Swanson, P.L., and Mercier, J. (2001). Three dimensional microseismic monitoring of a Utah longwall. *Proceedings of the 38th U.S. Rock Mechanics Symposium.* 1321-1333.

Erismann T.H. and Abele G. (2001). *Dynamics of Rockslides and Rockfalls*. Springer-Verlag: New York.

Farnbach J. (1975). The complex envelope in seismic signal analysis. *Bulletin of the Seismological Society of America* 65(4): 951-962.

Gale W.J., Heasley, K.A., Iannacchione A.T., Swanson P.L, Hatherly P., and King A. (2001). A rock damage characterization from microseismic monitoring. *Proceedings of the 38th U.S. Rock Mechanics Symposium,* 1313-1320.

Geiger L. (1912). Probability method for the determination of earthquake epicenters from the arrival time only (translated from Geiger's 1910 German article). *Bulletin of St. Louis University* 8(1). 56-71.

Gibbons M. (1978). Low frequency microseisms in relation to mine roof stability. *AE/MS in Geologic Structures and Materials: Proceedings of the 2nd Conference.* 246-257.

Gibowicz S.J. (1990). Keynote lecture: The mechanism of seismic events induced by mining. *Rockbursts and Seismicity in Mines: Proceedings of the 2nd International Symposium:* 3-27.

Goodman R.E. and Shi G.H. (1985). *Block Theory and its Application to Rock Engineering*. Prentice-Hall: Englewood Cliffs, NJ, 338 p.

Goodman R.E. (1989). *Introduction to Rock Mechanics*. John Wiley and Sons: New York.

Got J.L., Mourot P., and Grangeon J. (2010). Pre-failure behaviour of an unstable limestone cliff from displacement and seismic data. *Natural Hazards and Earth System Science* 10: 819-829.

Guzzetti F., Reichenbach P., and Wieczorek G.F. (2003). Rockfall hazard and risk assessment in the Yosemite Valley, California, USA; Monitoring, modeling, and mapping of mass movements. *Natural Hazards and Earth System Sciences* 3: 491-503.

Halliday D., Resnick R., and Walker J. (1993). *Fundamentals of Physics.* John Wiley and Sons: New York.

Hanks T.C. and Kanamori H. (1979). A moment magnitude scale. *Journal of Geophysical Research* 84(B5): 2348-2350.

Hardebeck J.L. and Shearer P.M. (2002). A new method for determining first-motion focal mechanisms. *Bulletin of the Seismological Society of America* 92(6): 2264-2276.

Hardebeck J.L. and Shearer P.M. (2003). Using S/P amplitude ratios to constrainteh focal mechanisms of small earthquakes. *Bulletin of the Seismological Society of America* 93(6): 2434-2444.

Hardy H.R. Jr. and Ersavci M.N. (1990). High frequency acoustic emission/microseismic studies associated with structural instabilities in underground mines. *Rockbursts and Seismicity in Mines: Proceedings of the 2nd International Symposium:* 199-204.

Hardy H.R. Jr. and Kimble E.J. (1991). Application of high frequency AE/MS techniques to rock slope monitoring. *AE/MS Activity in Geologic Structures Materials: Proceedings of the 5th Conference* 19: 457-477.

Helmstetter A. and Garambois S. (2010). Seismic monitoring of Séchilienne rockslide (French Alps); analysis of seismic signals and their correlation with rainfalls. *Journal of Geophysical Research* 115: F3: F03016. DOI: 10.1029/2009JF001532.

Iannacchione A.T., Batchler T., and Marshall T. (2004). Mapping hazards with microseismic technology to anticipate roof falls: A case study. *Proceedings of the 23rd International Conference on Ground Control in Mining:* 327-333.

Iannacchione A.T., Bajpayee T.S., and Edwards J.L. (2005). Forecasting roof falls with monitoring technologies: A look into the Moonee Colliery experience. *Proceedings of the 24th International Conference on Ground Control in Mining*.

Iannacchione A.T., Burke L.M., and Chapman M.C. (2005). Characterizing roof fall signatures with monitoring technologies: A look at the Moonee Colliery experience. *Proceedings of the 6th International Symposium on Rockbursts and Seismicity in Mines, Perth Australia.*

Iannacchione A.T., Esterhuizen G.S., Bajpayee T.S., Swanson P.L. and Chapman M.C. (2005). Characteristics of mining induced seismicity associated with rock falls and roof caving events. *Proceedings of the 40th U.S. Symposium on Rock Mechanics* 05-678.

Johnson J.B., Aster R.C., and Kyle P.R. (2004). Volcanic eruptions observed with infrasound. *Geophysical Research Letters* 31: L14604. DOI: 10.1029/2004GL020020.

Johnson J.B., Lees J.M., and Yepes H. (2006). Volcanic eruptions, lightning, and a waterfall: Differentiating the menagerie of infrasound in the Ecuadorian jungle. *Geophysical Research Letters* 33: L06308. DOI: 10.1029/2005GL025515.

Johnson J.B., Lees J., and Varley N. (2011). Characterizing complex eruptive activity at Santiaguito, Guatemala using infrasound semblance in networked arrays, *Journal of Volcanology and Geothermal Research,* 199(1-2), 1-14: ISSN 0377-0273, DOI: 10.1016/j.jvolgeores.2010.08.005.

Jost M.L. and Herrmann R.B. (1989). A student's guide to and review of moment tensors. *Seismological Research Letters* 60(2), 37–57.

Julian B.R. and Foulger G.R. (1996). Earthquake mechanisms from linear-programming inversion of seismic-wave amplitude ratios. *Bulletin of the Seismological Research Society of America* 86(4): 972-980.

Kanamori H. and Anderson D.L. (1975). Theoretical basis of some empirical relations in seismology. *Bulletin of the Seismological Society of America* 65(5): 1073-1095.

Kanamori H. (1977). The energy release in great earthquakes. *Journal of Geophysical Research* 82: 2981-2987.

Lacroix P. and Helmstetter A., (2011). Location of seismic signals associated with microearthquakes and rockfalls on the Sechilienne Landslide, French Alps. *Bulletin of the Seismological Society of America* 101: 341-353.

Lajtai E.Z. and Gadi A.M. (1989). Friction on a granite to granite interface*. Rock Mechanics and Rock Engineering* 22: 25-49.

Langstaff J.T. (1978). Interpretation of acoustic emission data: Star Mine. *Acoustic Emission/Microseismic in Geologic Structures and Materials: Proceedings of the 2nd Conference,* 163-178.

Lay T. and Wallace T. (1995). *Modern Global Seismology*. Academic Press.

Lee W.H.K and Lahr J.C. (1972). HYPO71: A computer program for determining hypocenter, magnitude, and first motion pattern of local earthquakes. *U.S. Geological Society Open File Report* 72-0224.

Leighton F. (1982). Case history of a major rock burst. *U.S. Bureau of Mines: Report of Investigation.*

Li D. (1989). Application of AE techniques to prediction of mining structure failure. *AE/MS Activity in Geologic Structures and Materials: Proceedings of the 4th Conference* 17: 181-187.

Luckett R., Baptie B., and Neuberg J. (2002). The relationship between degassing and rockfall signals at Soufriere Hills Volcano, Montserrat. *Geological Society of London, Memoirs* 21: 595-602. doi 10:1144/GSL.MEM.2002.021.01.28.

Maptek. (2011). I-Site Studio three dimensional LiDAR processing software, Version 3.2, http://www.maptek.com/products/i-site/i-site_studio.html (accessed 25 May 2011).

Marcak H. (1998). Model for changes in seismoacoustic parameters in mines. *Acoustic Emission/Microseismic in Geologic Structures and Materials: Proceedings of the 6th Conference,* 21, 339-355.

McSaveney M.J. and Downes G.L. (2002). Application of landslide seismology to some New Zealand rock avalanches. *Landslides : proceedings of the First European Conference on Landslides, Prague, Czech Republic, June 24-26, 2002.* Rybar, J., Stemberk J., and Wagner P. (eds.) Lisse, The Netherlands: A.A. Balkema. 649-654.

Minson S. and Dreger D.S. (2008), Stable Inversions for Complete Moment Tensors. *Geophysical Journal International* 174, 585-592.

Moore J.R., Sanders J.W., Haught R., Cuffey K.M., Glaser S.D. (2007). Seismic monitoring of rockfall, Helmet Mountain, British Columbia, Canada. *Proceedings: 1st Canada-U.S. Rock Mechanics Symposium*; Eberhardt E, Stead D, Morrison D (editors).

Moore J.R., Sanders J.W., Dietrich W.E., Glaser S.D. (2009). Influence of rock mass strength on the erosion rate of alpine cliffs. *Earth Surface Processes and Landforms* 34: 1339-1352.

Moran S.C., Matoza R.S., Garces M.A., Hedlin M.A.H., Bowers D., Scott W.E., Sherrod D.R., and Vallance J.W. (2008). Seismic and acoustic recordings of an usually large rockfall at Mount St. Helens, Washington. *Geophysical Research Letters* 35: L19302.

Morrison F., Gasperikova E., Washbourne J. (2004). *The Berkeley Course in Applied Geophysics*. http://appliedgeophysics.lbl.gov/ (last accessed October 9, 2011 at 10:49 am)

Myers S.C., Rock D., and Mayeda K. (2000). Feasibility of monitoring rock fall in Yosemite Valley using seismic methods; *LLNL report* UCRL-ID-137890.

Muir J. (1912). *The Yosemite*. The Century Company, New York.

Muir J. (1960). John Muir's studies in the Sierra, in Colby, W.E., ed.: San Francisco, Sierra Club, 103 p.

Nakamura A., Horiuchi S., and Hasegawa, A. (1999). Joint focal mechanism determination with source-region station corrections using short-period body-wave amplitude data. *Bulletin of the Seismological Society of America* 89(2): 373-383.

National Park Service Statistics (2011). Yosemite National Park Recreational Visitors.
http://www.nature.nps.gov/stats/viewReport.cfm (accessed 4 October, 2011).

Norris R. D. (1994). Seismicity of rockfalls and avalanches at three Cascade Range volcanoes: Implications for seismic detection of hazardous mass movements, *Bulletin of the Seismological Society of America* 84: 1925-1939.

Neumann M. and Makauch T. (1989). Analysis of microseismic activity prior to a rockburst in Campbell Red Lake Mines 'F-2' ore zone. *AE/MS Activity in Geologic Structures and Materials: Proceedings of the 4th Conference* 17, 225-240.

Obert L. and Duvall W. (1942). Use of subaudible noises for the prediction of rock bursts, part II. *U.S. Bureau of Mines Report of Investigation:* 3654.

Obert L. (1977). The microseismic method; discovery and early history. *Series on Rock and Soil Mechanics* 2(3): 11-12.

Pearce R.G. (1977) Fault plane solutions using relative amplitudes of P and pP. *Geophysical Journal of the Royal Astronomical Society* 60(3): 459-487.

Pearce R.G. and Rogers R.M. (1989). Determination of earthquake moment tensors from teleseismic relative amplitude observations. *Journal of Geophysical Research* 94: 775-786.

Reasenberg P. and Oppenheimer D. (1985). FPFIT, FPPLOT, and FPPAGE: Fortran computer programs for calculating and displaying earthquake fault-plane solutions. *U.S. Geological Society Open File Report* 85-739.

Reyes C.G., and West M.E. (2011). The Waveform Suite: A robust platform for manipulating waveforms in MATLAB, *Seismological Research Letters* **82:** 1: 104-110.

Richter C.F. (1935). An instrumental earthquake magnitude scale. *Bulletin of the Seismological Society of America* 25: 1-32.

Rosser N., Lim M., Petley D., Dunning S., and Allison R. (2007). Patterns of precursory rockfall prior to slope failure. *Journal of Geophysical Research* 112: F04014, doi: 10.1029/2006/JF000642

Roth M., and Blikra L.H. (2009). Seismic monitoring of an unstable rock slope at Aaknes, Norway. *Geophysical Research Abstracts* 11: EGU2009-3680: EGU General Assembly.

Rudajev V. (1990). Keynote address: Recent Polish and Czechoslovakian rockburst research and the application of stochastic methods in mine seismology. *Rockbursts and Seismicity in Mines: Proceedings of the 3rd International Symposium,* 157-161.

Shiotani T., and Ohtsu M. (1998). Evaluation of progressive slope failure by acoustic emission. *Progress in Acoustic Emissions IX,* II-70-II-79.

Spillman T., Maurer H., Green A.G., Heinke B., Willenberg H., and Husen S. (2007). Microseismic investigation of an unstable mountain slope in the Swiss Alps. *Journal of Geophysical Research* 112: B07301. DOI: 10.1029/2006JB004723.

Senfaute G., Duperret A., and Lawrence J.A. (2009). Micro-seismic precursory cracks prior to rock-fall on coastal chalk cliffs: a case study at Mesnil-Val, Normandie, NW France. *Natural Hazards and Earth System Science* 9 (5): 1625-1641.

Stevenson R. (1976). Microearthquakes at Flathead Lake, Montana: A study using automatic earthquake processing. *Bulletin of the Seismological Society of America* 66, 61-79.

Stock G.M., Bawden G.W., Green J.K., Hanson E., Downing G., Collins B.D., Bond S., and Leslar M. (2011a). High-resolution three-dimensional imaging and analysis of rock falls in Yosemite Valley, California. *Geosphere* 7: 2: 573-581.

Stock G.M, Collins B.D., Santaniello D.J., Wieczorek G.F., and Snyder JB. (2011b). Historic rock falls in Yosemite Valley (1857-2010). *U.S. Geological Survey Open-file Report (in review).*

Stock G.M. and Uhrhammer R.L. (2010). Catastrophic rock avalanche 3600 years BP from El Capitan, Yosemite Valley, California. *Earth Surface Processes and Landforms* 35: 8: 941-951.

Swanson P.L. and Sines C.D. (1991). Characteristics of mining-induced seismicity and rock-bursting in a deep hard-rock mine, *U.S. Bureau of Mines*.

Tilling R.I., Koyanagi R.Y., and Holcomb R.T. (1975). Rockfall seismicity -- correlation with field observations, Makaopuhi Crater, Kilauea Volcano, Hawaii. *Journal of Research, U.S. Geological Survey* 3: 345-361.

Uhrhammer RA. (1996). Yosemite rock fall of July 10, 1996. *Seismological Research Letters* 67: 47-48.

Uhrhammer R.A., Dreger D.S., and Romanowicz, B. (2001). Best practice in earthquake location using broadband three-component seismic waveform data. *Pure Applied Geophysics* **158**, 259-276.

Vandewater C.J., Dunne W.M., Mauldon M., Drumm E.C., and Bateman V. (2005). Classifying and assessing the geologic contribution to rockfall hazard. *Journal of Environmental & Engineering Geosciences* 11 (2):141–154.

Vassilou M.S. and Kanamori H. (1982). The energy release in earthquakes. *Bulletin of the Seismological Society of America* **72**(2): 371-387.

Vilajosana I., Surinach E., Abellán A., Khazaradze G., Garcia D., and Llosa J. (2008). Rockfall induced seismic signals: case study in Montserrat, Catalonia. *Natural Hazards and Earth System Sciences* 8: 805-812.

Wieczorek G.F., Alger C.S., and Synder J.B. (1989). Rockfalls in Yosemite National Park, California, in Brown W.M. II (ed.), *Landslides in central California: 28th International Geological Congress Field Trip Guidebook T381*: 56-62.

Wieczorek G.F., Synder J.B., Alger. C.S., Isaacson K.A. (1992). Rock falls in Yosemite Valley, California. *U.S. Geological Survey Open-File Report* 92-387.

Wieczorek G.F., Nishenko S.P., and Varnes D.J. (1995). Analysis of rock falls in the Yosemite Valley, California. *Rock Mechanics: Proceedings of the 35th U.S. Symposium*: 85-89.

Wieczorek G.F. and Jäger S. (1996). Triggering mechanisms and depositional rates of postglacial slope-movement processes in the Yosemite Valley, California. *Geomorphology* 15, 17-31.

Wieczorek G.F., Morrissey M.M., Iovine G., Godt J. (1998). Rock-fall hazards in the Yosemite Valley, California. *U.S. Geological Survey Open-file Report* 98-467.

Wieczorek G.F., Morrissey M.M., Iovine G., and Godt J. (1999). Rock-fall potential in the Yosemite Valley, California. *U.S. Geological Survey Open-file Report* 99-578.

Wieczorek G.F. and Snyder J.B. (1999). Rock falls from Glacier Point above Camp Curry, Yosemite National Park, California. *U. S. Geological Survey Open-File Report* 99-385, http://pubs.usgs.gov/of/1999/ofr-99-0385/.

Wieczorek G.F., Snyder J.B., Waitt R.B., Morrissey M.M., Uhrhammer R.A., Harp E.L., Norris R.D., Bursik M.I., and Finewood L.G. (2000). Unusual July 10, 1996 rock fall at Happy Isles, Yosemite National Park, California. *Geological Society of America Bulletin* 112, 75-85.

Wieczorek G.F. (2002). Catastrophic rockfalls and rockslides in the Sierra Nevada, USA. In *Catastrophic Landslides: Effects, Occurrence, and Mechanisms*, Evans S.G., and DeGraff J. (editors). Geological Society of America Reviews in Engineering Geology XV, 165-190.

Wieczorek G.F. and Synder J.B. (2004) Historical rock falls in Yosemite National Park, California. *U.S. Geological Survey Open-File Report* 03-0491.

Wieczorek G.F., Synder J.B., Borchers, J.W., and Reichenbach, P. (2007). Staircase Falls rockfall on December 26, 2003 and geologic hazards at Curry Village, Yosemite National Park, California. *U.S. Geological Survey Open-File Report* 07-1378, 14 p.

Wieczorek G.F., Stock G.M., Reichenbach P., Snyder J.B., Borchers J.W., and Godt J.W. (2008). Investigation and hazard assessment of the 2003 and 2007 Staircase Falls rock falls, Yosemite National Park, California, USA. *Natural Hazards and Earth System Sciences* 8: 421-432.

Wong, I.G. (1992) Recent developments in rockburst and mine seismicity research, *Rock Mechanics*, 1103.

Yosemite Association (1987). The walls came tumbling down: Yosemite National Park, *Yosemite Association* 49(2), spring 1987, 5.

Appendix A: Station Operation Log for Yosemite Rock Fall X7 Network

# Unique	# Days	%	X7 station deployment and tally of the number of unique locations.
0	5		
1	29	13%	
2	74	32%	
3	92	40%	
4	35	15%	

Date-Start	Date-End	# Days	LB03	LB05	GH08	MB02	MB07	MB06	MB04	GH08	MB04	GH08
		230	geophones						acc		HDF	
10/24/08	11/8/08	16				1						
11/9/08	11/9/08	1	1			1						
11/10/08	11/15/08	6	1									
11/16/08	12/11/08	26	1			1						
12/12/08	12/13/08	2	1	1		1		0			2	
12/14/08	12/21/08	8	1	1		1	1	0			2	
12/22/08	12/27/08	6	1	1		1		0			1	
12/28/08	1/2/09	6				1						
1/3/09	1/7/09	5										
1/8/09	1/8/09	1	1	1								
1/9/09	1/19/09	11	1	1		1		1				2
1/20/09	1/27/09	8	1	1		1						
1/28/09	1/29/09	2	1			1						
1/30/09	2/7/09	9	1			1						2
2/8/09	2/9/09	2	1			1						
2/10/09	2/10/09	1	1			1				1		2
2/11/09	2/13/09	3	1			1	1			1		2
2/14/09	2/16/09	3				1	1			1		2
2/17/09	2/17/09	1					1			1		2
2/18/09	2/19/09	2		1			1			1		2
2/20/09	2/20/09	1		1		1	1			1		3
2/21/09	3/2/09	10	1	1		1	1	1	1	1		3
3/3/09	3/3/09	1	1	1		1	1	1	1			
3/4/09	3/27/09	24	1	1		1	1		1			
3/28/09	3/31/09	4	1	1		1	1		1	1		2
4/1/09	4/4/09	4	1	1		1	1		1			
4/5/09	4/12/09	8	1	1		1	1	1	1	1		3
4/13/09	4/13/09	1	1	1		1	1	1	1			
4/14/09	4/16/09	3	1	1		1	1	1	1	1		3
4/17/09	4/21/09	5	1	1		1	1	1	1			
4/22/09	4/23/09	2	1	1		1	1	1	1	1		3
4/24/09	4/30/09	7	1	1		1	1	1	1			
5/1/09	5/6/09	6	1	1		1	1	1	1	1		1
5/7/09	5/10/09	4	1	1		1	1	1	1			
5/11/09	5/12/09	2	1		1	1		1				1
5/13/09	6/8/09	27	1		1	1						1
6/9/09	6/12/09	4	1			1						
6/13/09	6/14/09	2	1		1	1						1
6/15/09	6/15/09	1	1			1						

A.1 Station GH08 (Shady Valley), Accelerometer

Station GH08 was placed in Yosemite Valley during Phase 2 (winter 2007-08) and outfitted with an accelerometer and 3 barometric microphones. The station had intermittent power outages and data gap errors. The accelerometer may have been tilted (or slowly changing position) in the snow and frozen ground, which may account for some of the tilt in February, 2009.

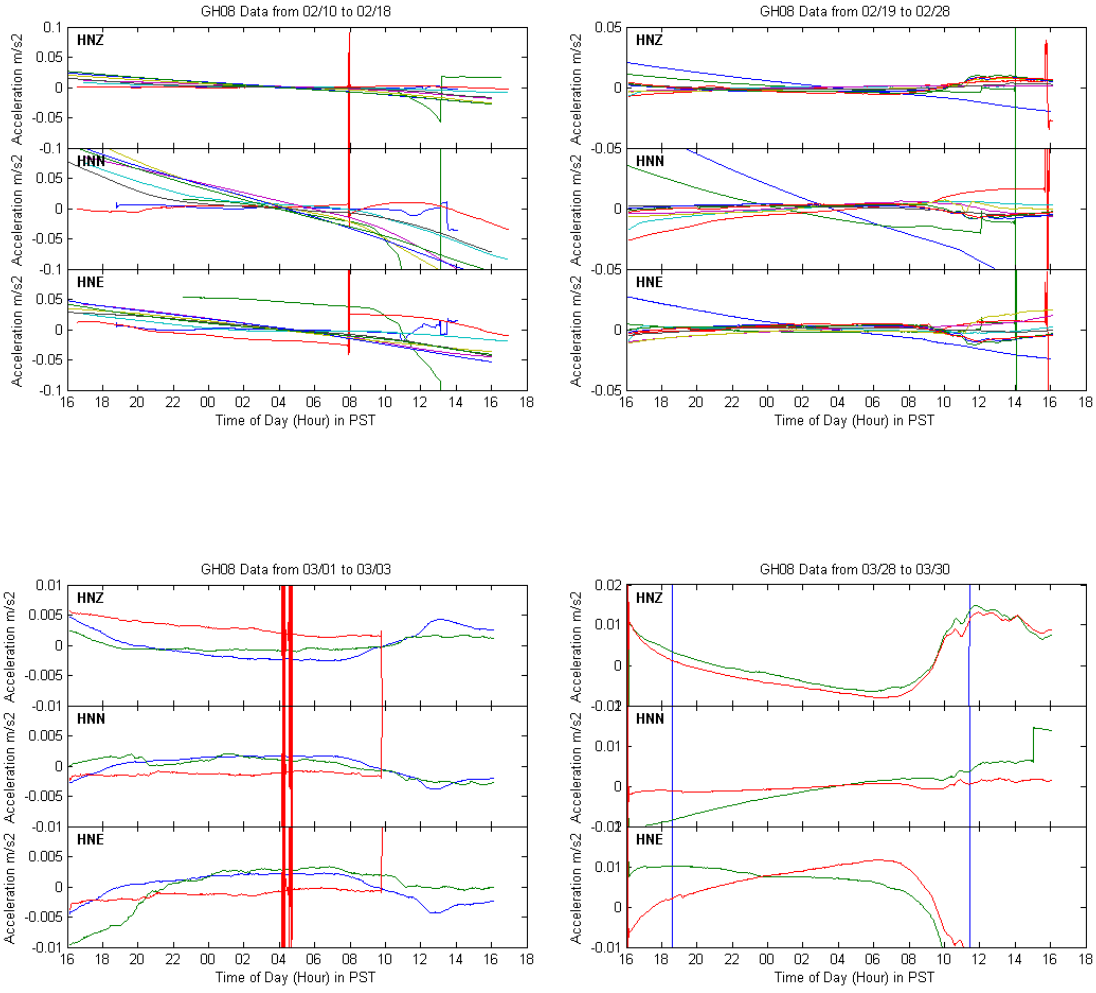

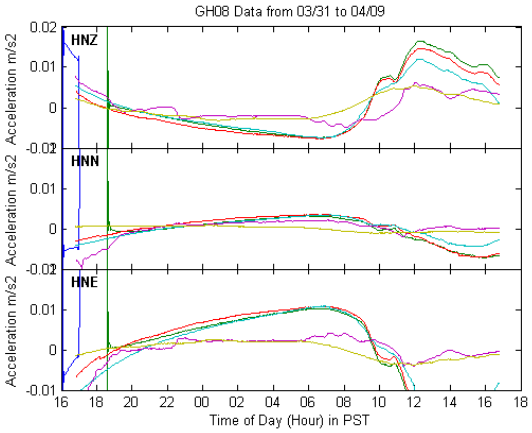
GH08 Data from 03/31 to 04/09
HNZ
HNN
HNE
Acceleration m/s2
Time of Day (Hour) in PST

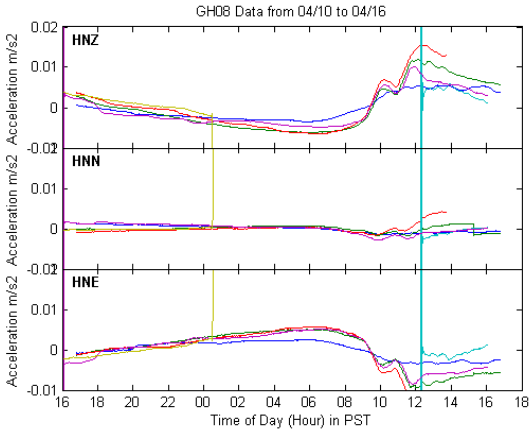
GH08 Data from 04/10 to 04/16
HNZ
HNN
HNE
Acceleration m/s2
Time of Day (Hour) in PST

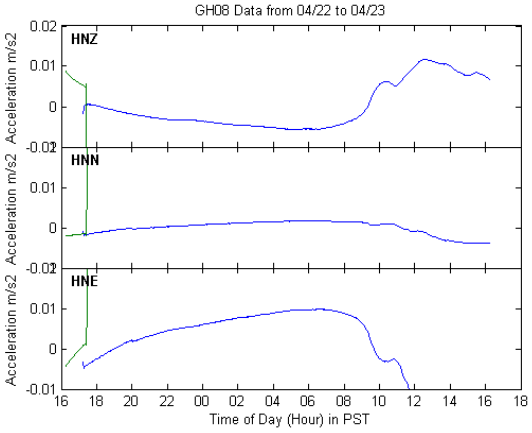
GH08 Data from 04/22 to 04/23
HNZ
HNN
HNE
Acceleration m/s2
Time of Day (Hour) in PST

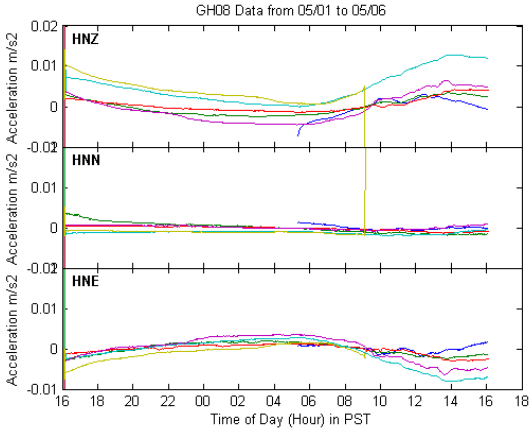
GH08 Data from 05/01 to 05/06
HNZ
HNN
HNE
Acceleration m/s2
Time of Day (Hour) in PST

A.2 Station GH08 (Shady Valley), Geophone

Station GH08 was placed in Yosemite Valley during Phase 2 (winter 2007-08) and outfitted with the geophone from MB07 (and 3 barometric microphones) after 05/10/2009. The normal gain for a geophone is x32, but the gain was left at x1 for this dataset, which may account for some of the noise. The station had intermittent power outages and data gap errors.

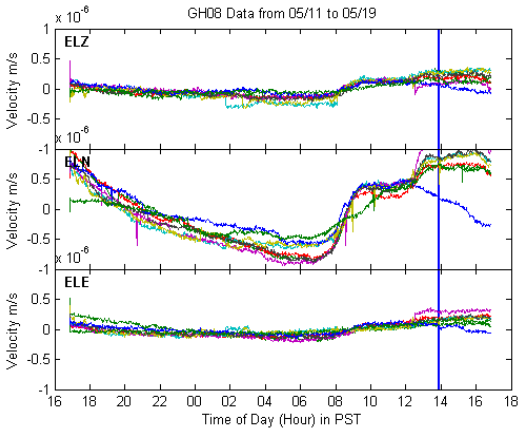

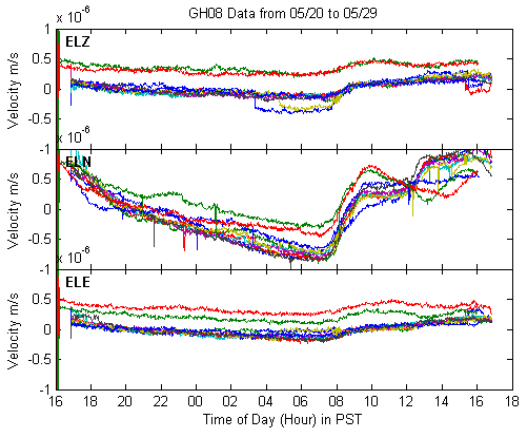

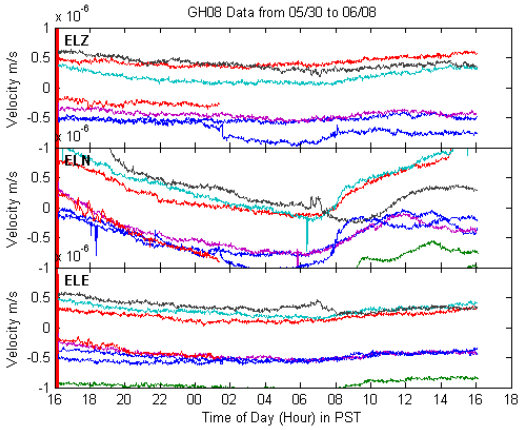

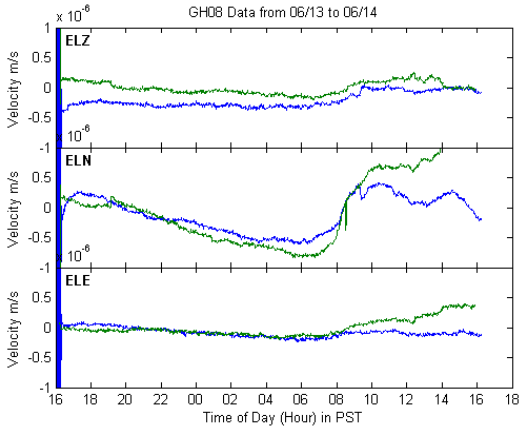

Appendix B: Record of Daily Instrument Fluctuations Attributed to Either Site Tilt or Instrument Drift

This Appendix shows most of the daily records plotted 10 days at a time with respect to time of day (PST). All records shown have been filtered and resampled at 0.0167 Hz, or one sample per minute

B.1 Station LB01 (Hot Ledge), Geophone

This geophone was placed on a small ledge (on Michael's Ledge) exposed to the elements during Phase 1 (winter 2007-08). This is the same location as station LB05 during the Phase 2 (winter 2008-09). The orientation of the components is shown in Table 1.

Table 1. LB01 geophone orientation.

Station LB01	+' direction	channel dip	Comment
EL2	N	20° down	
EL3	W	18° up	
EL1	Z (down)	69° down	240° azimuth
Instrument	SM-6 (8 Hz)		

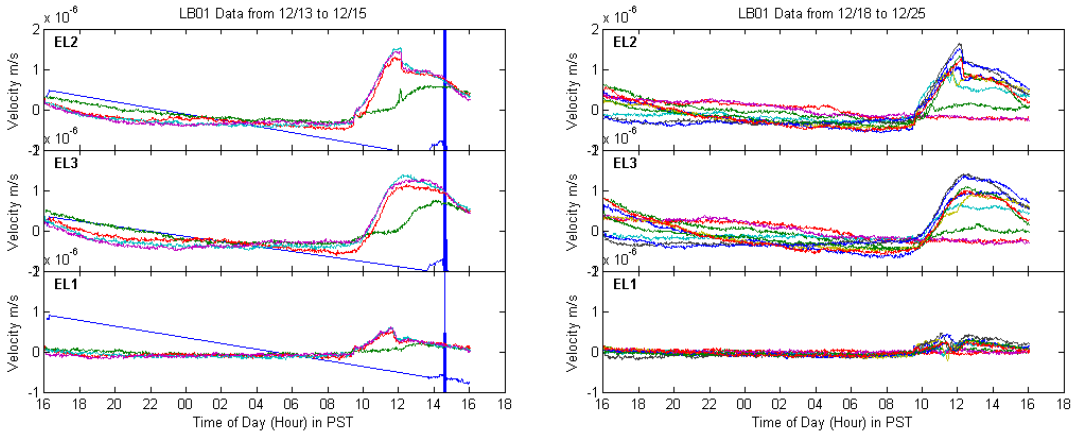

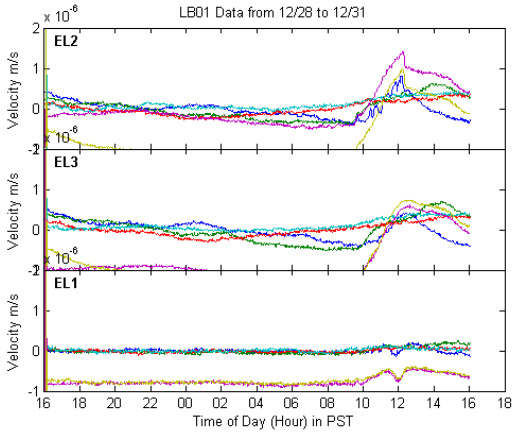
LB01 Data from 12/28 to 12/31
EL2
EL3
EL1
Velocity m/s
Time of Day (Hour) in PST

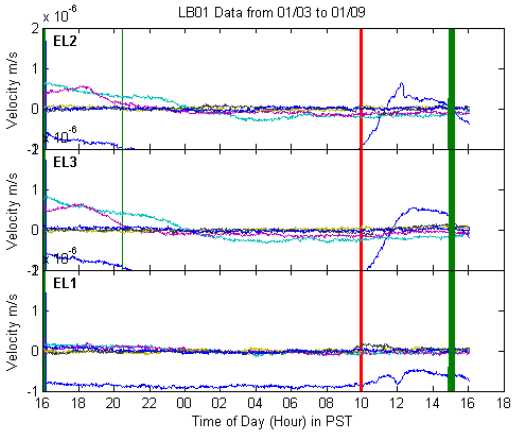
LB01 Data from 01/03 to 01/09
EL2
EL3
EL1
Velocity m/s
Time of Day (Hour) in PST

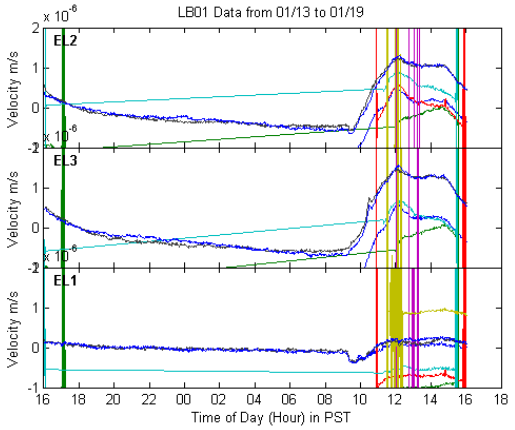
LB01 Data from 01/13 to 01/19
EL2
EL3
EL1
Velocity m/s
Time of Day (Hour) in PST

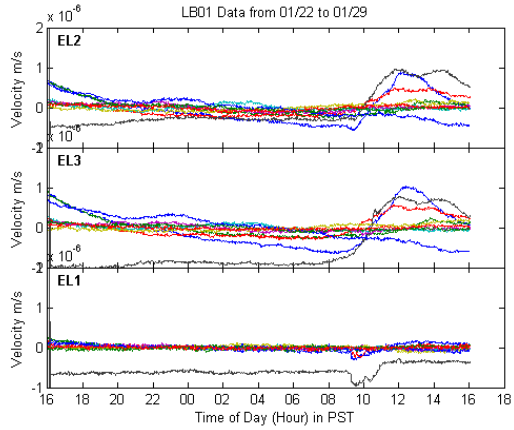
LB01 Data from 01/22 to 01/29
EL2
EL3
EL1
Velocity m/s
Time of Day (Hour) in PST

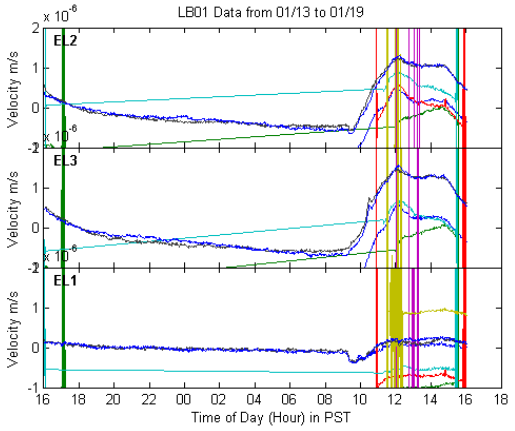
LB01 Data from 01/13 to 01/19
EL2
EL3
EL1
Velocity m/s
Time of Day (Hour) in PST

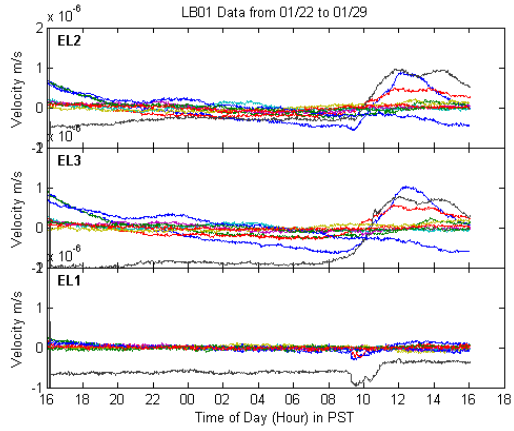
LB01 Data from 01/22 to 01/29
EL2
EL3
EL1
Velocity m/s
Time of Day (Hour) in PST

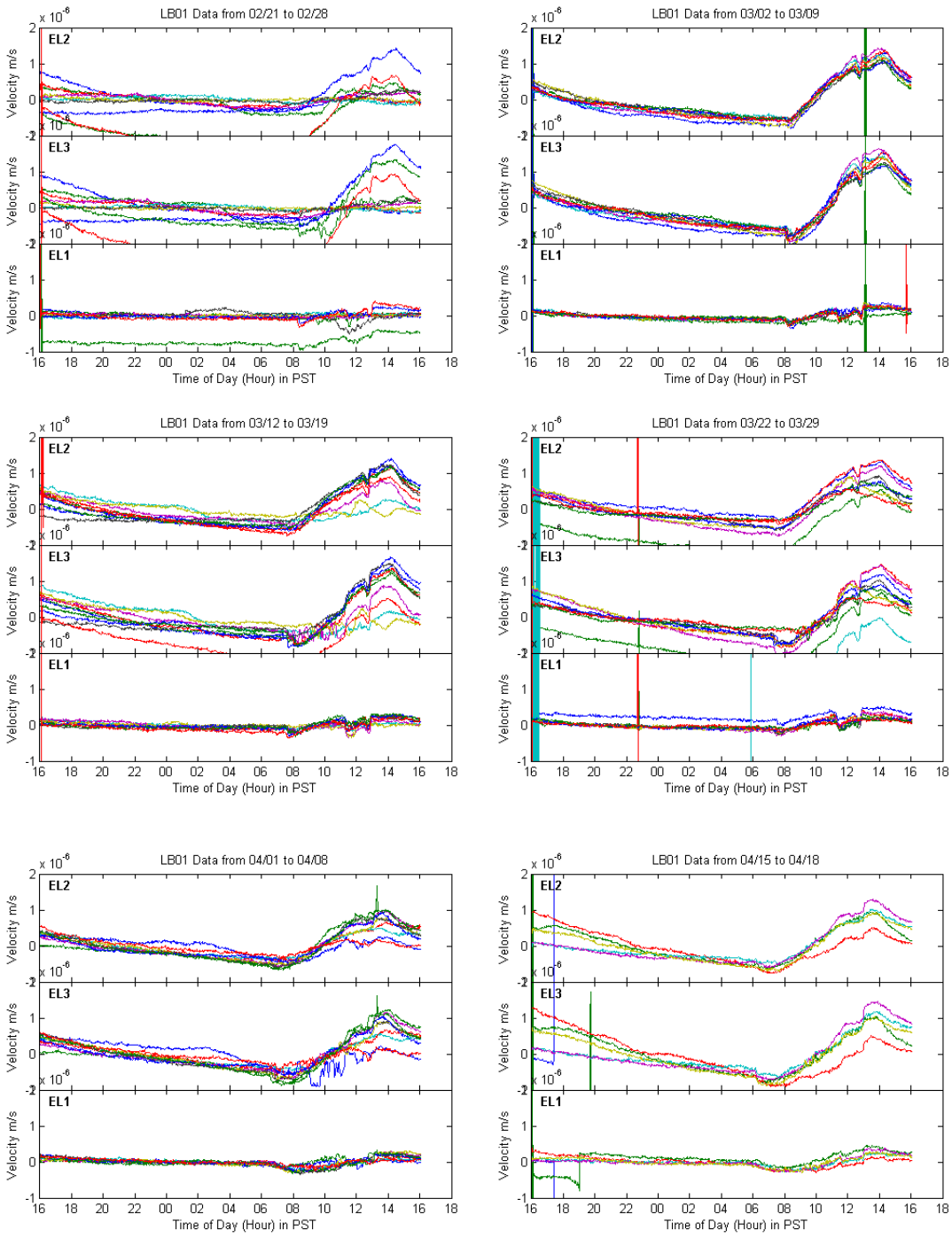

B.2 Station LB01 (Hot Ledge), Accelerometer

This accelerometer was placed on a small ledge (on Michael's Ledge) exposed to the elements during Phase 1 (winter 2007-08). The accelerometer used in this location was later placed at station GH08 during Phase 2. The orientation of the components is shown in Table 2.

Table 2. LB01 accelerometer orientation.

Station LB01	+' direction	channel dip	Comment
HN1	Z (up)	68° up	22° azimuth
HN2	N	15° down	
HN3	E	16° down	
Instrument	Reftek RT131A 02/03		

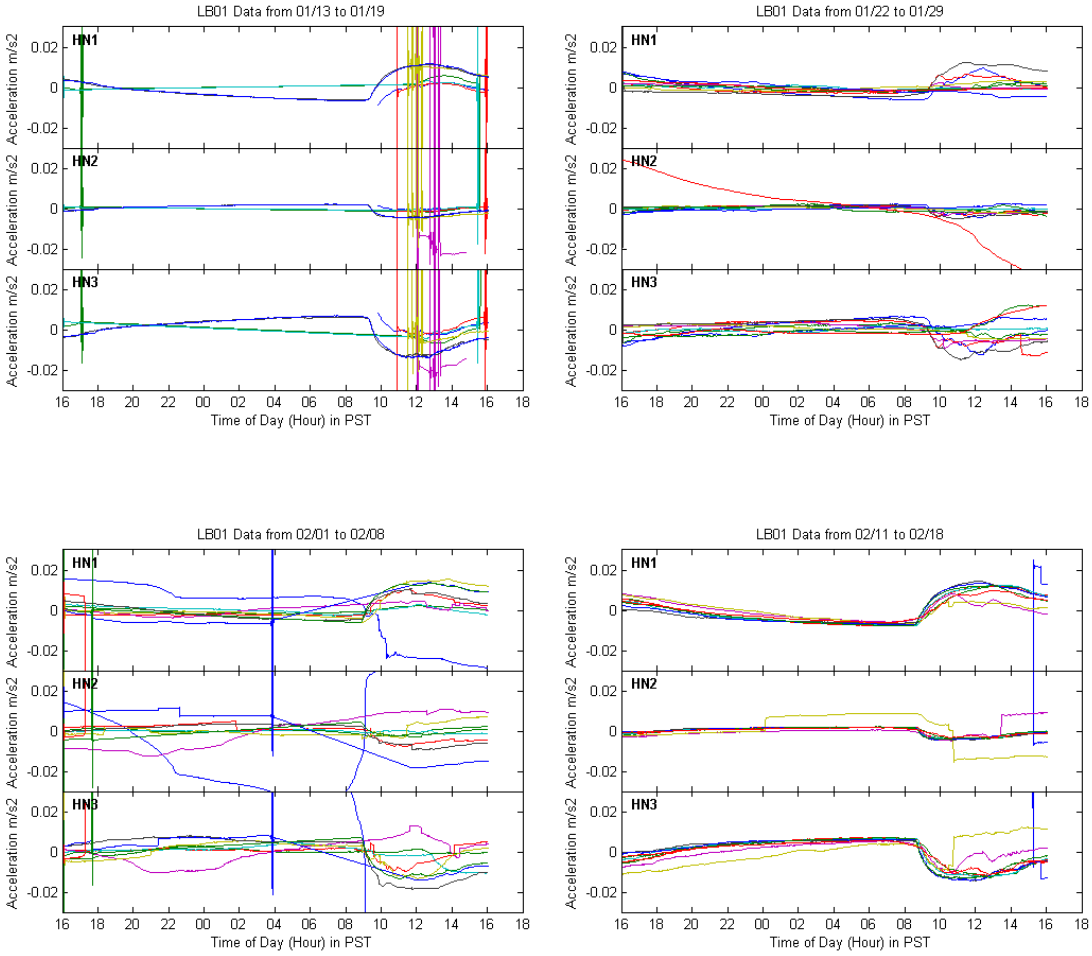

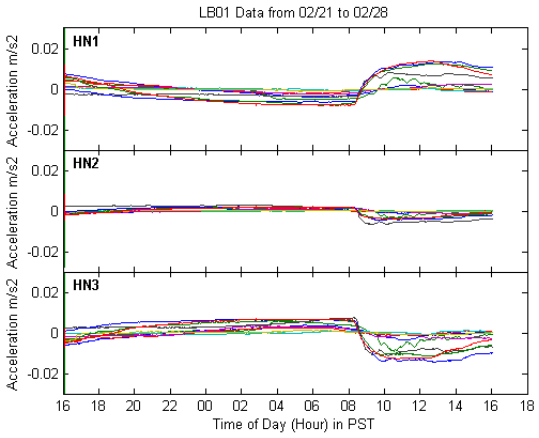
LB01 Data from 02/21 to 02/28
HN1
HN2
HN3
Acceleration m/s2
0.02
0
-0.02
16 18 20 22 00 02 04 06 08 10 12 14 16 18
Time of Day (Hour) in PST

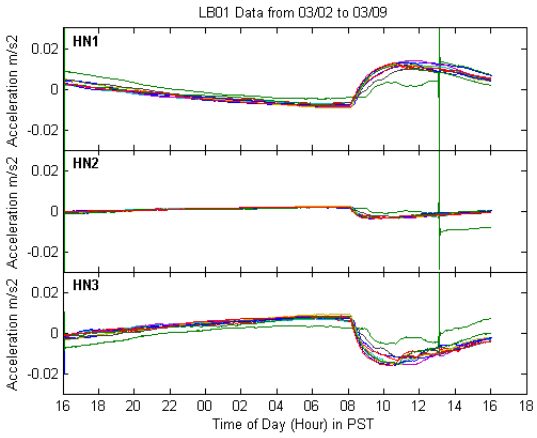
LB01 Data from 03/02 to 03/09
HN1
HN2
HN3
Acceleration m/s2
0.02
0
-0.02
16 18 20 22 00 02 04 06 08 10 12 14 16 18
Time of Day (Hour) in PST

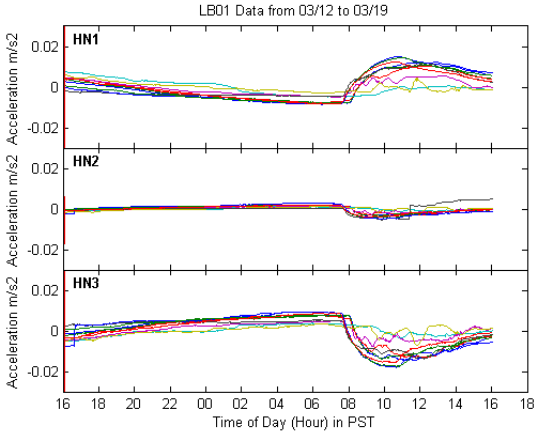
LB01 Data from 03/12 to 03/19
HN1
HN2
HN3
Acceleration m/s2
0.02
0
-0.02
16 18 20 22 00 02 04 06 08 10 12 14 16 18
Time of Day (Hour) in PST

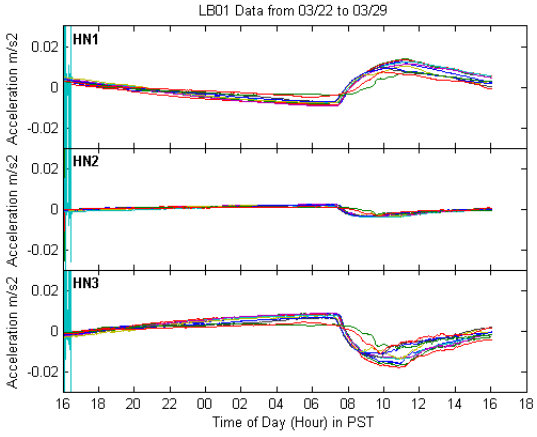
LB01 Data from 03/22 to 03/29
HN1
HN2
HN3
Acceleration m/s2
0.02
0
-0.02
16 18 20 22 00 02 04 06 08 10 12 14 16 18
Time of Day (Hour) in PST

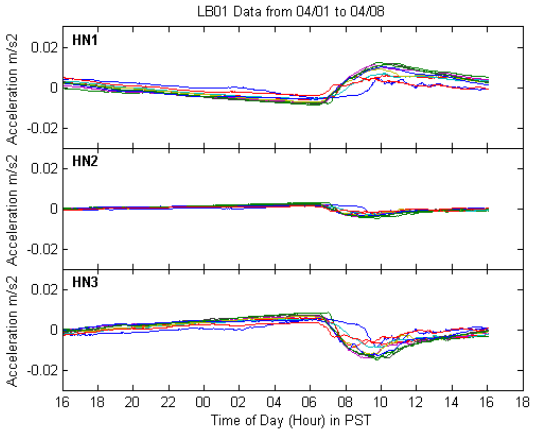
LB01 Data from 04/01 to 04/08
HN1
HN2
HN3
Acceleration m/s2
0.02
0
-0.02
16 18 20 22 00 02 04 06 08 10 12 14 16 18
Time of Day (Hour) in PST

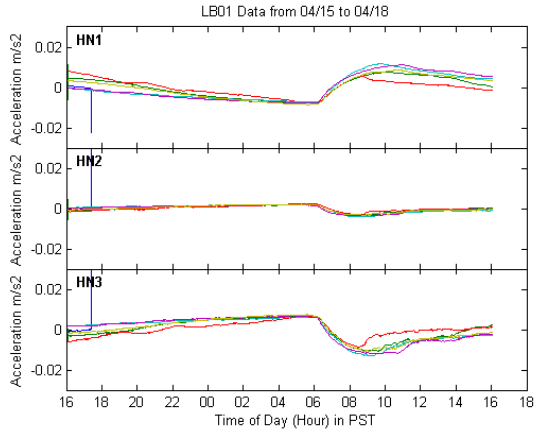
LB01 Data from 04/15 to 04/18
HN1
HN2
HN3
Acceleration m/s2
0.02
0
-0.02
16 18 20 22 00 02 04 06 08 10 12 14 16 18
Time of Day (Hour) in PST

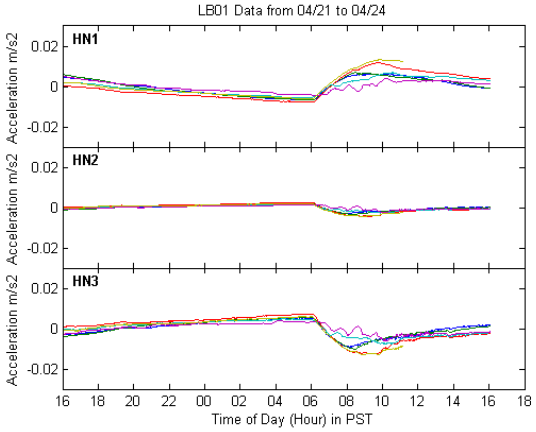
LB01 Data from 04/21 to 04/24
HN1
HN2
HN3
Acceleration m/s2
0.02
0
-0.02
16 18 20 22 00 02 04 06 08 10 12 14 16 18
Time of Day (Hour) in PST

B.3 Station LB03 (Hot Ledge), Geophone

This geophone was placed under sandbags on Michael's Ledge during Phase 2 (winter 2008-09).

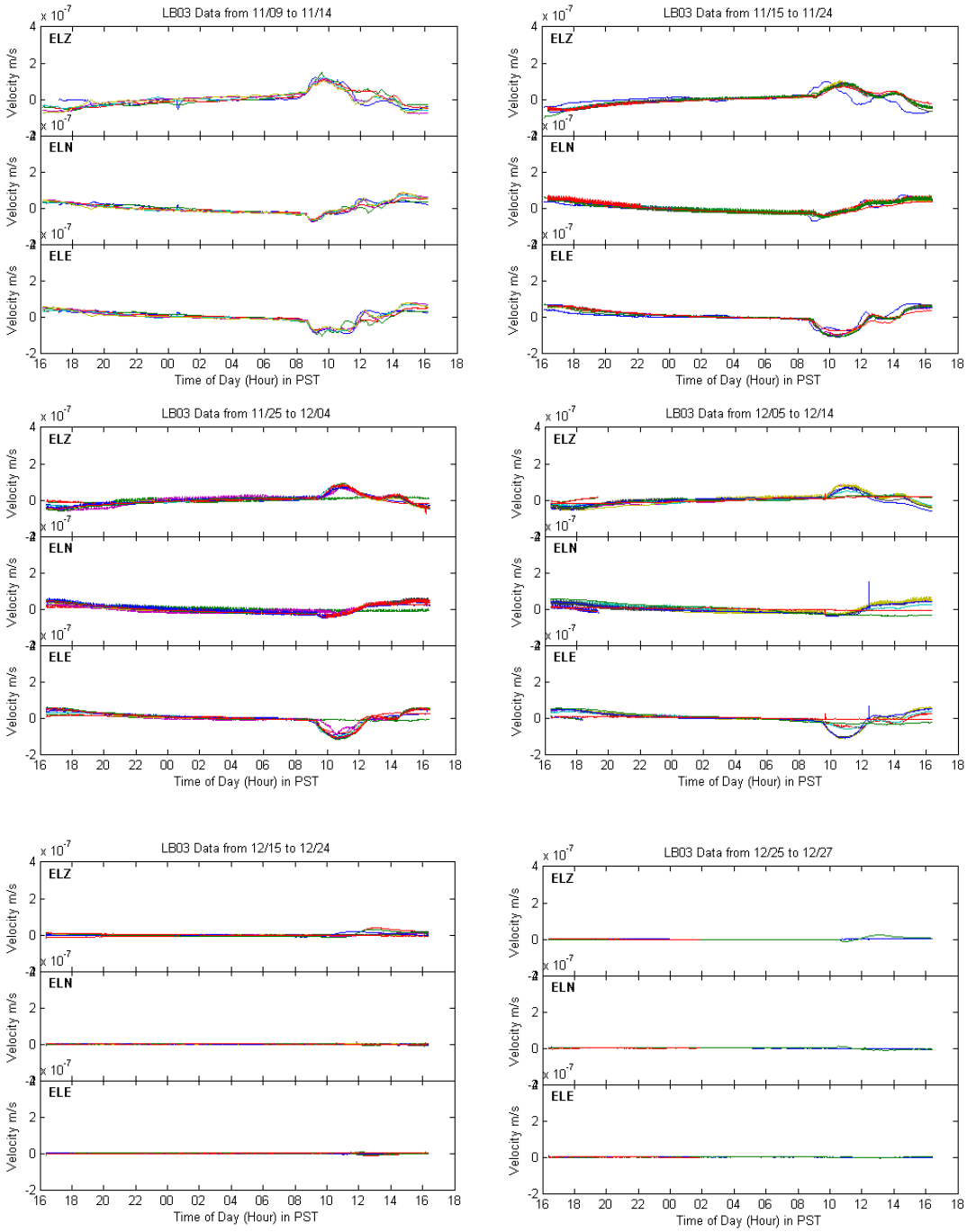

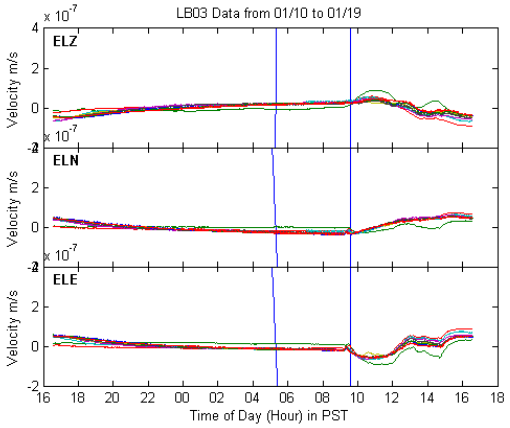
LB03 Data from 01/10 to 01/19
ELZ
ELN
ELE
x 10^-7
Velocity m/s
Time of Day (Hour) in PST

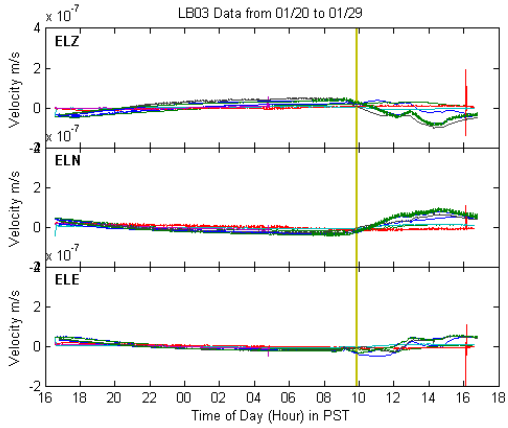
LB03 Data from 01/20 to 01/29
ELZ
ELN
ELE
x 10^-7
Velocity m/s
Time of Day (Hour) in PST

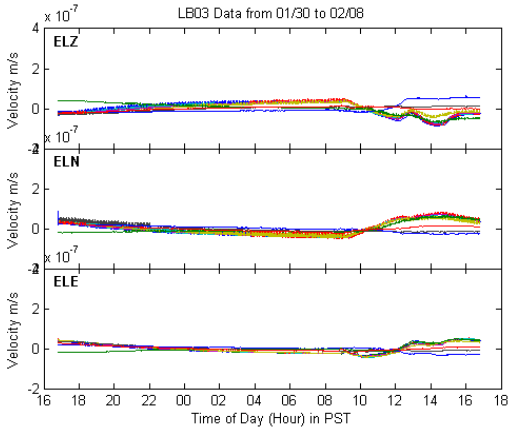
LB03 Data from 01/30 to 02/08
ELZ
ELN
ELE
x 10^-7
Velocity m/s
Time of Day (Hour) in PST

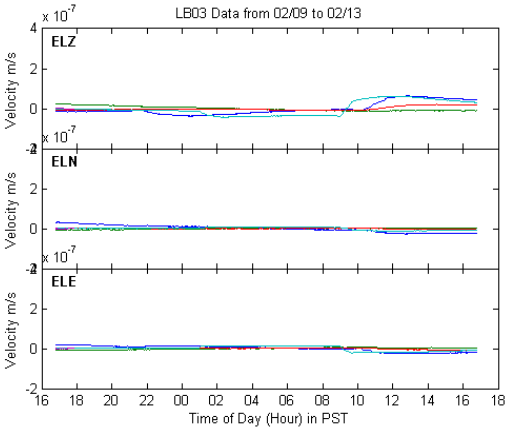
LB03 Data from 02/09 to 02/13
ELZ
ELN
ELE
x 10^-7
Velocity m/s
Time of Day (Hour) in PST

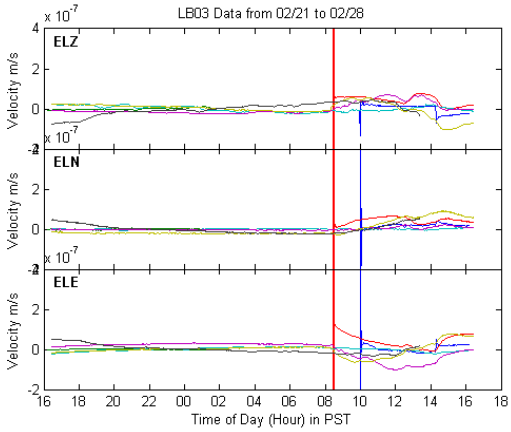
LB03 Data from 02/21 to 02/28
ELZ
ELN
ELE
x 10^-7
Velocity m/s
Time of Day (Hour) in PST

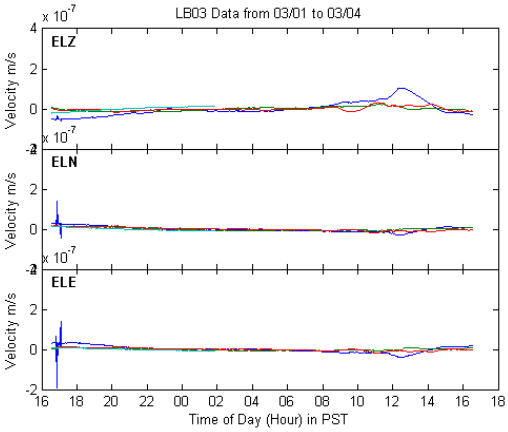
LB03 Data from 03/01 to 03/04
ELZ
ELN
ELE
x 10^-7
Velocity m/s
Time of Day (Hour) in PST

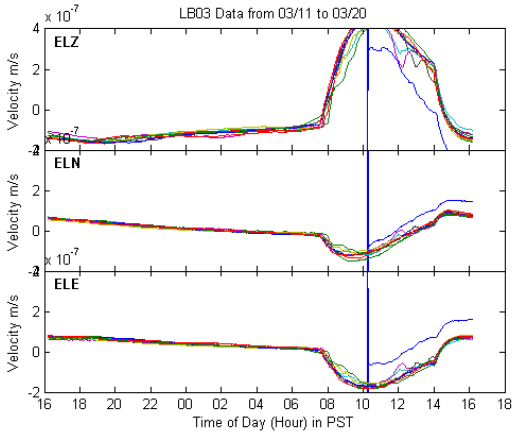
LB03 Data from 03/11 to 03/20
ELZ
ELN
ELE
Velocity m/s
Time of Day (Hour) in PST

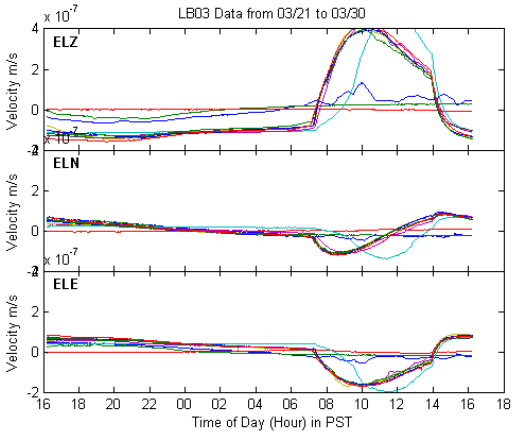
LB03 Data from 03/21 to 03/30
ELZ
ELN
ELE
Velocity m/s
Time of Day (Hour) in PST

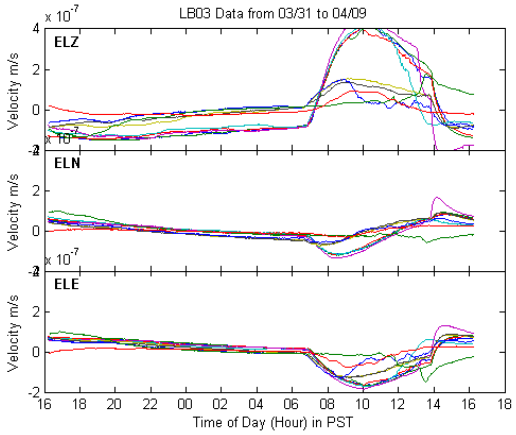
LB03 Data from 03/31 to 04/09
ELZ
ELN
ELE
Velocity m/s
Time of Day (Hour) in PST

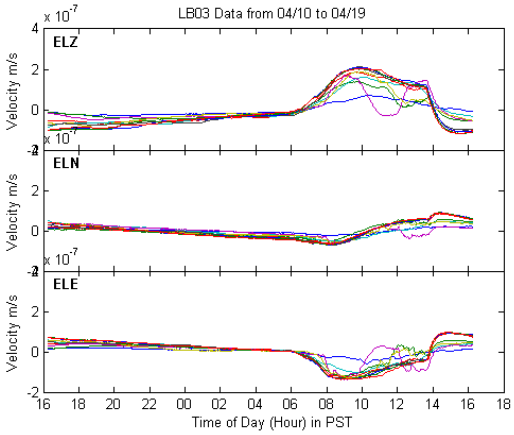
LB03 Data from 04/10 to 04/19
ELZ
ELN
ELE
Velocity m/s
Time of Day (Hour) in PST

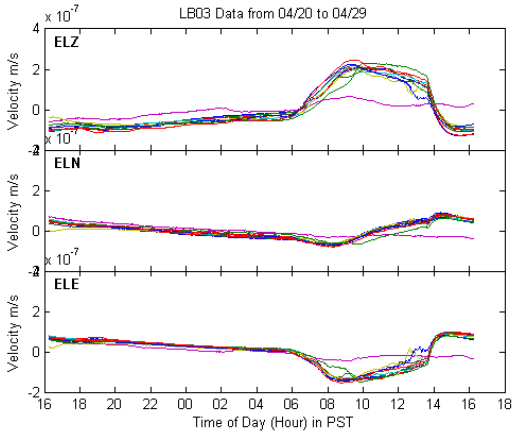
LB03 Data from 04/20 to 04/29
ELZ
ELN
ELE
Velocity m/s
Time of Day (Hour) in PST

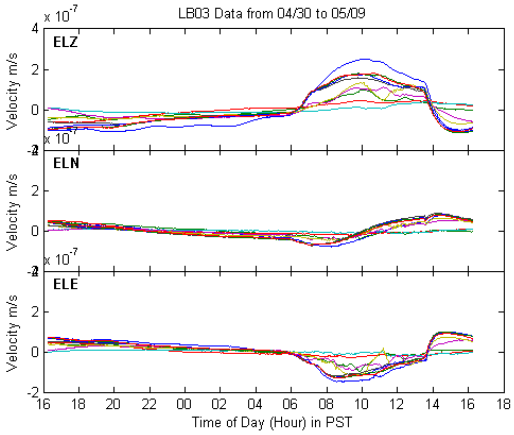
LB03 Data from 04/30 to 05/09
ELZ
ELN
ELE
Velocity m/s
Time of Day (Hour) in PST

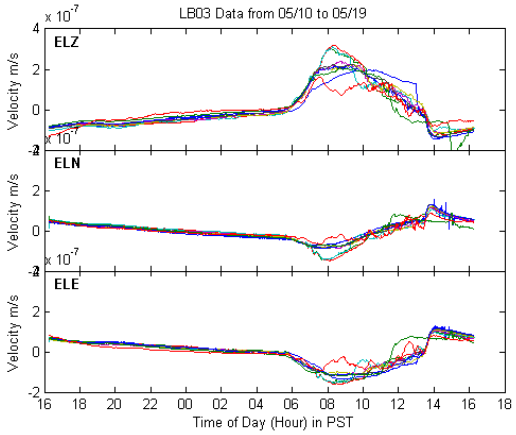
LB03 Data from 05/10 to 05/19
x 10^-7
ELZ
ELN
ELE
Velocity m/s
Time of Day (Hour) in PST

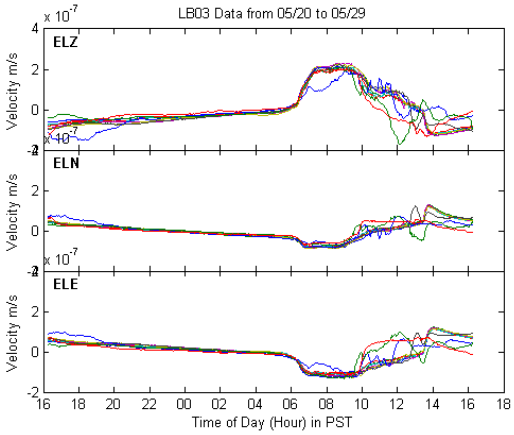
LB03 Data from 05/20 to 05/29
x 10^-7
ELZ
ELN
ELE
Velocity m/s
Time of Day (Hour) in PST

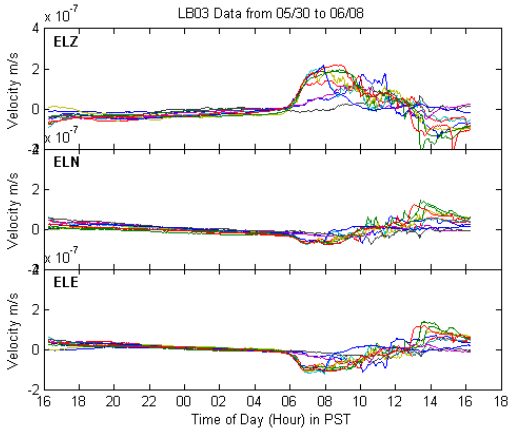
LB03 Data from 05/30 to 06/08
x 10^-7
ELZ
ELN
ELE
Velocity m/s
Time of Day (Hour) in PST

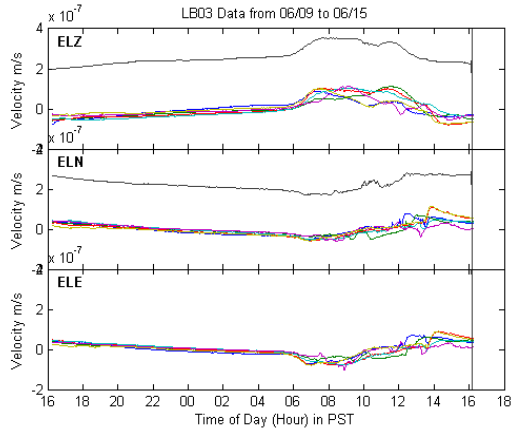
LB03 Data from 06/09 to 06/15
x 10^-7
ELZ
ELN
ELE
Velocity m/s
Time of Day (Hour) in PST

B.4 Station LB05 (Hot Ledge), Geophone

This geophone was placed on a small ledge (on Michael's Ledge) exposed to the elements during Phase 2 (winter 2008-08). This is the same location as station LB01 during the Phase 1 (winter 2007-08). The orientation of the components is shown in Table 3.

Table 3. LB05 orientation.

Station LB05	+' direction	channel dip	Comment
EL1	Z (down)	69° down	240° azimuth
EL2	N	20° down	
EL3	E	18° down	
Instrument	L-28 (4.5 Hz)		

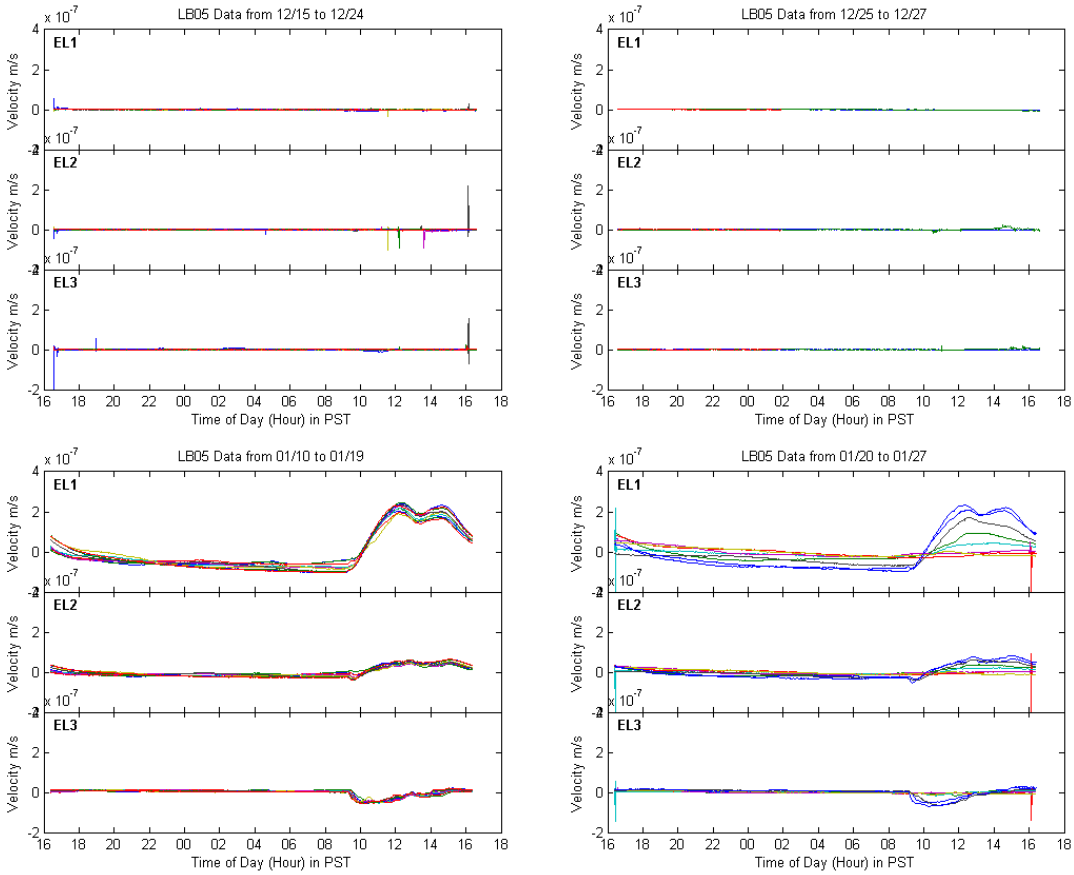

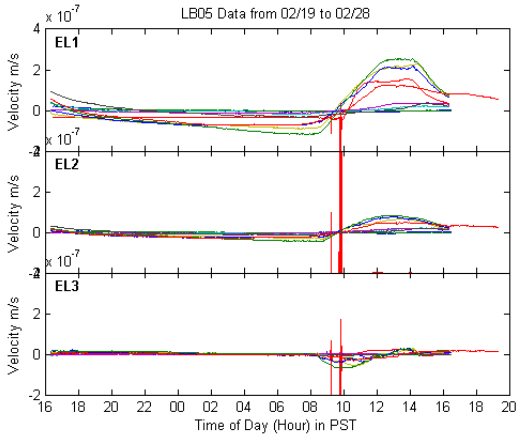
LB05 Data from 02/19 to 02/28
EL1
EL2
EL3
Velocity m/s
x 10^-7
Time of Day (Hour) in PST

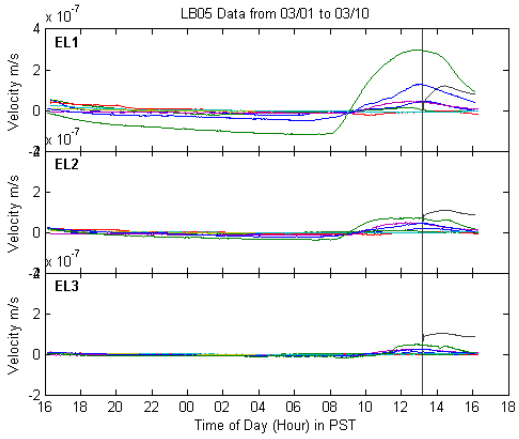
LB05 Data from 03/01 to 03/10
EL1
EL2
EL3
Velocity m/s
x 10^-7
Time of Day (Hour) in PST

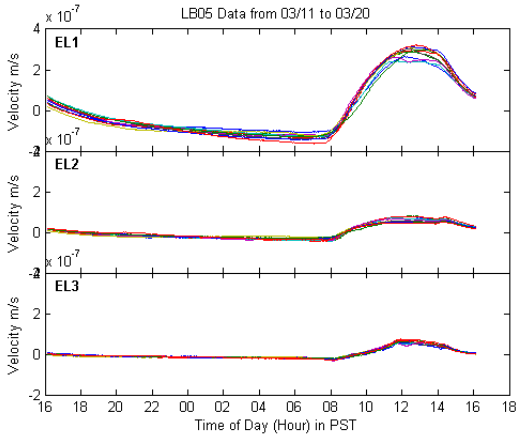
LB05 Data from 03/11 to 03/20
EL1
EL2
EL3
Velocity m/s
x 10^-7
Time of Day (Hour) in PST

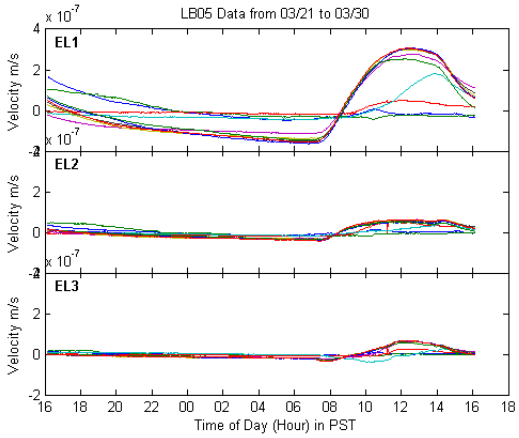
LB05 Data from 03/21 to 03/30
EL1
EL2
EL3
Velocity m/s
x 10^-7
Time of Day (Hour) in PST

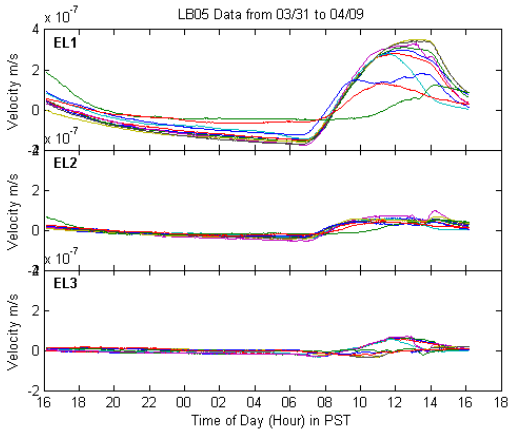
LB05 Data from 03/31 to 04/09
EL1
EL2
EL3
Velocity m/s
x 10^-7
Time of Day (Hour) in PST

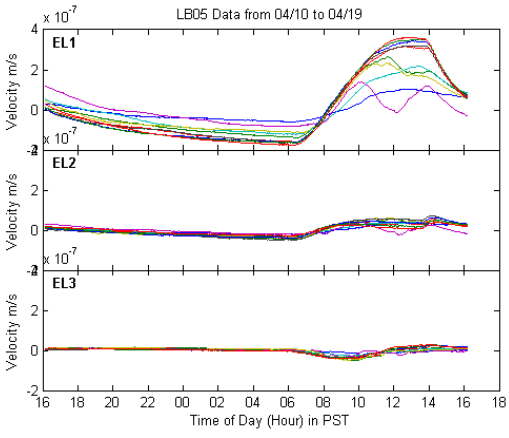
LB05 Data from 04/10 to 04/19
EL1
EL2
EL3
Velocity m/s
x 10^-7
Time of Day (Hour) in PST

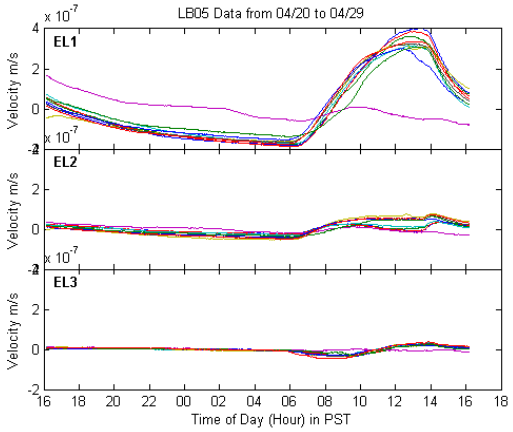
LB05 Data from 04/20 to 04/29
x 10^-7
EL1
EL2
EL3
Velocity m/s
Time of Day (Hour) in PST

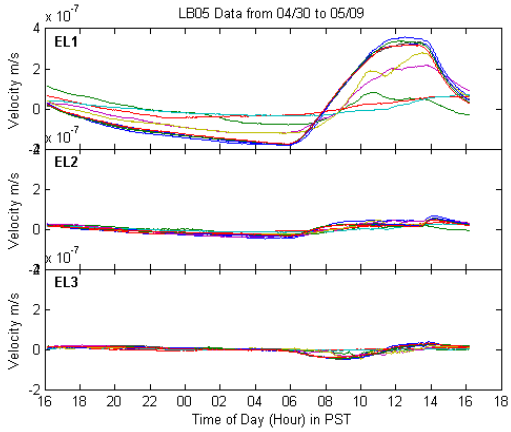
LB05 Data from 04/30 to 05/09
x 10^-7
EL1
EL2
EL3
Velocity m/s
Time of Day (Hour) in PST

B.5 Station MB06 (Mod. Ledge), Geophone

This geophone was placed under sandbags on Michael's Ledge during Phase 2 (winter 2008-09).

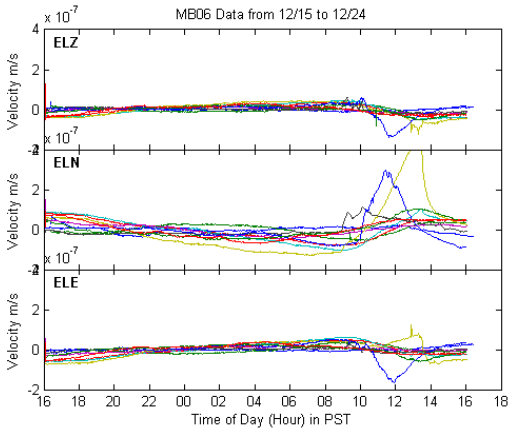

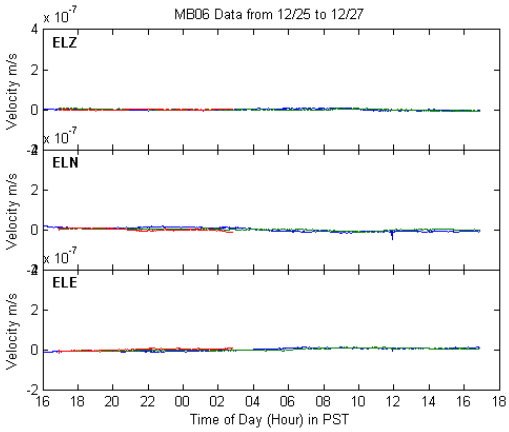

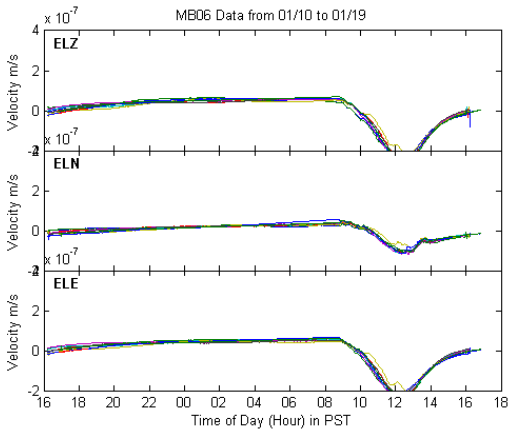

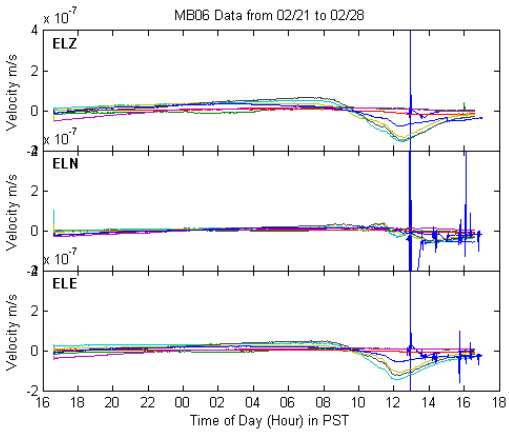

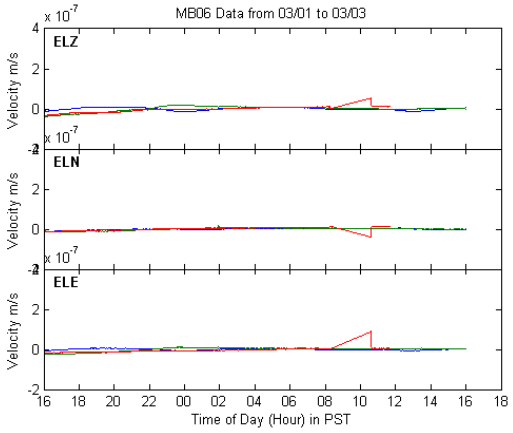

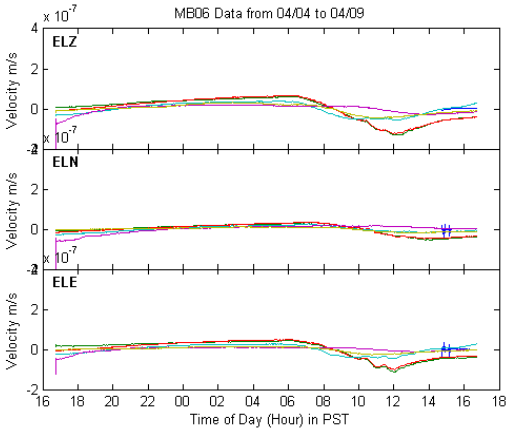

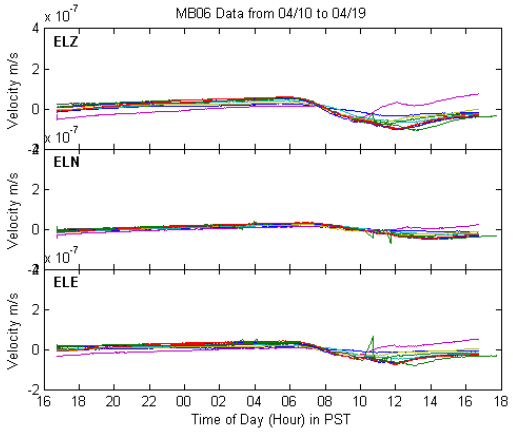
MB06 Data from 04/10 to 04/19
x 10^-7
ELZ
ELN
ELE
Velocity m/s
Time of Day (Hour) in PST

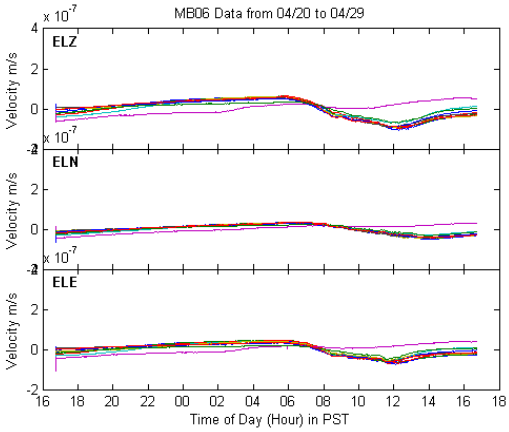
MB06 Data from 04/20 to 04/29
x 10^-7
ELZ
ELN
ELE
Velocity m/s
Time of Day (Hour) in PST

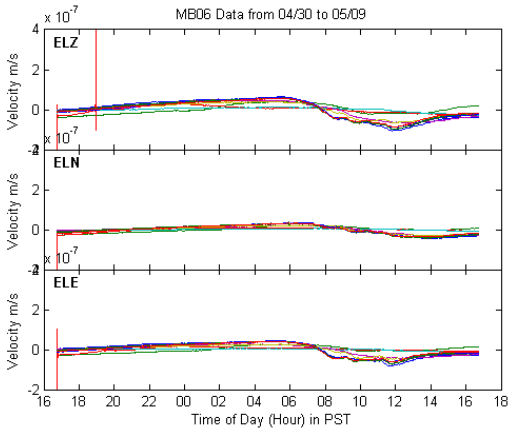
MB06 Data from 04/30 to 05/09
x 10^-7
ELZ
ELN
ELE
Velocity m/s
Time of Day (Hour) in PST

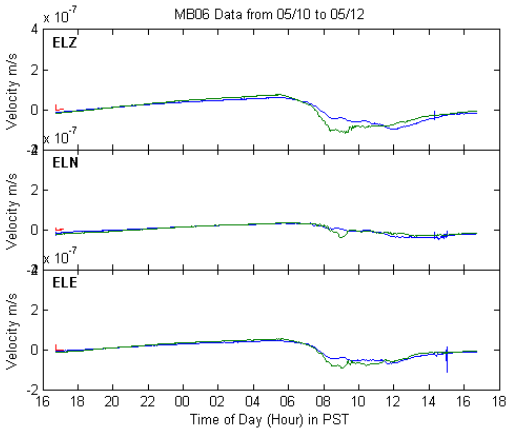
MB06 Data from 05/10 to 05/12
x 10^-7
ELZ
ELN
ELE
Velocity m/s
Time of Day (Hour) in PST

B.6 Station MB04 (Shady Ledge), Accelerometer

This accelerometer was mounted vertically on a rock wall under an overhang on Michael's Ledge during Phase 2 (winter 2007-08). Later laboratory tests revealed that channels 2 and 3 were reversed from the datasheet, and that channel 1 had a built-in 1g offset. The gain was set too high (x32) from installation until 02/21/2009 and most, but not all, of the data was not processed and is thus not displayed. This data also seems to show a higher reaction by the south component, while later, with the gain properly set to x1, it is the Z component that reacts to changes. The orientation of the components is shown in Table 4.

Table 4. MB04 orientation

Station MB04	**+' direction**	**channel dip**	**Comment**
HN1	E	10° up	offset by 1 g
HN2*	S	3° up	
HN3*	Z (up)	77° up	W azimuth
* HN2 and HN3 are reversed relative to instrument orientation sticker			
Instrument	Terratech SSA-320		

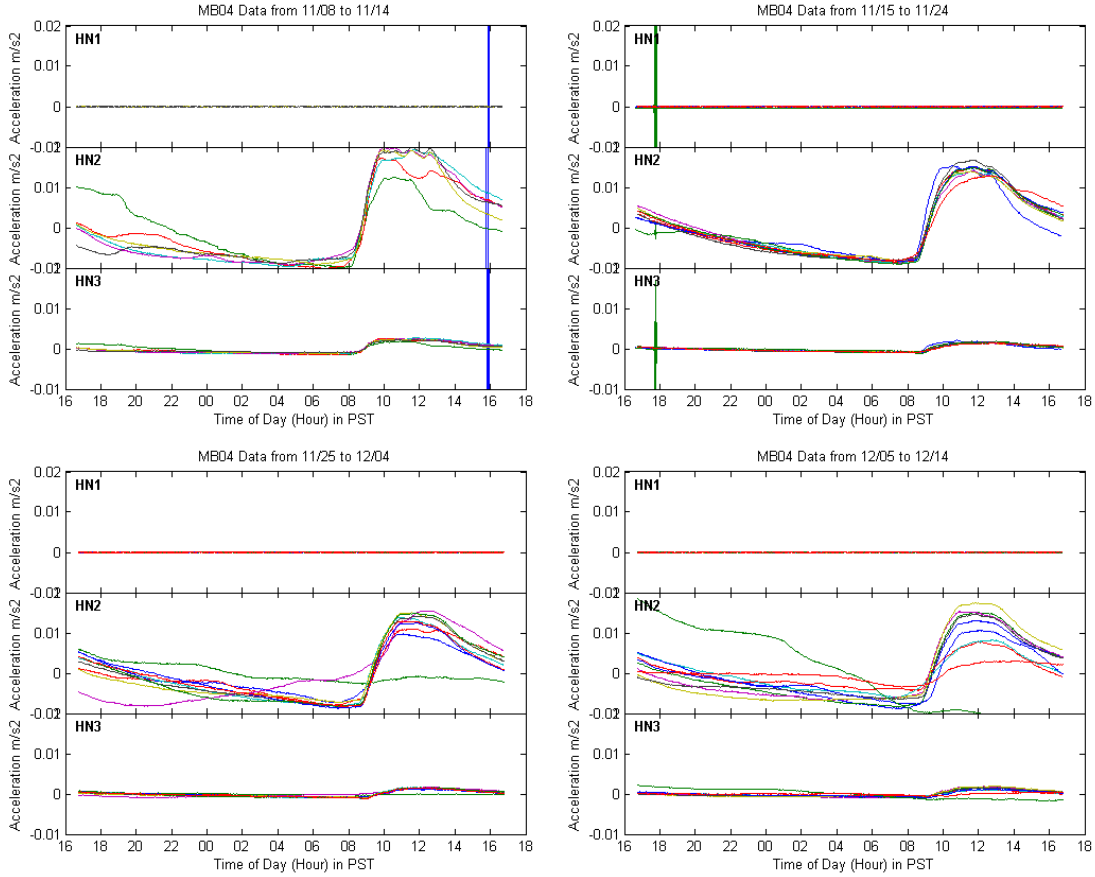

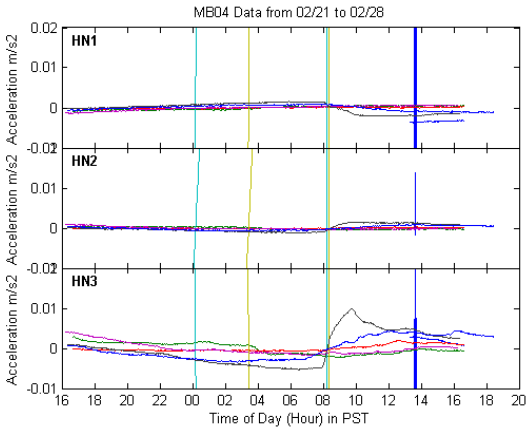
MB04 Data from 02/21 to 02/28
HN1
HN2
HN3
Acceleration m/s2
Time of Day (Hour) in PST

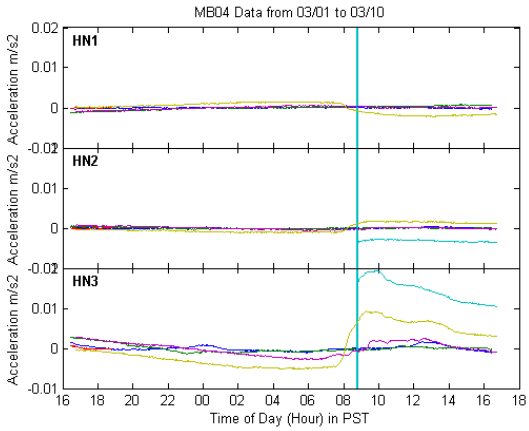
MB04 Data from 03/01 to 03/10
HN1
HN2
HN3
Acceleration m/s2
Time of Day (Hour) in PST

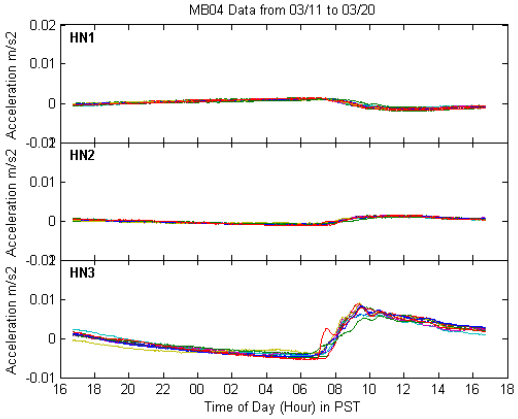
MB04 Data from 03/11 to 03/20
HN1
HN2
HN3
Acceleration m/s2
Time of Day (Hour) in PST

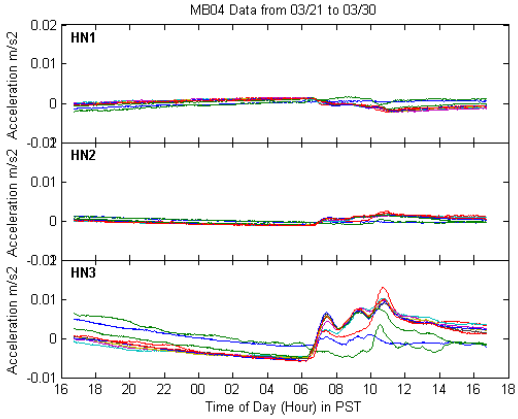
MB04 Data from 03/21 to 03/30
HN1
HN2
HN3
Acceleration m/s2
Time of Day (Hour) in PST

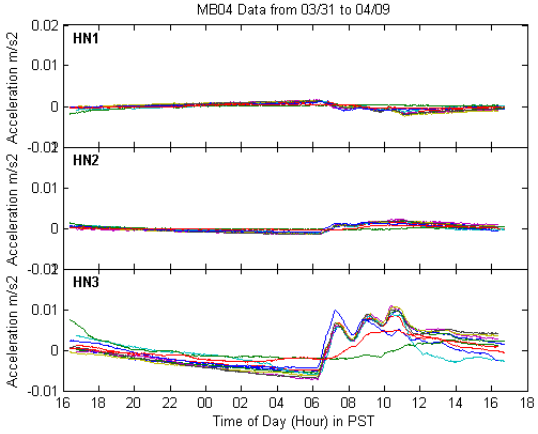
MB04 Data from 03/31 to 04/09
HN1
HN2
HN3
Acceleration m/s2
Time of Day (Hour) in PST

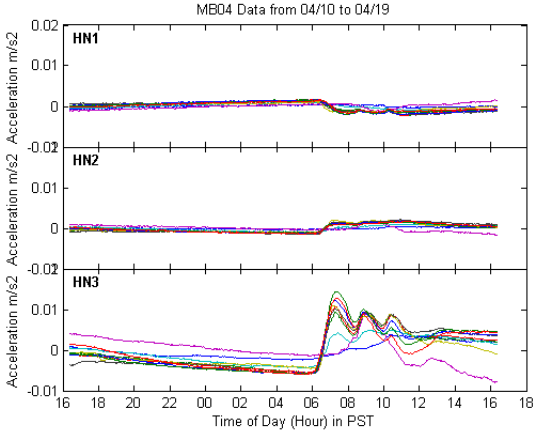
MB04 Data from 04/10 to 04/19
HN1
HN2
HN3
Acceleration m/s2
Time of Day (Hour) in PST

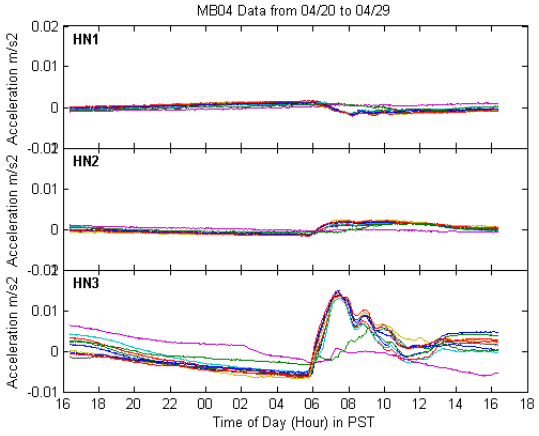
MB04 Data from 04/20 to 04/29
HN1
HN2
HN3
Acceleration m/s2
0.02
0.01
0
-0.01
-0.02
16 18 20 22 00 02 04 06 08 10 12 14 16 18
Time of Day (Hour) in PST

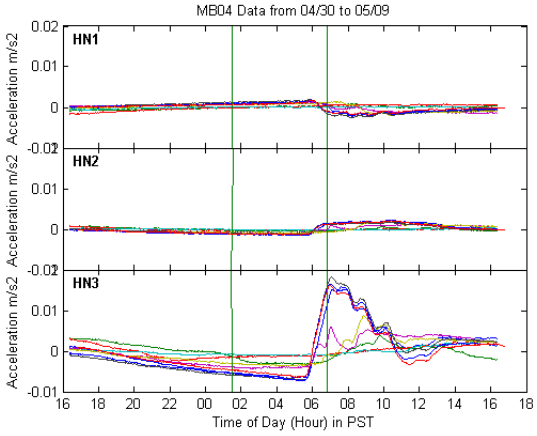
MB04 Data from 04/30 to 05/09
HN1
HN2
HN3
Acceleration m/s2
0.02
0.01
0
-0.01
-0.02
16 18 20 22 00 02 04 06 08 10 12 14 16 18
Time of Day (Hour) in PST

B.7 Station MB02 (Mod. Talus), Geophone

This geophone was placed under sandbags below a talus slope and adjacent to the cliff wall during Phase 2 (winter 2008-09).

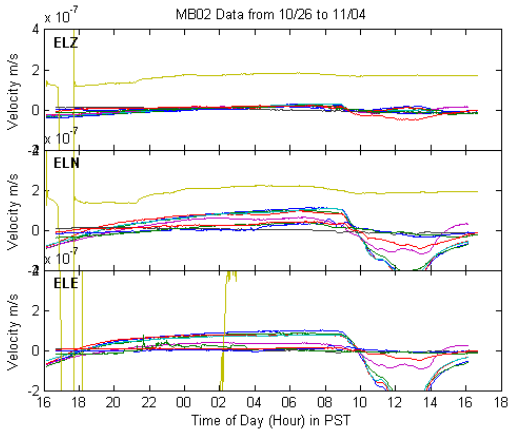

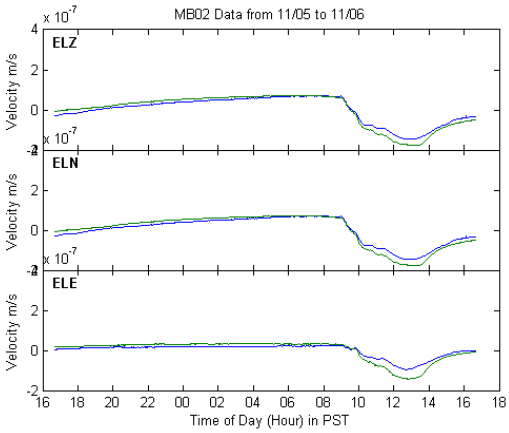

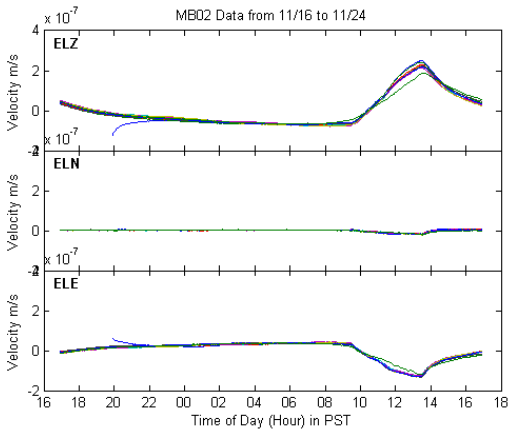

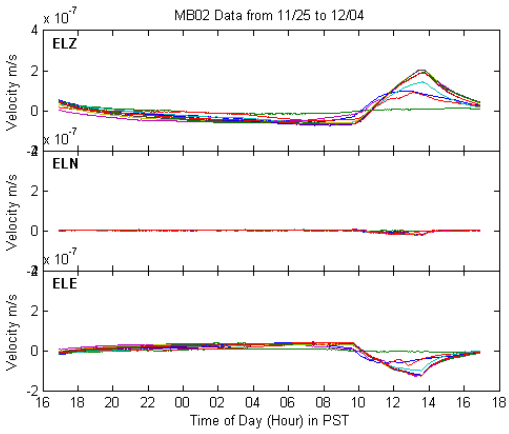

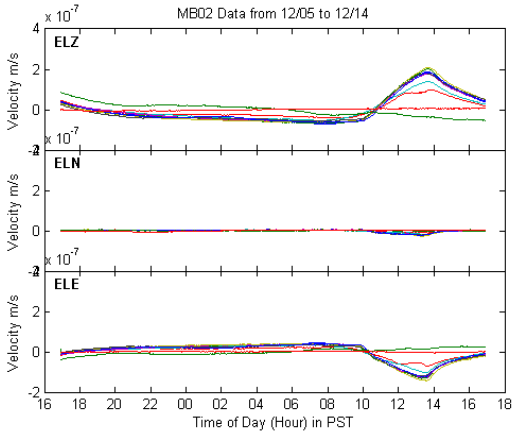

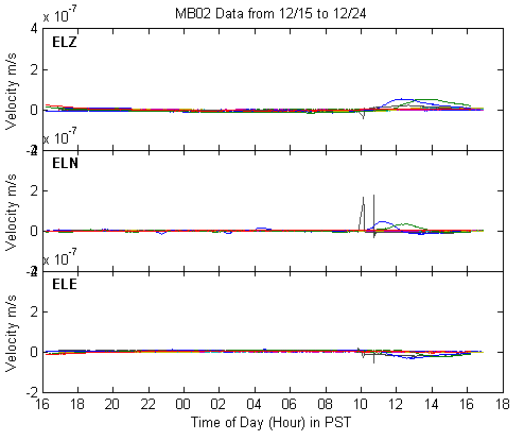

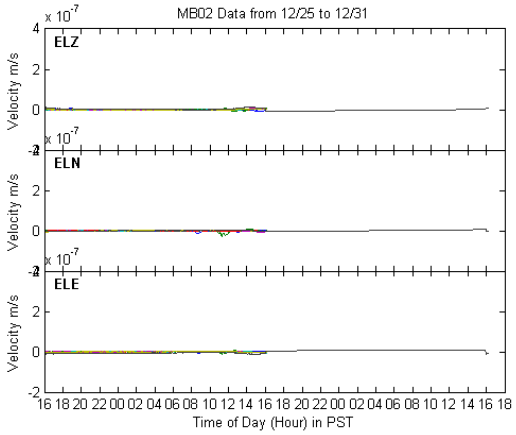
MB02 Data from 12/25 to 12/31
ELZ
ELN
ELE
Velocity m/s
Time of Day (Hour) in PST

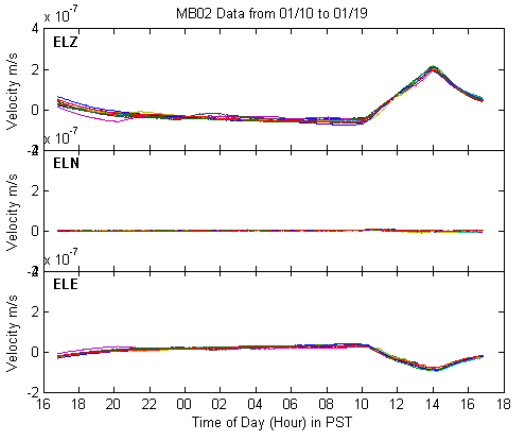
MB02 Data from 01/10 to 01/19
ELZ
ELN
ELE
Velocity m/s
Time of Day (Hour) in PST

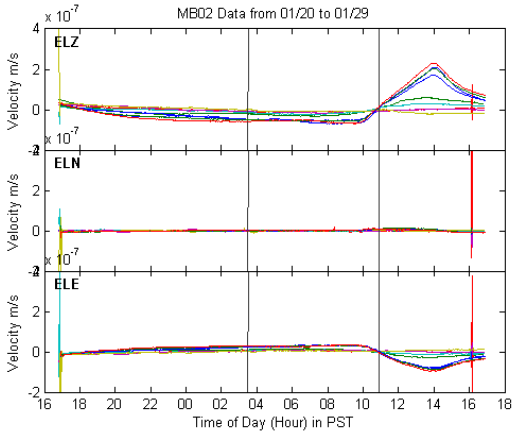
MB02 Data from 01/20 to 01/29
ELZ
ELN
ELE
Velocity m/s
Time of Day (Hour) in PST

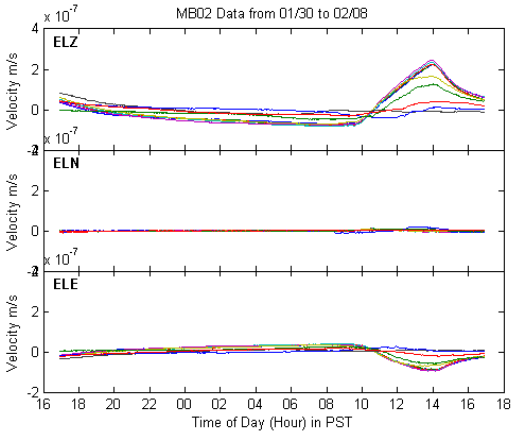
MB02 Data from 01/30 to 02/08
ELZ
ELN
ELE
Velocity m/s
Time of Day (Hour) in PST

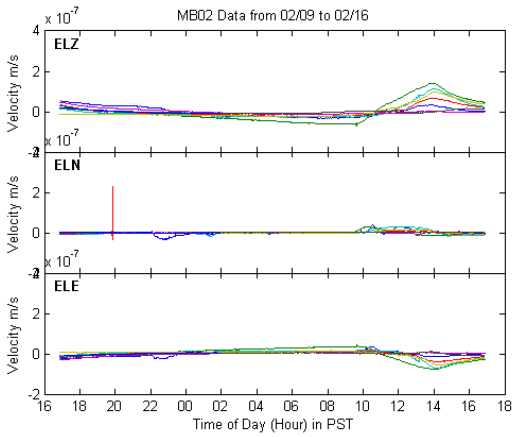
MB02 Data from 02/09 to 02/16
ELZ
ELN
ELE
Velocity m/s
Time of Day (Hour) in PST

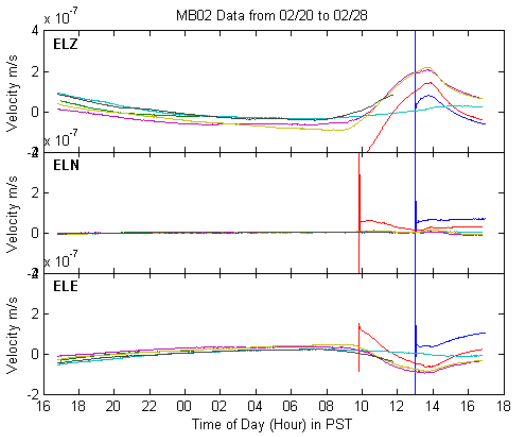
MB02 Data from 02/20 to 02/28
ELZ
ELN
ELE
Velocity m/s
Time of Day (Hour) in PST

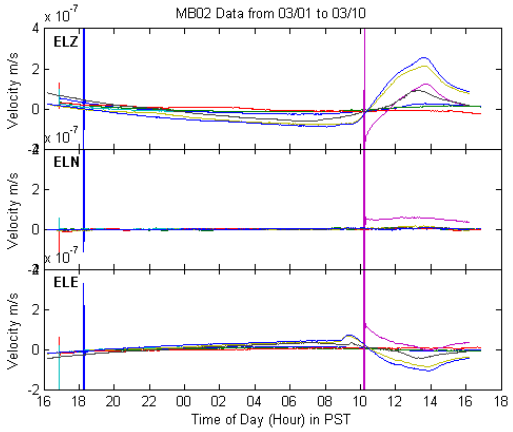
MB02 Data from 03/01 to 03/10
ELZ
ELN
ELE
Velocity m/s
x 10^-7
Time of Day (Hour) in PST

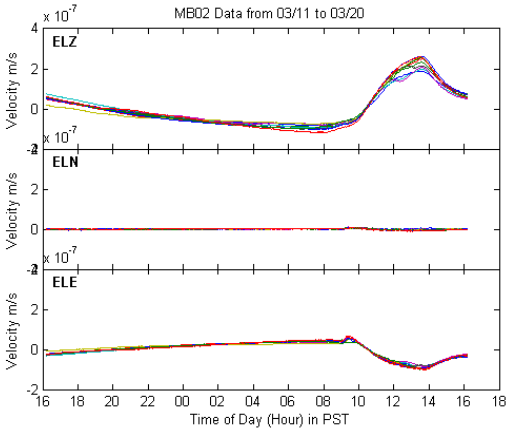
MB02 Data from 03/11 to 03/20
ELZ
ELN
ELE
Velocity m/s
x 10^-7
Time of Day (Hour) in PST

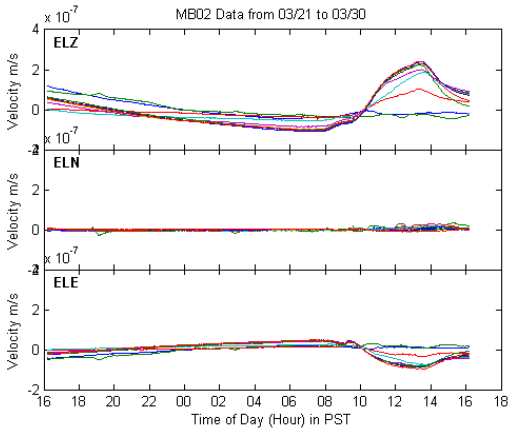
MB02 Data from 03/21 to 03/30
ELZ
ELN
ELE
Velocity m/s
x 10^-7
Time of Day (Hour) in PST

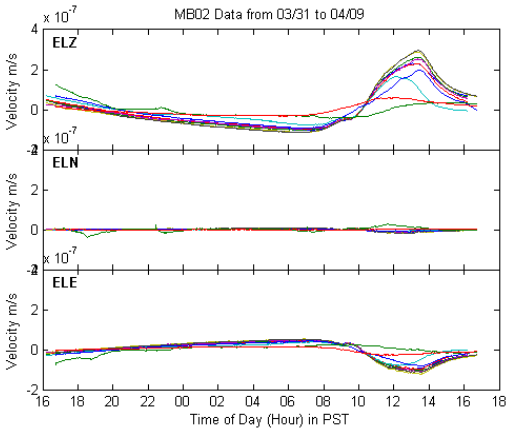
MB02 Data from 03/31 to 04/09
ELZ
ELN
ELE
Velocity m/s
x 10^-7
Time of Day (Hour) in PST

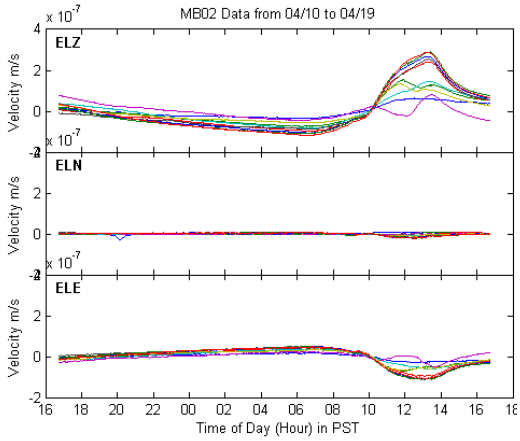
MB02 Data from 04/10 to 04/19
ELZ
ELN
ELE
Velocity m/s
x 10^-7
Time of Day (Hour) in PST

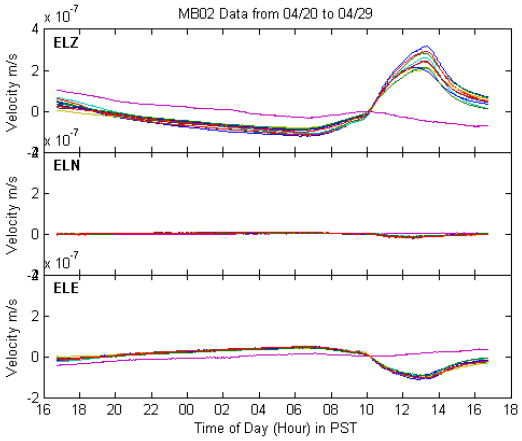
MB02 Data from 04/20 to 04/29
ELZ
ELN
ELE
Velocity m/s
x 10^-7
Time of Day (Hour) in PST

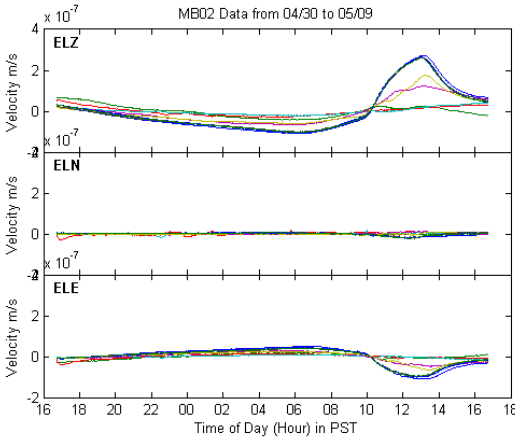
MB02 Data from 04/30 to 05/09
ELZ
ELN
ELE
Velocity m/s
Time of Day (Hour) in PST

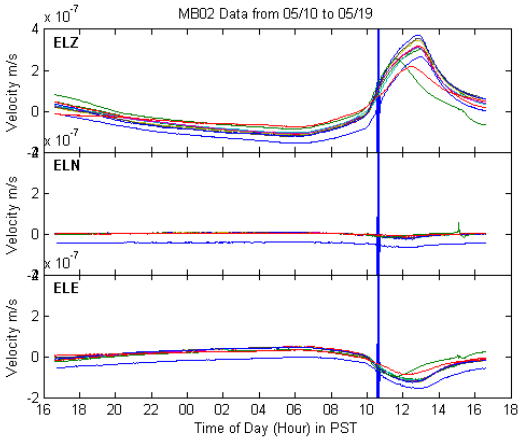
MB02 Data from 05/10 to 05/19
ELZ
ELN
ELE
Velocity m/s
Time of Day (Hour) in PST

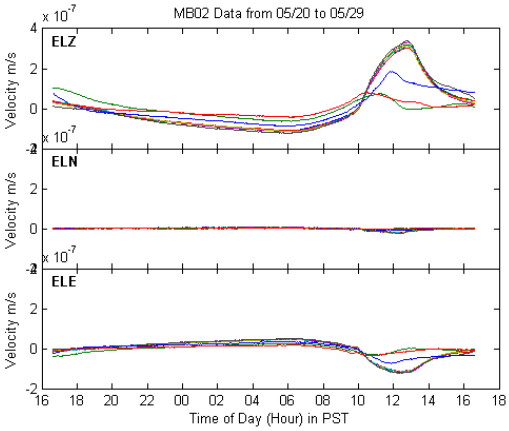
MB02 Data from 05/20 to 05/29
ELZ
ELN
ELE
Velocity m/s
Time of Day (Hour) in PST

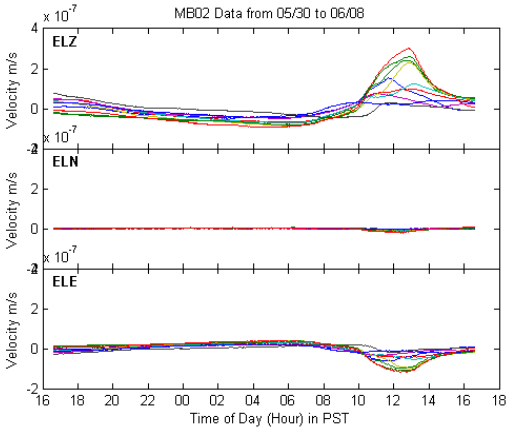
MB02 Data from 05/30 to 06/08
ELZ
ELN
ELE
Velocity m/s
Time of Day (Hour) in PST

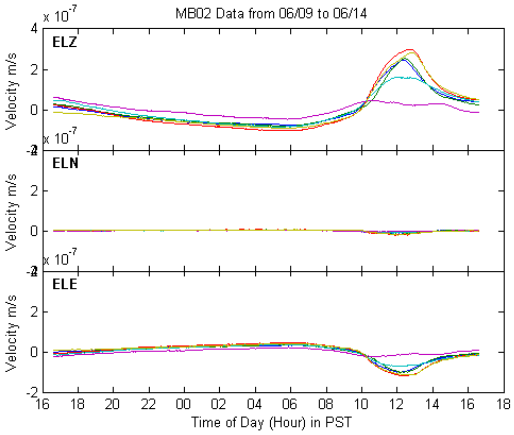
MB02 Data from 06/09 to 06/14
ELZ
ELN
ELE
Velocity m/s
Time of Day (Hour) in PST

B.8 Station MB07 (Mod. Talus), Geophone

This geophone was placed under sandbags below a talus slope and adjacent to the cliff wall during Phase 2 (winter 2008-09). It was discovered to have been tilted upon removal, and it is unknown when the instrumented tilted. Tilt dip was 34° from vertical with tilt direction azimuth (down) of 330°. This station also had some data gap errors. This instrument was later placed at station GH08 on 05/11/2009. The date from late 2008 to 02/11/2009 had serious power and data gap problems until the sampling rate was lowered to 500 sps.

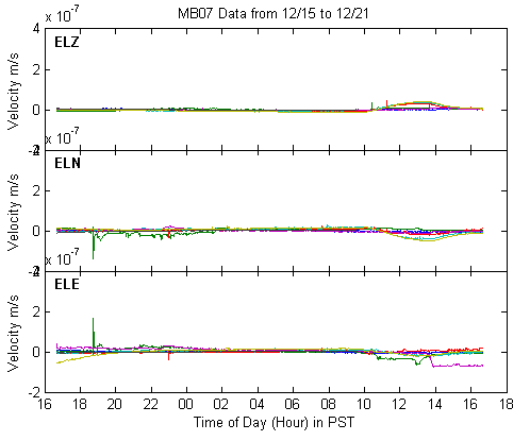

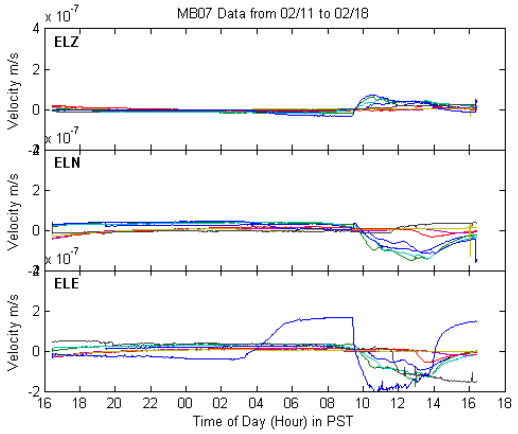

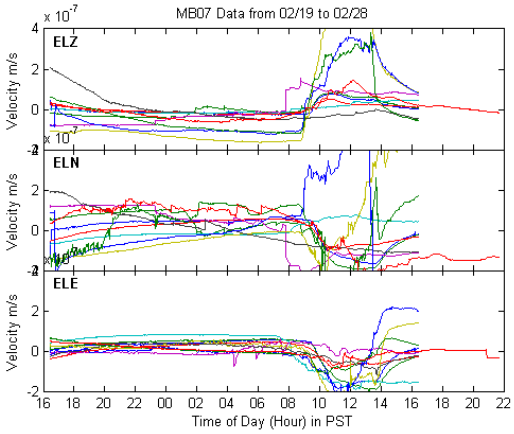

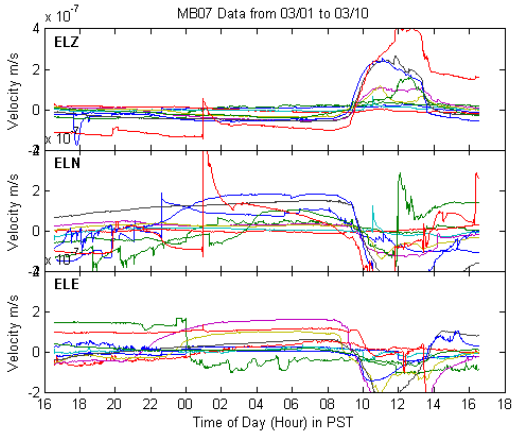
MB07 Data from 03/01 to 03/10
ELZ
ELN
ELE
Velocity m/s
Time of Day (Hour) in PST

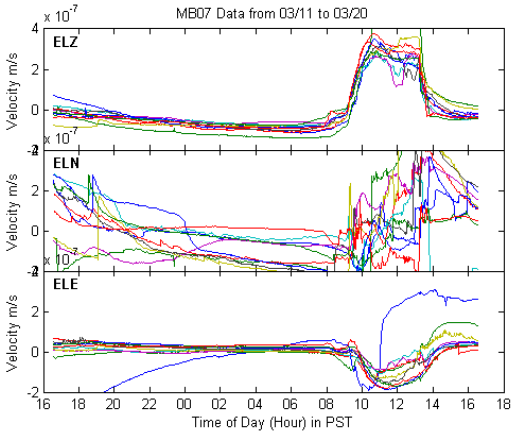
MB07 Data from 03/11 to 03/20
ELZ
ELN
ELE
Velocity m/s
Time of Day (Hour) in PST

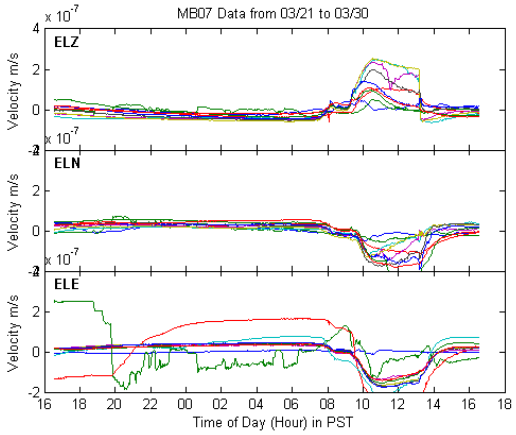
MB07 Data from 03/21 to 03/30
ELZ
ELN
ELE
Velocity m/s
Time of Day (Hour) in PST

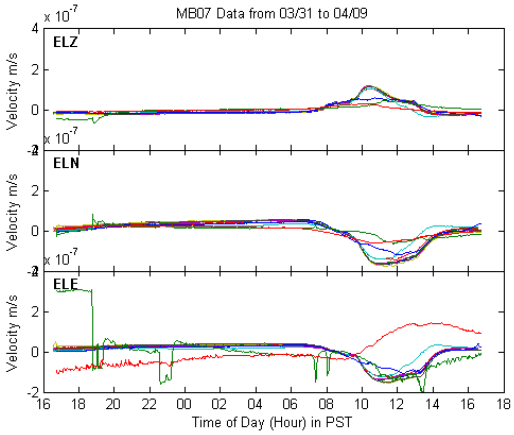
MB07 Data from 03/31 to 04/09
ELZ
ELN
ELE
Velocity m/s
Time of Day (Hour) in PST

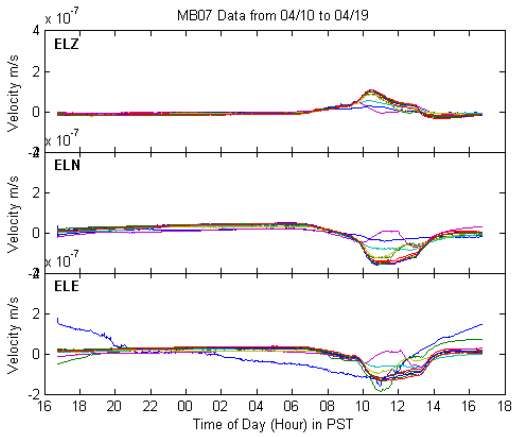
MB07 Data from 04/10 to 04/19
ELZ
ELN
ELE
Velocity m/s
Time of Day (Hour) in PST

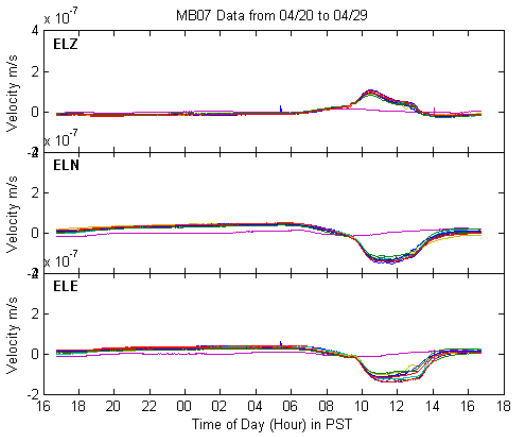
MB07 Data from 04/20 to 04/29
ELZ
ELN
ELE
Velocity m/s
Time of Day (Hour) in PST

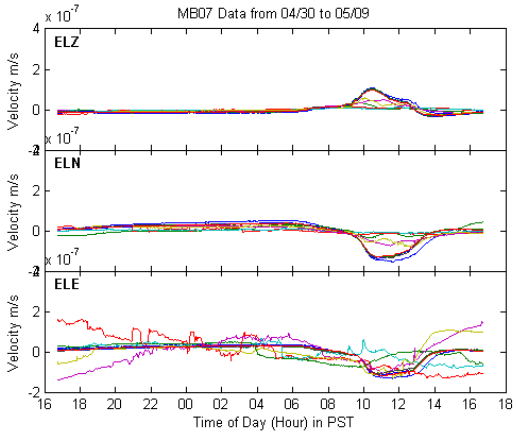
MB07 Data from 04/30 to 05/09
x 10^-7
ELZ
ELN
ELE
Velocity m/s
4
2
0
-2
16 18 20 22 00 02 04 06 08 10 12 14 16 18
Time of Day (Hour) in PST

B.9 Station GH08 (Shady Valley), Accelerometer

Station GH08 was placed in Yosemite Valley during Phase 2 (winter 2007-08) and outfitted with an accelerometer and 3 barometric microphones. The station had intermittent power outages and data gap errors. The accelerometer may have been tilted (or slowly changing position) in the snow and frozen ground, which may account for some of the tilt in February, 2009.

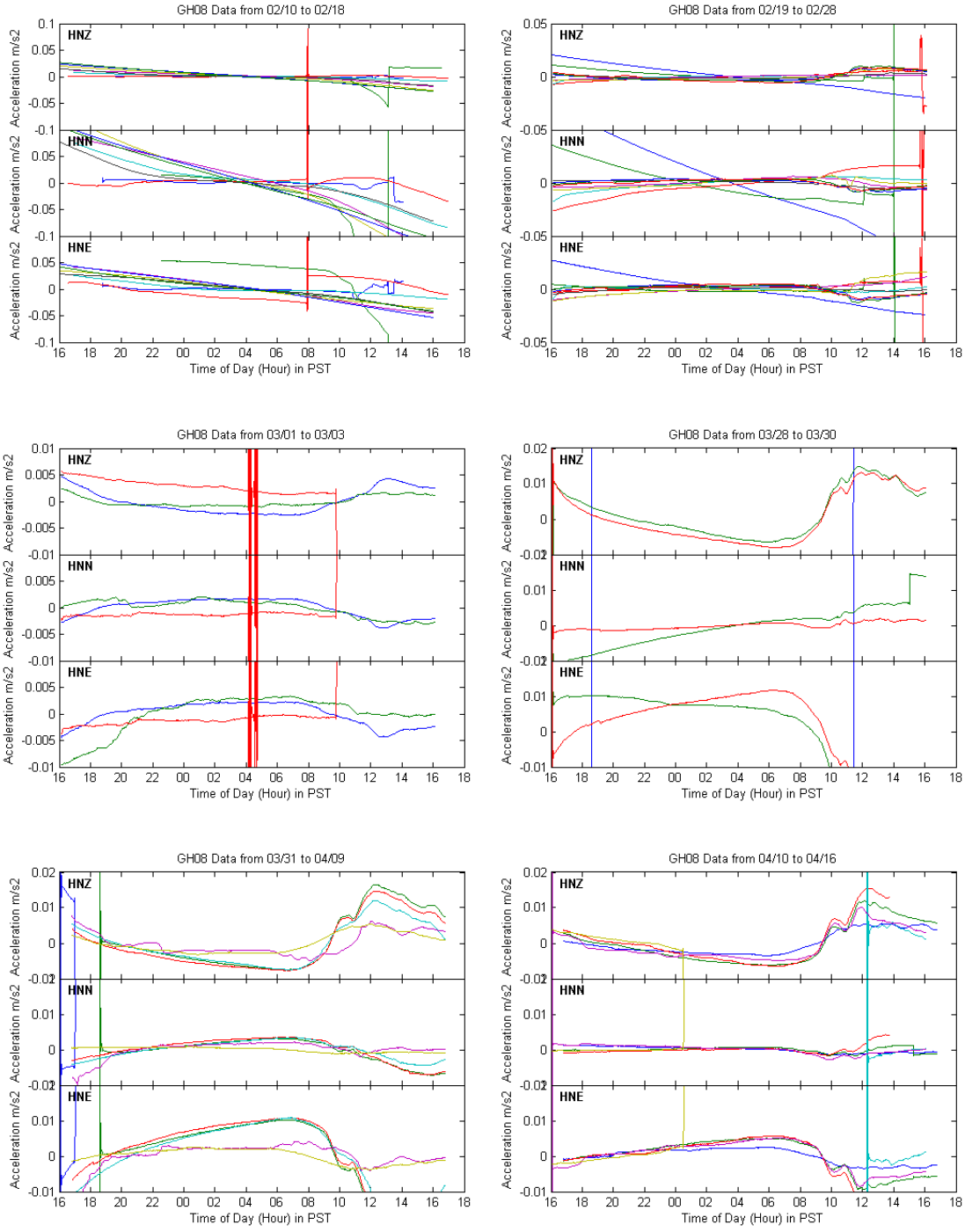

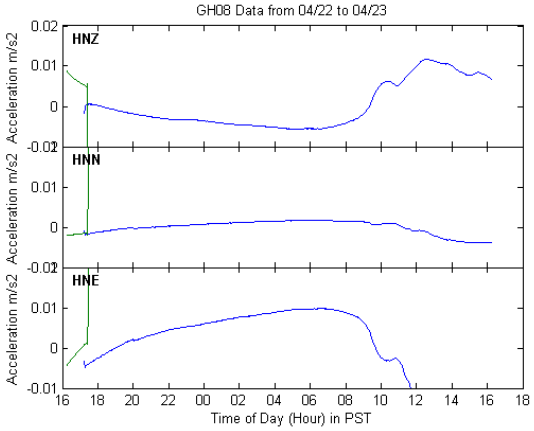
GH08 Data from 04/22 to 04/23
HNZ
HNN
HNE
Acceleration m/s2
Time of Day (Hour) in PST

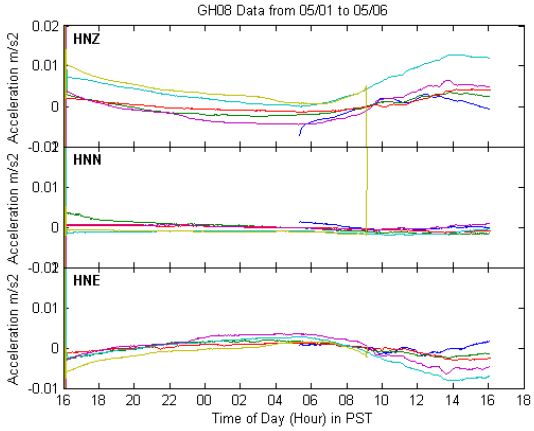
GH08 Data from 05/01 to 05/06
HNZ
HNN
HNE
Acceleration m/s2
Time of Day (Hour) in PST

B.10 Station GH08 (Shady Valley), Geophone

Station GH08 was placed in Yosemite Valley during Phase 2 (winter 2007-08) and outfitted with the geophone from MB07 (and 3 barometric microphones) after 05/10/2009. The normal gain for a geophone is x32, but the gain was left at x1 for this dataset, which may account for some of the noise. The station had intermittent power outages and data gap errors.